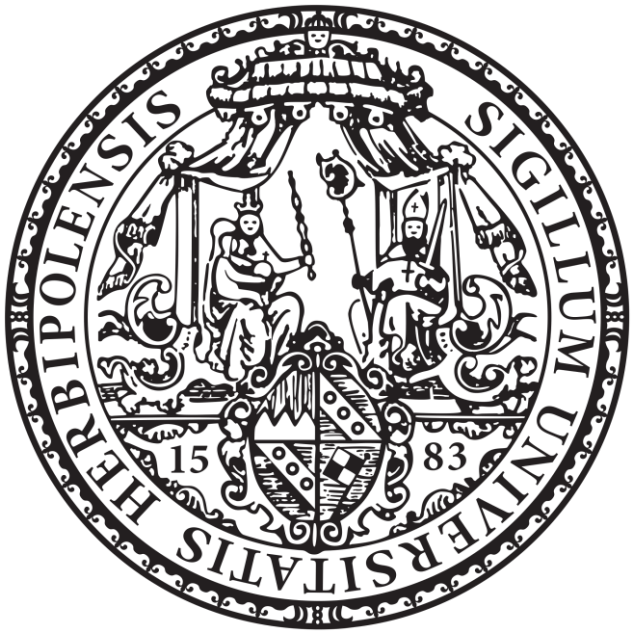

Functional peptide-based probes for the visualization of inhibitory synapses

***

Funktionelle peptidbasierte Sonden zur Visualisierung von hemmenden Synapsen

Doctoral thesis for a doctoral degree
at the Graduate School of Life Sciences,
Julius-Maximilians-Universität Würzburg,
Biomedicine Section

submitted by
Vladimir Khayenko
born in Kyiv, Ukraine
from Jerusalem, Israel
Würzburg 2022

Perseverance.

Dedicated to my Family.

Submitted on:

Members of the Thesis Committee:

Chairperson:	Prof. Dr. Markus Sauer
Primary Supervisor:	Dr. Hans M. Maric
Supervisor (Second):	Prof. Dr. Katrin G. Heinze
Supervisor (Third):	Prof. Dr. Philip Tovote

Date of public defence:

Date of receipt of certificates:

Contents

Acknowledgements

Nanos gigantum humeris insidentes.

First, I would like to thank Hans for giving me the opportunity to work, teach and learn at the University of Würzburg. This first chance in Germany was pivotal for me and my family. I am further grateful to you for trusting me to take the project in a different direction than you initially intended, letting me be creative and use my ideas. This approach paid off. You have taught me much and helped me to learn even more, and your support has allowed me to thrive. I wish you further success and thank you!

I further would like to thank Katrin and Philip. You both have been great mentors to me, were always there when I needed you and always helped me with word and deed.

Katrin, you and the Heinze team, especially Katharina, Hanna, Mike and Jürgen, were a big part of this work, and your professionalism and your support were fundamental to my accomplishments, thank you.

Philip, first, I want to thank you for the great collaboration that brought our scientific work to the next level, thank you for being open, responsive and involved. Furthermore, I am grateful for you picking up the mentorship banner at a critical time when I was left without the third mentor. Thank you for standing up to the task.

Dr. Christian Specht, Christian, you hosted me in the beautiful Paris, introduced me to ale and rugby and taught me how to image and work properly with neurons. You trained me in dSTORM and heavily invested in this project, you are a great part of it and its success. Lastly, you have been an excellent mentor and are a friend, thank you.

Sara Lourenco dos Reis, Sara, I was extremely lucky when you agreed to be a part of this work. I could not ever wish for a more committed, hard-working, smart, skilful and talented scientist to work with me. Thank you for everything.

Clemens Schulte, Clemens, my colleague, my peer, my mate. Thank you for the work, the support, the discussions, teaching me Inkscape and helping me make the figures. I wish you best of luck in your future endeavours.

Sonja, du warst mir eine kolossale Hilfe und hast mich immer mit Rat und Tat unterstützt. Ich bin froh, dass wir uns kennengelernt haben und gute Freunde werden konnten.

I am grateful to all the former Marics for good times and helpful discussions and especially to Noah Nordblom, Rafael Worschech and Melanie Hein, our talented and hard-working medical, master and bachelor students that contributed significantly to this work. I am grateful to all the current Marics for keeping the spirits high, taking interest in my work and being great mates. Ivan, Giorgia, Omkar, Christiane keep up the good work and good luck!

I am grateful to all the people that played smaller and bigger roles in this work. Thank you. Drs. Ora Schueler-Furman and Orly Avraham from the Hebrew University, Israel. Dr. Cataldo Schietroma from Abbelight, France. Drs. Carmen Villmann and Andreas Schlosser and their lab members from University of Würzburg. Drs. Eric Allemand and Fabrice Ango from INSERM, France. Dr. Antoine Triller from IBENS, France.

Finally, I want to thank to my Family. Lina, Gabi and Micha that make me happy and could handle without me on many weekends I spent in the lab, or many days on conferences and scientific stays. I promise, I will try very hard to get a job that will let us spend more time together. I want to thank my mother-in-law, Danka, for being there when we needed her and helping Lina in my absence. And I want to thank my sister, Sonya, that always roots for me and my mom, Olya, that lifts my spirits and is has an attentive ear to my concerns.

Abstract

Short functional peptidic probes can maximize the potential of high-end microscopy techniques and multiplex imaging assays and provide new insights into normal and aberrant molecular, cellular and tissue function. Particularly, the visualization of inhibitory synapses requires protocol tailoring for different sample types and imaging techniques and relies either on genetic manipulation or on antibodies that underperform in tissue immunofluorescence. Starting from an endogenous activity-related ligand of gephyrin, a universal marker of the inhibitory post-synapse, I developed a short peptidic multivalent binder with exceptional affinity and selectivity to gephyrin. By tailoring fluorophores to the binder, I have obtained Sylite, a probe for the visualization of inhibitory synapses, with an outstanding signal-to-background ratio, that bests the “gold standard” gephyrin antibodies both in selectivity and in tissue immunofluorescence. In tissue Sylite benefits from simplified handling, provides robust synaptic labeling in record-short time and, unlike antibodies, is not affected by staining artefacts. In super-resolution microscopy Sylite precisely localizes the post-synapse and enables accurate pre- to post-synapse measurements. Combined with complimentary tracing techniques Sylite reveals inhibitory connectivity and profiles inhibitory inputs and synapse sizes of excitatory and inhibitory neurons in the periaqueductal gray brain region. Lastly, upon probe optimization for live cell application and with the help of novel thiol-reactive cell penetrating peptide I have visualized inhibitory synapses in living neurons. Taken together, my work provided a versatile probe for conventional and super-resolution microscopy and a workflow for the development and application of similar compact functional synthetic probes.

Zusammenfassung

Kurze funktionelle peptidische Sonden können das Potenzial von High-End-Mikroskopietechniken und Multiplex-Imaging-Assays maximieren und neue Erkenntnisse über normale und abweichende Molekulare-, Zelluläre- und Gewebefunktionen liefern. Insbesondere die Visualisierung inhibitorischer Synapsen erfordert eine Anpassung des Protokolls an verschiedene Probentypen und Bildgebungsverfahren und ist entweder auf genetische Manipulationen oder auf Antikörper angewiesen, die in der Gewebeimmunfluoreszenz unterdurchschnittlich abschneiden. Ausgehend von einem endogenen aktivitätsbezogenen Liganden von Gephyrin, einem universellen Marker der hemmenden Postsynapse, habe ich einen kurzen peptidischen multivalenten Binder mit außergewöhnlicher Affinität und Selektivität zu Gephyrin entwickelt. Durch die Anpassung von Fluorophoren an das Bindemittel habe ich Sylite erhalten, eine Sonde für die Visualisierung inhibitorischer Synapsen mit einem hervorragenden Signal-Hintergrund-Verhältnis, das die "Goldstandard"-Gephyrin-Antikörper sowohl in der Selektivität als auch in der Gewebe-Immunfluoreszenz übertrifft. Im Gewebe profitiert Sylite von einer vereinfachten Handhabung, bietet eine robuste synaptische Markierung in rekordverdächtig kurzer Zeit und wird im Gegensatz zu Antikörpern nicht durch Färbungsartefakte beeinträchtigt. In der Super-Resolution-Mikroskopie lokalisiert Sylite präzise die Post-Synapse und ermöglicht genaue Messungen von Prä- zu Postsynapse. In Kombination mit ergänzenden Tracing-Techniken deckt Sylite die hemmende Konnektivität auf und erstellt Profile der hemmenden Eingänge und Synapsengrößen von erregenden und hemmenden Neuronen in der periaquäduktalen Grau Hirnregion. Schließlich habe ich nach Optimierung der Sonde für die Anwendung in lebenden Zellen und mit Hilfe eines neuartigen thiolreaktiven zelldurchdringenden Peptids hemmende Synapsen in lebenden Neuronen visualisiert. Insgesamt lieferte meine Arbeit eine vielseitige Sonde für konventionelle und superauflösende Mikroskopie und einen Arbeitsablauf für die Entwicklung und Anwendung ähnlicher kompakter funktioneller synthetischer Sonden.

Abbreviations

AA	Amino acid
A488	Alexa Fluor 488
A555	Alexa Fluor 555
A647	Alexa Fluor 647
AAV	Adeno-associated virus
ABC	ammonium bicarbonate
ACN	Acetonitrile
AGC	Automatic gain control
AZ	Active zone
BBB	Blood brain barrier
BSA	Bovine serum albumin
CNS	Central nervous system
DAD	Diode array detector
DAPI	4’,6-diamidino-2-phenylindole
DCM	Dichloromethane
DIC	N,N'-Diisopropylcarbodiimide
DIEA	N,N-Diisopropylethylamine
dm	dorsomedial
DMEM	Dulbecco's Modified Eagle Medium
DMF	Dimethylformamide
DMSO	Dimethyl sulfoxide
dSTORM	direct stochastic optical reconstruction microscopy
DTT	Dithiothreitol
eGFP	enhanced green fluorescent protein
eYFP	enhanced yellow fluorescent protein
FA	Formic acid
FBS	Fetal bovine serum
FDR	False discovery rate
Flp	Flippase
Fmoc	Fluorenylmethyloxycarbonyl
GABA	gamma-aminobutyric acid
GFP	Green fluorescent protein
GK	Guanylate kinase
Gly	Glycine
GPHN	Gephyrin
HCD	Higher-energy collisional dissociation
HPLC	High-pressure liquid chromatography
HRP	Horseradish peroxidase
IP-MS	Immunoprecipitation-Mass Spectrometry
ITC	Isothermal titration calorimetry
LC-MS	Liquid Chromatography-Mass Spectrometry
MAGUK	Membrane-associated guanylate kinase
MOC	Mander’s overlap coefficient
MS	Mass spectrometry
NA	Numerical apperture
ND	Asparagine-aspartate
NHS	N-Hydroxysuccinimide
NMDA	N-methyl-D-aspartate
NMI	1-Methylimidazole / N-methylimidazole
Oxyma	Ethyl cyanohydroxyiminoacetate

PAG	Periaqueductal gray
PALM	Photoactivated localization microscopy
PBS	Phosphate-buffered saline
PCC	Pearson's correlation coefficient
PDZ	PSD-95/Discs large/Zona occludens-1
PEG	Polyethylene glycol
PEI	Polyethylenimine
pip	Piperidine
PSD	Post synaptic density
PSF	Point spread function
RIM	Rab3-interacting molecule
ROI	Region of interest
RT	Room temperature
SBR	Signal-to-background ratio
SD	Standard deviation
SEC	Size-exclusion chromatography
SEM	Standard error of the mean
SH3	Src-homology-3
SRRF	Super-resolution radial fluctuations
SSC	Saline-sodium citrate
STED	Stimulated emission depletion
TCEP	Tris(2-carboxyethyl)phosphine
TFA	Trifluoroacetic acid
TFMSA	Trifluoromethanesulfonic acid
THPTA	Tris((1-hydroxy-propyl-1H-1,2,3-triazol-4-yl)methyl)amine
TIPS	Triisopropyl silane
TNB	5-thio-2-nitrobenzoic acid
VGAT	Vesicular GABA trasporter
vGluT2	Glutamate transporter
vl	ventrolateral

Copyright disclaimer

1. Introduction

Neuroscience relies on a plethora of scientific disciplines, techniques and methods to study the nervous system. There, light microscopy plays a central role in the study of the microscopic components, like the neuronal synapse, the basic communication and information transfer unit of the brain. Synapse studies on the nanoscale provide insight on the ultrastructure, molecular organization, synaptic strength and the underlying mechanisms involved in normal and aberrant function[2,3]. Synapse visualization on the micro- and macroscale allows mapping of the inhibitory and excitatory connectivity and is relevant for neural circuit tracking[4]. Finally, for histology and histopathology synapse detection in native tissue can be of a significant value, as it can help profile the neural connectivity in a healthy brain and see the connectivity changes in disease states[5].

On the brink of the millennium the development of advanced optical imaging methods has accelerated and today a plentitude of super-resolution microscopy techniques and tissue imaging approaches are available[6]. These new methods enabled multiplex and multiscale studies of the brain, from whole organ imaging[7] to the counting of single receptors at the synapse[2]. However, along with the development of new imaging approaches came a strong demand for new fluorescent tags, since the classical fluorescent affinity probes, the antibodies, would often underperform in tissue staining[8] and their size became a limiting factor in super-resolution microscopy. Firstly, the tissue imaging, especially of thick samples or whole organs, would benefit from new affinity probes that efficiently penetrate the intricate tissue matrix[9], or from new fluorescent proteins that endure tissue fixation and emit in longer wavelengths[6]. Secondly, super-resolution assays benefit from new tags with small size, since the smaller the tag is and the closer it is to the surface of the target protein, the higher localization precision gets, and, by extension, the resolution[10].

In the following chapters I will outline the importance of the inhibitory synapses and describe the development and application of a new small-size peptide-based affinity probe in conventional fluorescence microscopy, super-resolution studies of the synapse and in profiling and mapping of the inhibitory synapses in brain tissue.

1.1. Synaptic inhibition, inhibitory receptors and gephyrin

Main message:

- Neuronal inhibitory circuits regulate the excitability of the brain.
- The immediate inhibitory signal transduction occurs at glycinergic and GABAergic synapses.
- Gephyrin is the protein that scaffolds the glycinergic, GABAergic and mixed synapses.

Synaptic inhibition is a fundamental process modulating the flow of information in the neurons. Synaptic inhibition is directly related to the neuronal activity levels, it dynamically regulates neuronal excitability, prevents hyperexcitability and controls the processing and routing of information in neuronal circuits. Two basic types of brain inhibitory circuits involve: a) *Feedforward inhibition*, where an excitatory innervation activates both excitatory and inhibitory neurons and, in turn, inhibitory neurons regulate the activity of the activated excitatory neurons, b) *Feedback inhibition*, where the activated inhibitory neurons inhibit the activity of the activating excitatory neurons (Fig.1)[11].

Synaptic inhibition in the central nervous system (CNS) is mediated mainly by glycine (Gly) and γ-aminobutyric acid ($GABA_A$) receptors[12,13]. The former are largely located in the spinal cord and the brainstem, whereas the latter are present essentially in all CNS neurons[12]. GlyRs and $GABA_A$Rs are ligand-gated channels that are selectively permeable to anions, Cl^- and HCO_3^-. Under physiological conditions and normal neuronal function, activation of

GlyRs and $GABA_AR$s reduces the depolarization caused by parallel excitatory input, by balancing out the cation influx from excitatory receptors by anion influx, effectively shunting the excitation (depolarization)[13].

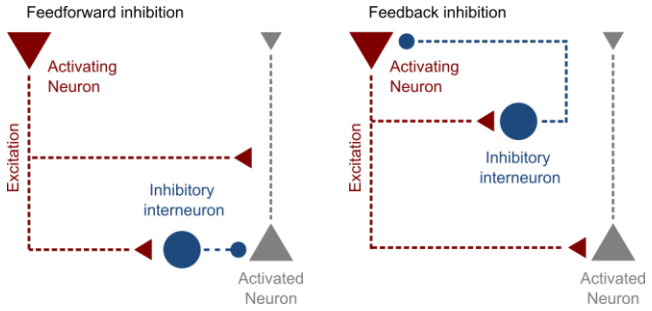

Figure 1. Inhibitory circuits. *Feedforward inhibition.* Activating cell triggers an action potential in the inhibitory interneuron and the pyramidal cell, the activated pyramidal cell receives shortly after an inhibitory input from the interneuron. *Feedback inhibition.* Action potentials in the pyramidal cell lead to excitation in the inhibitory interneuron, which in turn inhibits the pyramidal cell.

GlyRs and $GABA_AR$s, alongside nicotinic acetylcholine and serotonin receptors, belong to the Cys-loop receptor family, that derives its name from a 13-amino-acid loop in the extracellular domain formed by a disulfide bond of two cysteines. Cys-loop receptors share common structural features of five subunits, each with four transmembrane domains, that are circularly arranged with an ion-conducting pore in the center[14].

GlyR has five different receptor-forming subunits, α_{1-4} and β, however, in human only α_{1-3} and β are expressed[15]. Functional GlyRs are formed either from α homomers or from α and β heteropentamers with evidence pointing to 2:3[12,15], 3:2[16] or 4:1[17] stoichiometry. Most adult glycine receptors are α_1 and β heteropentamers, however also α_3 and β heteropentamers are abundant in the spinal cord neurons[18]. The α_2 subunit is expressed primarily during the nervous system development but has also been shown to be present in adults, in areas with sparce glycinergic innervation, like the cerebral cortex[12,15].

Unlike the α subunits, the β subunit alone does not form functional glycine receptors. However, the β subunit contributes to the glycine binding site in heteromeric receptors and is crucial for the clustering of the receptors at the post synaptic sites via the interaction with gephyrin, the main scaffold protein of the inhibitory synapse[15,19]. Glycine receptors devoid of β subunits are not enriched at the post-synapse, but at the extrasynaptic and presynaptic sites they play a role in mediating the tonic inhibition[15] and enhancing the neurotransmitter release in different CNS areas[20].

$GABA_A$ receptors, unlike GlyRs, have 19 different receptor-forming subunits: α_{1-6}, β_{1-3}, γ_{1-3}, δ, ε, π, θ, and ρ_{1-3}, however, the common $GABA_AR$ is a heteropentamer that has two α subunits, two β subunits, and one γ subunit. Not coincidentally, GABA binds at the interface between the α and β subunits, leading to a structural change that opens the anion pore[12,13]. The synaptic $GABA_AR$s are composed of αβγ subunits that have been shown to interact with intracellular proteins regulating $GABA_AR$ transport to- and anchoring at the synapses[21]. The most widespread and abundant synaptic receptor variations $\alpha_1\beta_2\gamma_2$, $\alpha_1\beta_3\gamma_2$ and $\alpha_2\beta_3\gamma_2$ all contain subunits that were shown to directly or indirectly interact with gephyrin[21–23], and the current list of gephyrin interactors encompasses $\alpha_{1/2/3/5}$, $\beta_{2/3}$ and γ_2 subunits[19,22,24–29]. Moreover, the γ_2 subunit, which is virtually present in all synaptic $GABA_AR$s[21], and gephyrin are interdependent, knock-out of either of the components results in the loss of synaptic $GABA_AR$ clusters[23].

As hinted beforehand, the common denominator of the inhibitory synapses is the scaffold protein gephyrin, that orchestrates the clustering of GlyRs and $GABA_AR$s at the post synaptic density (PSD). Notably, gephyrin's concentration at the inhibitory synapses closely correlates with the number of inhibitory receptors and the synaptic strength[30–32]. Gephyrin has two domains, an N-terminal G-domain connected by a long unstructured linker to a C-terminal E-domain[33]. The E domain harbors a universal receptor binding pocket that accepts an intracellular loop located between transmembrane domains 3 and 4 of $GABA_AR$ subunits $\alpha_{1,3}$ and of the GlyR β subunit[24,26]. Structural studies of gephyrin have shown that the G domain forms homotrimers, while the E-domain

forms homodimers, allowing the formation of gephyrin network at the inhibitory PSD[19,33]. While the non-synaptic soluble gephyrin forms trimers[18], the multimeric gephyrin scaffold at the PSD takes on two-dimensional latticed arrangement[2,34], which resembles hexagonal honeycomb organization[19,33].
To summarize, synaptic inhibition is dependent on the inhibitory receptors that are clustered at the synapses via a direct interaction to gephyrin or an indirect gephyrin interaction through auxiliary proteins (Fig. 2).

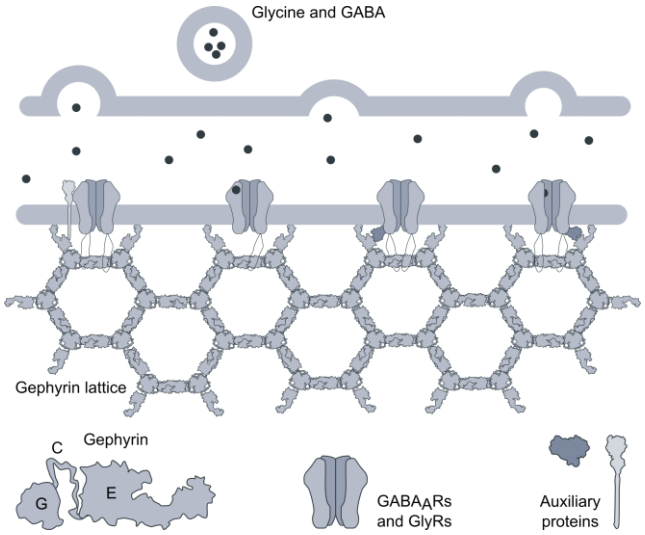

Figure 2. The inhibitory synapse. Glycine and GABA receptors are clustered at the inhibitory post-synapse either via direct interaction to gephyrin, indirectly via mediator proteins or the combination of both. Several interactions can occur simultaneously anchoring the receptor at the PSD. Gephyrin consists of an N-terminal "G" domain, C-terminal "E" domain, and the unstructured "C" linker region. With two N-terminal and one C-terminal bond per molecule the basic requirement for the gephyrin lattice formation is met. Note that the gephyrin lattice is rotated 90° for illustration purposes, at the synapse the lattice is parallel to the cell membrane.

1.2. Visualization of the inhibitory synapses

Main message:

- Gephyrin is the most robust pan-inhibitory synapse marker that correlates with receptor numbers and synaptic strength.
- Commonly inhibitory synapses are visualized through genetic tagging of gephyrin or with immunofluorescence.
- Genetic manipulations inherently affect cell function and morphology.
- Antibodies used in immunofluorescence underperform in tissue labeling and have sub-optimal localization precision for super-resolution microscopy.
- New fluorescent tags, mitigating the weaknesses of "classical" probes, are being developed.

The common markers used for the visualization of inhibitory synapses are, naturally, the molecular components of the inhibitory transmission. Fluorescent tagging of GABA$_A$R γ2 subunit[35,36] is frequently used to visualize synapses having GABAergic input, and GlyR α1 tagging is used for the visualization of glycinergic synapses[2]. A more inclusive marker is the vesicular GABA transporter (VGAT), also known as vesicular inhibitory amino acid transporter, a presynaptic protein involved in vesicular storage and subsequent exocytosis of glycine and GABA[37]. However, VGAT is not a quantitative marker, as its expression is higher in nerve endings rich in GABA, compared to those rich in glycine only[38]. Additionally, some sub-populations of nerve endings rich in glycine and GABA lack VGAT, there the neurotransmitter exocytosis probably relies on other proteins[38], in these populations synaptic sites cannot be detected using VGAT tagging.

Gephyrin is a universal marker for inhibitory synapses, considering that staining for any one of $GABA_A$ or glycine receptor subunits would overlook receptors that do not include that subunit. And, in contrast to VGAT, gephyrin is integral to the inhibitory synapse and is directly correlated to receptor numbers and the synaptic strength, making it a suitable marker for quantitative microscopy[2].

Gephyrin is often visualized using genetic tagging, i.e., fusion of gephyrin with a fluorescent protein and expression of the chimera via transfection or viral transduction (infection). eGFP, mCherry, mEos2 and other fluorescent gephyrin chimeras have successfully been used for synapse studies both in fixed and live cells[2,39,40], and in conditional expression in transgenic animals[41]. However, induced secondary gephyrin expression has an inherent drawback, as it can cause morphological or functional effects in cells[41–43]. To overcome overexpression and, by extension, the unwanted morphological and functional effects, transcriptional control mechanisms could be applied. Recently, two alternative methods of genetic tagging were described. The first method describes an exogenic transcriptional control system, that is coupled to an expression of eGFP fused anti-gephyrin nanobody (antibody-like light-weight protein), with the coding plasmid delivered via transfection or infection to the cells. This control system matches the expression level of the protein tag with that of its endogenous target, minimizing off-target labeling and unwanted functional effects[44]. The second method relies on the generation of fluorescent protein-gephyrin knock-in mice where expression levels, subcellular distribution of the endogenous protein and synaptic function are largely preserved[2,32], most likely due to the native control and regulation mechanisms.

To summarize, genetic tagging can induce aberrant cell function and morphology, therefore thorough evaluation of the impact of genetic interference and careful interpretation of the data is needed. Newer methods of genetic tagging that include transcriptional control mechanisms are preferrable, however their application is arguably more complex, as it requires even more rigorous controls to ensure that the multicomponent machinery properly works. Furthermore, the availability of the new genetically tagged models is limited, and *de novo* generation of these models is not straightforward, especially of the knock-in animals.

A powerful alternative to genetic tagging is immunostaining of endogenous proteins, a technique that is easily applicable to *post vivo* samples. There is a vast variety of commercial anti-gephyrin antibodies, however commercial antibody reliability, especially in tissue immunostaining, was shown to be below 50%[8]. Nevertheless, several gephyrin antibodies have become the 'gold standard' for gephyrin labeling and have been used for decades[30,45–47]. Yet the antibodies' large size and their tendency to crosslink the target proteins can affect labeling performance, particularly in tissue and other complex samples[8,48]. Additionally, the size of the antibodies is disadvantageous in super-resolution microscopy studies, where smaller probes are preferred since they increase localization precision and resolution[9,10]. Therefore, past years have seen a significant development of alternative affinity probes, protein-based, like Fabs (antibody-derived antigen-binding fragments) and nanobodies, and synthetic, like aptamers or small-molecule ligands[49–51]. Recent work described the development and application of nanobodies as immunolabels for neuronal proteins, including gephyrin, and showed with the example of Homer1, a marker of excitatory synapses, that nanobodies can successfully be used for tissue staining and, due to their small size, enhance the obtained spatial resolution in super-resolution microscopy[52]. However, no positive examples of gephyrin nanobody staining or any gephyrin staining data analysis were shown, in fact only one gephyrin nanobody from a ~180 nanobody library was mentioned to work in tissue staining, and none worked in cell assays[52].

The only non-antibody affinity probe that has been successfully used to label gephyrin was TMR-2i[53], a synthetic probe derived from the binding sequence of the intracellular loop of the GlyR β subunit, the strongest endogenous binder of the universal receptor binding pocket of gephyrin. However, the probe had low selectivity and low signal to background ratio, limiting its usability in light microscopy. A succinct summary of the inhibitory synapse visualization methods is shown in Table 1.

Table 1. Summary of published labeling methods for gephyrin¨

Class	Type	Examples	Cell imaging	Tissue imaging	Live imaging	Super-Resolution	Notes
Affinity probes	Protein based	mAb7a[2,54]	Yes	Restricted	No	Yes, depends on a secondary antibody	Isoform- and phosphoselective
		mAb3B11[41]	Yes	Restricted	No	Yes, depends on a secondary antibody	Indiscriminate for active neuronal isoforms
	Synthetic	TMR2i[53]	Restricted	No	No	No	Low selectivity and contrast
		Sylite	Yes	Yes	No	Yes (dSTORM)*	Binds active neuronal isoforms
Genetic tags	Fused tags	eGFP[39,41]	Yes	Yes, with additional anti-eGFP staining	Yes	Not tested	Secondary gephyrin expression
		mEos2[2]	Yes	Not tested	Yes	Yes (PALM)*	Secondary gephyrin expression
		mRFP[2,32,40]	Yes	Yes	Yes	Restricted (SRRF)**	Knock-in mouse
	Intrabodies	GPHN-FingR-GFP[44]	Yes	Not tested	Yes	Not tested	Integrated expression regulation, fibronectin III-based probe
		GC52-EGFP[52]	Yes	Not tested	Yes	Not tested	Single monomeric variable camelid antibody domain

*dSTORM and Photoactivated localization microscopy (PALM) are single molecule localization techniques that require specific fluorophores that have stochastic blinking behaviour under certain conditions. ~20 nm average resolution[55].

**Super-Resolution radial fluctuations (SRRF) is a fluorophore independent super-resolution algorithm that analyses image sequences of one sample to generate a super-resolution image with an average resolution of ~110 to ~200 nm[56].

1.3. Functional peptide-based gephyrin probes

Main message:

- Immunological probes used in immunofluorescence inherently target various isoforms of the same protein.
- Peptide probes developed from an endogenous ligand of a protein would target the protein isoforms that have the binding site for the ligand.
- A linear gephyrin binding motif derived from GlyR can serve as a lead to develop a peptide probe targeting gephyrin isoforms that form the synapse.

Antibodies and the recent, smaller, immunoprobes like Fabs or nanobodies are raised against protein fragments and, after maturation, would bind their antigen, however, the epitope they bind to may have no relation to any functional site of the protein. This would typically result in labeling of active and inactive forms of the protein by the immunoprobes.

A peptide probe derived from an endogenous ligand of the target protein can retain the specificity to a certain function-carrying site of the protein, i.e., the peptide probe would have an advantage of functional targeting, selectively binding the active forms of the protein of interest.

Gephyrin is a multifunctional protein, with numerous isoforms and post-translational modifications. In non-neural tissues it participates in the molybdenum cofactor biosynthesis that is essential for a diverse set of two electron transfer reactions, a crucial process for viability throughout all kingdoms of life[57]. In neural tissues gephyrin governs the formation, maintenance, size, density and the receptor composition of inhibitory synapses through the myriad of its isoforms and post-translational modifications[58,59]. Recently a common structural feature of synaptic gephyrin isoforms was noted, in primary neurons gephyrin isoforms having a complete E domain were forming synaptic clusters, while isoforms with an altered E domain were not[58]. In turn, integral gephyrin E domain forms the receptor binding pocket that directly anchors GlyRs and several $GABA_AR$ variations[24,26,60,61]. Thereby, the logical lead for the development of a functional peptide-based gephyrin probe, which selectively targets the synaptic gephyrin, would be its strongest endogenous ligand – a GlyR segment that binds to the receptor binding pocket formed by the complete E domain.

Already in 1995 Meyer et al. have shown that a large, 49-amino acid fragment of GlyR β intracellular loop, which starts at position 378 of the subunit, interacts with gephyrin, and then further pinpointed the interaction region to 18 amino acids located in positions 394-411[62]. Later, structural studies confirmed a direct high affinity interaction of the large fragment with gephyrin and specifically with the gephyrin E domain[63] and provided first crystal structure of gephyrin E domain universal receptor binding pocket with a significantly shorter 13 amino acid

peptide, a fragment of the GlyR β loop (398-410)[64]. Further research showed that even an 8-amino acid long peptide from the core binding sequence of the GlyR β loop (398-405) retains high affinity to the E domain, with a dissociation constant (K_D) of ~20 µM compared to ~2 µM K_D of the larger fragment[65].
In 2017 Maric et al., used peptide microarrays to explore point mutation influence in the core binding motif on the interaction with gephyrin E domain[53]. Based on the microarray several binding-enhancing point mutations were discovered and a high affinity "2i" peptide carrying the mutations and a polyarginine motif was produced. This peptide had an antagonistic effect on the GlyR firing, and when conjugated to Tamra, red-light emitting rhodamine fluorophore, was shown to label gephyrin clusters in fixed cells (the aforementioned TMR-2i). Subsequently, we exploited peptide microarrays with brain lysate to further refine the binders for native gephyrin[66] (Fig. 3).

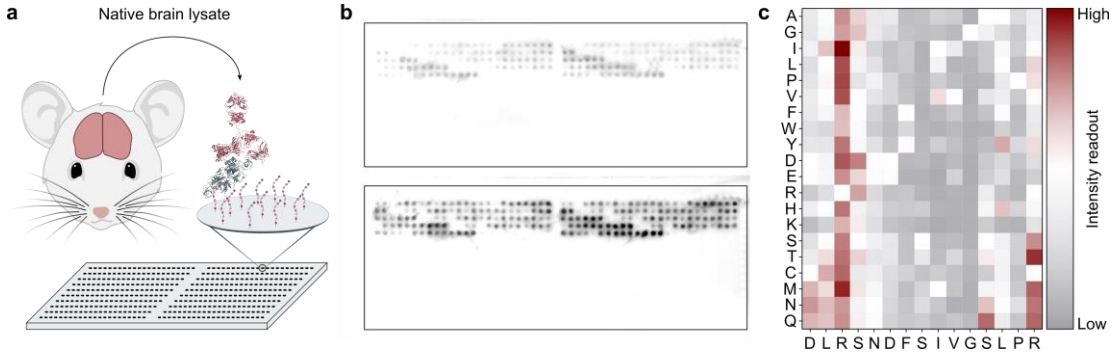

Figure 3. Gephyrin core binding sequence and binding enhancing mutations determination with brain lysate. a) Mouse brain was homogenized and applied on peptide microarrays, gephyrin was detected with anti-gephyrin antibody. b) Representative microarray readout, here, gephyrin binder microarrays with chemiluminescence readout. On the top is 4-fold dilution of the sample applied to the microarray on the bottom. c) Heatmap generated from the signal intensity readout of the peptide microarray with brain lysate – stronger signal correlates to stronger binding. On the X axis is the gephyrin binding motif, on the Y axis are point mutations with the 20 common amino acids for each position of the gephyrin binding motif.

While most monomeric peptides have a formidable low µM affinity, dimeric peptides were shown to be superior binders of gephyrin. A study exploring the dimerization of a 19 amino acid fragment of the GlyR β loop (398-416) showed a 25-fold affinity increase of the dimeric peptide over the monomer[67]. Further exploration of dimerization strategies and binding motifs led to shortened dimeric binders that had mid- to low nanomolar affinity and shorter binding sequences of up to 8 amino acids[65]. However, these dimers required two reaction-purification cycles, since the dimerization relied on a di-maleimide linker that would connect two peptide monomers carrying a cysteine. To simplify the synthesis route, shorten the synthesis time and increase the yields, an on-resin dimerization via lysine was explored[1]. Microarray data regarding the optimal linker length of the dimer was inconclusive, yet the process enabled the production of low nanomolar affinity dimeric gephyrin binders in one-pot reaction (Fig. 4, Appendix A). These studies have uncovered the potential of multimeric gephyrin binders and paved way for further exploration and exploitation of short dimeric peptides as potential inhibitory neurotransmission modulators and fluorescent probes.

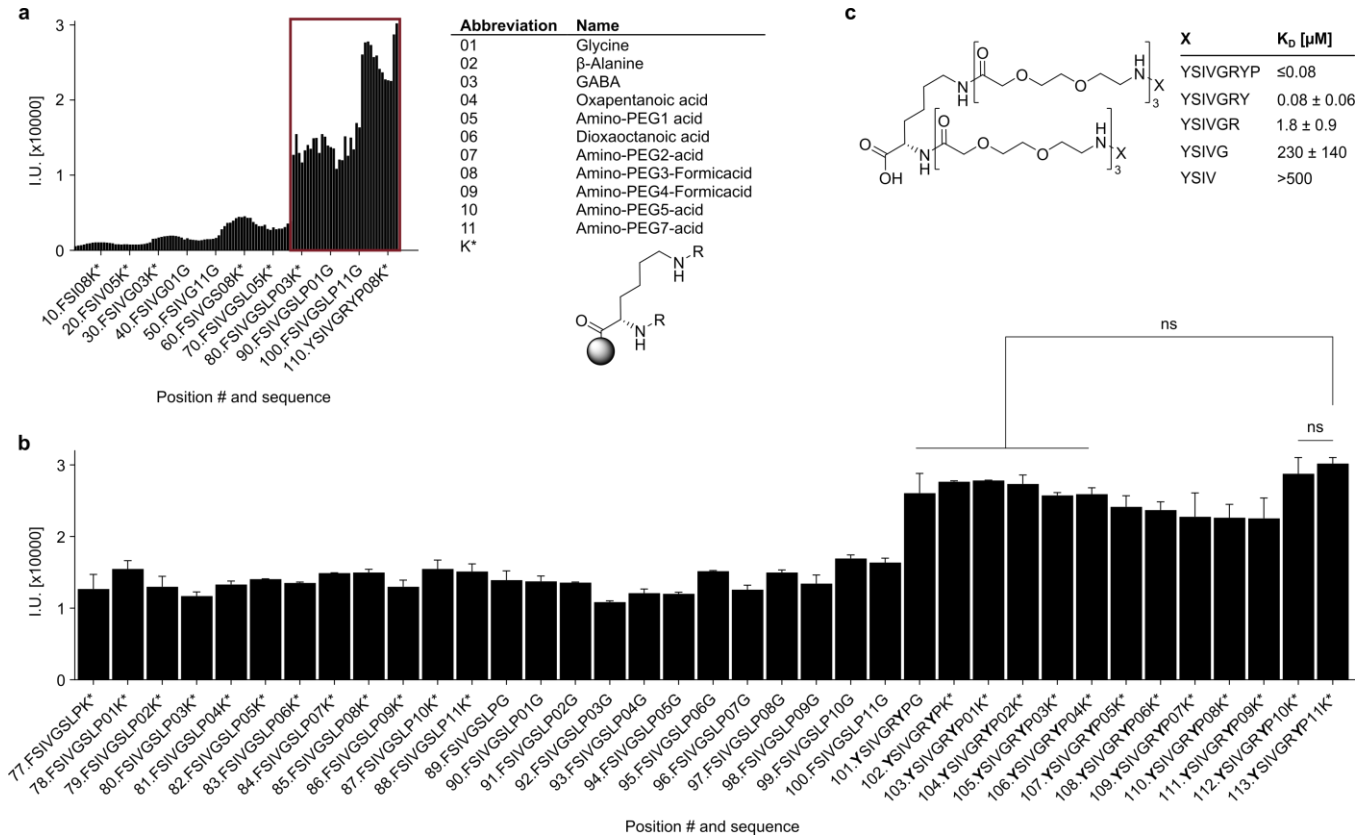

Figure 4¨. Peptide dimers synthesized in one-pot reaction retain strong binding to gephyrin. a) A luminescence readout of gephyrin binding to the peptide microarray, containing different mono- and dimeric binders. Signal strength correlates with the number of molecules bound. Lysine is the fork enabling the simultaneous synthesis of identical dimer branches. b) Zoom-in on the box from a), no significant difference in signal intensity can be determined between mono- and dimeric gephyrin binders. Significance determined with ANOVA with a follow up Dunnett's test for multiple comparisons. c) Tri-aminodioaxaoctanoic acid linker was used before the gephyrin binding sequence of 8 to 4 amino acids. ITC assays showed progressing affinity increase for binders with longer binding sequences and low nanomolar affinity for the 8-mer binder.

1.4. The aim of this study

In this study I pursued one aim and one objective:

<u>The aim</u>

Establishment of a new class of affinity probes, functional peptide-based probes derived from endogenous ligands, together with the general probe development concept.

<u>The objective</u>

Production of a versatile fluorescent probe for the visualization of inhibitory synapses that would serve as a fundamental microscopy tool for neurosciences.

Small size fluorescent probes can overcome the shortcomings of the antibodies, both in labeling performance, be that better localization precision or enhanced tissue penetration, and in selectivity. To date, only a fraction of the available affinity (or covalent) labels for fluorescence microscopy are not immuno-based, and even fever are functional or activity-based, i.e., targeting the functional or active forms of the protein.

I anticipated that through the evolution of a binding motif derived from an endogenous ligand of a target protein a small-sized probe with a unique selectivity profile could be developed. Gephyrin was an ideal target protein to

test this assumption. First, gephyrin, as the scaffold protein of the inhibitory synapse and its most prominent marker, is of high interest to the scientific community. Therefore, a gephyrin probe would have practical application and could be used and evaluated by a big audience. Secondly, gephyrin directly clusters GlyRs and a subset of $GABA_ARs$ through a universal binding pocket, hence, a probe derived from GlyR, the strongest endogenous binder of gephyrin, should retain the binding specificity of the endogenous ligand. Thirdly, gephyrin is concentrated and unsaturated at the inhibitory synapse, i.e., a considerable proportion of gephyrin molecules will have an unoccupied receptor binding pocket that could be targeted by the functional probe.
Thus, I hypothesized that the peptidic gephyrin probe, derived from the endogenous ligand, the glycine receptor, would be as good or better than the antibodies in visualizing the inhibitory synapses in cells and tissue.

2. Methods

Unless otherwise noted, all resins and reagents were purchased from IRIS biotechnologies, Carl Roth or Sigma and used without further purifications. All solvents used were HPLC grade. All water-sensitive reactions were performed in anhydrous solvents under positive pressure of argon. Statistical analysis was preformed using GraphPad Prism.

YSIVGSYPRRRRRRRRR peptide, with noted >95% purity, was purchased from ChinaPeptides (Suzhou, China) and directly used for further conjugation to fluorophores. Post hoc mass spectrometry analysis of conjugated product showed that the peptide was provided as a mixture of YSIVGSYPRRRRRRRR (8 arginines) and YSIVGSYPRRRRRRRRR (9 arginines) peptides (Appendix B).

2.1. Materials, equipment and instruments

Equipment and consumables

Unless further stated, all equipment and consumables are listed in the tables 1 and 2. Protected trademarks have not been marked separately.

Table A: Equipment and instruments

Device	Source	Product name
Balances	*A&D Company, Ltd.* *Mettler-Toledo, LLC* *KERN & SOHN GmbH*	FZ-300i XS105 ABT120-5DNM
Box	*Raaco GmbH*	Raaco Assorter Polypropylen box
Centrifuges	*VWR International, Ltd.* *Eppendorf SE* *Biozym Scientific, GmbH*	Micro Star 17R Mega Star 1.6R Concentrator 5301 Mini Centrifuge
Columns	*Phenomenex, Inc.*	Onyx™ Monolithic Semi-PREP C18, LC Column 100 x 10 mm Onyx™ Monolithic C18, LC Column 100 x 4.6 mm Onyx™ Monolithic C18, LC Column 50 x 2 mm
Freeze dryer	*Uniequip, GmbH*	Unicryo MC-2L-60°C
Heat Block	*Labnet International, Inc.*	Digital Dual Block Dry Bath
High-performance liquid chromatography (HPLC) setups	*Shimadzu Corporation* *Thermo Fisher Scientific, Inc.*	Shimadzu Prominence Analytical HPLC Ultimate 3000 Preparative HPLC
Imaging systems	*GE Healthcare, Inc.* *Azure Biosystems, Inc.*	ImageQuant™ LAS 4000 c400
Ionizer	*KERN & SOHN GmbH*	YBI-01A
Laminar flow cabinet	*BDK Luft- und Reinraumtechnik GmbH*	BDK-S 1200
Liquid chromatography-mass spectrometry (LC-MS) setup	*Agilent Technologies, Inc.*	Agilent 1260 Infinity II LC
Microarray contact printer	*CEM GmbH*	Slide Spotter
Microscopes	*Leica Microsystems, GmbH* *Olympus Europa SE & Co. KG* *Nikon Europe B.V.*	DMI 6000 DMi8 SP5 SP8 Olympus Ix83 Eclipse Ti
Microscopy imaging chamber	*Life Imaging Services*	Ludin Chamber Type 1, screwing tool and holder (10900/10910/10604)

Shakers	*Scientific Industries, Inc.* *Heathrow Scientific,* *Edmund Bühler GmbH* *LLC*	Mini-100 Orbital-Genie TiMix 5 Digital Orbital Shaker
Peptide synthesizer	*CEM GmbH*	MultiPep 2
pH-meter	*VWR International, Ltd.*	pHenomenal pH 1100 L
Pipettes	*Eppendorf SE*	Eppendorf Research plus 0.1-2.5 µl 2-20 µl 20-200 µl 100-1000 µl
Pipette (multichannel)	*Brand, GmbH*	Transferpette S-12
Pipette (stepper)	*Eppendorf, AG*	Multipette M4
Pipette controller	*Brand, GmbH*	Accu-jet pro
Sonicator	*EMAG AG*	Emmi-H22
Spectrophotometer	*Cole-Parmer, Ltd.*	Jenway 7205
Thermometer	*IKA Works, Inc.*	ETS-D5
Thermoshaker	*Eppendorf, AG*	Eppendorf Thermomixer comfort
Vortex	*Scientific Industries, Inc.*	Vortex-Genie 2
Water bath	*Phoenix Instrument*	WB5

Table B: Consumables

Consumable	**Source**	**Product name**
Conical tube	*Sarstedt AG & Co. KG*	15/50 ml
Coverslips	*Hartenstein, GmbH* *VWR International, Ltd.*	24 mm x 60 mm, thickness 1, DK60 Ø 18 mm, thickness 1, 631-0153P
Gloves	*VWR International, Ltd.*	NITRILE Light
Microarray slides	*Intavis Peptide Services GmbH & Co. KG*	CelluSpot
Microscope slides	*Thermo Fisher Scientific, Inc.*	AGAA000001#02E
Pipette tips	*Biozym Scientific, GmbH* *Eppendorf SE*	200/1000 µL epTips 0.1-10 µL
Reaction tubes	*Sarstedt AG & Co. KG*	1.5/2/5 mL
Water purification system	*Thermo Fisher Scientific, Inc.*	TKA xCAD Plus
Well plates	*Eppendorf, AG* *CEM GmbH* *Sarstedt AG & Co. KG*	Deepwell Plate 96/1000 µl 384 well plate TC 6/12 well plate, Standard F

Chemicals

Table C: Protected amino acids, derivatives, reagents and resins used in peptide synthesis

Derivative	**Code**	**Chemical name**	**Source**	**Identifier**
DIEA	-	N,N-Diisopropylethylamine	*Carl Roth GmbH*	2474.3
DCM	-	Dichloromethane	*Merck KGaA*	32222-m
OxymaPure	-	Ethyl(hydroxyimino)cyanoacetate	*Iris Biotech GmbH*	RL-1180
DIC	-	N,N'-Diisopropylcarbodiimide	"	RL-1015
DMF	-	Dimethylformamide	"	SOL-004
Rink amide linker	1	Fmoc-Rink-Amide-Linker	"	RL-1027
PEG-linker	2	Fmoc-O_2Oc-OH	"	FAA1435
L-Lys(N3)	-	Fmoc-L-Lys(N3)	"	FAA1793
Di-Fmoc-Lysine	-	Fmoc-L-Lys(Fmoc)-OH	"	FAA1391
L-Alanine	A	Fmoc-L-Ala-OH*H_2O	"	FAA1005

β-Alanine	B	Fmoc-beta-Ala-OH	"	FAA1300
L-Cysteine	C	Fmoc-L-Cys(Trt)-OH	"	FAA1040
L-Aspartic acid	D	Fmoc-L-Asp(tBu)-OH	"	FAA1020
L-Glutamic acid	E	Fmoc-L-Glu(tBu)-OH*H_2O	"	FAA1045
L-Phenylalanine	F	Fmoc-L-Phe-OH	"	FAA1175
Glycine	G	Fmoc-Gly-OH	"	FAA1050
L-Histidine	H	Fmoc-L-His(Trt)-OH	"	FAA1090
L-Isoleucine	I	Fmoc-L-Ile-OH	"	FAA1110
L-Lysine	K	Fmoc-L-Lys(Boc)-OH	"	FAA1125
L-Leucine	L	Fmoc-L-Leu-OH	"	FAA1120
L-Methionine	M	Fmoc-L-Met-OH	"	FAA1150
L-Asparagine	N	Fmoc-L-Asn(Trt)-OH	"	FAA1015
L-Proline	P	Fmoc-L-Pro-OH*H_2O	"	FAA1185
L-Glutamine	Q	Fmoc-L-Gln(Trt)-OH	"	FAA1043
L-Arginine	R	Fmoc-L-Arg(Pbf)-OH	"	FAA1010
L-Serine	S	Fmoc-L-Ser(tBu)-OH	"	FAA1190
L-Threonine	T	Fmoc-L-Thr(tBu)-OH	"	FAA1210
L-Valine	V	Fmoc-L-Val-OH	"	FAA1245
L-Tryptophan	W	Fmoc-L-Trp-(Boc)-OH	"	FAA1225
L-Tyrosine	Y	Fmoc-L-Tyr(tBu)-OH	"	FAA1230
L-Glutamic acid, free side chain	-	Fmoc-Glu-OH	*Bachem AG*	4025278
Glycine, Boc protected	-	Boc-Gly-OH	*Merck KGaA*	8.530000
Cys-Wang resin	-	Fmoc-L-Cys(Trt)-Wang Resin	*Iris Biotech GmbH*	WAA11306
2-Chlorotrityl chloride resin	-		"	BR-1065
TentaGel resin	-	-	*Intavis Peptide Services GmbH & Co. KG*	32.900

Table D: Chemicals

Trivial name	**IUPAC name or abbreviation**	**Identifier**	**Source**
Acetonitrile	C_2H_3N	34851	*Merck KGaA*
Aminoguanidine hydrochloride	CH_6N_4 HCl	396494	*Merck KGaA*
Ammonium chloride	NH_4Cl	213330	*Merck KGaA*
Copper sulfate	$CuSO_4$	84845.230	*VWR International, Ltd.*
Diethyl ether	$(C_2H_5)_2O$	5920.3	*Carl Roth GmbH*
Dimethyl sulfoxide	DMSO	34869	*Merck KGaA*
Disodium phosphate	Na_2HPO_4*H_2O	4984.1	*Carl Roth GmbH*
DTNB	5,5'-Dithiobis(2-nitrobenzoic acid)	D218200	*Merck KGaA*
Ethanol	EtOH	51976	*Merck KGaA*
Formic acid	CH_2O_2	84865.180	*VWR International, Ltd.*
Glycine	$C_2H_5NO_2$	3187.1	*Carl Roth GmbH*
Methanol	MeOH	34860	*Merck KGaA*
Monopotassium phosphate	KH_2PO_4	3904.1	*Carl Roth GmbH*
Paraformaldehyde	$OH(CH_2O)_nH(_{n=8\text{-}100})$	00380-250	*Polysciences, Inc.*
Piperidine	$C_5H_{11}N$	A122.4	*Carl Roth GmbH*
Potassium chloride	KCl	P017.1	*Carl Roth GmbH*
Sodium chloride	NaCl	0962.1	*Carl Roth GmbH*
Sodium ascorbate	$C_6H_7NaO_6$	11140	*Merck KGaA*
Sucrose	$C_{12}H_{22}O_{11}$	S0389	*Merck KGaA*
THPTA	Tris(3-hydroxypropyltriazolylmethyl)amin	F4050	*Lumiprobe GmbH*

Triflic acid	CF_3SO_3H	158534	*Merck KGaA*
Trifluoroacetic acid	$C_2HF_3O_2$	P088.3	*Carl Roth GmbH*
Triisopropylsilane	$C_9H_{22}Si$	233781	*Merck KGaA*
Triton X-100	$C_{14}H_{22}O(C_2H_4O)_n$	3051.3	*Carl Roth GmbH*
Water	H_20	34877	*Merck KGaA*

Table E: Fluorophores

Fluorophore	Source	Identifier
Sulfo-Cyanine 5, NHS ester	*Bio-Techne GmbH*	5436
Sulfo-Cyanine 5, NHS ester	*Lumiprobe GmbH*	23320
Sulfo-Cyanine 5, maleimide	*Lumiprobe GmbH*	23380
Sulfo-Cyanine 5, alkyne	*Lumiprobe GmbH*	B33B0
Sulfo-Cyanine 3, maleimide	*Lumiprobe GmbH*	21380
Cyanine 5, NHS ester	*Lumiprobe GmbH*	43020
Silicon Rhodamine, NHS ester	*Spirochrome AG*	SC003
Alexa 647, NHS ester	*Thermo Fisher Scientific, Inc.*	A37573
Perylene monoimide, NHS ester	*Peneva group, University of Jena*	-

Solutions and buffers

For all solutions and media, a TKA xCAD system (*Thermo Fisher Scientific Inc.*) purified water of the quality *aqua bidest* was used. Unless otherwise indicated, pH values were adjusted by means of NaOH or HCl.

Table F: Buffers and solutions

Buffer/Solution	Composition	Specifications
Blocking solution (Immunostaining & Microarray)	Bovine serum albumin (BSA) Phosphate buffered saline (PBS)	3 % (w/v) 1 x
Blocking solution (Microarray)	Powdered milk Phosphate buffered saline (PBS)	2-5 % (w/v) 1 x
Fixation solution	Paraformaldehyde (PFA) Sucrose Na_2HPO_4 NaH_2PO4	4 % (w/v) 1 % (v/v) 0.1M pH 7.4 Phosphate buffer
Cell-medium	DMEM (+ 4500 mg/l (D)-glucose, + GlutaMAX & pyruvate) penicillin/streptomycin solution FCS	 1% (v/v, 10,000 U/ml) 10% (v/v)
HEK 293 starvation-medium	DMEM (+ 4500 mg/l (D)-glucose, + GlutaMAX & pyruvate) penicillin/streptomycin solution FCS	 1% (v/v, 10,000 U/ml) 2% (v/v)
Permeabilization solution	Triton X-100 PBS	0.1 % (v/v) 1 x
Phosphate-buffered saline (PBS) pH 7.4, 1x	NaCl KCl $Na_2HPO_4*H_2O$ KH_2PO_4	137 mM 2.7 mM 10 mM 1.8 mM
Saline-sodium citrate (SCC) pH 7, 1x	NaCl trisodium citrate	150 mM 15 mM

Trypsin-EDTA-Solution	500 BAEE units porcine trypsin and 180 µg EDTA, 4Na per mL in PBS without calcium and magnesium	T4299, *Merck KGaA*

Commercial cell lines and antibodies

Table G: Commercial cell lines

Cell line	Description	Identifier	Source
HEK 293	Human embryonic kidney cells	ACC 305	*DSMZ GmbH*
COS-7	African green monkey kidney cells	ACC 60	*DSMZ GmbH*

Table H: Primary and secondary antibodies

Name	Applied dilution	Identifier	Source
Mouse monoclonal anti-gephyrin mAb7a	1:1000 (Immunofluorescence) 1:2500 (Microarray)	147 011	*Synaptic Systems GmbH* (Göttingen, Germany)
Mouse monoclonal anti-gephyrin mAb3B11	1:1000 (Immunofluorescence) 1:2500 (Microarray)	147 111	*Synaptic Systems GmbH* (Göttingen, Germany)
Mouse monoclonal anti-PSD-95 mAb108E10	1:1000 (Immunofluorescence)	124 011	*Synaptic Systems GmbH* (Göttingen, Germany)
Goat polyclonal anti-mouse, Alexa Fluor 647-conjugate	1:1000 (Immunofluorescence)	A-21235	*Thermo Fisher Scientific Inc.* (Waltham, U.S.)
Goat polyclonal anti-mouse, Alexa Fluor 555-conjugate	1:1000 (Immunofluorescence)	A-21422	*Thermo Fisher Scientific Inc.* (Waltham, U.S.)
Goat polyclonal anti-mouse, Alexa Fluor 488-conjugate	1:1000 (Immunofluorescence)	115-545-003	*Jackson ImmunoResearch Laboratories Inc.* (West Grove, U.S.)
Goat polyclonal anti-mouse, DyLight650-conjugate	1:1000 (Immunofluorescence)	84545	*Thermo Fisher Scientific Inc.* (Waltham, U.S.)
Goat polyclonal anti-mouse, HRP-conjugate	1:5000 (Microarray)	31430	*Thermo Fisher Scientific Inc.* (Waltham, U.S.)

2.2. Ethical approval statement

Approval for the experiments involving animals reported here was obtained from the relevant authorities. Experiments at the Institute of Clinical Neurobiology (Würzburg) were approved by the local veterinary authority (Veterinäramt der Stadt Würzburg, Germany) and government (Regierung von Unterfranken, Würzburg, Germany, FBVVL 568/200-324/13; TVA 55.2.2-2532-2-509/1067). Experiments in Paris are authorized by the Ministry of Agriculture and the Direction départementale des services vétérinaires de Paris (Ecole Normale Supérieure, animalerie des rongeurs, license B 75-05-20).

2.3. Peptide microarrays

Production of solid support cellulose membranes for peptide synthesis

The original procedure described by R. Frank[68] was adapted and optimized. Hardened low ash Whatman paper was dried in a desiccator overnight, then incubated for 3 hours with a mixture of 0.24 M N,N'-

diisopropylcarbodiimide (DIC), 0.2 M 1-methylimidazole (NMI), 0.2 M 9-fluorenylmethyloxycarbonyl-β-alanine (Fmoc-β-Ala) in dimethylformamide (DMF). Then, the membranes were washed thrice with DMF and thrice with ethanol and dried overnight in a desiccator. Finally, the membranes were cut to discs (4 mm diameter, average loading: 130 nmol/disc) to fit in the synthesis plates.

Synthesis of peptide microarrays

The peptide microarrays were synthesized using a Celluspot-based approach[66,69] using a MultiPep RSi robot (CEM GmbH) on the cellulose membranes. Synthesis was initiated by Fmoc deprotection using 20% piperidine (pip) in DMF followed by washing with DMF and ethanol. Peptide chain elongation was achieved using a coupling solution with amino acids (AAs, 0.5 M), Ethyl cyanohydroxyiminoacetate (Oxyma, 1 M) and DIC (1 M) in DMF (1:1:1, AA:Oxyma:DIC). Couplings were carried out thrice for 30 min, followed by capping (4% acetic anhydride in DMF) and washes with DMF and ethanol. Synthesis was finalized by deprotection with 20% pip in DMF for 10 min, followed by washing with DMF and ethanol. Dried discs were transferred to 96 deep-well blocks and treated, while shaking, with sidechain deprotection solution, consisting of 90% trifluoracetic acid (TFA), 2% dichloromethane (DCM), 5% H_2O and 3% triisopropylsilane (TIPS) (150 µL/well) for 1.5 h at room temperature (RT). Afterwards, the deprotection solution was removed, and the discs were solubilized overnight at RT, while shaking, using a solvation mixture containing 88.5% TFA, 4% trifluoromethanesulfonic acid (TFMSA), 5% H_2O and 2.5% TIPS. The resulting peptide-cellulose conjugates (PCCs) were precipitated with ice-cold ether and spun down at 2000×g for 10 min at 4°C, followed by two additional washes of the formed pellet with ice-cold ether. The pellets were then dissolved in dimethyl sulfoxide (DMSO) to give final stocks. PCC solutions were mixed 2:1 with saline-sodium citrate (SSC) buffer (150 mM NaCl, 15 mM trisodium citrate, pH 7.0) and transferred to a 384-well plate. For transfer of the PCC solutions to white coated CelluSpot blank slides (76×26 mm, Intavis AG), a SlideSpotter (CEM GmbH) was used. After completion of the printing procedure, slides were left to dry overnight.

Mono- and dimeric gephyrin binders peptide microarray

The microarray contained 113 mono- and dimeric peptides derived from the glycine receptor β gephyrin binding motif of different length (Appendix A). The microarray slides were blocked for 1 h. in 0.1% (w/v) bovine serum albumin (Carl Roth) in phosphate-buffered saline (PBS; 137 mM NaCl, 2.7 mM KCl, 10 mM Na_2HPO_4, 1.8 mM KH_2PO_4, pH 7.4). After blocking, the slides were incubated for 1 h. with 160 pM of gephyrin E domain, that was subsequently detected with anti-gephyrin mAb3B11 (Synaptic Systems, 147 111) and a secondary horseradish peroxidase (HRP) conjugated antibody (G-21040, Invitrogen). The antibodies were 1:10000 diluted and applied in blocking buffer for 30 min., with x3 PBS washes between the antibodies and after the application of the secondary antibody. Chemiluminescent readout was obtained (resolution 1200x1600, 60s exposure time) after application of 200 µl of SuperSignal™ West Femto Maximum Sensitivity Substrate (Thermo Fischer Scientific Inc., Waltham, U.S.; Cat: 34094) per slide using a DNR MicroChemi camera-based reader (DNR Bio-Imaging Systems Ltd., Jerusalem, Israel).

Anti-gephyrin mAb7a peptide microarray binding assay

The microarray contained 241×15AA long peptides representing a full positional scan of the gephyrin protein (GPHN-1 isoform) with a 12AA overlap between the peptides and additional 45 Ser 268/270 phosphorylated peptide versions (Appendix C). The microarray slides were blocked for 1 h. in 2% (w/v) skimmed milk powder (Carl Roth) in PBS. After blocking, the slides were incubated for 30 min. with 1:2500 dilution of anti-gephyrin mAb7a (Synaptic Systems, 147 011). mAb7a was detected with a secondary 1:5000 diluted HRP-coupled Anti-mouse antibody (G-21040, Invitrogen). The antibodies were applied in blocking buffer for 30 min., with x3 PBS washes between the antibodies and after the application of the secondary antibody. Chemiluminescent readout was obtained ("High sensitivity" mode (highest resolution; 1536 x 1024), 1s exposure time) after application of 200 µl of SuperSignal™ West Femto Atto Ultimate Sensitivity Substrate (Thermo Fischer Scientific Inc., Waltham, U.S.; Lot: A38554) per slide using a ImageQuant™ LAS 4000 imaging system (GE Healthcare Inc., Chicago, U.S.). Binding intensities were acquired with FIJI using the "Microarray Profile" plugin (OptiNav). The error range and the relative standard deviation were defined by comparing the intensities of each peptide duplicate on the respective array.

Gephyrin E domain for microarrays, expression and purification

Gephyrin P2 splice variant E domain (amino acids 318–736) was expressed in *E. Coli* and purified as described earlier[66]. Concisely, the protein was purified using via Intein-tag (Chitin beads, New England BioLabs), and after self-cleavage the protein was obtained by size-exclusion chromatography (SEC) column (HiLoad 16/600 Superdex 200pg, GE Healthcare) on an ÄKTA explorer system (GE Healthcare). The protein was bought from the protein expression facility at the Rudolf-Virchow-Center, University of Würzburg.

2.4. Synthesis of peptide-based probes

Peptide synthesis

Peptides were produced using standard solid phase peptide synthesis with Fmoc chemistry. 2-chlorotrityl resin (1.6 mmol/g) was swollen in dry DCM for 30 min., then, the desired amino acid (1eq), Boc-Gly-OH (1eq) and 4 eq. of dry DIEA in dry DCM were added to the resin slurry. After overnight reaction at RT with agitation, the resin was capped with MeOH and washed with DCM and DMF. Deprotection and conjugation cycles followed, where 20% piperidine solution in DMF was used to remove the Fmoc protecting group. After washes the peptide chain was elongated by adding AA (4 eq.) with Oxyma (4 eq.) and DIC (4 eq.). Capping was done with DIEA (50 eq.) and acetic anhydride (50 eq.) in N-Methyl-2-pyrrolidone for 30 min. Coupling efficiency was monitored by measuring the light absorption of the dibenzofulvene–piperidine adduct in 20% pip solution after deprotection, using the following empirical formula:

$$\boxed{c_i = \frac{6.1206}{Abs.(290nm)}}$$

The concentration (c_i) in mM is determined from an absorption ($Abs.$) read at 290 nm in a quartz cuvette that has 1 cm -long optical path.

The peptides were cleaved from the resin using a cocktail of 90% TFA, 5% H_2O, 5% Triisopropylsilane, for 2 to 4 hours at RT. Then, the peptides were precipitated in ice-cold ether and afterwards purified with HPLC and analyzed by LC-MS as described below.

Fluorophore conjugation

The purified peptides or peptide dimers were conjugated with fluorophores either via NH_2-terminus using N-Hydroxysuccinimide (NHS) coupled dyes or via thiol side chain of cysteine using maleimide coupled dyes. Shortly, for NHS coupling 1 eq. of peptide was dissolved in DMF with 3 eq. of DIEA and a fluorophore-NHS was added (1 eq. for standard peptides, 2eq. for peptide dimers) and agitated overnight at 4°C. Maleimide conjugation was done with similar stoichiometry agitated overnight at RT, with pH 7.4 phosphate buffer (100 mM) as a solvent and a minimal addition of DMF to facilitate dissolution.

For the copper-catalyzed alkyne-azide cycloaddition the following general protocol for 1 mL reaction volume was used:

1.5 eq. of alkyne-dye was mixed with 1 eq. azide-peptide in 0.87 mL 1:1 DMSO-Phosphate buffer (100 mM, pH7), to yield a final concentration of 1.5 mM and 1 mM, respectively. 12.5 µL of $CuSO_4$ 20 mM water-based solution was premixed with 25 µL 50 mM water-based solution of THPTA (tris-hydroxypropyltriazolylmethylamin) and added to the peptide-dye mix, for the final concentration of 0.25 mM and 1.25 mM, respectively. 50 µL of 100 mM aminoguanidine hydrochloride and 50 µL of 100 mM sodium ascorbate were successively added to the mix, to final concentrations of 5 mM. The reaction vessel was sealed with parafilm and agitated overnight at RT. For thiol-containing peptides, 5 mg of DTT (dithiothreitol) can be added to the reaction vessel after the completion of the reaction, to break the disulfide bridges. The product can de directly purified from the reaction mixture with semi-preparative HPLC.

Purification and characterization of peptides and fluorescent probes

The fluorescent probes were purified from the crude reaction mix by reverse phase HPLC using water acetonitrile gradient with 0.1% formic acid (FA). LC-MS validation was performed with similar gradient and LC-MS grade solvents. Semi-preparative HPLC was performed on Shimadzu Prominence equipped with a diode-array detector (DAD) system using a C18 reverse-phase column (Phenomenex Onyx Monolithic HD-C18 100×4.6 mm or Onyx

Monolithic C18 100×10 mm). VK7, VK10, VK11, VK13, VK14 were analysed after purification with Thermo Scientific LTQ Velos, linear ion trap mass spectrometer. Purity and structural identity of all other probes were verified using a DAD equipped 1260 Infinity II HPLC with a C18 reverse-phase column (Onyx Monolithic C18 50×2 mm), coupled to a mass selective detector single quadruple system (Agilent Technologies) in ESI+ mode.

2.5. *Ex-cellulo* characterization of gephyrin probes

Isothermal titration calorimetry (ITC)

Measurements were performed using an ITC200 (MicroCal) at 25 °C and 1,000 rotations per minute (rpm) stirring in PBS pH 7.4. Specifically, 40 µL of a 200 µM gephyrin E solution was titrated into the 200 µL sample cell containing 10 µM and 20 µM of Sylite and SyliteM, respectively. In each experiment, a volume of 2.5 µL of ligand was added at a time resulting in 15 injections and a final molar ratio between 1:2 (SyliteM) and 1:4 (Sylite). The dissociation constant (K_D) and stoichiometry (N) were obtained by data analysis using NITPIC, SEDPHAT and GUSSI[70]. Measurements were conducted three times for each probe and are given as mean values with their standard deviations.

Pulldowns with cellulose conjugated peptides

Cellulose membrane bound peptides were produced using µSPOT solid phase peptide synthesis[66]. After completion of the automated peptide synthesis, cellulose bound peptides side chains were deprotected with 90% TFA, 5% H_2O, 5% Triisopropylsilane for 3 hrs at RT, followed by washing with 5×2 mL H_2O. Afterwards, cellulose disks were left do dry overnight in a fume hood and stored at 4°C until use. For pulldowns, discs were first blocked in 2% (w/v) bovine serum albumin (BSA) in PBS for 1 hour at 25°C. Subsequently, one disc was incubated with 100 µL of mouse brain homogenate mixed with 100 µL of 10 mM tris(2-carboxyethyl)phosphine (TCEP) in PBS for 45 min at 30°C. After washing with 3×300 µL PBS, 50 µL loading buffer (NuPAGETM LDS-sample buffer, ThermoFisher Scientific) were added and incubation at 70°C for 2×5 min with a brief vortex in between followed. Samples were stored at -80°C until preparation for mass spectrometric proteomic analysis. As non-binding analogues of SyliteM and Sylite FSI**GV**SYPRRRRRRRRR, and (YSI**GV**SYPRpeg)$_2$KC, respectively, were used. These sequences contain a binding-abolishing AA swap, described earlier[53].

Mass spectrometric analysis of pulldowns

Performed by the group of Dr. Andreas Schlosser, RVZ, Würzburg University, Germany

Alkylation of the eluate was achieved by reduction with 50 mM dithiothreitol for 10 min at 70°C and 650 rpm in a thermoshaker followed by addition of 2-iodoacetamide to a final concentration of 120 mM and incubation in the dark for 20 min. Afterwards, cold acetone was added in a 4.5:1 ratio and overnight incubation at -20°C followed. Then, the samples were centrifuged at 12,000 g for 20 min at 4°C. Pellets were washed with 4×1 mL of cold acetone with 5 min centrifugations at 12,000 g in between. Next, pellets were left to dry under ventilation for 10 min. The protein pellet was resuspended in 50 µL of 8 M urea in 100 mM ammonium bicarbonate (ABC) using a bioruptor (diagenode) with 3 cycles for 30 sec. Afterwards, 50 µL of 100 mM ABC were added, followed by addition of 0.25 µg endoproteinase LysC. After incubation for 2 hrs in a thermoshaker at 30°C and 900 rpm, 100 µL of 100 mM ABC and 0.25 µg trypsin were added. Following overnight incubation at 37°C, the samples were acidified using 20 µL of 10% TFA. Stage tips were prepared by insertion of three C18 disks into a pipette tip. Each Stage tip was pre-washed with 50 µL methanol, followed by 50 µL of 60% acetonitrile (ACN) with 0.3% (v/v) FA, followed by equilibration with 2x50 µL of a 2% ACN solution with 0.3% (v/v) TFA. After sample loading, the tips were centrifuged for 10 min at 2,000 g and washed with 3×50 µL of 2% ACN with 0.3% (v/v) TFA. Elution was achieved using 2×50 µL of 60% ACN with 0.3% (v/v) FA, then the samples were lyophilized for storage until solubilization in 25 µL of 2% ACN with 0.1% (v/v) FA.

NanoLC-MS/MS analyses were performed on an Orbitrap Fusion (Thermo Scientific) equipped with a PicoView Ion Source (New Objective) and coupled to an EASY-nLC 1000 (Thermo Scientific). Peptides were loaded on capillary columns (PicoFrit, 30 cm×150 µm ID, New Objective) self-packed with ReproSil-Pur 120 C18-AQ, 1.9 µm (Dr. Daniel Maisch) and separated with a 60 min linear gradient from 3% to 30% acetonitrile and 0.1% FA at a flow rate of 500 nL/min.

Both MS and MS/MS scans were acquired in the Orbitrap analyzer with a resolution of 60,000 for MS scans and 7,500 for MS/MS scans. Higher-energy C-trap dissociation (HCD) fragmentation with 35% normalized collision energy was applied. A Top Speed data-dependent MS/MS method with a fixed cycle time of 3 sec was used. Dynamic exclusion was applied with a repeat count of 1 and an exclusion duration of 30 sec; singly charged precursors were excluded from selection. Minimum signal threshold for precursor selection was set to 50,000. Predictive automatic gain control (AGC) was used with AGC a target value of 2×10^5 for MS scans and 5×10^4 for MS/MS scans. EASY-IC was used for internal calibration.

Raw MS data files were analyzed with MaxQuant version 1.6.2.2. Database search was performed with Andromeda, which is integrated in the utilized version of MaxQuant. The search was performed against the UniProt *mus musculus* reference proteome database (download time: August 2020). Additionally, a database containing common contaminants was used. The search was performed with tryptic cleavage specificity with 3 allowed miscleavages. Protein identification was under control of the false-discovery rate (FDR; <1% FDR on protein and PSM level). In addition to MaxQuant default settings, the search was performed against following variable modifications: Protein N-terminal acetylation, Gln to pyro-Glu formation (N-term. Gln) and oxidation (Met). Carbamidomethyl (Cys) was set as fixed modification. Further data analysis was performed using R scripts developed in-house. LFQ intensities were used for protein quantitation. Proteins with less than two razor/unique peptides were removed. Missing LFQ intensities in the control samples were imputed with values close to the baseline. Data imputation was performed with values from a standard normal distribution with a mean of the 5% quantile of the combined log10-transformed LFQ intensities and a standard deviation of 0.1. For the identification of significantly enriched proteins, boxplot outliers were identified in intensity bins of at least 300 proteins. Log2 transformed protein ratios of sample versus control with values outside a 1.5x (significance 1) or 3x (significance 2) interquartile range, respectively, were considered as significantly enriched.

The IP-MS table of the enriched proteins that bound the peptidic probes is in Appendix D.

Modeling of the Sylite/gephyrin supracomplex

Performed by Dr. Orly Avraham, from the Schueler-Furman lab of the Hebrew University of Jerusalem, Israel

Generation of the Sylite bound to gephyrin E domain was carried out using the Rosetta FlexPepDock refinement protocol[71] using the crystal structure of gephyrin E domain bound to glycine receptor (GlyR) β subunit peptide (PDB ID: 4pd1) as a scaffold. Peptide residues where mutated using the Rosetta Fixed Backbone protocol to correspond to the binding sequence of Sylite. Following this process, the linker and dye were added to demonstrate the feasibility of the dimer formation.

2.6. Cell cultures

HEK293 and COS-7 cell cultures and transfection

HEK293 and COS-7 cells were cultured in DMEM (GIBCO), supplemented with GlutaMax and pyruvate (GIBCO), 10% fetal bovine serum (GIBCO) and 1% Penicillin/Streptomycin (Sigma) at 37°C and with 5% CO_2. Stable HEK293 cells expressing eGFP-gephyrin were grown with 0.4 mg/mL of the selective antibiotic G418.

The cells were plated on 0.15 mm thick 18 mm glass coverslips (HEK293 on coverslips that were coated with 35 µg/ml Poly-D-Lysine) in a 12-well plate and were transfected with 1 µg plasmid DNA per coverslip using PEI (Polyethylenimine). The transfection was performed at 60-80% confluence. Shortly before transfection the medium was changed to fresh DMEM. The DNA was added to 100 µl DMEM without additives and mixed, 4 µl fresh PEI (1 mg/ml) was added, mixed immediately and incubated for 20 min at RT. The transfection mix was pipetted drop-wise on cells while swirling, and incubated overnight. The medium was changed to fresh DMEM with 2% FBS after 12-24 hours, and on the following day the cells were fixed and used for staining.

The following constructs were used for transient transfection of HEK293 and COS-7 cells: eGFP-gephyrin P1[59] and eGFP - pEGFP-C2 (Clontech) constructs were provided by Prof. Matthias Kneussel (ZMNH, Germany); Venus-gephyrin[72] and pHluorin-tagged GlyR β-loop transmembrane protein[73] constructs (supplied by Dr. Christian G. Specht); gephyrin isoform constructs (Appendix E,F) provided by Prof. Eric Allemand (INSERM, France) and Dr.

Fabrice Ango (INSERM, France); PSD-95-eGFP constructs were provided by Dr. Daniel Choquet (CNRS, Bordeaux, France, Appendix F)

Culture and infection of primary neurons

Primary murine hippocampal neurons

Primary murine hippocampal neurons were prepared from wildtype CD-1 mice (Jackson Laboratory) at embryonic day 17 (E17). Hippocampal neurons were grown in neurobasal medium (21103-049 Life Technologies, Massachusetts, USA) supplemented with 1% 200 mM L-Glutamine (25030-024 Life Technologies, Massachusetts, USA), 1% B27 (17504-044 Life Technologies, Massachusetts, USA). 50% of the medium was exchanged every 7 days in culture. 60,000 hippocampal neurons were seeded on 18 mm glass coverslips. Neurons were taken for experiments after three weeks in culture (day in vitro 21 = DIV21).

Primary murine cortical neurons

All procedures involving animals were in compliance with the regulations of the French Ministry of Agriculture and the Direction départementale des services vétérinaires de Paris (Ecole Normale Supérieure, animalerie des rongeurs, license B 75-05-20). Primary murine cortical neurons were dissociated from wildtype C57BL/6J mice (Janvier, France) at embryonic day 17 (E17) and cultured on 18 mm glass coverslips in neurobasal medium containing B27, glutamax and penicillin/streptomycin (all from Gibco). Where required, neurons were infected at day in vitro 1 to 5 (DIV1-5) with lentivirus driving the expression of full-length gephyrin tagged at its N-terminus with mEos2[16]. Neurons were used for experiments after two to three weeks in culture (DIV15-21).

2.7. Animals and surgeries

Performed by Sara L. Reis, from the Tovote lab, UKW, Würzburg University, Germany

Experimental subjects were 3- to 6-month-old offspring of C57BL/6 mice with mutated Slc17a6$^{tm1.1(flpo)Hze}$ (VgluT2-IRES2-FlpO) or Slc6a13$^{tm1.1Ncd}$ (Vgat2-2A-FlpO-D) genes (both lines from Jackson Laboratory) crossed with GlyT2-Cre mice initially provided by U. Zeilhofer (University Zurich). Before surgeries, mice were co-housed with littermates (2–5 per cage) in a temperature (22–24 °C) and humidity (40–60%) controlled environment, after surgery mice were individually housed in the same conditions. Mice were maintained with unrestricted access to food and water on a 12-h light/dark cycle, with tissue processed during the light phase. All mice were randomly assigned to experimental conditions, with approximately equal numbers of male and female mice.

Injection of viruses

Isoflurane (cp-pharma, induction 4%, maintenance 1-2%) in oxygen-enriched air was used to anaesthetize mice fixed in a stereotactic frame (Kopf Instruments 1900 series). Eyes were lubricated with an ophthalmic ointment and body temperature was maintained at 32–37 °C with a heat pad. Fur was shaved and the incision site was sterilized with Cutasept solution before beginning surgical procedures. Local injections of 200 µL ropivacainhydrochlorid (Naropin; 5mg/mL, AspenGlobal) was injected subcutaneously before opening of the scalp. Buprenophine (10 µL of 0.3 mg/mL, Bayer) was injected subcutaneously to ensure no pain. After completion of surgery, intraperitoneal injections of meloxicam were administered to alleviate pain (30µl of 5 mg/ml, Metacam; Boehringer). A craniotomy was made at the injection site with a round 0.5 mm drill bit (David Kopf). A volume of 200-300 nL virus solution was pressure-injected intracranially using calibrated glass pipets (5µl microcapillary tube; Sigma-Aldrich) pulled in Narishige PC-100 connected to a PDES-02X (npi electronics). Unilateral targeting of dmPAG and vlPAG was achieved with the following coordinates: dmPAG AP -3.20mm, ML +0.2mm, DV -2.00mm; vlPAG AP -4.80mm, ML +0.60mm, DV -3.00mm. The capillary was then manually slowly lowered until the desired injection depth was reached.

To discover glycinergic vlPAG intra-connectivity inputs a cre-dependent anterogradely transported AAV: AAV2/5-CAG- Floxed-SypGFP rev-WPRE was used

To study glycinergic vlPAG projections to dmPAG, we combined a vlPAG injection of a cre-dependent, anterogradely transported adeno-associated virus (AAV): AAV2/5/CAG-Floxed-Synaptophysin-10xMyc-.rev-WPRE with a dmPAG injection of a Flp-dependent AAV: AAV2/1/hsyn-Cre^{off}/Flp^{on}-EYFP.

2.8. Sample preparation and fluorescent labeling

Live cell labeling

1 eq. of either Sylite 1.2, MH1 or MH1peg were mixed with 5 eq. of either CPP_1 or CPP_2 in PBS and incubated at RT for 15 minutes. After the incubation the solutions were diluted 1:4 with DMEM to produce 1-10 µM concentrated solutions of the probes and the corresponding five times higher concentration of the CPPs. Then, neurons or HEK293 cells expressing eGFP-gephyrin were washed thrice with warm PBS and incubated either at 37°C or at 4°C with 1-10 µM of either Sylite 1.2, MH1 or MH1peg and 5 equivalents of either CPP_1 or CPP_2 in DMEM for 30 minutes. Before imaging the cells were washed thrice with PBS and imaged in phenol red free DMEM at RT.

Cell fixation and immunocytochemistry

For "Probe screening I" coverslips with HEK293 cells were washed with PBS and fixed with ice cold methanol at −20 °C for 10 min. After washing with PBS, the fixed cells were blocked for 1 h with 3% (w/v) BSA, then the peptide probes (VK7, VK10, VK11, VK13, VK14 and SyliteM) were applied at 50 nM in blocking buffer for 1h. After washes the coverslips were mounted on microscope slides with mowiol.

In all other experiments neurons, COS-7 and HEK293 cells were fixed in 0.1 M sodium phosphate buffer pH7.4 containing 4% paraformaldehyde (EM grade, Polysciences) and 1% sucrose for 10-20 min at 37°C. After three rinses in PBS, the cells were permeabilized in PBS containing 0.1% Triton X-100 for 10 min at room temperature, rinsed again and blocked for 1 h in PBS with 3% BSA. Primary and secondary antibodies were applied sequentially in blocking solution for 1 hour. The fluorescent probes were applied together with the primary antibody, unless otherwise mentioned. Primary antibodies: mAb7a (147 011), mAb3B11 (147 111), mAb108E10 (124 011), Synaptic Systems. Secondary antibodies were purchased from ThermoFisher: anti-mouse conjugated IgG with AlexaFluor (A) 647 (A-21235), A555 (A-21422), A488 (A-27023) or DyLight650 (84545). Unless otherwise noted the SyliteM, Sylite and TMR2i were applied with 50 nM concentration, SyliteCy3 with 25nM, C5-2xIETAV with 10 µM and both primary and secondary antibodies with 1:1000 concentration.

Brain section preparation and staining

Performed by Sara L. Reis, form the Tovote lab, UKW, Würzburg University, Germany

Wildtype C57BL/6J mice (Jackson Laboratory) were transcardially perfused via the left ventricle with ice-cold PBS followed by ice-cold 4% paraformaldehyde (in PBS). Brains were then removed, post-fixed in 4% PFA for 2 hours, cryoprotected in 30% sucrose/PBS for 48-72 hours and cut on a cryostat (Leica CM1950) in 50µm coronal slices. The immunohistochemistry was performed in free floating sections. Tissue sections were blocked with blocking solution (10% Donkey serum (Bio-rad) with 0.3% TritonX in PBS) for 1 hour at RT, then fluorescent probes and primary antibodies were applied in blocking solution for 1 hour at RT, or 24/72 hours at 4°C. Then slices were washed 3 times with PBS and incubated with secondary antibody for 1 hour or 2 hours for the 24/72 hours staining protocol at RT. When no antibodies were applied the slices were incubated for 1h at RT with the probes. Labelled sections were then incubated with DAPI (1:5000) for 5 min at RT and washed again with PBS. Lastly, the sections were mounted onto a gelatin-coated slides using mowiol as the mounting medium. Following primary antibodies were used: gephyrin mouse mAb7a 1:1000 and mouse mAb3B11 1:1000. The fluorophore-tagged secondary antibody used was Alexa 555 donkey anti-mouse (1:1000).

Brain tissue staining of the operated mice for anatomical tracing of inhibitory circuits

Performed by Sara L. Reis, form the Tovote lab, UKW, Würzburg University, Germany

Four weeks after injection, mice were sacrificed, transcardially perfused with 4% paraformaldehyde in PBS, brains were extracted and processed for histology as described above.

To evaluate the intra-connectivity of vlPAG GlyT2 neurons immunohistochemistry was performed in free floating sections as described above with the following primary antibody chicken anti-GFP 1:1000 (Abcam; #: ab13970) and fluorophore-tagged secondary antibody Alexa 488 donkey anti-chicken 1:1000 (Jackson ImmunoResearch, 705-545-155).

To assess active local vlPAG inputs onto dmPAG glutamatergic vs GABAergic neurons, immunohistochemistry was also performed as described above with the following primary antibodies chicken anti-GFP 1:1000 (Abcam; cat nb: ab13970) and goat anti-Myc 1:500 (Abcam, ab9132). The fluorophore-tagged secondary antibody used was Alexa

488 donkey anti-chicken 1:1000 (Jackson ImmunoResearch, 705-545-155) and Cy3 donkey anti-goat 1:1000 (Jackson ImmunoResearch, 703-165-147), respectively. Sylite was used to label post-synaptic active zones.
The sections were mounted onto a gelatin-coated slides using mowiol as the mounting medium.

2.9. Microscopy

Unless otherwise stated the coverslips with samples were inserted in an imaging chamber (Ludin Chamber Type 1, Life Imaging Services) and imaged in PBS. The measurements were taken from distinct samples with a sample size ≥ 2, for each group. A series of images, used to generate the datapoints, were acquired from different regions of the sample, each region having a distinct group of cells.

Probe screening in HEK293 cells

HEK293 cells expressing eGFP-gephyrin were fixed and stained as described above. Labeled samples were imaged on a Leica TCS SP5 confocal microscope equipped with an HCX PL APO lambda blue 63.0×/1.40-NA oil UV objective. Images were taken using a 100-Hz scanner, 8-bits, a pixel size of 60.1 nm^2, a pinhole of 95.5 µm (1 AU). For excitation Argon laser at 488 nm (output power 20%, intensity 1%) and HeNe 633 nm laser (intensity 2%) were used. Emission light was registered with Leica HyD detectors set to the following spectral ranges: 500-570 nm, gain 15 (eGFP channel); 645-715 nm, gain 13 (Cy5 channel). Image acquisition was performed in sequential frame scan mode, with sequential 488 nm and 633 nm excitation and acquisition in corresponding ranges.

Probe screening in COS-7 cells

COS-7 cells expressing Venus-gephyrin or pHluorin-tagged GlyR β-loop transmembrane protein were fixed and stained as described above. Various probes and probe concentrations were applied (Fig. 6). Wide field imaging of labelled cells was done on an inverted Nikon Eclipse Ti microscope with a 100x oil-immersion objective (NA 1.49) using an Andor iXon EMCCD camera (16-bit, image pixel size: 160 nm). The following excitation and emission filters were chosen: excitation 485/20, emission 525/30 for A488 and unconverted (green) mEos2; ex. 560/25, em. 607/36 for Cy3; exc. 650/13, em. 684/24 for A647 or Cy5 (Sylite). Generally, 10 images were acquired at a frame rate (exposure time) of 100 ms and at variable illumination intensity using a mercury lamp (Intensilight, Nikon) and neutral density filters to maximize the signal while avoiding saturation. All images in one fluorescent channel were taken with constant settings to ensure comparability.

Probe profiling in COS-7 cells

COS-7 expressing either eGFP or gephyrin-eGFP were labeled with either Sylite, SyliteM or TMR2i and imaged on an inverted Leica DMI6000B microscope with a 100x oil-immersion objective (NA 1.49) using a Leica DFC9000 GTC VSC-05760 sCMOS camera (16-bit, 2x2 binning, image pixel size: 130 nm). The following excitation and emission filters were chosen: excitation 470/40, emission 525/50 for gephyrin-eGFP and soluble eGFP; ex. 545/25, em. 605/70 for TMR2i (Tetramethylrhodamine); exc. 628/40, em. 692/40 for Sylites (Sulfo-Cyanine 5 – Cy5), 10 images were acquired at a frame rate (exposure time) of 100 ms and constant illumination intensity to ensure comparability. n≥8.

Imaging of HEK293 cells expressing different gephyrin isoforms

Images of transiently transfected HEK293 cells were acquired with the above-described setup. The following excitation/emission filters were chosen: ex. 545/25, em. 605/70 for mScarlet, exc. 628/40, em. 692/40 for Sylites, and mAb7a/mAb3B11 with secondary DyLight650 Antibody. 10 images were acquired at a frame rate (exposure time) of 100 ms and constant illumination intensity to ensure comparability. n≥5.

SyliteCy3 profiling in HEK293 cells

HEK293 expressing either eGFP or gephyrin-eGFP were labeled with SyliteCy3 and imaged with the above-described setup. The following excitation/emission filters were chosen: excitation 470/40, emission 525/50 for gephyrin-eGFP and soluble eGFP; ex. 545/25, em. 605/70 for SyliteCy3. 10 images were acquired at a frame rate (exposure time) of 100 ms and constant illumination intensity to ensure comparability. n=10.

Live cell imaging

Live HEK293 cells expressing gephyrin-eGFP were co-incubated with gephyrin probes and CPPs as described above and imaged on an inverted Leica DMi8 microscope with a 100x oil-immersion objective (NA 1.49) using a Leica

DFC9000 GTC VSC-12299 sCMOS camera (16-bit, 2x2 binning, image pixel size: 130 nm) with the DFT51011 filter cube. The following excitation and emission filters were chosen: excitation 479/33, emission 519/25 for gephyrin-eGFP and soluble eGFP; exc. 638/31, em. 695/58 for the probes (Sulfo-Cyanine 5 – Cy5), 10 images were acquired at a frame rate (exposure time) of 100 ms and constant illumination intensity to ensure comparability. n≥3.
The gephyrin puncta in the green channel and the corresponding puncta in the far-red channel were manually counted. Per condition the total number of the corresponding far-red puncta were divided by the total number of green puncta to determine the labeling efficiency.
Live primary hippocampal neurons were co-incubated with MH1peg and CPP_2 as described above and imaged on an inverted Leica DMI6000B microscope with a 100x oil-immersion objective (NA 1.49) using a Hamamatsu-Flash4-USB3-002889 sCMOS camera (16-bit, 4x4 binning, image pixel size: 260 nm). The following excitation and emission filters were chosen: exc. 628/40, em. 692/40 for gepyhrin probes (Sulfo-Cyanine 5 – Cy5), 10 images were acquired at a frame rate (exposure time) of 200 ms and constant illumination intensity to ensure comparability. n≥10.

PSD-95 probe evaluation in HEK293 cells

HEK293 expressing either eGFP or PSD-95-eGFP were labeled with C5-2xIETAV and imaged on an inverted Leica DMI6000B microscope with a 100x oil-immersion objective (NA 1.49) using a Leica DFC9000 GTC VSC-05760 sCMOS camera (16-bit, 2x2 binning, image pixel size: 130 nm). The following excitation and emission filters were chosen: excitation 470/40, emission 525/50 for eGFP; em. 692/40 for C5-2xIETAV (Cyanine 5 – C5). 10 images were acquired at a frame rate (exposure time) of 100 ms and constant illumination intensity to ensure comparability. n≥10.

Neuron imaging

Primary murine hippocampal neurons were imaged on an inverted Leica DMI6000B microscope with a 100x oil-immersion objective (NA 1.49) using a Leica DFC9000 GTC VSC-05760 sCMOS camera (16-bit, 4x4 binning, image pixel size: 260 nm). The following excitation and emission filters was chosen: ex. 545/25, em. 605/70 for red fluorophores, exc. 628/40, em. 692/40 for far-red fluorophores. 10 images were acquired at a frame rate (exposure time) of 100 ms and constant illumination intensity to ensure comparability. n≥6.
Wide field imaging of primary murine cortical neurons was done on an inverted Nikon Eclipse Ti microscope with a 100x oil-immersion objective (NA 1.49) using an Andor iXon EMCCD camera (16-bit, image pixel size: 160 nm). The following excitation and emission filters were chosen: excitation 485/20, emission 525/30 for Alexa Fluor 488 and unconverted (green) mEos2; ex. 560/25, em. 607/36 for Cy3; exc. 650/13, em. 684/24 for Alexa Fluor 647 or Cy5 (Sylite). 10 images were acquired at a frame rate (exposure time) of 100 ms and at variable illumination intensity using a mercury lamp (Intensilight, Nikon) and neutral density filters to maximize the signal while avoiding saturation. All images in one channel were taken with constant settings to ensure comparability. n≥5.

Dual-color dSTORM super-resolution imaging

Neurons were fixed at DIV20 and immuno-labelled with primary rabbit anti-RIM1/2 antibody (Synaptic Systems, No. 140203, 1:250 dilution) and mouse anti-gephyrin antibody (Synaptic Systems, mAb7a, No. 147011, 1:500; Synaptic Systems, mAb3B11, No. 147111, 1:1000) in blocking buffer for 2 hours. CF680-conjugated goat anti-rabbit secondary antibody (Biotium, No. 20818, one dye per IgG, 1:250) was co-applied with Alexa Fluor 647 (A647) – coupled donkey anti-mouse (1:500) or with Sylite at a final concentration of 500 nM for 2 h. Coverslips were mounted in dSTORM buffer (Abbelight SMART-kit) on cavity slides (Heinz Herenz, No 1042001), sealed with twinsil (Picodent) and imaged. The measurements were taken from distinct samples with a sample size ≥ 3, for each group.
All three fluorophores (Cy5, A647, CF680) photo-switch under reducing and oxygen-free buffer conditions, making them suitable for dSTORM single molecule imaging[74], which enables the localization of the emitters with sub-diffraction localization precision. Thanks to their close spectral proximity, Cy5 or A647 were excited and acquired simultaneously with CF680 in the same dSTORM buffer (Abbelight SMART-Kit) using a 640 nm laser (Oxxius), and their respective signals discriminated after single molecule localization using a spectral demixing strategy[75]. To implement spectral demixing dSTORM of SyliteD – (Cy5 or gephyrin-A647) and RIM1/2-CF680 we used a dual-view Abbelight SAFe360, equipped with two Hamamatsu Fusion sCMOS cameras and mounted on an Olympus Ix83

inverted microscope with a 100X 1.5NA TIRF objective. The SAFe360 uses astigmatic PSF engineering to extract the axial position and achieves quasi-isotropic 3D localization precision, and a long-pass dichroic mirror to split fluorescence from single emitters on the two cameras.
Single molecule localization, drift correction, spectral demixing, data visualization and cluster analysis[76] (DBSCAN) were performed with Abbelight NEO software, using a neighborhood radius eps = 150 nm and minPts = 50 minimum neighbors for the antibody labelling. To compensate for the lower number of detections generated by Sylite we adjusted the DBSCAN parameters to eps = 200 nm and minPts = 10. To measure the distance between presynaptic RIM and the postsynaptic gephyrin cluster, the centers of mass of the segmented clusters were determined in each fluorescence channels The Euclidean distance representing the average distance between the two-point clouds was then calculated for each cluster.

Wide field and confocal imaging of brain sections

The brain sections were mounted with mowiol on microscopy slides. Wide-field 20x microscopy of brain sections was done with a Zeiss Axio Imager 2 equipped with a Plan-Apochromat 20x/0.8 M27 objective. Images were taken with an Axiocam 506 and pixel size of 0,454 x 0,454 µm. For excitation of DAPI a wavelength of 353 nm with LED-Module 385nm (power 6.08%) and for the probes a wavelength of 650nm with LED-Module 630nm (power 22.50%) was used. Emission wavelength for DAPI was 465nm and for the probes 673nm. Image acquisition was set using Zeiss Tiles module.
Labeled samples were imaged on a Leica SP8 (Leica) confocal microscope equipped with an HC PL APO CS2 63.0×/1.40-NA oil UV objective. Images were taken using a 200-Hz resonant scanner, 12-bits, a voxel size of 58 × 58 × 170 nm^3, a pinhole of 108.7 µm (1 AU). For excitation violet 405 nm LASOS diode laser (power 1-2%), yellow-green 561 nm DPSS laser (power 1-4%), red 633 nm HeNe laser (power 1-2%) were used. Emission light was registered with Leica PMT detectors set to the following spectral ranges: 415-465 nm, gain 750-850V (DAPI channel); 575-620 nm, gain 800-950V (Sulfo-Cyanine 3 channel); 645-700 nm, gain 750-850V (Cy5 channel). Image acquisition was performed in sequential frame scan mode, with concurrent 405 nm and 633 nm excitation and acquisition in corresponding ranges, followed by 561 nm excitation with an acquisition in Sulfo-Cyanine 3 channel. Bleaching was compensated with a linear gain increase of 30-40 V for an hour. The measurements were taken from distinct samples with a sample size of 4 for each group.

2.10. Image processing and analysis

2D image processing and analysis

Image processing and analysis were carried out using Fiji[77] (**F**iji **I**s **J**ust **I**mageJ) with JACoP[78] (**J**ust **A**nother **Co**localization **P**lugin) plugin for colocalization analysis. Macros and scripts (Appendix G) were written by V.K.
mEos2-gephyrin single synapse segmentation and intensity recording was done with Icy[79] 2.0.3.0 using "Wavelet Spot Detector" function in a custom protocol written by V.K. (Appendix H). mEos2-gephyrin synaptic puncta were segmented, average intensity of individual punctum was determined and compared to the average intensity of the corresponding punctum in the far-red spectrum for either mAb7a with a secondary A647 antibody or the staining of Sylites.

Synaptophysin-GFP image processing

PAG was sectioned in 50 µm thick slices, then each third slice was imaged sequentially to reconstruct PAG and trace the glycinergic pathways from vlPAG (8-9 slices per animal from 3 animals). Overview of the labelled PAG sections was obtained with Zeiss Axio Imager 2 microscope equipped with a Plan-Apochromat 20x/0.8 M27 objective. Images were taken with an Axiocam 506 and pixel size of 0,454 x 0,454 µm using LED-Module 475nm (power 11.12%) with an emission wavelength of 517nm. Image acquisition was set using Zeiss Tiles module. Zen connect was used to precisely perform z-stack in the region of interest. Z-stacks were then converted in 2D images using maximal orthogonal projection of Zen Blue Software. Quantification of the synaptic inputs from the ipsilateral was performed with machine learning based Zen Intelesis software. The software was trained by manual Synaptophysin-eGFP cluster segmentation. ROI's of the subregions of the PAG were performed using anatomical features of the region and the total number of synaptic inputs in that region of interest (ROI) was divided by the

ROI area to obtain synaptic density. The following nomenclature for the subregions of the PAG nuclei was used: dorsal medial periaqueductal grey (dmPAG), dorsal lateral periaqueductal grey (dlPAG), lateral periaqueductal grey (lPAG), ventrolateral periaqueductal grey (vlPAG) (Supplementary Figure 7).

dmPAG image processing

Overview of the labeled samples was obtained with a Zeiss Axio Imager 2 microscope equipped with a Plan-Apochromat 5x/0.16 objective. Images were taken with an Axiocam 506 and pixel size of 2,724 x 2,724 µm. For excitation of DAPI a wavelength of 353 nm with LED-Module 385nm (power 3-6%), for the GFP a wavelength of 488nm with LED-Module 475nm (power 20-24%) and for the SynMyc a wavelength of 548nm with LED-Module 555nm (power 25-30%) was used. Emission wavelength for DAPI was 465nm, GFP was 517 and SynMyc 561. Image acquisition was set using Zeiss Tiles module.

Labeled samples were imaged on a Leica SP8 (Leica) confocal microscope equipped with an HC PL APO CS2 63.0×/1.40-NA oil UV objective. Images were taken using a 200-Hz resonant scanner, a voxel size of 59 × 59 × 170 nm, a pinhole of 108.7 µm (1 AU). For excitation blue 488 nm argon laser (power 1-3%), yellow-green 561 nm DPSS laser (power 1-3%), red 633 nm HeNe laser (power 1-3%) were used. Emission light was registered with Leica PMT detectors set to the following spectral ranges: 500-550 nm, gain 750-850V (green channel); 575-620 nm, gain 750-850V (red channel); 645-700 nm, gain 750-850V (far-red channel). Image acquisition was performed in sequential frame scan mode, with concurrent 488 nm and 633 nm excitation and acquisition in corresponding ranges, followed by 561 nm excitation with an acquisition in the red channel. Bleaching was compensated with a linear gain increase of 30-40 V for an hour.

Subsequently, deconvolution using a computed PSF was applied (Huygens Professional package, Scientific Volume Imaging), and 3D volumetric representation, segmentation and modeling was done (Imaris, Oxford Instruments).

3D image processing

Confocal data was deconvoluted using a computed PSF (Huygens Professional package, Scientific Volume Imaging) with the following settings: Logarithmic vertical mapping function; manual background estimation, according to the intensity baseline; max. 40 iterations, background to noise ratio of 5, 0.05 quality threshold, optimized iteration mode, auto brick layout. 3D and volumetric representation, segmentation and modeling of the deconvoluted images were done in Imaris (Oxford Instruments).

The volumetric representation and segmentation were done with the following settings:

<u>Wild-type hippocampal tissue</u>

mAb3B11, mAb7a and Sylites (synapse segmentation): No smoothing, 10% intensity threshold, >800 Voxels volume threshold (~0.5 μm^3). DAPI (nuclei segmentation): 0.468 µm (8 pixels) smoothing, 5% intensity threshold, 10000 Voxels volume threshold.

<u>Periaqueductal gray tissue from infected recombinant mice</u>

Gephyrin labeled with Sylite segmentation: No smoothing, 5% intensity threshold, >0.1 μm^3 volume threshold. Synaptophysin, labeled with goat anti-MYC antibody and donkey anti-goat Cy3 antibody segmentation: No smoothing, 5% intensity threshold, >0.1 μm^3 volume threshold. Neurons, labeled with chicken anti-eGFP antibody, and donkey anti-chicken Alexa 488 antibody segmentation: smoothing 0.117 µm (2 pixels), 2-10% intensity threshold, >2 μm^3 volume threshold.

Inhibitory synapse density in neurons was calculated by dividing total in-neuron gephyrin volume (voxels) by total neuron volume (voxels) in each tissue section of dmPAG. Gly+ synapse density: the total volume of gephyrin clusters (voxels) in proximity to synaptophysin (<1 µm distance) was divided by total neuron volume (voxels). Gly- synapse density: the total volume of gephyrin clusters (voxels), excluding the ones in proximity to synaptophysin, was divided by total neuron volume (voxels).

3. Results

This chapter is focusing on the results regarding the design, development, characterization and application of functional anti-gephyrin peptide-based probes that visualize the inhibitory synapse. Parts of the results presented here have been published in an article by Khayenko et al. (2022)[1] in Angewandte Chemie International Edition.

3.1. Fluorophores impact the binding of peptidic gephyrin probes

TMR2i (Tetramethylrhodamine-FSIVGRYP9R) was the first synthetic fluorescent probe that has been successfully used to label gephyrin[53]. To improve the usability of synthetic gephyrin probes for light microscopy and to expand the implementation to super resolution microscopy and tissue labeling an improvement in probe selectivity combined with a fluorophore exchange was required.

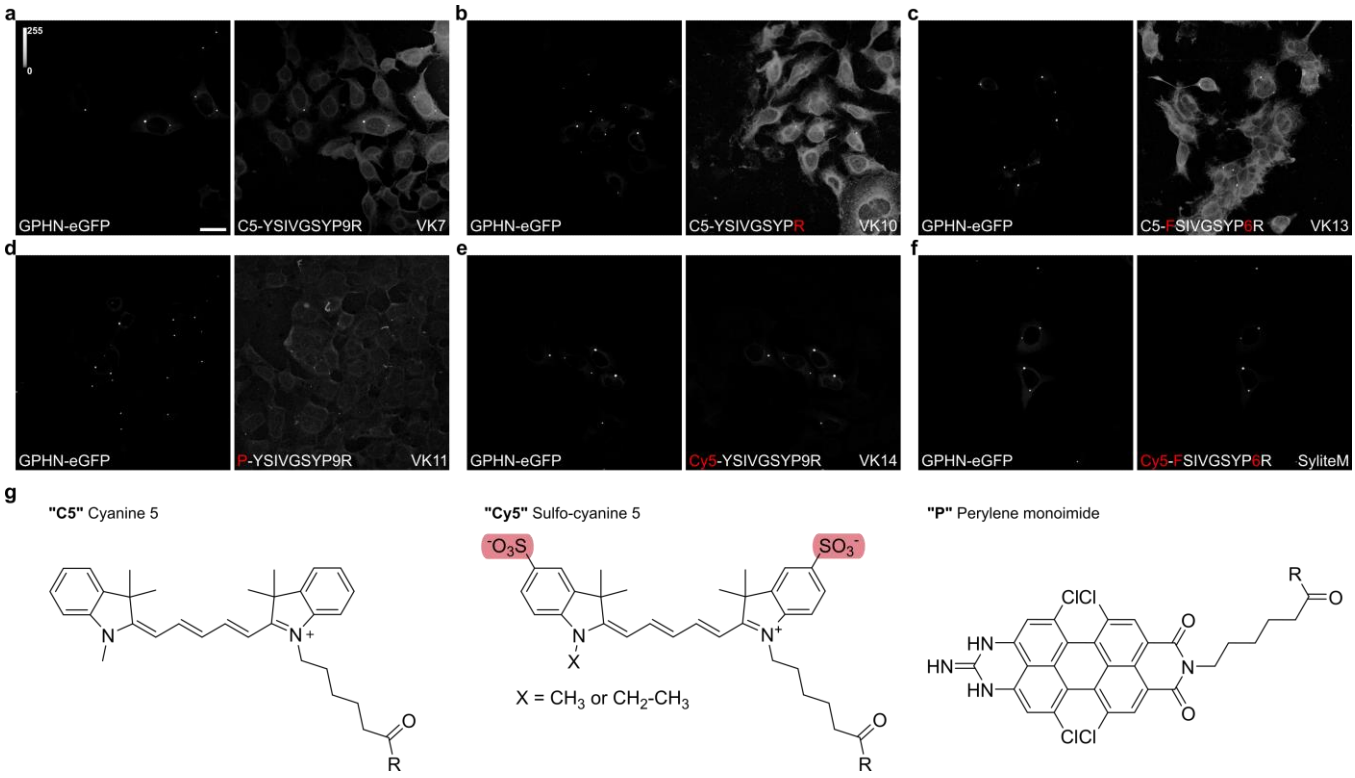

Figure 5. Fluorophores influence the binding of anti-gephyrin peptides. a-f) Representative images of fixed HEK293 cells expressing gephyrin-eGFP, stained with various anti-gephyrin peptidic probes, all applied with 50 nM concentration. Scale bar 20 µm. a) Staining of the gephyrin clusters is visible with the Cyanine 5 conjugated YSIVGSYPRRRRRRRRR gephyrin binding peptide, however, significant background staining is observed. b) Binder with a single arginine and otherwise unchanged sequence retains binding to gephyrin clusters, but even more background staining is observed. c) Binder with terminal Y to F exchange and the 9 to 6 truncation of the polyarginine sequence retains binding to gephyrin clusters but does not reduce the background staining. d) Probe with Cyanine 5 to perylene monoamide swap had reduced gephyrin cluster staining and did not reduce off target binding. e+f) Sulfo-Cyanine 5 conjugated gephyrin binders both with unchanged and with modified binding sequence clearly visualized the gephyrin clusters and had the lowest observed background staining. g) Chemical structures of the fluorophores used for the conjugation with the probes. The differences between C5 and Cy5 are highlighted in red.

First, I produced a modified version of TMR2i, by performing an N-terminal conjugation of the YSIVGSYP9R peptide to cyanine 5, a dye applicable in direct Stochastic Optical Reconstruction Microscopy (dSTORM)[80], a super-resolution microscopy technique. Then I applied the probe on fixed HEK293 cells expressing gephyrin (GPHN) eGFP chimera where it showed on-target staining, however, background staining was present as well (Fig. 5A). Since the probe consisted of three nominal parts: a) a fluorophore, b) gephyrin binding sequence and c) polyarginine motif (that contributes to solubility and could facilitate cell permeation in potential live-cell application), changes could have been done in any of the parts to improve the labeling contrast. Therefore, I have synthesized analogous

probes either having the same peptide sequence, but a different fluorophore, or probes having the same fluorophore (cyanine 5), but a different peptide sequence (Appendix B).
Probes harboring the cyanine 5 fluorophore and with alterations in the peptide sequence, i.e., without polyarginine, or with terminal Y to F switch and a shortened polyarginine motif, did not show an improvement in labeling contrast (Fig. 5B,C). Probe having perylene monoamide, a super-resolution compatible fluorophore[81], and an unaltered peptide sequence had worse labeling contrast than the original probe (Fig. 5A,D,G), while sulfo-cyanine 5 containing probes, both with unaltered and altered binding sequences had a superior labeling contrast (Fig. 5E-G).
To summarize, fluorophore swap had the strongest impact on probe performance. Changes in peptide sequence, with mutations that do not hinder the binding (Fig. 3), did not markedly influence the staining outcome. Conversely, sulfo-cyanine 5 conjugated probes, with or without sequence alteration had the best labeling contrast. Lastly, adoption of the sulfo-cyanine 5 dye was favorable, as it is widely used in dSTORM super-resolution microscopy[74].

3.2. Dimeric gephyrin probe is superior to monomers

ITC experiments showed higher affinity for dimeric gephyrin binders when compared with monomers[65,67] and the microarrays suggested that point mutations further contribute to the binding potency[53], however, the microarray comparison of dimers was inconclusive, showing equal potency for mutant mono- and dimeric binders with different linker lengths[1] (Fig. 4).

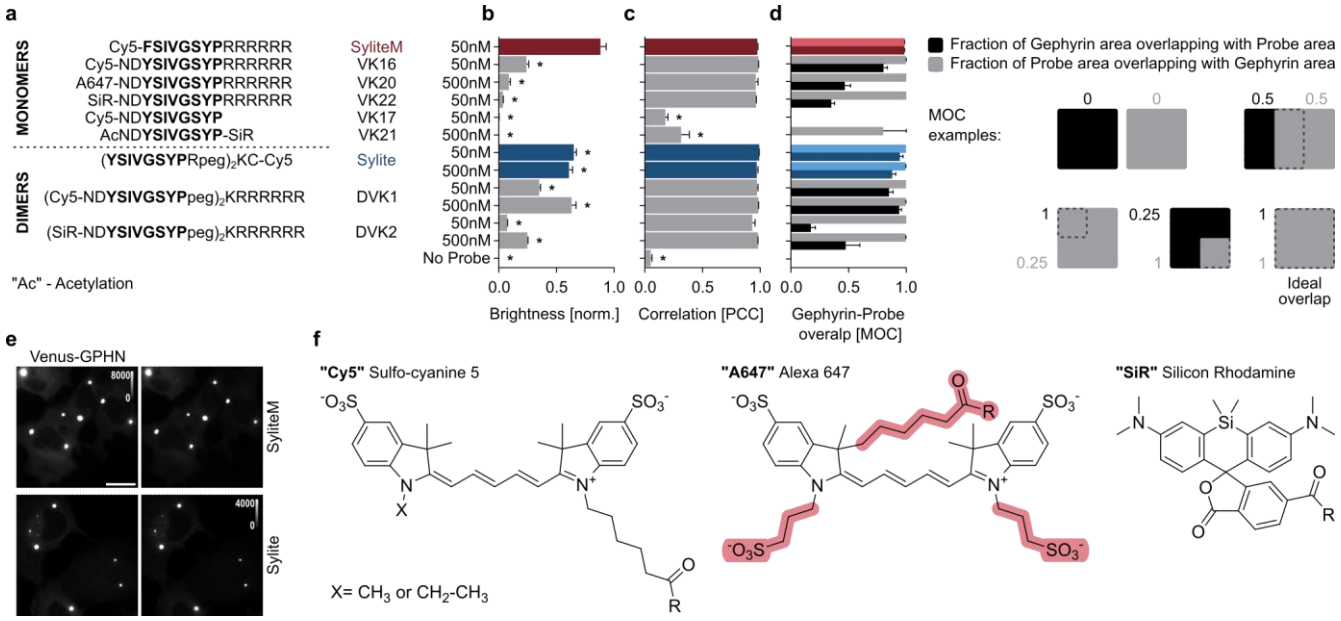

Figure 6¨. N-terminal binding sequence elongation does not improve probe performance. Systematic comparison of the gephyrin labeling efficiency of the synthesized fluorescent probes in COS-7 cells expressing Venus-gephyrin. a) Sequences of dimeric and monomeric probe variants and probe concentrations. b) Comparison of the relative probe brightness. All probes are conjugated with far-red fluorophores, the average signal intensity coming from gephyrin clusters in far-red channel was divided by the corresponding average signal intensity of gephyrin clusters in green channel. Note that SyliteM is the brightest probe followed by Sylite. *P<0.0001. Mean ± SEM. n ≥3. Significance was determined with ANOVA followed by Dunnett's test for multiple comparisons with SyliteM's brightness. c) Pearson's Correlation Coefficients (PCC) of fluorescent probes and Venus-gephyrin. Next to the control only VK17 and VK21 show an incomplete correlation with gephyrin. *P<0.0001. Mean ± SEM. n ≥3. Significance was determined with ANOVA followed by Tukey's test for multiple comparisons. d) Mander's overlap coefficients (MOC) - proportional coappearance of gephyrin and probe signals. When both MOC values reach 1 there is an exclusive overlap of the two signals, meaning there is no unspecific staining or underlabeling of the target. Far-red signals coming from VK20, VK21, VK22 and DVK2 overlap almost completely with Venus-gephyrin, however Venus-gephyrin has only partial overlap with these probes, indicating under-labeling of the target. e) Representative images of fixed COS-7 cells expressing Venus-gephyrin (left) stained with SyliteM or Sylite (right). Scale bar 20 µm. f) Chemical structures of the fluorophores used for the conjugation with the probes. Cy5 and A647 are dSTORM compatible fluorophores, the differences between Cy5 and A647 are highlighted in red. SiR is Stimulated Emission Depletion (STED) super-resolution microscopy compatible fluorophore.

Integrating the microarray data on native gephyrin binders (Fig. 3) and the data from the preceding probe screening (Fig. 5) I have synthesized a set of mono- and dimeric probes (Appendix B), all having a core binding sequence capable of binding gephyrin (YSIVGSYP or FSIVGSYP) and the same linker structure. Except Sylite and SyliteM, all probes contained N-terminal asparagine-aspartate (ND) core binding sequence elongation that could contribute to gephyrin binding (Fig. 3) and some had a polyarginine sequence. Additionally, I further explored the inclusion of different super-resolution capable fluorophores (Fig. 6A,F).

The probes were tested on fixed COS-7 cells expressing gephyrin tagged with Venus fluorescent protein (Venus-GPHN). Image analysis of the staining showed that the dimeric Sylite and the monomeric SyliteM were the brightest probes and had the highest correlation and overlap with gephyrin (Fig. 6B-E). Comparison of the SyliteM and VK16 monomers showed that N-terminal ND elongation of the binding sequence does not enhance the probe performance, but rather diminishes it, reducing the probe labeling capacity and the brightness (Fig. 6B,D). Furthermore, substitution of the Cy5 fluorophore to A647 or SiR further reduced the probe performance, affirming

the fluorophore effect on the probe performance. Interestingly, deletion of the polyarginine sequence (VK17) further hampered the probe labeling capacity, this change was inconspicuous for VK10 (Fig. 5B), speculatively, since VK10 had a better performing binding sequence, without ND elongation, and a secondary effect of the polyarginine deletion was unremarkable.
Dimer comparison once again validated the fluorophore effect on probe performance. Although having the same sequence and architecture, DVK1 conjugated to Cy5 performed better than DVK2 conjugated to SiR. Sylite, a shorter dimer, lacking the ND elongation and the polyarginine sequence, carrying the Cy5 fluorophore on the linker, instead of a direct conjugation to the binding sequence, performed better than the aforementioned dimers. It was as bright as DVK1 in a 10-fold reduced concentration, while also having one fluorophore per molecule instead of two (Fig. 6A,B). This suggests that the on-target binding of Sylite was more efficient.

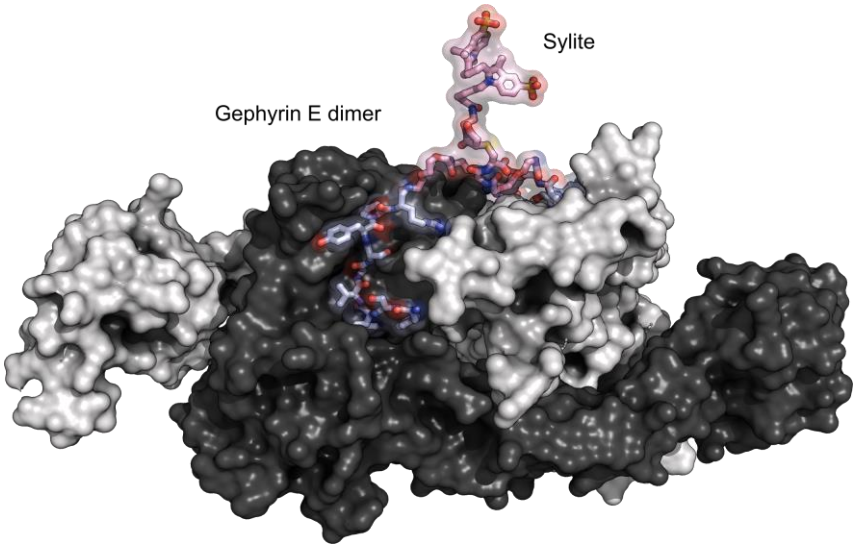

Figure 7¨. Sylite simultaneously binds to two gephyrin molecules. Rosetta FlexPepDock structural model of Sylite bound to the gephyrin (GPHN) E domain dimer. In light blue is the binding sequence, in pink is the linker and the fluorophore; the two gephyrin E domains are shown in black and white. Sylite can simultaneously bind two gephyrin molecules.
**The model was produced in collaboration with Dr. Orly Avraham and Prof. Ora Schueler-Furman from the Hebrew university of Jerusalem, Israel.*

We further used in-silico modeling to investigate Sylite's mode of binding to gephyrin. The model shows probe attachment to universal receptor binding pocket in gephyrin E domain[26,67] and implies simultaneous attachment of the probe to two gephyrin molecules, emphasizing the importance of avidity for the dimeric probes (Fig. 7). To provide a robust and unambiguous probe evaluation I conducted a follow up assay with alternative gephyrin construct, where I directly compared TMR2i, SyliteM and Sylite for gephyrin visualization. COS-7 cells expressing either eGFP-gephyrin (eGFP-GPHN) or eGFP alone, as a control, were fixed and stained with the fluorescent probes. Gratifyingly, SyliteM with the sulfo-cyanine 5 fluorophore, and the optimized binding sequence performed better than TMR2i, while the Sylite dimer performed better than SyliteM. Sylite showed both complete correlation with gephyrin and a remarkable signal-to-background ratio (SBR) of 492, a 172-fold increase over TMR2i and 14-fold increase over SyliteM (Fig. 8). Next, using isothermal titration calorimetry (ITC) we determined the affinity of Sylites to the purified gephyrin E domain. SyliteM showed an average K_D of 205 nM, while Sylite an even higher affinity of 17.5 nM, a remarkable 11-fold affinity increase over the monomer. Additionally, we confirmed the expected 1:2 binding stoichiometry of the dimeric probe (Fig. 9A). We then proceeded to mass-spectrometric analysis of the interactome of Sylite. We used the non-fluorescent peptide probes bound to cellulose membranes to retain proteins from mouse brain homogenate, and then, after protein digestion, analysed the bound fractions. Gephyrin was the only protein with high abundance, high enrichment and represented by multiple unique peptide fragments binding to Sylite, confirming the probe selectivity for gephyrin within the whole brain proteome (Fig.

9B, Appendix D). The monovalent SyliteM probe retained additional proteins, demonstrating that probe dimerization not only enhanced affinity but also target selectivity.

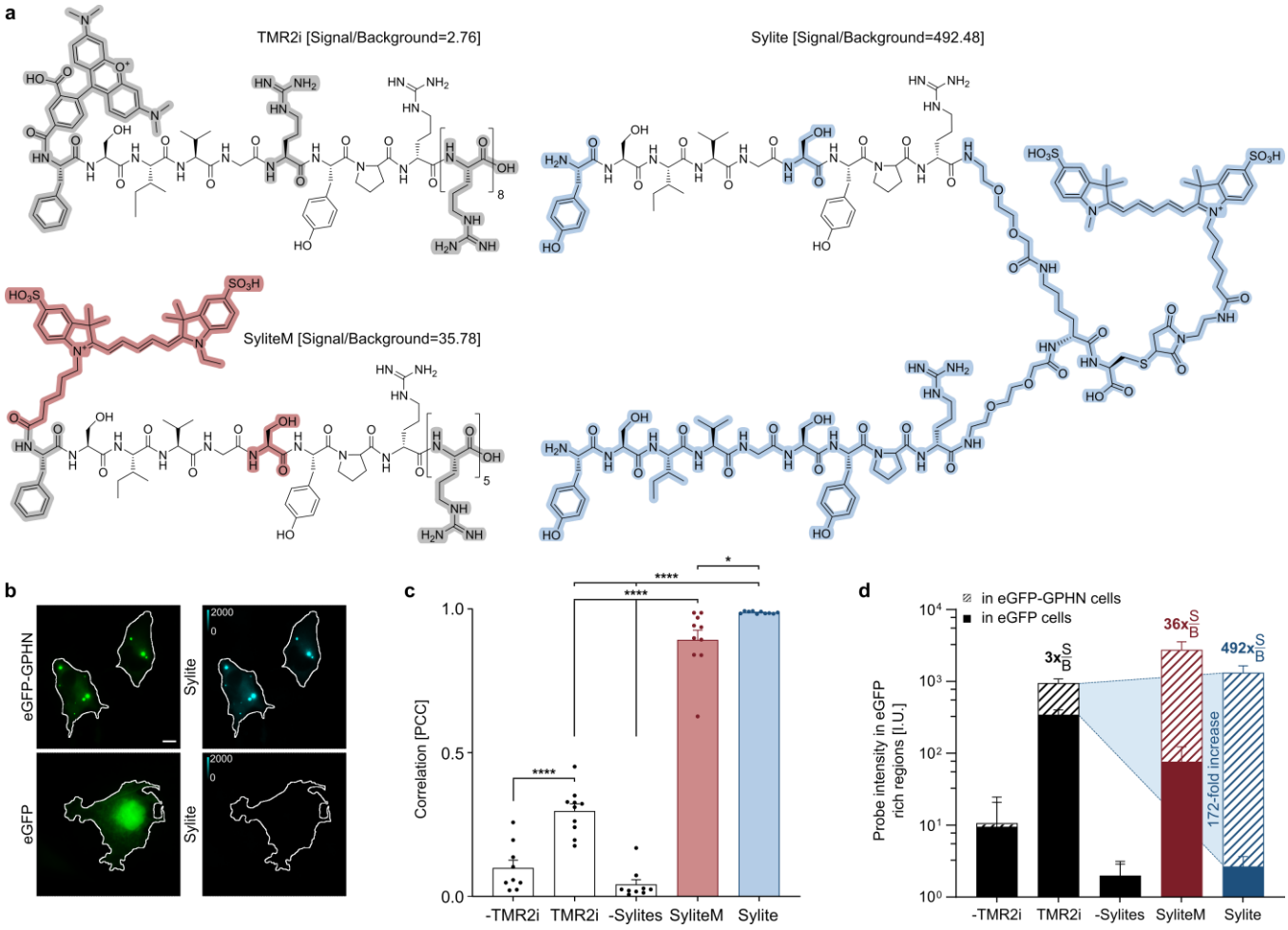

Figure 8¨. Evolution of peptide-based gephyrin probes. a) Chemical structures of TMR2i, SyliteM and Sylite. The stepwise evolution of the TMR2i to Sylite involves fluorophore tailoring with binding sequence changes, resulting in an improvement of one order-of-magnitude in the SBR (SyliteM, in red are the changes, in gray are the obsolete components). Dimerization and the relocation of the fluorophore to the linker yields another order-of-magnitude improvement in SBR (Sylite, changes in blue). b) Fixed COS-7 cells expressing either eGFP-gephyrin or eGFP (green) stained with 50 nM of Sylite (cyan). Scale bar 10 µm. c) Probe to gephyrin correlation in fixed COS-7 cells. Sylite achieves a complete correlation of the probe with gephyrin. Both Sylite and the monomer SyliteM have a significantly higher correlation to gephyrin than the earlier reported fluorescent probe TMR2i. The negative control (unlabeled cells) in the red channel is shown as "-TMR2i", that in the far-red channel as "-Sylites". Mean±SEM. Significance determined with ANOVA, using Dunnet's test for multiple comparisons,*P<0.05, ****P<0.0001. d) Labeling contrast of gephyrin with the synthetic peptide probes. The logarithmic Y axis represents the average signal intensity of the probe in eGFP-rich regions of the COS-7 cells. Sylite and SyliteM have 492 and 36 signal-to-background ratios (rounded), respectively. TMR2i has a target to off-target labeling ratio of ≈3. The negative control (unlabeled cells) in the red channel is shown as "-TMR2i", that in the far-red channel as "-Sylites". N≥8 samples per condition. Mean±SD.

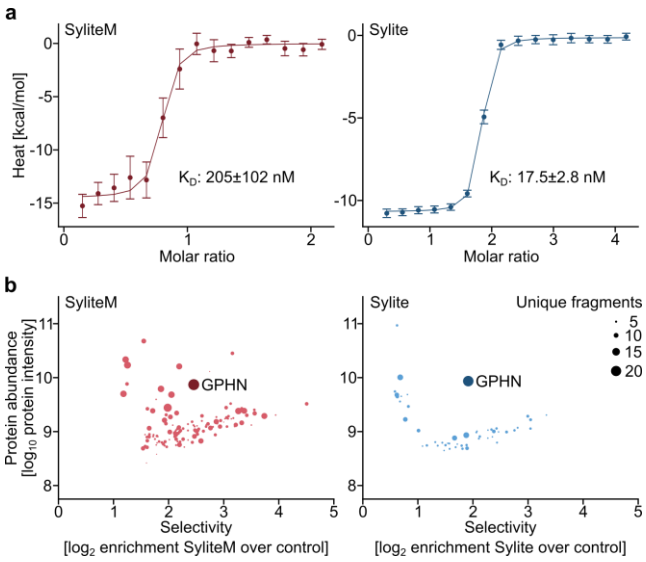

Figure 9¨. Probe dimerization enhances affinity and selectivity to gephyrin. a) ITC measured heat signature of Sylite and SyliteM titrated with gephyrin E domain. Both probes exhibit nanomolar affinity, with the dimeric Sylite having 10-fold affinity increase over the monomer. N=3. Error bars are auto generated with NITPIC software and indicate SD. b) Quantitative mass spectrometric analysis of Sylite and SyliteM pull-downs. Non-fluorescent versions of Sylite and SyliteM were used to pull down proteins from mouse brain homogenate and the protein fractions were subsequently digested and analyzed with LC-MS/MS. The size of the circle corresponds to the number of unique peptides identified for each protein. Left: SyliteM retains additional proteins that have high intensity and abundantly represented in the pool, even though gephyrin is the most prominent. Right: Gephyrin is the only protein with high abundance, selectivity and multiple fragments in the Sylite pull-down.

3.3. Sylite targets synaptic gephyrin

Gephyrin is a multifunctional protein with numerous isoforms and post-translational modifications, some of which are specific for neurons, others have functions unrelated to neurotransmission, such as molybdenum cofactor biosynthesis in non-neural tissues[57]. A recent study has shown that in neurons gephyrin isoforms having an E domain with the universal receptor binding pocket form synaptic clusters, while isoforms having a compromised E domain do not[58]. Unlike antibodies that are raised against protein fragments that are not necessarily exclusive or related to specific protein activity, Sylite is a functional probe designed to bind receptor binding competent gephyrin isoforms, i.e., isoforms that exhibit functional roles in neurons. Comparison of the binding profiles of eleven gephyrin isoforms expressed in HEK293 cells revealed that both Sylite and SyliteM, but not the tested antibodies, exclusively label gephyrin isoforms that have GlyR and $GABA_AR$ binding capacity (Fig. 10, Appendix E,F). Interestingly, no gephyrin labeling was observed with the widely used mAb7a antibody in HEK293 cells, probably due to the phosphorylation state of gephyrin in the cells. Microarray profiling of mAb7a binding (Fig. 11, Appendix C) confirmed that in contrast to Sylite, mAb7a binding depends on the presence of a phosphorylated (pSer270) epitope in the linker region of gephyrin[54]. Thus, mAb7a labels only a sub-population of synaptic gephyrin isoforms and phosphorylation variants. mAb3B11 antibody appears to target an epitope in 349-510 AA region of gephyrin, located in the beginning of the E domain, and does not differentiate between receptor clustering capable and uncapable isoforms (Fig. 12). A proteome analysis by Dos Reis et al.[58] showed that a peptide derived from the GlyR β gephyrin core binding motif, which shares sequence similarity and targets the same gephyrin binding site as Sylite[26,53], pulled gephyrin isoforms that comprise 95% of the gephyrin brain proteome from a whole brain lysate[58]. These data combined advocate that Sylite is a universal probe for neuronal gephyrin that detects active synapses and could quantify functionally relevant receptor binding sites.

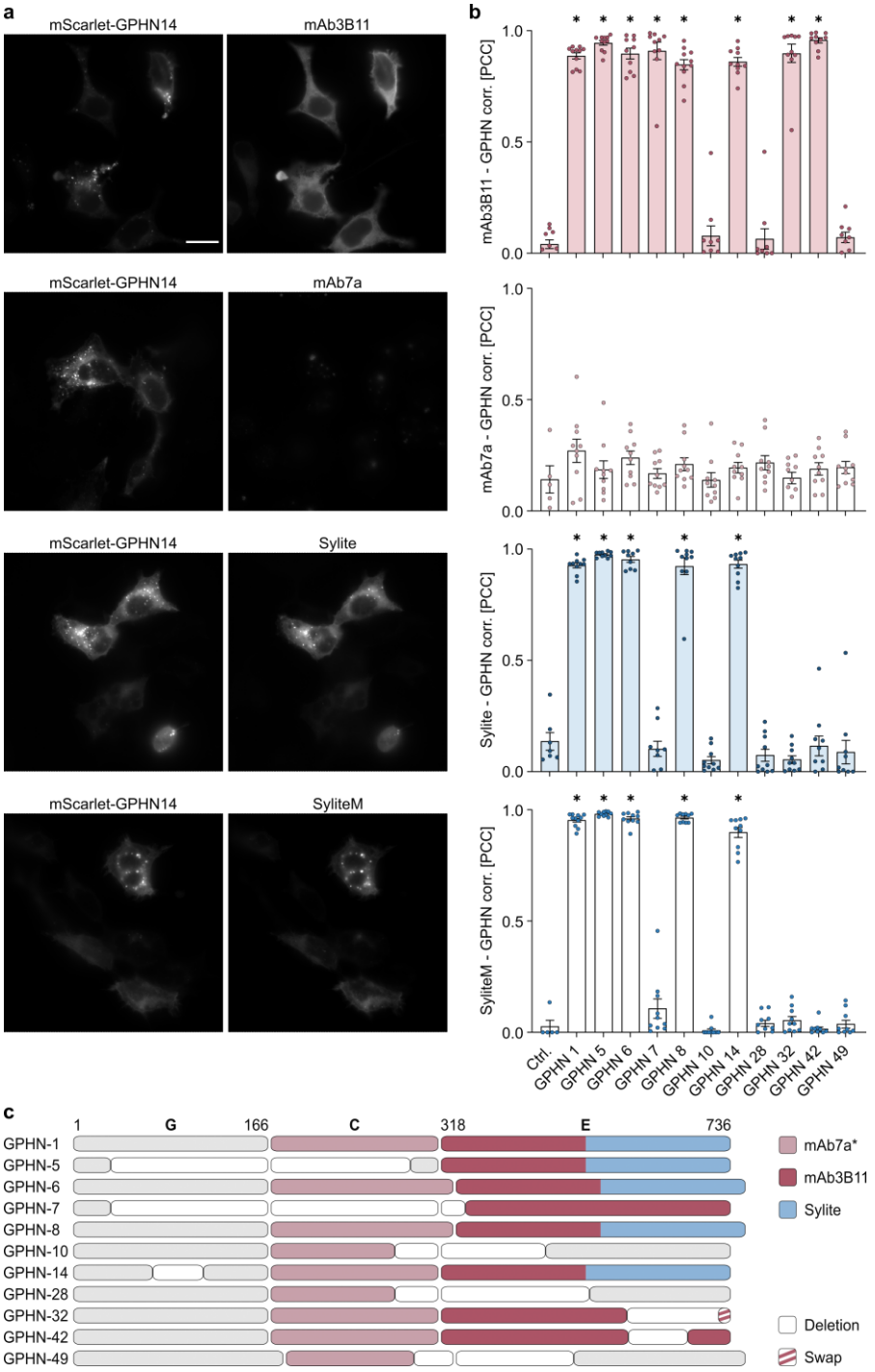

Figure 10¨. Sylite specifically labels gephyrin isoforms with receptor binding capability. a) Left: Fixed HEK293 cells expressing mScarlet-gephyrin isoform 14. Right: Co-labeling of gephyrin with either mAb3B11, mAb7a, or Sylites. mAb3B11 stains gephyrin in the transfected cells but does not resolve the fine puncta visible in the top image. mAb7a does not label recombinant gephyrin in HEK293 cells. Sylites label mScarlet-gephyrin and resolve the fine puncta where the recombinant protein accumulates. Scale bar 10 µm. b) Colocalization analysis of probes with gephyrin isoforms expressed in HEK293 cells. Control indicates stained cells expressing soluble mScarlet. Both peptide probes label 1,5,6,8 and 14 isoforms of gephyrin. mAb7a does not stain recombinant gephyrin in HEK293 cells; mAb3B11 stains all isoforms except 10,28,49. Mean±SEM. Significance determined with Brown-Forsythe and Welch ANOVA tests with Dunnet's T3 test for multiple comparisons to the control. * P<0.0001. c) Interaction of probes with different gephyrin isoforms. The isoform GPHN-1 represents the primary structure of gephyrin[82]. Blank boxes indicate deletions, elongated boxes additions, striped box - substitution. Sylite (blue) binds isoforms that contain a receptor binding pocket in the E domain. The antibodies target both receptor clustering competent and binding deficient isoforms. mAb7a (rose) binds a short linear *Ser270 phosphorylated epitope in the linker region (C), while mAb3B11 (raspberry) interacts with an epitope in the E domain.

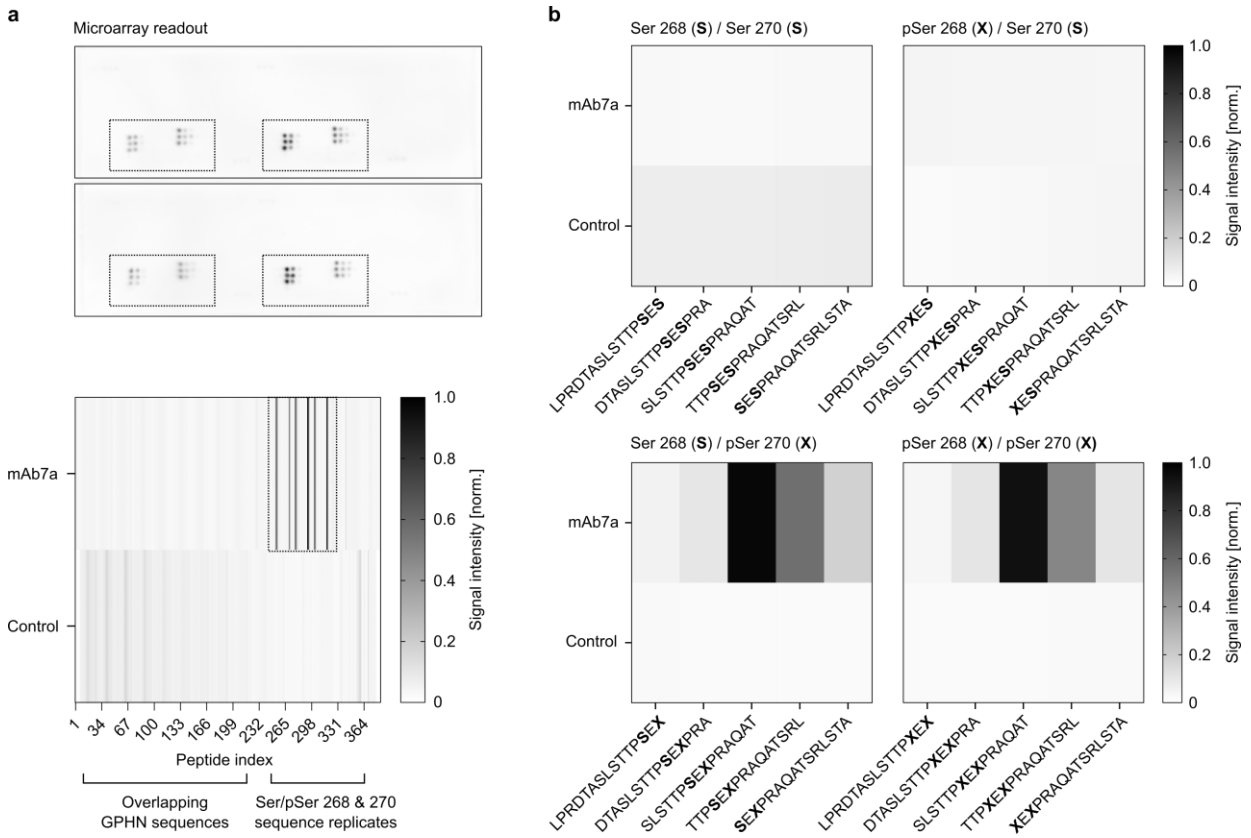

Figure 11¨. Gephyrin mAb7a explicitly binds a phosphorylated epitope. a) Representative examples (top) and averaged intensities as density blots (bottom) of mAb7a binding overlapping gephyrin fragments. The GPHN-1 isoform sequence was displayed in microarray format in the form of 15 AA peptides overlapping 12 AA with and without phosphorylations. mAb7a antibody binding was visualized with a secondary anti-mouse HRP conjugated antibody. Top panel: boxed - triplicates of phosphorylated peptide sequences. Bottom: a positional intensity readout, boxed is the region with phosphorylated sequence replicates. Intensities normalized to the highest intensity detected in the array. b) Averaged normalized intensity readout of the boxed region in a) X represents the phosphoserine. Chemiluminescent readout reports SLSTTPSEXPRAQAT as the primary mAb7a epitope. Thus, indicating that phosphorylation of Serin 270 is necessary and sufficient for binding while phosphorylation of Ser 268 does not appear to affect binding.

Figure 12¨. Binding sites of gephyrin probes. mAb7a targets a short linear phosphorylated epitope on the linker (C) region of gephyrin. mAb3B11 targets an epitope in 349-510 AA region of gephyrin, located in the beginning of the E domain, Sylite explicitly targets the receptor binding pocket in the E domain of gephyrin.

3.4. Multicolor Sylites visualize the inhibitory synapses in neurons

In fluorescence microscopy simultaneous imaging of two or more spectral channels is typically necessary for an evaluation of a biological question. Having flexibility in fluorophore and spectral channel choice is advantageous as this can save time and resources, in particular the need to re-adjust an experimental procedure or acquire new antibodies. I therefore produced a Sylite probe emitting in the red spectrum, conjugated to sulfo-cyanine 3 (Cy3), expanding the spectral range of Sylites. Sylite[Cy3] performs comparably to the earlier synthesized Sylite[Cy5]: Colocalization analysis in mammalian cells expressing eGFP-gephyrin showed a close linear relationship between the probe and gephyrin, while no correlation was observed in cells expressing eGFP only (Fig. 13), confirming the selectivity of the probe for gephyrin.

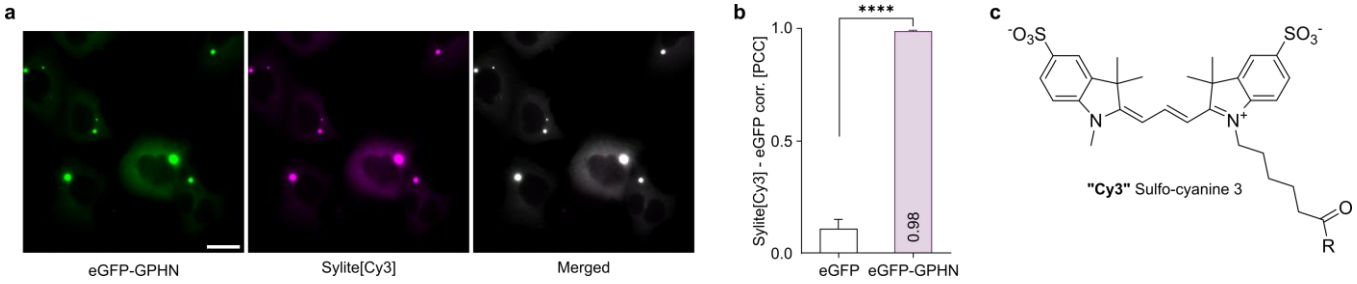

Figure 13¨. Sylite[Cy3] colocalizes with eGFP-gephyrin in mammalian cells. a) Fixed HEK293 cells expressing eGFP-gephyrin (GPHN) chimera (green) stained with Sylite[Cy3] (magenta), a full GPHN-Sylite overlap (white) is observed. Scale bar 20 µm. b) Sylite[Cy3] correlation with eGFP. Pearsons' correlation coefficient [PCC] of 0.98 indicates a near-complete correlation of Sylite to eGFP-GPHN, with no correlation to eGFP. n≥10 for each group. Significance determined with Mann-Whitney test, **** P<0.0001. c) Chemical structure of sulfo-cyanine 3, the two methylated indolinesulfonate units are connected with a three-unit carbon chain with conjugated double bonds, while in sulfo-cyanine 5 a five-unit carbon chain with conjugated double bonds connects the indolinesulfonates.

Next, I stained primary murine neurons with Sylites and mAb3B11. Both Sylite[Cy5] and Sylite[Cy3] visualized the inhibitory synapses and the diffuse gephyrin in neuronal cell bodies, as confirmed by the co-staining of primary hippocampal neurons with gephyrin 3B11 antibody (Fig. 14). Noteworthy, the relative intensity of the synaptic clusters relative to diffuse staining, i.e., synapse labeling contrast, with Sylite was higher than the one with mAb3B11. This finding is in line with the data from the previous chapter, where we substantiated that Sylite targets synaptic gephyrin, whereas the 3B11 antibody is not exclusive for synaptic isoforms. Lastly, the co-labeling with mAb3B11 did not affect the labeling contrast with Sylite. Interestingly, the colocalization of Sylite with mAb7a was lower than with mAb3B11 (Fig. 15A,C), leading me to investigate the nature of Sylite and mAb7a interaction with gephyrin in neurons. I stained cortical neurons expressing gephyrin-mEos2 fluorescent protein chimera with Sylite and mAb7a. Then, I performed colocalization analysis and compared the mEos2 intensity of individual synapses with that of Sylite or mAb7a (detected with a secondary antibody). Although both probes colocalized well with recombinant gephyrin in neurons (Fig. 15B,D), linear regression analysis of fluorescent intensities of synaptic puncta revealed a 2-fold closer prediction interval for Sylite compared with mAb7a, indicating a closer linear correlation between Sylite and mEos2-gephyrin signals (Fig. 15E). The higher scattering observed with mAb7a on the other hand suggests that the antibody staining exhibits non-linear scaling with synaptic gephyrin, in agreement with our previous finding that the mAb7a antibody specifically targets a phosphorylated variant of gephyrin. Taken together, our data demonstrate a linear, stoichiometric relationship between Sylite and gephyrin, making it suitable for quantitative microscopy.

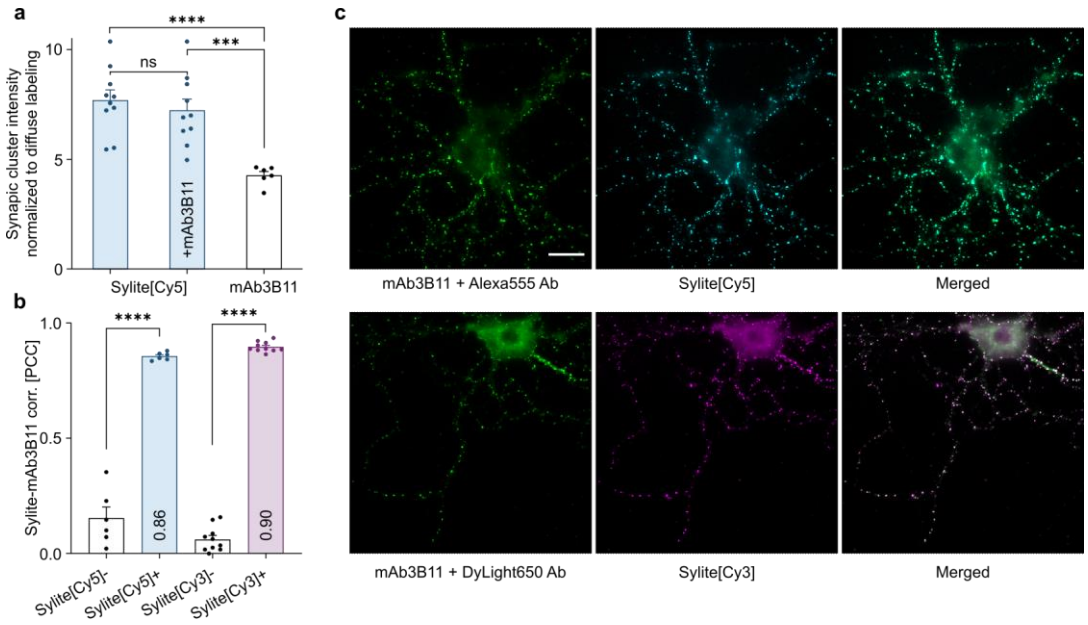

Figure 14¨. Sylites visualize neuronal synapses. a) Synapse labeling contrast with Sylite[Cy5] and mAb3B11 with a secondary Alexa 555 antibody. The synaptic cluster intensity was normalized to the diffuse signal within the cells. In samples stained with Sylite a higher labeling contrast of the synapses is seen. Co-labeling with mAb3B11 does not impact Sylite's labeling contrast of the synapses. Significance determined with ANOVA, using Tukey's test for multiple comparisons, ***P=0.0002, ****P<0.0001. b) Pearson's correlation coefficients (PCC) of mAb3B11 and Sylite signals confirm high degrees of co-localization. The negative control in the far-red channel (unlabeled) is shown either by "Sylite[Cy3]-" for cells labeled only with Sylite[Cy3], or by "Sylite[Cy5]-" for cells labeled only with mAb3B11 and Alexa555 secondary antibody. Significance determined with Welch's t-test. P<0.0001. c) Primary wild-type hippocampal neurons fixed and stained with Sylite[Cy5] or Sylite[Cy3]. Top: Co-labeling with mAb3B11 and a secondary Alexa 555 conjugated antibody (green) and with Sylite (cyan). Bottom: Anti gephyrin mAb3B11 and secondary DyLight650 conjugated antibody (green) and SyliteCy3 co-staining (magenta). Scale bar 10 µm.

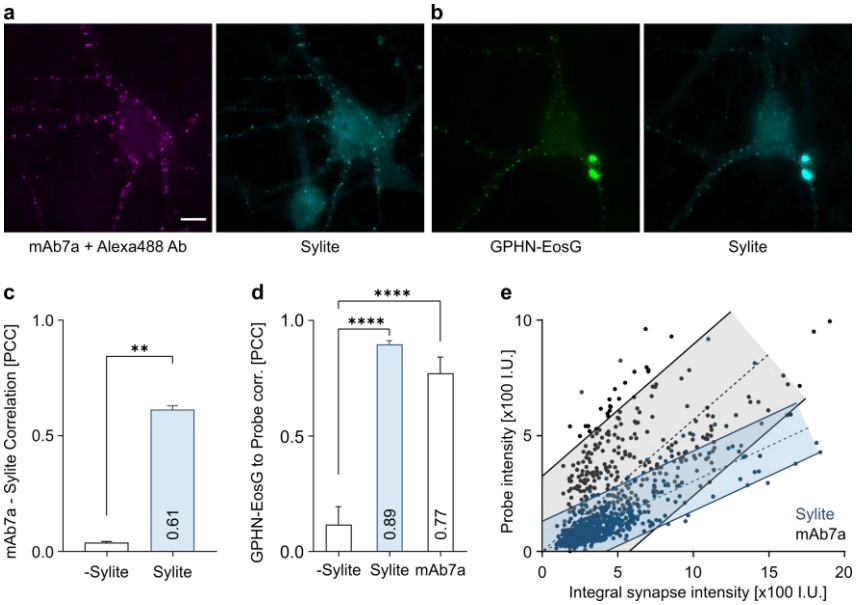

Figure 15¨. Sylite scales linearly to gephyrin a) Fixed DIV21 cortical neurons co-stained with Sylite (Cy5, 500 nM, green) and mAb7a (magenta). Scale bar 10 µm. b) Fixed cortical neurons expressing mEos2-gephyrin (green), with Sylite (Cy5, 500 nM) staining of the fixed sample (cyan). c) Sylite staining correlates with the staining of mAb7a, but the degree of correlation is lower than with mAb3B11. "-Sylite" is a negative control with only a secondary mouse A488 antibody applied. Mean ± SEM. n≥5. Significance determined with Mann-Whitney test. P<0.0025. d) Pearson's correlation coefficients (PCC) of mEos2-gephyrin expressing neurons with the counterstain of SyliteM, Sylite or mAb7a. The probes show high correlation wit recombinant gephyrin in neurons. Mean±SEM. n≥5. Significance determined using one-way ANOVA with a follow up Tukey's test for multiple comparisons. P<0.0001. e) Intensity dependence of synapse labeling with mAb7a or Sylite compared to the internal reference signal mEos2-gephyrin in infected neurons. Higher signal scattering is observed with mAb7a (grey), while Sylite (blue) has a constant and less variable linear labeling behavior. Shaded regions indicate the 90 % prediction interval. 10 pairs of images were used for each probe.

3.5. Nanoscopy with Sylite affirms the inhibitory synapse ultrastructure

**Super-resolution microscopy was performed in collaboration with Abbelight, Cachan, France and with Dr. Chrisitan Specht, INSERM, Le Kremlin-Bicêtre, France*

At inhibitory synapses numerous post-synaptic proteins assemble in sub-synaptic domains (SSDs) where gephyrin plays a central role in stabilization and scaffolding of the proteins[2,83]. Recent work showed that at the inhibitory synapse the pre-synaptic neurotransmitter release site, the active zone (AZ), is aligned to the SSD, forming a structural unit called trans-synaptic nanocolumn[3]. To determine the distance between the inhibitory SSD and AZ we labeled gephyrin and Rab3-interacting molecule (RIM) protein, which is enriched in areas where neurotransmitter vesicle fusion occurs[84], and studied the samples with dSTORM nanoscopy. RIM labeling was performed with primary anti-RIM1/2 and CF680-conjugated secondary antibodies and gephyrin was labeled either with Sylite or with commercial antibodies and AF647-conjugated secondary antibodies. Dual-color 3D-dSTORM imaging using spectral de-mixing showed that the Sylite detections closely matched the distribution of RIM in the AZ (Fig. 16A,B), confirming the close association between the AZ containing RIM and SSD containing gephyrin[3,30]. The measured mean Euclidian distance between Sylite and RIM1/2-CF680 detections was 129±24 nm (mean±SD), in agreement with the estimated molecular sizes separating the two proteins[3]. The direct comparison with mAb7a and mAb3B11 gephyrin labeling confirmed that Sylite provides a precise read-out of the location of the synaptic gephyrin scaffold and receptor binding sites at inhibitory synapses (Fig. 16C).

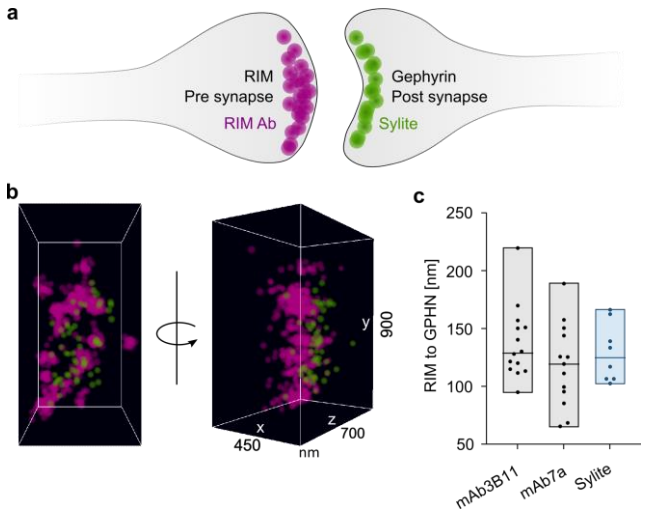

Figure 16¨. Super-resolution imaging and nanometric measurements with Sylite. a) Neuronal synapse illustrating presynaptic RIM1/2 labeling using a CF680 secondary antibody (magenta) and postsynaptic gephyrin labeling with Sylite (green). b) Dual-color dSTORM visualization of single molecule detections using spectral de-mixing is shown as planar projection and *en face* view of a single synapse. c) RIM to gephyrin center of mass distance measurements were conducted with RIM1/2-CF680 and either gephyrin antibodies or Sylite. In all cases an average distance of ≈130 nm was determined. Bars indicate the full range of individual measurements, the in-bar line indicates the median value.

3.6. Sylite bests antibodies in tissue penetration and visualizes brain synapses in 2D and 3D

**Immunohistochemistry was performed by Sara L. Dos Reis, AG Tovote, Würzburg university*

Immunohistochemistry of inhibitory synapses is an elaborate and time-consuming procedure that is generally restricted to thin brain sections (≤16 µm) to obtain reliable labeling[85]. In turn, the high tissue fragmentation inherently causes information loss and further increases the time cost, as data acquisition from multiple fragments and the following brain region reconstruction require more time. Here, we demonstrate that Sylite effectively penetrates 50 µm-thick tissue sections, achieving high-contrast labeling within just one hour using a standard, straightforward immunohistochemistry protocol.

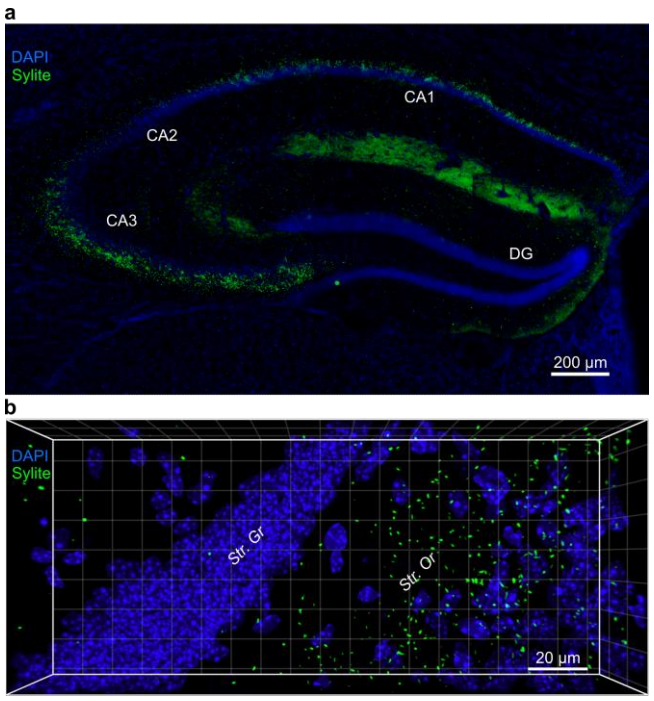

Figure 17¨. Sylite maps inhibitory synapses in brain tissue on macro- and microscale. Tissue synapse staining after 24-hour incubation with Sylite. a) Wide field 2D image of dorsal hippocampus section stained with DAPI nuclear staining (blue) and Sylite (green). A high density of distinct synaptic puncta is visible in CA1 and especially CA3 regions. b) 3D-confocal microscopy of Sylite (24-hours) staining in a ventral hippocampus section. Synapses appear in the stratum oriens. Str. Or—*stratum oriens*; Str. Gr—*stratum granulosum*.

We visualized inhibitory synapses and their distribution using epifluorescence microscopy with 20x magnification, giving us a macro-overview of the inhibitory synapse distribution in the hippocampus (Fig. 17A). Next, we incubated the hippocampal sections for 1, 24 and 72 hours with Sylite, and either mAb3B11 or mAb7a, then imaged the sections with a confocal microscope, deconvoluted the image stacks, and reconstructed 3D images. Sylite-visualized synapses were observed in the stratum oriens of the CA3 region of the ventral hippocampus, an area densely packed with inhibitory interneurons[86] (Fig. 17B). Sylite detected synaptic clusters throughout the entire section, demonstrating a complete penetration of the probe already after 1 hour of incubation. Similarly, after 24 hours Sylite synapse staining was equally good, 3D visualization of synapses obtained with Sylite showed smooth and well-defined shapes of different sizes, in agreement with the known diversity of shapes and sizes of inhibitory synapses in the CNS[87] (Fig. 18A). In contrast, after 24 hours, the antibody distribution appeared to have a “sandwich”-like pattern, with the strongest labeling near the surfaces of the sections while the center remained largely unlabeled (Fig. 18B). Furthermore, unlike Sylite, mAb7a did not have a pronounced region-specific staining (Fig. 19A,B). Strikingly, even after 72 hours of incubation with Sylite we did not observe any significant background

fluorescence, but the antibodies appeared to lose binding specificity causing staining artefacts and loss of any observable localization in specific regions of the tissue section (Fig. 19C,D).

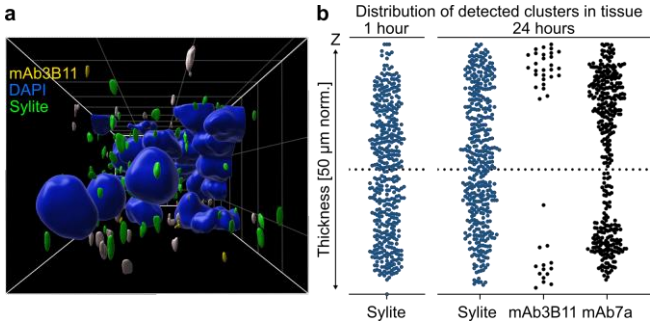

Figure 18¨. Sylite bests antibodies in tissue penetration. a) 3D volumetric representation of nuclei and inhibitory synapses. Side view of a rendered image stack from a section co-labeled for gephyrin for 24 hours with mAb3B11 and with Sylite. Green—Sylite, yellow—mAb3B11, blue—DAPI nuclear staining. Sylite and mAb3B11 co-labeled synapses are shown in white. Squares show a 10×10 µm grid. b) Distribution of Sylite and antibody labeling along the Z axis (depth) in 50 µm-thick mouse hippocampal sections after 1 and 24-hour staining. The top and bottom black lines indicate the section extremities, the dashed line the center. Violin plots represent the distribution of the detected clusters. The hourglass shape of antibody labeling indicates skewed antibody distribution, towards the surfaces of sections.

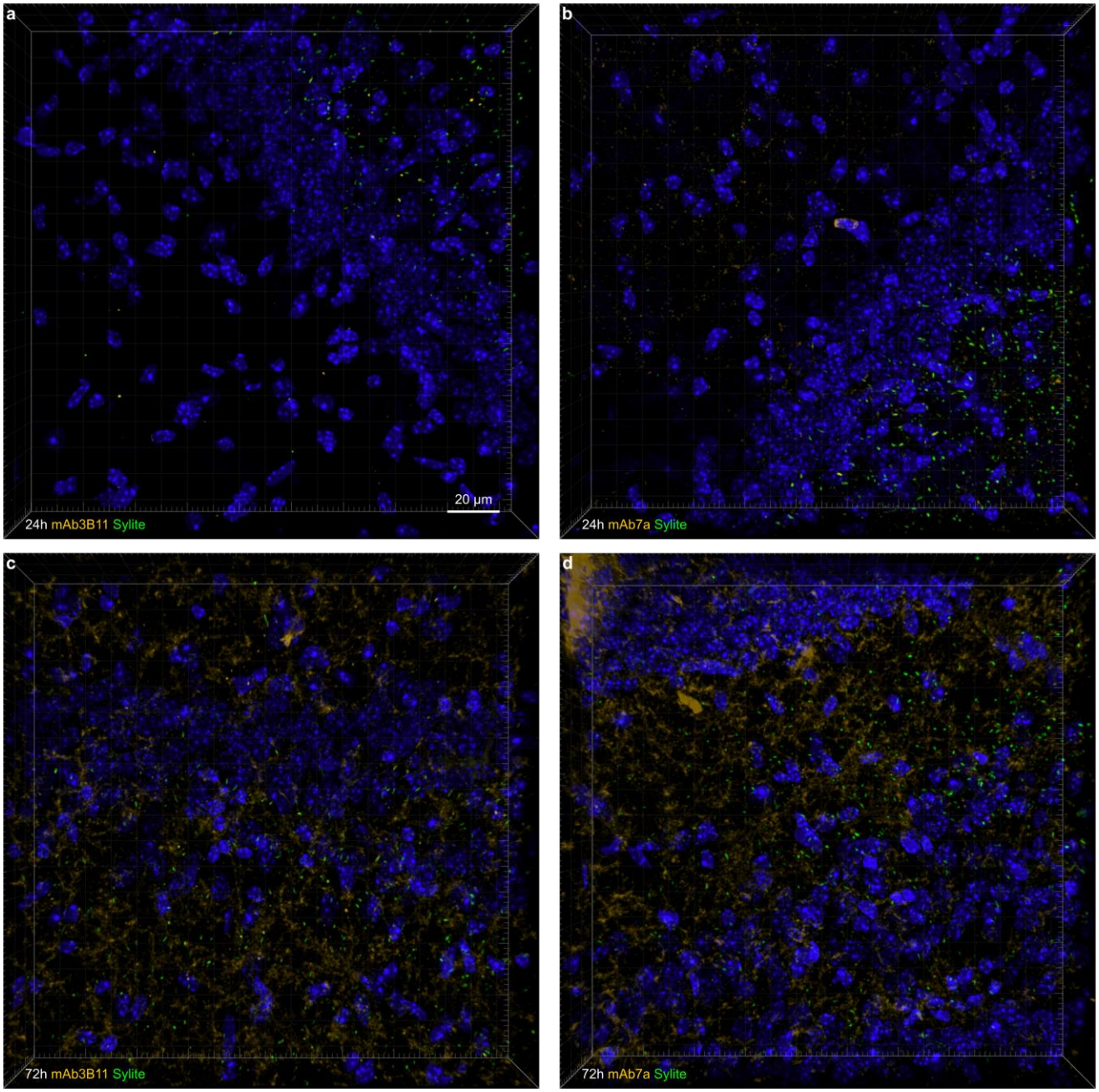

Figure 19¨. Sylite retains high-contrast artefact-free synapse labeling in tissue. 24-hour (a-b) or 72-hour (c-d) tissue slab staining with Sylite (green) and a) mAb3B11 or b) mAb7a with a secondary Alexa 555 conjugated antibody (gold). DAPI nuclear staining in blue. a) Both Sylite and mAb3B11 stainings appear to be region-specific, although the antibody labeling is sparce. b) mAb7a does not have pronounced region-specific staining and does not appear to be artefact-free. Sylite synapse staining is region-specific. c,d) Both mAb3B11 and mAb7a appear to lose binding specificity, staining is not region-specific and has imaging artefacts. Sylite staining is unaffected by longer incubation times, synapses are visualized with high contrast and in specific regions.

3.7. Sylite reveals local inhibitory circuits in the midbrain periaqueductal gray region

**Immunohistochemistry and glycinergic tracking was performed by Sara L. Dos Reis, AG Tovote, Würzburg University*

The mammalian nervous system is composed of a complex network of specialized synaptic connections that coordinate the neuronal flow of information. The periaqueductal gray (PAG) is a midbrain region that plays an important role in orchestrating the defense reaction in response to a perceived threat[4]. It has been postulated that intra-PAG circuitry supports integration of multiple defense components, such as switching between active and passive behavioral coping patterns[88]. However, the precise circuit mechanisms and their neuroanatomical substrates remain to be elucidated. To study the local inhibitory circuits created by the glycinergic neurons in the ventrolateral PAG (vlPAG), we sought to clarify their intra-PAG connectivity on the anatomical level using Sylite.

We used genetically modified mice expressing GlyT2 promotor-driven Cre recombinase[89], i.e., mice that express Cre recombinase in glycinergic neurons, as GlyT2 is a membrane protein of glycinergic neurons that recaptures glycine. Then we injected an adeno-associated virus (AAV) carrying a plasmid with Cre recombinase-dependent Synaptophysin-eGFP chimera coding region (Appendix F) in ventrolateral (vl) posterior PAG and tracked the glycinergic projections. We observed that these neurons locally project from the posterior ventrolateral (vl) to the anterior dorsomedial (dm) part of the PAG, while passing through the lateral (l) PAG (Fig. 20).

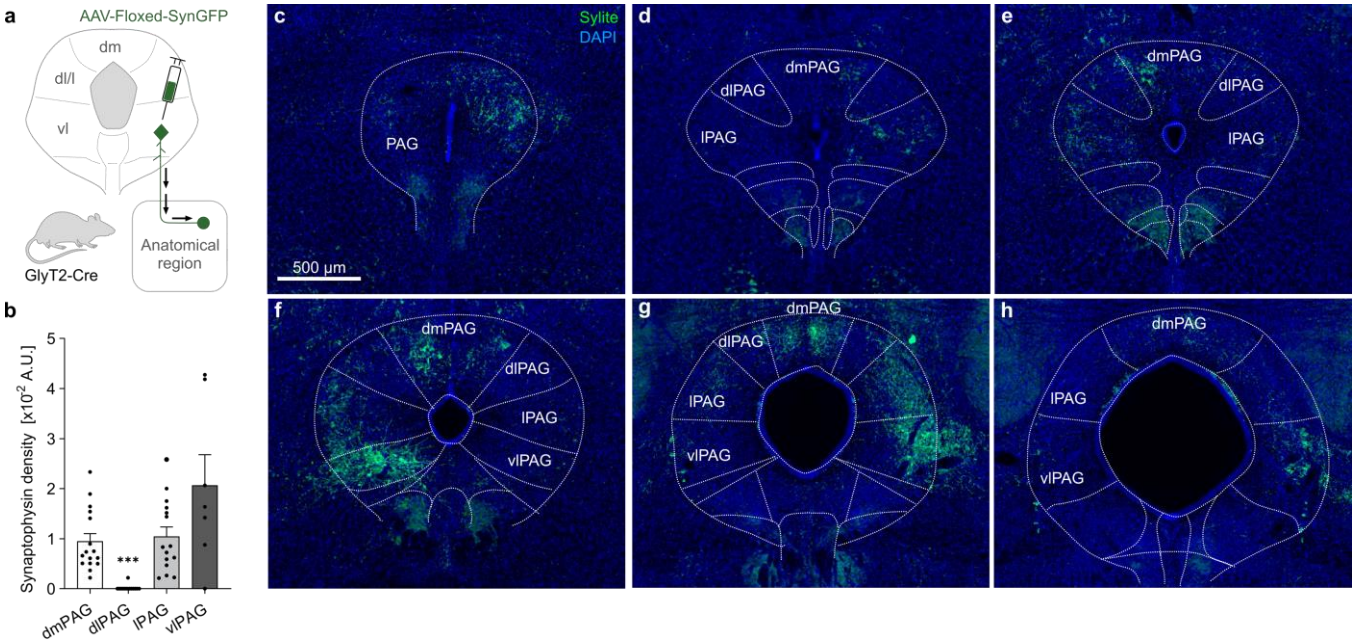

Figure 20¨. Glycinergic neurons from vlPAG project locally to lPAG and dmPAG. a) Anatomical tracing scheme of the injections and expression localizations in the periaqueductal gray. GlyT2-Cre recombinant mice were injected in posterior vlPAG with AAV carrying a plasmid with Cre recombinase-dependent Synaptophysin-eGFP chimera coding region. The synaptophysin-eGFP projections of the glycinergic neurons were traced and localized in specific anatomical regions of the PAG. b) Glycinergic projections from vlPAG are observable in lPAG and dmPAG, but not in dlPAG. Synaptophysin density: total synaptophysin in a specific anatomical region (μm^2) was divided by the total area of the region (μm^2) in each tissue section of dmPAG and plotted, mean±SEM, brain sections from three different animals were used. Significance determined with a Kruskal-Wallis test with a subsequent Dunn's multiple comparison test. P≤0.0001. c-h) Projection pattern of glycinergic vlPAG inputs to the different subregions of the PAG. Terminals of GlyT2+ vlPAG projection neurons were labelled by AAV-mediated expression of GFP fused to presynaptic marker synaptophysin from the more anterior (c) to the more posterior (h) part of the PAG.

We next aimed at characterizing the inhibitory post-synapse and identifying the target output cells of the glycinergic vlPAG neurons. To this purpose, GlyT2-Cre mice were crossed with either with glutamate transporter (vGluT2) promotor-driven Flippase (Flp) recombinase expressing mice or with vesicular $GABA_A$ transporter (VGAT) promotor-driven Flippase (Flp) recombinase expressing mice. This created mouse lines, expressing Cre recombinase in glycinergic neurons and Flp recombinase either in neurons expressing vGluT2, i.e., glutamatergic neurons, or in neurons expressing VGAT, i.e., GABAergic neurons. Next, we injected viruses in the mice brains: a)

AAV carrying a plasmid with Cre recombinase-dependent synaptophysin-Myc coding region and b) AAV carrying a plasmid with Flp recombinase-dependent enhanced yellow fluorescent protein (eYFP) coding region. This created eYFP labeled glutamatergic or GABAergic neurons in the anterior PAG, while vlPAG glycinergic projections expressed Myc tagged synaptophysin (Fig. 21). The mice were then sacrificed, and their brains harvested, cut and stained with Sylite to visualize the inhibitory post-synaptic sites. Further, we used anti-Myc and anti eYFP antibodies, to visualize the glycinergic projections and the GABAergic or the glutamatergic neurons, respectively (Fig. 21, Fig. 22A–C).

After the imaging of the brain tissue and the segmentation of the imaged components, I assessed the size of the post-synaptic densities visualized by Sylite. Gephyrin clusters having glycinergic input from vlPAG neurons were larger than clusters without the glycinergic input (Fig. 22D). This observation is in line with previous findings that reported larger individual gephyrin clusters in the spinal cord, a region rich in glycinergic neurons, compared with those in the cortex that are mostly GABAergic[2].

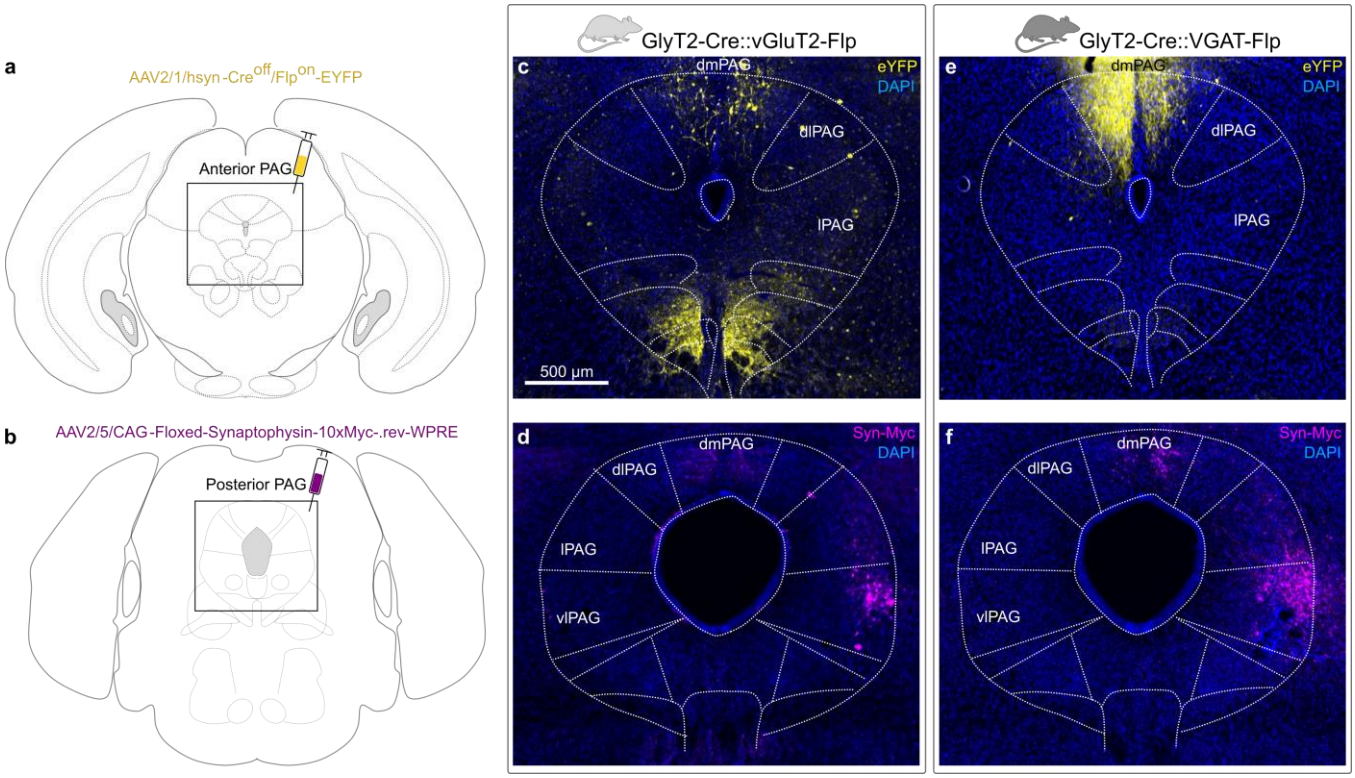

Figure 21¨. Recombinant protein expression at viral injection sites in the PAG. a) AAV2/1/hsyn-Cre^{off}/Flp^{on}-EYFP virus was injected in anterior PAG. b) AAV2/5/CAG-Floxed-Synaptophysin-10xMyc-.rev-WPRE virus was injected in posterior PAG. c-d) After viral infections, at injection sites, GlyT2-Cre::vGluT2-Flp mice express eYFP in glutamatergic neurons, i.e., neurons expressing a glutamate transporter in the membrane of synaptic vesicles and Myc-synaptophysin in glycinergic neurons, i.e., neurons expressing GlyT2, a membrane protein that recaptures glycine. Virally infected dmPAG glutamatergic neurons pattern. e-f) After viral infections, at injection sites, GlyT2-Cre::VGAT-Flp mice express eYFP in GABAergic neurons, i.e., neurons expressing vesicular GABA transporter proteins and Myc-synaptophysin in glycinergic neurons, i.e., neurons expressing GlyT2, a membrane protein that recaptures glycine. Virally infected dmPAG glutamatergic neurons pattern.

Next, I investigated vlPAG glycinergic projections to dmPAG and identified the glycinergic presynapses close to both glutamatergic and GABAergic dmPAG gephyrin sites (Fig. 22E, left), suggesting that vlPAG glycinergic neurons may exert inhibitory effects in the two functionally different dmPAG neuron classes. Interestingly, gephyrin density was higher in dmPAG GABAergic compared to glutamatergic neurons (Fig. 22E, middle and right), suggesting that GABAergic dmPAG neurons receive overall strong inhibitory inputs. Taken together, our data demonstrate the usefulness of Sylite to identify target output cells of specific inhibitory neurons and further determine the precise location and size of their synapses.

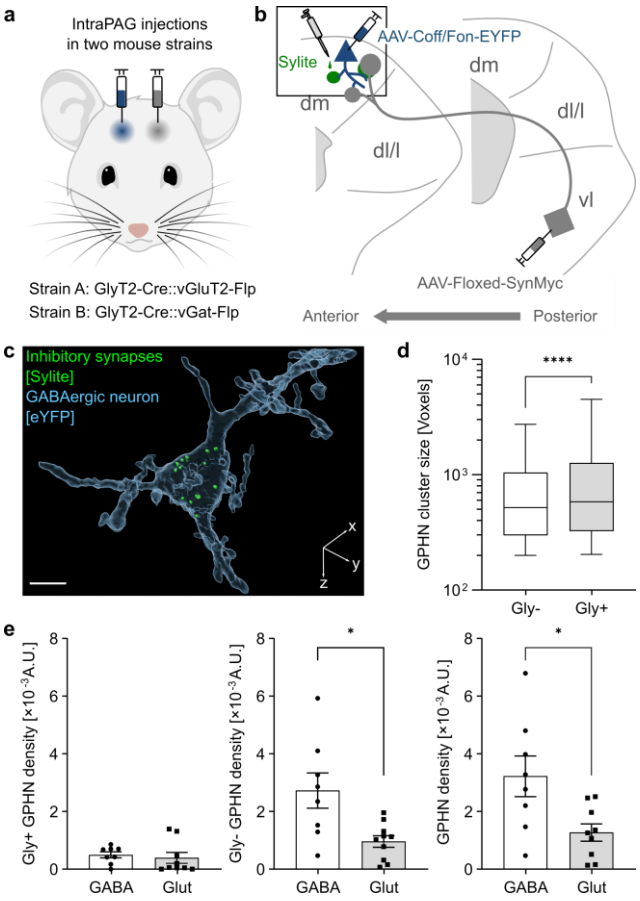

Figure 22¨. Mapping and characterization of inhibitory inputs in the periaqueductal gray. a) GlyT2-Cre::vGluT2-Flp or GlyT2-Cre::vGat-Flp recombinant mice were injected in posterior vlPAG with adeno-associated virus (AAV) carrying a plasmid with Cre recombinase-dependent Synaptophysin-Myc chimera coding region (gray). An additional injection was done in the dmPAG with AAV carrying a plasmid with Cre-off Flippase (Flp) recombinase-on eYFP fluorescent protein coding region (blue). b) Anatomical tracing scheme of the injections and expression localizations in the periaqueductal gray. Glycinergic neurons project from vlPAG to dmPAG (gray). In dmPAG, depending on the mouse genotype, either GABAergic or glutamatergic neurons express soluble eYFP (blue). PAG brain sections from both mice strains were stained with Sylite (green). Box—the region of interest. c) 3D volumetric reconstruction of a single dmPAG GABAergic neuron cell body (light blue, transparent) from a brain section. Multiple gephyrin clusters (green) are found in the soma. Scale bar 10 µm. d) Glycinergic synapses are on average larger than non-glycinergic synapses in dmPAG. Box (25th to 75th percentiles) and whiskers (5th to 95th percentiles) plot representing gephyrin (GPHN) cluster size distribution. Significance determined with unpaired t-test with Welch's correction, P<0.0001. e) Higher inhibitory synapse density is observed in GABAergic neurons in dmPAG. Inhibitory synapse densities: total in-neuron gephyrin volume (voxels) was divided by total neuron volume (voxels) in each tissue section of dmPAG and plotted, mean±SEM. The density of inhibitory synapses having glycinergic input (Gly+) does not differ between GABAergic and glutamatergic neurons (left), while higher non glycinergic (Gly-) synapse density is observed in GABAergic neurons (middle). Total inhibitory synapse density in GABAergic neurons is higher than in glutamatergic neurons (right). Data sets were checked for normality with D'Agostino-Pearson test. A single outlier was removed using Grubbs' method with α=0.05. Significance determined with unpaired t-test with Welch's correction, P<0.05, 8 (4 per animal) brain sections from GlyT2-Cre::vGat-Flp mice and 9 (3 per animal) sections from GlyT2-Cre::vGluT2-Fl mice were used.

3.8. Visualization of inhibitory synapses in living neurons

Visualization of gephyrin and the PSD in living neurons underlies the study of synaptic dynamics like the inhibitory synapse formation and disassembly, and synaptic plasticity[90–92]. The initial designs of gephyrin probes contained cell penetrating entities (Fig. 6A, Fig. 8A), but due to unconvincing live-cell performance (data not shown) I switched the focus to the development of Sylite, an exclusively *post-vivo* affinity probe. However, with a recent advancement in intracellular delivery method of larger molecules[93,94] I decided to revisit live gephyrin probes.

At the core of the novel delivery method stood in situ conjugation of the cargo molecule to an excess of a cell penetrating peptide (CPP) via a disulphide bond, and the application of this reaction mix on a living cell culture. The excess of the CPP would react with the cell membrane and facilitate the penetration of the cargo-CPP conjugate. In turn, the disulphide bond between CPP and the cargo would be reduced in the cytosol, separating the cargo from the CPP, allowing unhindered activity of the cargo molecule within the cell [93,94].

The first iteration of the live probe, Sylite 1.2, repeated Sylite's structure, with an additional PEG linker with an azide for further conjugation of Cy5 (Fig. 8A, Fig. 23, Appendix B), while cysteine retained a free thiol, for in-situ conjugation to a thiol-reactive CPP (Fig. 24, Appendix B). The thiol reactive CPPs, contained a cysteine, with a 5-thio-2-nitrobenzoic acid (TNB) modified thiol. TNB is a good electron withdrawing and leaving group, prevents CPP dimerization that can occur in CPPs with unmodified cysteine, and assures quick and efficient reaction with the free thiol[95] of the probe.

Initial experiments with Sylite 1.2 and CPP_1 showed limited gephyrin labeling efficacy in live mammalian cells expressing eGFP-gephyrin. With 10 µM concentration of Sylite 1.2 partial gephyrin cluster labeling was observed, while with the lower 1 µM concentration the labeling was ineffective (Fig. 25A, Table 2). Thus, I have designed and synthesized two additional live probes, MH1 and MH1peg (Appendix B). MH1, differs from Sylite 1.2 in the slightly different linker design, lack of arginine in the binding sequence and acetylation of the terminal amines (Fig. 23) that decreases the overall probe charge, increases lipophilicity and increases the biological stability[96]. MH1peg is similar to MH1, but has an additional pegylation of the terminal amines (Fig. 23), to further reduce degradation by proteolytic enzymes[97]. Moreover, I synthesized another CPP, CPP_2 (Fig. 24, Appendix B), that has a peg linker between the oligoarginine sequence and the cysteine-TNB, giving the group a flexible handle and thereby increasing its spatial freedom and, likely, the potency.

Table 2. Probe labeling efficiency of gephyrin clusters in HEK293 cells

	Sylite 1.2	CPP1	CPP2		Sylite 1.2	CPP2
30 minutes incubation at RT	1 µM	3,2%	16,1%	30 minutes incubation at 4 °C	1 µM	13,3%
	10 µM	7,4%	36,2%		5 µM	47,5%
	MH1				**MH1**	
	1 µM	21,4%	82,6%		1 µM	41,2%
	5 µM	84,2%	84,1%		2 µM	47,8%
	10 µM	37,7%	59,2%		5 µM	84,6%
	MH1peg				**MH1peg**	
	1 µM	31,8%	82,9%		1 µM	73,1%
	5 µM	90,9%	89,5%		2 µM	65,2%
	10 µM	51,9%	75,3%		5 µM	92,0%

In "%" are shown the colocalization coefficient of gephyrin clusters in the green and the far-red fluorescent channels. I.e., the proportion of the eGFP-gephyrin clusters in the green channel that have corresponding clusters in the far-red channel that are visualized by the probe.

Following experiments showed that all probes performed better in tandem with CPP_2 than with CPP_1 and that MH1 and MH1peg performed better than Sylite 1.2 (Table 2). Additionally, the optimal concentration range for gephyrin staining with CPP_2 is 1-5 µM, with MH1peg labeling about 90% of gephyrin clusters when at 5 µM concentration. Nonetheless, upon incubation of the probes with living cells at room temperature off-target fluorescence was observable, either as diffuse signal or combined with grainy particles (Figures 25-27, panels A,B). Whereas diffuse signal is evidently non-bound probe that diffuses through the cytosol, the grainy fluorescent particles resemble Lysotracker distribution within a cell[98] and imply lysosomal engulfment of the probe. To improve the labeling by reducing the active cell uptake[93,94], I have incubated the living cells with increasing probe concentrations and CPP_2 at 4 °C for 30 minutes and then immediately visualized the cells in fresh DMEM at room temperature. The resulting labeling had visibly less off-target fluorescence, with MH1peg labeling over 90% of gephyrin clusters at 5 µM concentration (Table 2, Figures 25-27, panel C).

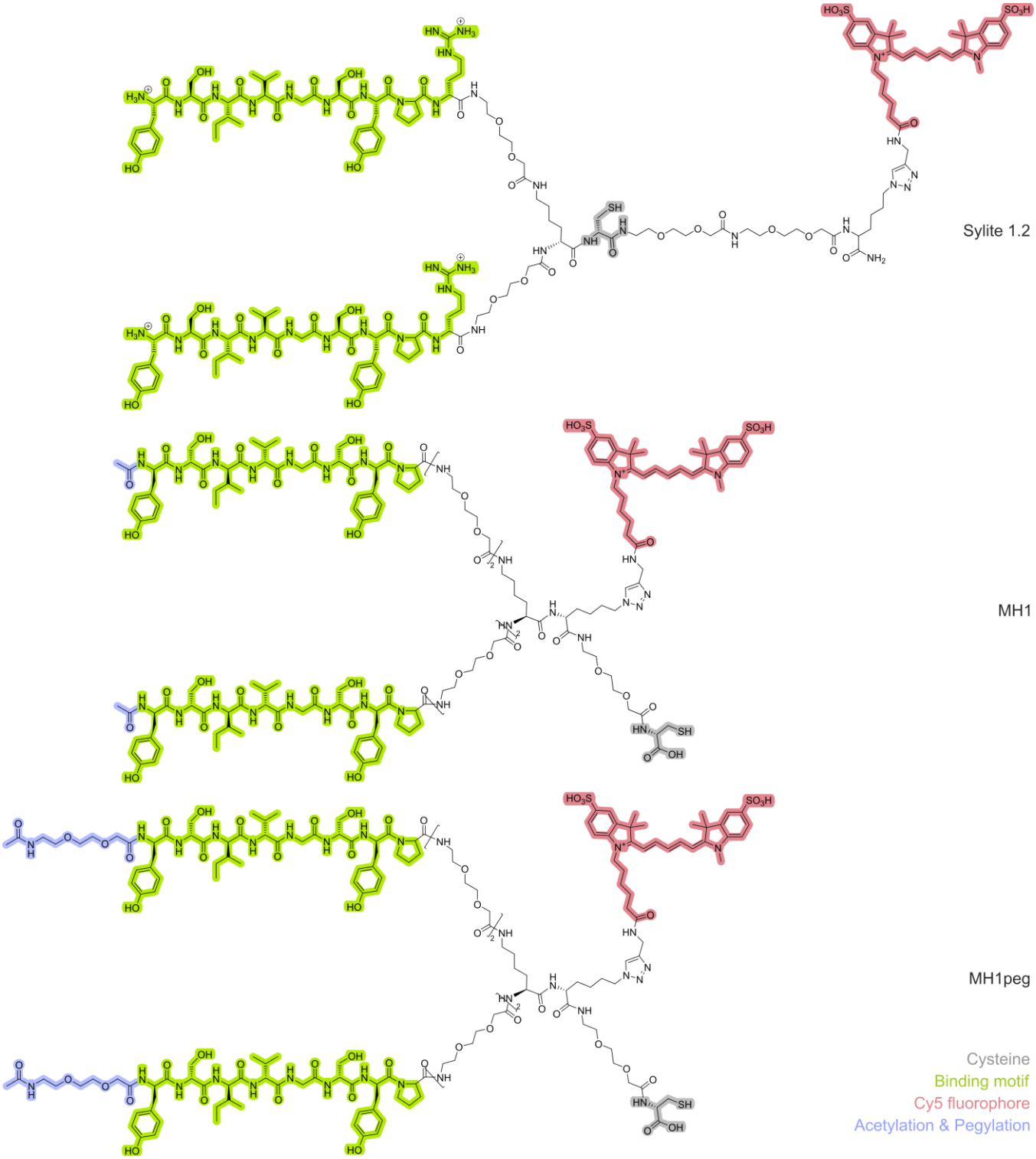

Figure 23. Synthetic probes for in-vivo gephyrin visualization. Sylite 1.2 is a direct derivate of Sylite, with identical binding motifs and linker that connects the peptides. The major difference between Sylite and Sylite 1.2 is the appearance of the PEG spacer after cysteine, along with azido-lysine for subsequent conjugation with sulfo-cyanine 5. Compared to Sylite 1.2, MH1 has shorter binding motifs that lack arginine, but are acetylated at the N-terminal amines, to decrease the overall probe charge. Additionally, MH1 linker structure is different from that of Sylite 1.2. To compensate the lack of arginine in the binding chain there is an additional amino-dioxaoctanoic unit, and the cysteine is not embedded anymore within the linker, potentially giving it more spatial freedom. MH1peg is a modest modification of MH1, having an acetylated peg spacer on the N-terminal amines, to further increase its enzymatic stability towards exopeptidases.

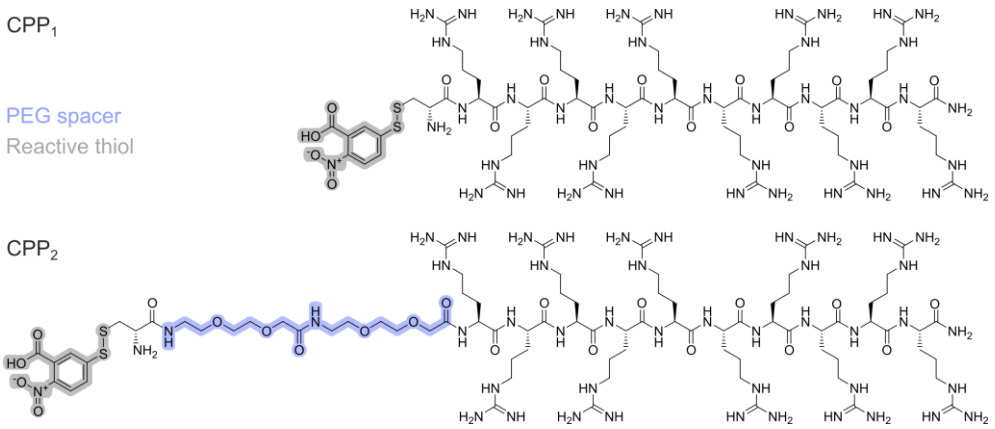

Figure 24. Thiol-reactive cell penetrating peptides. Both CPP_1 and CPP_2 have an oligoarginine motif connected with a TNB-modified cysteine. CPP_2 has a PEG spacer between the arginine motif and the TNB-cysteine, giving it more spatial freedom.

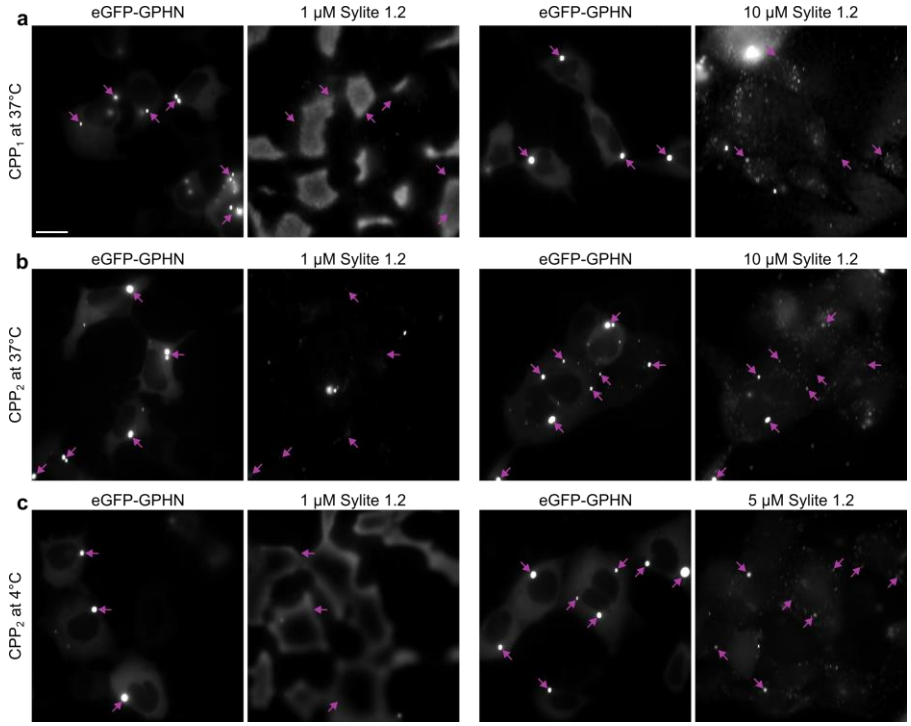

Figure 25. Sylite 1.2 labels gephyrin clusters in living HEK293 cells. Exemplary images of Sylite 1.2 staining of living HEK293 cells expressing eGFP-gephyrin. Scale bar 20 µm. a) After 30 minutes of co-incubation of CPP_1 with Sylite 1.2 at 37 °C the cells were washed and imaged in phenol red free DMEM at RT. Left, at 1 µM concentration Sylite 1.2 appears to associate with the cell membrane and fails to stain the gephyrin clusters. Right, at 10 µM Sylite 1.2 stains some of the gephyrin clusters, significant off-target fluorescence is observable. b) After 30 minutes of co-incubation of CPP_2 with Sylite 1.2 at 37 °C the cells were washed at imaged in phenol red free DMEM at RT. Left, at 1 µM concentration Sylite 1.2 fails to stain gephyrin clusters. Right, at 10 µM Sylite 1.2 stains some of the gephyrin clusters, some off-target fluorescence is observable. c) After 30 minutes of co-incubation of CPP_2 with Sylite 1.2 at 4 °C the cells were washed at imaged in phenol red free DMEM at RT. Left, at 1 µM concentration Sylite 1.2 appears to associate with the cell membrane and fails to stain the gephyrin clusters. Right, at 5 µM Sylite 1.2 stains some of the gephyrin clusters, some off-target fluorescence is observable.

Encouraged by the high degree of gephyrin cluster labeling and good visualization contrast with MH1peg at 5 µM concentration I have continued to the labeling of living wild-type hippocampal neurons. After 30-minute incubation at 4 °C with MH1peg I immediately imaged the cells. Gratifyingly, I observed the characteristic synaptic puncta withing the living neuron, along with strong fluorescence in the axon initial segment in numerous neurons (Fig. 28).

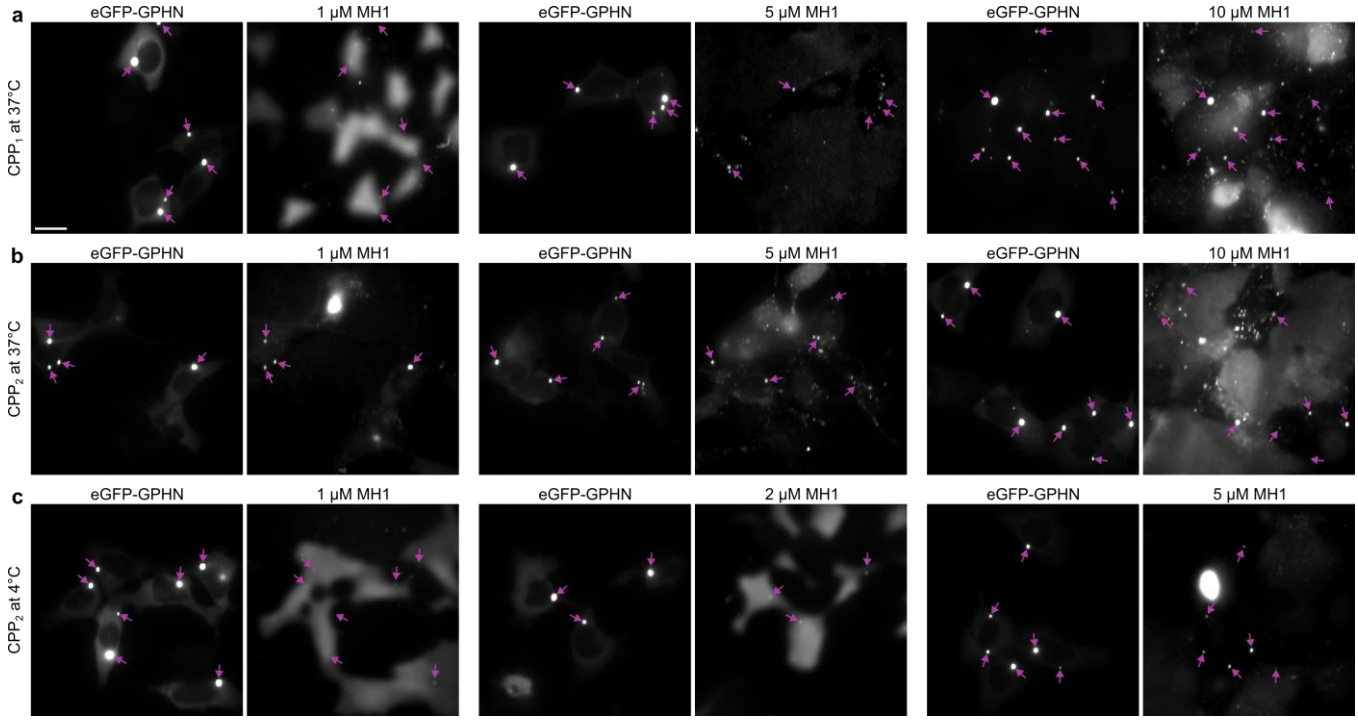

Figure 26. MH1 successfully labels gephyrin clusters in living HEK293 cells. Exemplary images of MH1 staining of living HEK293 cells expressing eGFP-gephyrin. Scale bar 20 µm. a) After 30 minutes of co-incubation of CPP_1 with MH1 at 37 °C the cells were washed and imaged in phenol red free DMEM at RT. Left, at 1 µM concentration MH1 appears to associate with the cell membrane and minimal co-staining of gephyrin clusters is observed. Middle, at 5 µM MH1 stains some of the gephyrin clusters, off-target fluorescence is observable. Right, at 10 µM MH1 gephyrin staining efficiency and visualization contrast increases, along with increase in off-target fluorescence. b) After 30 minutes of co-incubation of CPP_2 with MH1 at 37 °C the cells were washed and imaged in phenol red free DMEM at RT. Left, at 1 µM concentration MH1 successfully stains gephyrin clusters, some off-target fluorescence is observable. Middle, at 5 µM MH1 successfully stains the gephyrin clusters, some increase in off-target fluorescence is observable. Right, at 10 µM MH1 successfully stains gephyrin clusters and visualization contrast increases, along with increase in off-target fluorescence. c) After 30 minutes of co-incubation of CPP_2 with MH1 at 4 °C the cells were washed and imaged in phenol red free DMEM at RT. Left, at 1 µM concentration MH1 appears to associate with the cell membrane minimal co-staining of gephyrin clusters is observed. Middle, increase to 2 µM does not change the staining behavior. Right, at 5 µM MH1 successfully stains the gephyrin clusters, some off-target fluorescence is observable, evidently less than in comparable condition at 37 °C, b) middle panel.

To summarize, gephyrin probes with a free thiol can be delivered within living cells with the help of thiol-reactive cell penetrating peptides. However, the labeling efficiency of the probes appears to be dependent on the probe lipophilicity and, apparently, on its ability to withstand degradation and lysosomal engulfment. Here, MH1peg, the more lipophilic probe with N-teminal pegylation, which helps avoid exopeptidase degradation, performed better. An additional factor in probe efficiency was the CPP. Here CPP_2 with TNB-cysteine on the flexible PEG handle performed better. Lastly, probe application at 4 °C, to avoid active cellular uptake, visually improved the background fluorescence.

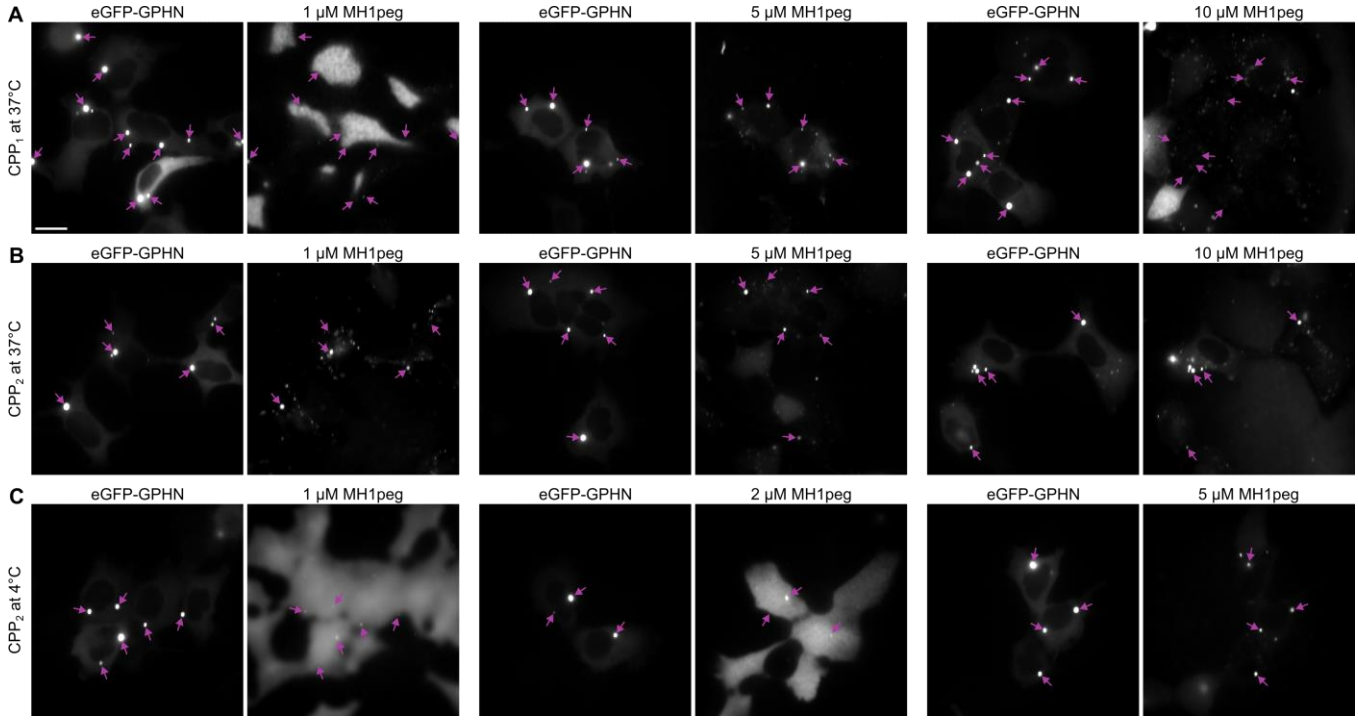

Figure 27. MH1peg successfully labels gephyrin clusters in living HEK293 cells. Exemplary images of MH1peg staining of living HEK293 cells expressing eGFP-gephyrin. Scale bar 20 µm. a) After 30 minutes of co-incubation of CPP_1 with MH1peg at 37 °C the cells were washed and imaged in phenol red free DMEM at RT. Left, at 1 µM concentration MH1peg appears to associate with the cell membrane and minimal co-staining of gephyrin clusters is observed. Middle, at 5 µM MH1peg successfully stains the gephyrin clusters, off-target fluorescence is observable. Right, at 10 µM MH1peg the gephyrin visualization contrast observably drops, due to strong increase in off-target fluorescence and the overall staining efficiency decreases. b) After 30 minutes of co-incubation of CPP_2 with MH1 at 37 °C the cells were washed and imaged in phenol red free DMEM at RT. Left, at 1 µM concentration MH1peg successfully stains the larger gephyrin clusters, off-target fluorescence is observable. Middle, at 5 µM MH1 successfully stains the gephyrin clusters, some off-target fluorescence is observable, however is less noticeable than in previous condition, likely due to increased visualization contrast. Right, at 10 µM MH1 successfully stains gephyrin clusters with good visualization contrast, some off-target fluorescence is noticable. c) After 30 minutes of co-incubation of CPP_2 with MH1 at 4 °C the cells were washed and imaged in phenol red free DMEM at RT. Left, at 1 µM concentration MH1peg appears to associate with the cell membrane minimal co-staining of gephyrin clusters is observed. Middle, increase to 2 µM does not change the staining behavior. Right, at 5 µM MH1peg successfully stains the gephyrin clusters, some off-target fluorescence is observable, evidently less than in comparable condition at 37 °C, b) middle panel.

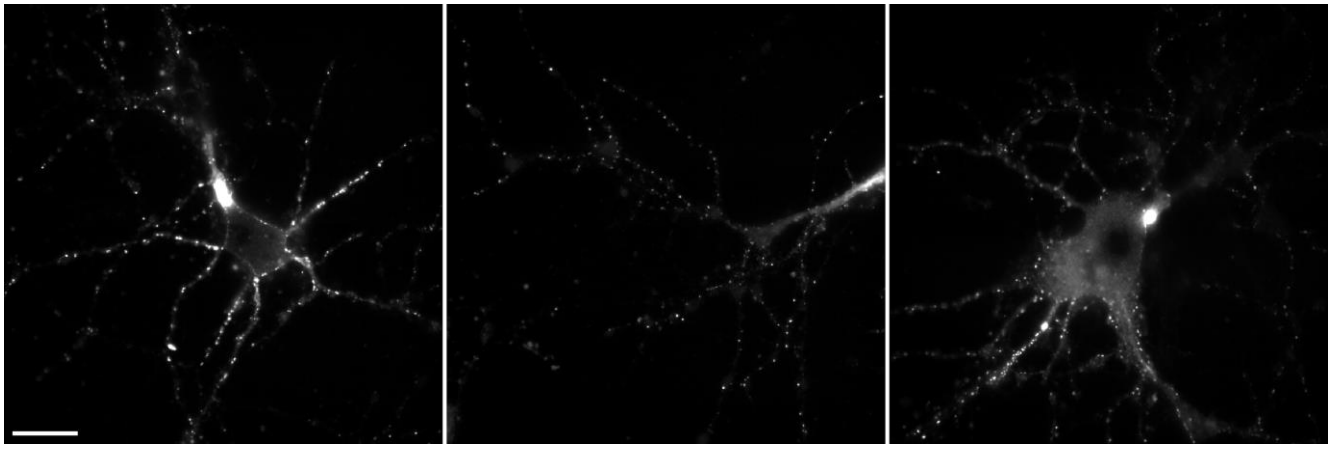

Figure 28. MH1peg visualizes the inhibitory synapses in live wild-type hippocampal neurons. Exemplary images of the primary neurons stained for gephyrin by co-incubation with 5 µM MH1peg and CPP_2 at 4 °C. The cells were washed and imaged in phenol red free DMEM at RT. Characteristic synaptic puncta are observable, alongside with strong fluorescence in the axon initial segment. Scale bar 20 µm.

3.9. A probe derived from NMDA receptor visualizes PSD-95, the hallmark protein of the excitatory PSD

PSD-95 is a member of the membrane-associated guanylate kinase (MAGUK) family of scaffolding proteins. PSD-95 and other MAGUKs participate in the regulation of synaptic composition of receptors, synaptic plasticity, and are responsible for the formation of the PSD. PSD-95 is the prototype of the PSD-95 subfamily of MAGUKs which includes PSD-95, PSD-93, SAP102, and SAP97[99]. These proteins are highly structurally similar, and all contain two closely placed PSD-95/Discs large/Zona occludens-1 (PDZ) domains, and a tridem of another PDZ domain a Src-homology-3 (SH3) domain and a guanylate kinase (GK) domain that form a supramodule involved in the multimerization of single protein molecules[100] (Fig. 29).

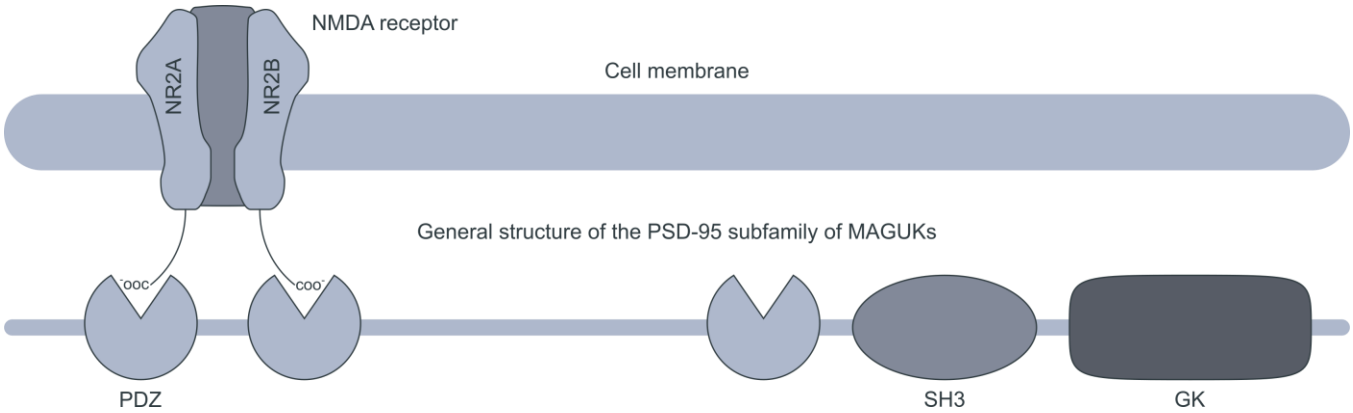

Figure 29. MAGUK PSD-95 subfamily scaffolding proteins share a common structure. PSD-95, PSD-93, SAP102, and SAP97 share a common structure. A tandem of closely placed PDZ domains and a tridem of PDZ, SH3 and GK. Unstructured C-terminals of NMDA glutamate receptor NR2A and NR2B subunits interact with the PDZ domain tandem. PDZ: PSD-95/Discs large/Zona occludens-1; SH3: Src-homology-3; GK: Guanylate Kinase.

A primary function of PSD-95 family of MAGUKs is to bind and stabilize proteins at synapses, like the methyl-D-aspartate (NMDA) glutamate receptor. The PSD-95 PDZ domain tandem directly interacts with the C-terminal "ESDV" motif of the NR2A and NR2B subunits of the NMDR receptor[99]. Commonly, NMDA receptors consist of two NR1 subunits and two NR2 subunits of which there are four types: NR2A, NR2B, NR2C, NR2D. However, synaptic neurotransmission is mediated through NMDA receptors with NR2A and NR2B subunits, but not through NMDARs with NR2C and NR2D, substantiating the tight relationship of NR2A/B with the PDZ domains of synaptic MAGUKs[101]. Furthermore, deletion of the "ESDV" motif or mutations in C-terminal domain within NR2B disrupt surface and synaptic expression of NMDARs[99].

Based on the C-terminal fragment of NR2B subunit various neuroprotective peptide-based compounds are being developed and clinically tested[102,103]. These compounds bind the PDZ domains and inhibit the interaction of PSD-95 family of MAGUKs with NMDA receptors and with neuronal nitric oxide synthase, potentially ameliorating post-stroke effects[103–105]. Yet, no small molecule or peptide-based fluorescent probe for the visualization of excitatory synapses was developed. Therefore, I decided to explore the potential of peptidic compounds derived from NR2A/B, the endogenous ligands of PSD-95, as fluorescent probes.

One of the NR2B derived compounds, UCCB01-125, is a dimeric peptide-based PDZ domain binder. Although this compound is clinically inactive, because it does not penetrate the blood-brain barrier (BBB), it has an exceptional low-nanomolar affinity to PDZ domains[103,105]. Yet, a fluorescent probe, especially an antibody analogue for post-vivo samples, does not have to penetrate the BBB. Based on UCCB01-125, I have designed and synthesized a dimeric fluorescent probe, C5-2xIETAV, with an identical to UCCB01-125 binding motif, but a different amine-functionalized linker which I used for the conjugation of cyanine 5 fluorophore (Fig. 30A, Appendix B). After successful synthesis I tested the probe on mammalian cells that transiently express PSD-95-eGFP (Appendix F) or eGFP, that I fixed and stained with C5-2xIETAV. Gratifyingly, with 10 µM concentration of the probe, I saw

fluorescent signal correlation of the probe with PSD95-eGFP. Furthermore, the probe did not stain the control HEK293 cells expressing soluble eGFP only (Fig. 30B,C).

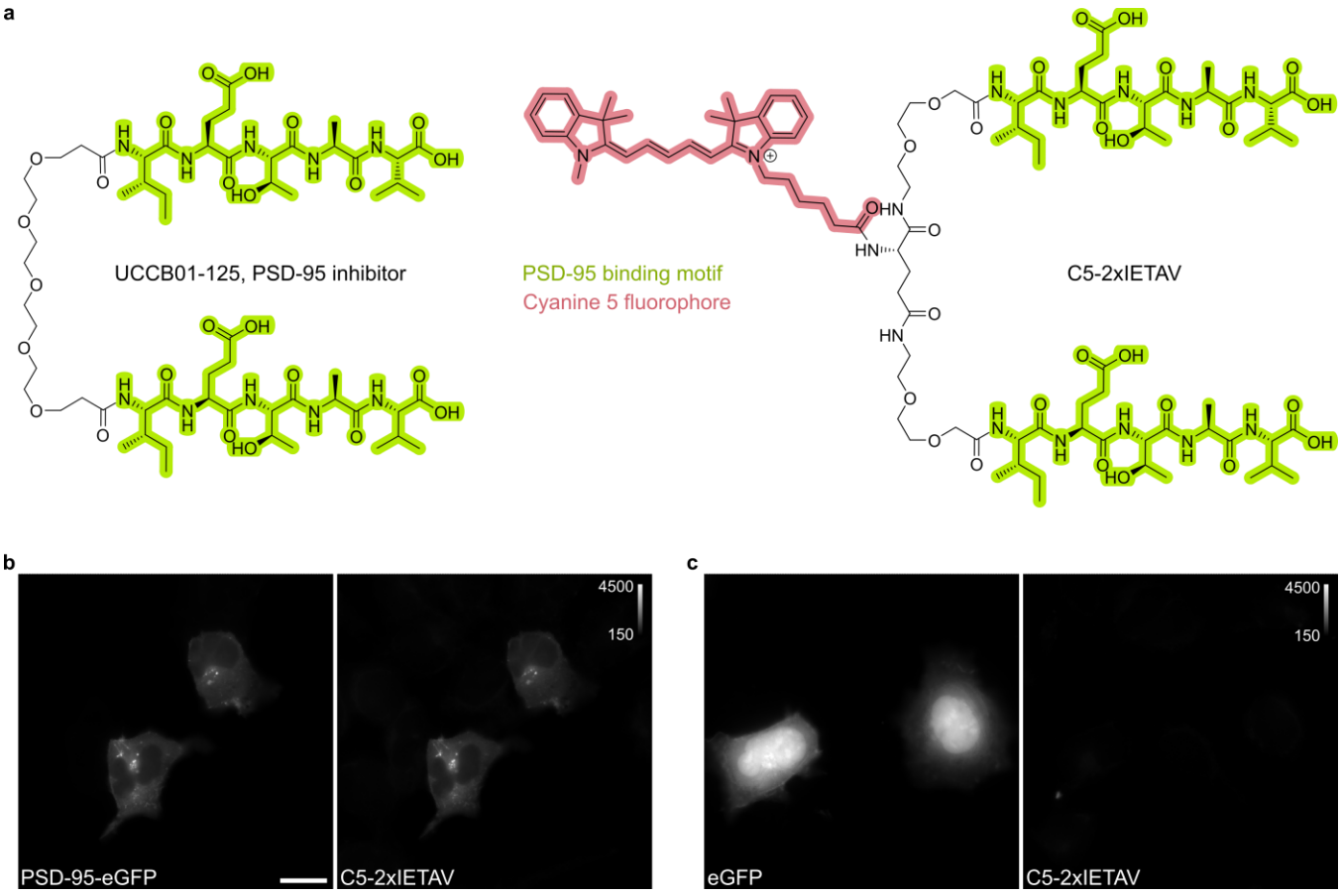

Figure 30. Synthetic dimeric peptide-based probe labels PSD-95. a) Chemical structures of the PSD-95 inhibitor UCCB01-125[103] and the C5-2xIETAV fluorescent probe. Both molecules have identical binding motifs (green), C5-2xIETAV has a slightly different linker and the cyanine 5 fluorophore (red). b-c) HEK293 cells transiently expressing PSD-95-eGFP or soluble eGFP as a control were fixed with 4% PFA and stained with 10 µM of C5-2xIETAV peptidic probe. Scale bar 20 µm. b) The signal of the fluorescent PSD-95 (left) overlaps with the signal of the peptidic probe (right). c) The probe signal is imperceptible (right) and does not correspond to the eGFP signal coming from the soluble eGFP in HEK293 cells (left).

Next, I fixed wild-type hippocampal neurons and co-stained them with 10 µM C5-2xIETAV and with primary PSD-95 antibody and a secondary Alexa555-conjugated antibody. Here, I did not observe notable signal correlation. The characteristic synaptic puncta were visualized with PSD-95 antibody, C5-2xIETAV, however, displayed a different fluorescent signal pattern (Fig. 31). This discrepancy in signal correlation could be explained by the possible higher selectivity of the PSD-95 antibody that was raised against recombinant PDZ domain of PSD-95. The probe on the other hand could interact with multiple PDZ domains of the MAGUK PSD-95 subfamily that the parent compound UCCB01-125 binds to. Additionally, the dye conjugation could further affect the probe selectivity in neurons.

Nevertheless, these initial experiments provide additional proof of principle of probe development from endogenous ligands. With further probe evolution, as was done with Sylite, a selective and effective probe for PSD-95 could be produced. A probe that would visualize the excitatory PSD.

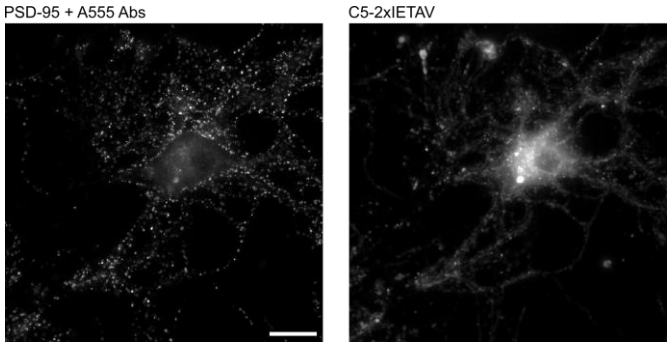

Figure 31. Co-labeling of wild-type neurons with PSD-95 antibody and C5-2xIETAV. The neurons were fixed and stained with PSD-95 antibody (#124011, synaptic systems) together with a secondary Alexa 555 antibody and 10 µM C5-2xIETAV. The fluorescent pattern produced by the antibodies (left) does not match to the pattern produced by the probe. Scale bar 20 µm.

4. Summary and Discussion

The proteins of our cells engage in myriads of interactions with each other, mediating various biological functions. A significant proportion of protein-protein interactions (PPIs) are carried out via “hot-spots” or “hot-segments”, i.e., linear peptide stretches or contiguous segments through which the binding takes place[106]. Both the binding interface and the binding protein fragments are lucrative targets for pharmacological intervention that could modulate PPIs[106–108]. The modulators of these interactions are often derived from the hot-spots and the hot-segments, and therefore are either peptides or peptidomimetics[108].

For neurosciences such compounds are of a particular interest, as they could have a more selective neuropharmacology than the currently available therapeutics[109,110] and also be engineered into novel fluorescent probes suitable for multiplex micro- and nanoscale studies of the brain[6,49].

In this work I have pursued the development of a new fluorescent probe for gephyrin, a hallmark protein of the inhibitory synapse, and described the general strategy for the development of functional probes derived from a “hot-spot” regions of endogenous ligands. Furthermore, I have exemplified the broad applicability of the peptidic probe and its advantages over the conventional affinity probes, the antibodies.

Four decades ago, gephyrin was discovered when it was co-purified with the glycine receptor[111], since then gephyrin became a monumental research topic and its interaction with inhibitory receptors received the due attention. The gephyrin binding motif of the GlyR β subunit was located and thoroughly studied[62,112], the GlyR β binding pocket in the gephyrin E domain was identified[64] and later recognized as a universal binding pocket that interacts with several $GABA_AR$ subunits[24,26]. Anticlimactically, it took twenty years since the discovery of the GlyR β gephyrin binding motif to propose the use of GlyR β derived binders as pharmacological tools for the modulation of inhibitory neurotransmission[65,67]. A pioneering study by Maric et al. explored the use of the GlyR β derived peptide probe as a pharmacological tool and as a fluorescent probe[53]. In a series of proof-of-concept experiments GlyR β derived peptide affected the glycinergic conductivity after its intraneural injection, and when conjugated with 5-carboxytetramethylrhodamine the probe (TMR2i) labelled gephyrin clusters. This work has inspired the rational development of gephyrin probes applied in this study, i.e., the evolution of an endogenous activity-related ligand to a compact synthetic high-affinity binder, probe multimerization for increased avidity, affinity and selectivity, as well as fluorophore screening and tailoring. Our efforts yielded a probe with straightforward and robust labeling delivering high-contrast visualization of inhibitory synapses and versatility of application both in microscopy and nanoscopy.

The potential effect of the hydrophilic-lipophilic balance of the fluorophore on probe performance

Of note, extensive fluorescent probe library synthesis was not the aim of this work, but a means to achieve the aim, i.e., to produce a universally applicable easy-to-use probe for the inhibitory synapses. Nevertheless, interesting insights, like the one below, were the incidental outcome of comparison of the different fluorescent probes.

The GlyR β binding motif was thoroughly profiled with peptide microarrays both in Maric et al. 2017[53] with recombinant gephyrin E domain and in Schulte, Khayenko et al. 2020[66] with native brain gephyrin. Based on these studies I had to my disposal a few potential sequence modifications that contributed to binding in microarray format, which I first applied in a monomeric peptide binder “YSIVGSYPRRRRRRRRR” and then conjugated it to cyanine 5 fluorophore. The probe labeled recombinant gephyrin in mammalian cells, but off-target staining was evident. To determine the cause of the non-selective staining I synthesized probes with the same fluorophore, but with changes in amino acid sequence, and probes with the same sequence, but with different fluorophores. The change of the fluorophore had the strongest effect on the probe staining, and although the modifications of the binding sequence seemingly affected the staining quality, the impact was second to the fluorophore change.

A plausible explanation for this phenomenon is the fluorophores’ hydrophilicity. Cy5, having two “sulfo” groups, is more hydrophilic than cyanine 5, and when conjugated to “YSIVGSYPRRRRRRRRR” the probe had evidently less

off-target staining than the cyanine 5 probe. Furthermore, off-target staining was also evident with perylene monoimide conjugated peptide, this is in line with its reduced hydrophilicity compared to Cy5 (according to logD prediction https://disco.chemaxon.com).

Another example is "NDYSIVGSYPRRRRRR" conjugated to Cy5 or to A647, a more hydrophilic analogue of Cy5 that has two additional "sulfo" groups. A647 conjugated probe needed to be applied in a 10-fold higher concentration than otherwise identical Cy5 probe to see any labeling, and even then it performed worse, by incompletely staining gephyrin in COS-7 cells.

To summarize, empirically, the fluorophore hydrophilic-lipophilic balance proved to be a major determinant of the probe functionality. When comparing molecules with the same basic structure, substitution of cyanine 5 to more hydrophilic Cy5 reduced the off-target labeling, presumably by reducing the unspecific interaction to lipidic components of the cell. Conversely the introduction of an even more hydrophilic A647 reduced the labeling efficiency, perhaps by increasing the interactions with aquatic buffers used in the assays, thereby washing the probe off. Changes in amino acid sequence proved to be less dramatic, as both more hydrophilic "YSIVGSYPRRRRRRRRR" and less hydrophilic "FSIVGSYPRRRRRR" performed equally well when conjugated to Cy5, however, Cy5 - "NDYSIVGSYPRRRRRR" conjugate performed worse than the latter probes, although the peptide's hydrophilicity is in the same range. Here, the N-terminal elongation with amino acids may have negatively impacted the interaction with the binding pocket.

Similarly to monomers, the hydrophilic-lipophilic balance of fluorophores may affect the dimeric probe performance, but in dimers there is an additional variable – the avidity, and since I synthesized a limited number of dimers no robust comparison could be made.

Notwithstanding the effect of hydrophilic-lipophilic balance, unspecific labeling caused by interactions of the three-dimensional structures of the fluorophores to binding sites of indeterminate cellular targets cannot be disregarded. To have a decisive conclusion on the effect of hydrophilic-lipophilic balance of the fluorophores on the performance of gephyrin probes, more probe analogues with the same binding sequence and different fluorophores should be synthesized and applied on cells. At the same time log D, an octanol-water partition coefficient that is used to predict lipophilicity[113] of the different fluorophores should be empirically calculated, and then cross-correlated to the staining performance of the probes.

Dimerization improves gephyrin probe affinity and selectivity through avidity

The probe dimerization mimics the native interaction of the inhibitory receptors to gephyrin[19,67] thereby not only increasing affinity but also selectivity through avidity. The pulldown experiments with the mouse brain lysate corroborated the increased selectivity of the dimer versus the monovalent probe, and the ITC measurements showed an order of magnitude affinity increase of Sylite over SyliteM and confirmed the 1:2 binding stoichiometry to the gephyrin E domain. Furthermore, the *in-silico* model asserted the mode of binding of the dimeric Sylite to the universal binding pocket of gephyrin, has shown simultaneous binding of the dimer to two gephyrin molecules and defined the structural requirements for a dimeric gephyrin probe.

Image analysis of mammalian cells expressing fluorescent gephyrin stained with TMR2i, SyliteM and Sylite was fully in-line with *ex-cellulo* characterization of the probes. SyliteM, the monomeric probe with the optimized binding sequence and the tailored fluorophore showed an order of magnitude improvement of signal-to-background ratio over TMR2i. In turn, Sylite showed another order of magnitude improvement over SyliteM, and an overall 172-fold increase in signal-to-background ratio over TMR2i, and a remarkably low background fluorescence (Fig. 8D) that correlates with the high selectivity of the dimer demonstrated in the pulldown experiment.

Sylite is a universal, selective, functional marker of inhibitory synapses

A very recent study investigated different gephyrin isoforms and their involvement in the formation of inhibitory synapses[58]. The researchers have shown that gephyrin isoforms having an intact E domain form synaptic cluster, while isoforms with altered E-domains, that lose the capacity to form the universal receptor binding pocket[26], display diffuse distribution in neurons and impaired synaptic clustering. Additionally, the researchers noted that

in tissue immunostaining none of the four commercial gephyrin antibodies they used singly labeled all inhibitory synapses.

In contrast to antibodies that are raised against protein fragments that are not necessarily related to specific protein activity, Sylite is a functional probe designed to bind receptor binding competent E domain of gephyrin, labeling gephyrin isoforms that exhibit functional roles in neurons. The gephyrin isoform staining confirms this expectation, with Sylite exclusively labeling isoforms with an intact E domain. My data combined with the aforementioned observations fully support the selectivity of Sylite for synaptic gephyrin, with all its isoform diversity, and thereby for the inhibitory synapses.

Naturally, some skepticism arises regarding the capacity of Sylite to stain the synapses, since it likely competes with the endogenous receptors for gephyrin. However, evidence points to an excess of receptor binding sites on the gephyrin lattice at the PSD[19], additionally Sylite may replace the lower affinity[24] receptor loops from binding pocket. Finally, empirical evidence confirms that Sylite staining colocalizes and correlates with the fluorescently tagged gephyrin (Fig. 15B,D) in neurons and with anti-gephyrin mAb3B11 staining in wild-type neurons (Fig. 14).

High versatility, ease of application and robust tissue staining position Sylite as a valuable alternative to antibodies

Sylite is easily implemented in standard immunostaining protocols for cell or tissue samples, where it can be used complimentary to or instead antibodies, visualizing inhibitory synapses in a one-step application, effectively avoiding the need to use two antibodies to detect inhibitory synapses. Sylite is available as a far-red, Cy5, or as a red, Cy3, conjugate giving spectral range flexibility to the user, and, potentially, other fluorophores could be tailored to the probe.

Sylite, conjugated to the Cy5 fluorophore, is compatible with dSTORM, a single molecule localization microscopy technique with an average resolution of 10-30 nm, the currently best in commonly used super-resolution techniques[55]. Combined with dSTORM Sylite enables nanoscale studies of the inhibitory synapse, such as the pre-to-post synapse distance measurements conducted here.

In tissue, likely due to its small size, Sylite succeeded where antibodies failed. Sylite completely stained synapses through the tissue thickness, achieving full labeling in one hour, while antibody staining required 24 hours and even then, the labeling was localized at tissue extremities, with limited penetration to the middle of the section. Moreover, Sylite does not require complex immunohistochemistry protocols, enabling greatly simplified and accelerated tissue processing without imaging artifacts often observed with antibodies.

Furthermore, our data showed that Sylite can be fully integrated in advanced and multiplexed anatomical tracing techniques that are used to study cell-type- and projection-specific neuronal connectivity, i.e., neuronal circuits. Due to its high labeling efficiency in tissue, Sylite easily visualized the inhibitory postsynaptic densities and provided information on their shapes and sizes, complementing the viral delivery systems that commonly do not provide specific information on the post-synaptic site [4].

Visualization of inhibitory synapses in living neurons

The next major application of Sylites is gephyrin visualization in a living cell. Starting from an identical scaffold of Sylite I have made Sylite 1.2, that had an elongated difunctional linker with an azide and a thiol group. To the azide I've clicked an alkyne modified dye, and the thiol served for in-situ conjugation of thiol-reactive cell penetrating peptide. With the help of the CPP the compound is delivered in the living cell, then the CPP is cleaved in the cytosol from the fluorescent probe. In optimal conditions Sylite 1.2 stained about 45% of the gephyrin clusters, therefore, I have designed more lipophilic and biologically stable derivatives of the probe. Both new probes, MH1 and MH1peg, bested Sylite 1.2, optimally staining about 90% of gephyrin clusters. In turn, MH1peg performed slightly better than MH1, both in terms of labeling efficiency and reduction of background fluorescence. Additionally, in all cases the off-target fluorescence was reduced when the probe was incubated at 4°C with the cells, as at this temperature the active uptake is hampered. When applied on wild-type hippocampal neurons MH1peg showed characteristic synaptic puncta withing the living neuron, along with strong fluorescence in the axon initial segment. Three major conclusions can be drawn from these assays:

a) Probe scaffold that works well in post-vivo samples will not necessarily work well in living cells.

b) Probe lipophilicity increase and N-terminal acetylation and pegylation, which also increase the probe stability, had a positive effect on the probe performance.
c) Although the delivery method that relies on thiol-reactive cell penetrating peptide is not relying on active cell uptake, at physiological conditions the cargo can still be engulfed in lysosomes and other acidic vesicles. Brief probe incubation with the cells at 4°C ameliorates the background fluorescence that appears to originate in lysosomes.
The new fluorescent probes successfully visualize gephyrin in living cells and likely occupy receptor binding sites on gephyrin scaffold, and therefore can be of great value for the study of synaptic dynamics, synaptic transmission and neuropharmacology. Indeed, further probe applications in living neurons will surely lead to new discoveries in the study of the synapse.

Development of new fluorescent probes for PSD-95

Sylite, that visualizes the inhibitory synapse, was a success, yet it was a lone example of a functional fluorescent probe developed from an endogenous ligand of the protein. A potential lead compound for a new peptide-based fluorescent probe that could visualize a different key protein, PSD-95, the scaffolding protein of the excitatory synapse, was UCCB01-125. UCCB01-125 is a dimeric peptidic binder derived from the NMDA receptor, an endogenous ligand of PSD-95, that binds to PDZ domains of the protein.
Based on UCCB01-125 I have designed and synthesized a fluorescent probe, C5-2xIETAV, that successfully visualized PSD-95 in recombinant mammalian cells, in neurons, however, the probe did not perform as I expected. The probe fluorescent signal did not correlate with the signal of the PSD-95 antibody, and I did not observe the characteristic synaptic puncta that were visualized with the antibody. Further evaluation of the probe, desirably in a neuronal model expressing fluorescently tagged PSD-95, could provide further insight into probe functionality. Nevertheless, this probe provides an additional proof of principle that endogenous ligands are a potentially infinite pool for the development of peptide-based probes.
Furthermore, C5-2xIETAV, unlike Sylite, was not developed following a thorough analysis of the binding sequence and no significant probe optimization took place, rather a known binder of PSD-95 was modified with a linker capable of dye-conjugation. I expect that with a comprehensive analysis of the PSD-95 binding sequences from the NMDA receptor an optimized binder can be designed, and with further fluorophore tailoring and extensive *ex-cellulo* and *in-cellulo* evaluation an optimal functional fluorescent peptide-based probe can be put forward.

Through systematic improvements of the binding sequence, fluorescent dye tailoring and dimerization to enable simultaneous attachment to two gephyrin molecules, I produced a selective and affine probe for the inhibitory synapse. Sylite is easily applicable in common immunolabeling assays, has remarkable advantages over antibodies both in selectivity for synaptic gephyrin and in tissue staining and can be used for microscopy or nanoscopy of the inhibitory synapse and the study of neuronal circuits.
Furthermore, by modifying Sylite's binding scaffold and introducing a bi-functional linker with an azide for dye conjugation and a thiol for in-situ functionalization with a thiol-reactive CPP I obtained a probe that efficiently visualizes gephyrin in living cells. This probe opens new avenues for the study of synaptic dynamics and neuropharmacology.
Finally, this work shows with the example of C5-2xIETAV, a fluorescent probe for PSD-95, that Sylite is not an isolated case and other peptidic probes derived from endogenous ligands can be developed. With a comprehensive analysis of PSD-95 binding motifs of NR2A/B, a superior binder can be designed, and with subsequent probe evolution functional synthetic probes for the *post-vivo* and *in-vivo* visualization of excitatory synapses can be produced.

5. Future prospectives and implications

Sylite, an accessible versatile imaging tool for neurosciences

The current "gold standard" for the visualization of inhibitory synapses are antibodies, they however, have certain limitations in immunostaining assays and microscopy. Their first inherent drawback is the lack of selectivity for synaptic gephyrin isoforms, since they bind epitopes that are not necessarily related to protein activity or function. This can result in an incomplete staining of the synapses due to antibody specificity to a sub-population of synaptic gephyrin, or, if the antibody does not distinguish synaptic isoforms, in false-positive detection of "synapses"[54,58]. Their second inherent drawback is their size. Both for super-resolution microscopy and in tissue staining smaller probes are beneficial. In super resolution microscopy the smaller the probe is, the better is the localization precision and the resolution[10,50,114,115], and in tissue staining, the better is the penetration and the target staining. And an additional benefit of using antibody alternatives in tissue staining is the reduction of artifacts from antibody crosslinking and aggregation[9,48].

Sylite overcomes these limitations. Sylite is a synthetic probe 50-fold smaller than an antibody that is selective for synaptic gephyrin isoforms and with proven efficacy in cell and tissue staining and in super resolution microscopy. Sylite's full potential in nanoscopy remains to be uncovered, as it can be used for the inhibitory PSD profiling and evaluation of synaptic strength, e.g., by the counting of the available receptor binding sites, counting of gephyrin molecules or the determination of the volume of the PSD. Furthermore, Sylite is a reliable probe in histochemical assays, as it can label large tissue volumes robustly, quickly and without imaging artifacts often observed with antibodies. These qualities make it invaluable both for fundamental and medical research, like histopathology, where often complex and lengthy tissue processing, which augments antibody staining, is not an option. In this regard, the clinical significance of gephyrin in epilepsy was postulated[116,117] and as it may be involved in other neurological disorders[118] timely research could shed light on epilepsy pathogenesis and possible treatments.

To sum up, Sylite is a powerful, versatile and reliable microscopy tool for neurosciences with an untapped potential. I expect that Sylite will facilitate new findings that could not previously been made because of the limitations of the current fluorescent probes. This, however, will only happen if Sylite becomes broadly available to the scientific community so it can be gradually implemented as a standard label in fluorescent microscopy.

Sylive, a tool for live imaging and pharmacological research

MH1peg, Sylite-derived probe that visualizes gephyrin in living cells is a new means for the study of synaptic dynamics, Sylive. Gephyrin localization, trafficking and its interaction with inhibitory receptors can be studied in genetically unmodified living cells. Furthermore, the impact of occupation of free receptor binding sites, whether the probe competes with glycine or GABA receptors, and the implication of these processes on neurotransmission can and should be evaluated. In perspective, interference in receptor interaction with gephyrin could be a selective way to modulate inhibitory neurotransmission.

Development strategy for new synthetic peptide-based probes

The rational development of peptide-based probes described in this work involves the evolution of an endogenous activity-related ligand to a short peptidic high-affinity binder, probe multimerization for increased avidity, affinity and selectivity, as well as fluorophore screening and tailoring.

The first step in the development of a peptide-based probe is the identification of hot-spots or hot-segments involved in PPIs of the target protein. Often these data is found in reported crystal structures, which can specifically reveal the principles of protein-protein binding modes. Both gephyrin and PSD-95 crystal structures and their models depicting the interaction with ligands[26,105] were of fundamental importance for the development of Sylite and UCCB01-125, that served as a scaffold for the PSD-95 fluorescent probe. Alternatively, the linear motifs involved in interactions can be identified with the help of peptide microarrays, where an entire sequence of a protein is displayed as a library of short (usually 15 to 25 AA) overlapping peptides[119].

Then, after the identification of the hot-spot, a binding sequence profiling takes place, where a core binding sequence is determined and possible affinity-enhancing mutations are explored, this also could be done in a

microarray format[53,66]. Alternatively high-throughput screening of various peptide binders can be performed with high-performance and high-pressure size exclusion chromatography[120].
Next, an architectural and/or chemical modification is done. In case of gephyrin and PSD-95 probes dimerization is beneficial because it allows simultaneous binding to two binding sites[1,105]. For MH1peg additional pegylation and acetylation of terminal amines was done, to increase the lipophilicity and improve biological stability in live cells. Other common peptide binder modifications are stapling (synthetic brace constraining a peptide in a certain conformation), cyclization and introduction of D-amino acids, usually done to improve proteolytic stability and/or cell permeability[108,121].
Finally, fluorophore tailoring needs to be done. As the experience with gephyrin probes showed, fluorophores can significantly impact the performance of peptidic binders, therefore an initial screening can be performed to determine which fluorophore suits better for the probe. As mentioned in the previous section, hydrophilicity (or lipophilicity) of the fluorophore could play a significant role, therefore a good benchmark is to test the same probe scaffold with the cyanine family of fluorophores, as they are all structurally very similar, with cyanine 5 having no sulfo groups, sulfo-cyanine 5 – two, and Alexa647 – four.
Taken together the rational probe development is a valid approach that is potentially applicable to any protein target that has a binding pocket for a hot-spot or a hot-segment of an endogenous ligand. I expect that in the future this approach will gain further popularity and more probes for microscopy and pharmacological applications will be developed.

References

1. Khayenko, V. *et al.* A Versatile Synthetic Affinity Probe Reveals Inhibitory Synapse Ultrastructure and Brain Connectivity**. *Angewandte Chemie International Edition* (2022) doi:10.1002/anie.202202078.
2. Specht, C. G. *et al.* Quantitative nanoscopy of inhibitory synapses: Counting gephyrin molecules and receptor binding sites. *Neuron* **79**, 308–321 (2013).
3. Yang, X., le Corronc, H., Legendre, P., Triller, A. & Specht, C. G. Differential regulation of glycinergic and GABAergic nanocolumns at mixed inhibitory synapses. *EMBO Rep* **22**, (2021).
4. Tovote, P. *et al.* Midbrain circuits for defensive behaviour. *Nature* **534**, 206–212 (2016).
5. Dejanovic, B. *et al.* Changes in the Synaptic Proteome in Tauopathy and Rescue of Tau-Induced Synapse Loss by C1q Antibodies. *Neuron* **100**, 1322-1336.e7 (2018).
6. Choquet, D., Sainlos, M. & Sibarita, J.-B. Advanced imaging and labelling methods to decipher brain cell organization and function. *Nat Rev Neurosci* **22**, 237–255 (2021).
7. Ueda, H. R. *et al.* Whole-Brain Profiling of Cells and Circuits in Mammals by Tissue Clearing and Light-Sheet Microscopy. *Neuron* **106**, 369–387 (2020).
8. Berglund, L. *et al.* A genecentric human protein atlas for expression profiles based on antibodies. *Molecular and Cellular Proteomics* **7**, 2019–2027 (2008).
9. Fornasiero, E. F. & Opazo, F. Super-resolution imaging for cell biologists. *BioEssays* **37**, 436–451 (2015).
10. Lelek, M. *et al.* Single-molecule localization microscopy. *Nature Reviews Methods Primers* **1**, (2021).
11. Fröhlich, F. Microcircuits of the Neocortex. in *Network Neuroscience* (ed. Fröhlich, F.) 85–95 (Elsevier, 2016). doi:10.1016/B978-0-12-801560-5.00007-0.
12. Tovar, K. R. & Westbrook, G. L. Ligand-Gated Ion Channels. in *Cell Physiology Source Book* 549–562 (Elsevier, 2012). doi:10.1016/B978-0-12-387738-3.00031-7.
13. Prescott, S. A. Synaptic Inhibition and Disinhibition in the Spinal Dorsal Horn. in *Progress in Molecular Biology and Translational Science* vol. 131 359–383 (Elsevier B.V., 2015).
14. Thompson, A. J., Lester, H. A. & Lummis, S. C. R. The structural basis of function in Cys-loop receptors. *Q Rev Biophys* **43**, 449–499 (2010).
15. Zeilhofer, H. U., Acuña, M. A., Gingras, J. & Yévenes, G. E. Glycine receptors and glycine transporters: targets for novel analgesics? *Cellular and Molecular Life Sciences* vol. 75 447–465 Preprint at https://doi.org/10.1007/s00018-017-2622-x (2018).
16. Patrizio, A., Renner, M., Pizzarelli, R., Triller, A. & Specht, C. G. Alpha subunit-dependent glycine receptor clustering and regulation of synaptic receptor numbers. *Sci Rep* **7**, 1–11 (2017).
17. Zhu, H. & Gouaux, E. Architecture and assembly mechanism of native glycine receptors. *Nature* **599**, 513–517 (2021).
18. Patrizio, A., Renner, M., Pizzarelli, R., Triller, A. & Specht, C. G. Alpha subunit-dependent glycine receptor clustering and regulation of synaptic receptor numbers. *Sci Rep* **7**, (2017).
19. Specht, C. G. Fractional occupancy of synaptic binding sites and the molecular plasticity of inhibitory synapses. *Neuropharmacology* **169**, 107493 (2020).
20. Turecek, R. & Trussell, L. O. Presynaptic glycine receptors enhance transmitter release at a mammalian central synapse. *Nature* **411**, 587–590 (2001).
21. Mortensen, M., Patel, B. & Smart, T. G. GABA Potency at GABAA Receptors Found in Synaptic and Extrasynaptic Zones. *Front Cell Neurosci* **6**, (2012).
22. Groeneweg, F. L., Trattnig, C., Kuhse, J., Nawrotzki, R. A. & Kirsch, J. Gephyrin: a key regulatory protein of inhibitory synapses and beyond. *Histochem Cell Biol* **150**, 489–508 (2018).
23. Essrich, C., Lorez, M., Benson, J. A., Fritschy, J.-M. & Lüscher, B. Postsynaptic clustering of major GABAA receptor subtypes requires the γ2 subunit and gephyrin. *Nat Neurosci* **1**, 563–571 (1998).

24. Maric, H.-M., Mukherjee, J., Tretter, V., Moss, S. J. & Schindelin, H. Gephyrin-mediated γ-Aminobutyric Acid Type A and Glycine Receptor Clustering Relies on a Common Binding Site. *Journal of Biological Chemistry* **286**, 42105–42114 (2011).
25. Brady, M. L. & Jacob, T. C. Synaptic localization of α5 GABA (A) receptors via gephyrin interaction regulates dendritic outgrowth and spine maturation. *Dev Neurobiol* **75**, 1241–1251 (2015).
26. Maric, H. M. *et al.* Molecular basis of the alternative recruitment of GABAA versus glycine receptors through gephyrin. *Nat Commun* **5**, 5767 (2014).
27. Kowalczyk, S. *et al.* Direct binding of GABAA receptor β2 and β3 subunits to gephyrin. *European Journal of Neuroscience* **37**, 544–554 (2013).
28. Mukherjee, J. *et al.* The Residence Time of GABAARs at Inhibitory Synapses Is Determined by Direct Binding of the Receptor 1 Subunit to Gephyrin. *Journal of Neuroscience* **31**, 14677–14687 (2011).
29. Yamasaki, T., Hoyos-Ramirez, E., Martenson, J. S., Morimoto-Tomita, M. & Tomita, S. GARLH Family Proteins Stabilize GABA A Receptors at Synapses. *Neuron* **93**, 1138-1152.e6 (2017).
30. Crosby, K. C. *et al.* Nanoscale Subsynaptic Domains Underlie the Organization of the Inhibitory Synapse. *Cell Rep* **26**, 3284-3297.e3 (2019).
31. Charrier, C. *et al.* A crosstalk between β1 and β3 integrins controls glycine receptor and gephyrin trafficking at synapses. *Nat Neurosci* **13**, 1388–1395 (2010).
32. Maynard, S. A. *et al.* Identification of a stereotypic molecular arrangement of endogenous glycine receptors at spinal cord synapses. *Elife* **10**, 1–22 (2021).
33. Kasaragod, V. B. & Schindelin, H. Structure–Function Relationships of Glycine and GABAA Receptors and Their Interplay With the Scaffolding Protein Gephyrin. *Front Mol Neurosci* **11**, (2018).
34. Tao, C.-L. *et al.* Differentiation and Characterization of Excitatory and Inhibitory Synapses by Cryo-electron Tomography and Correlative Microscopy. *The Journal of Neuroscience* **38**, 1493–1510 (2018).
35. Bannai, H. *et al.* Bidirectional Control of Synaptic GABAAR Clustering by Glutamate and Calcium. *Cell Rep* **13**, 2768–2780 (2015).
36. Lorenz-Guertin, J. M., Bambino, M. J. & Jacob, T. C. γ2 GABAAR Trafficking and the Consequences of Human Genetic Variation. *Front Cell Neurosci* **12**, (2018).
37. Juge, N., Omote, H. & Moriyama, Y. Vesicular GABA transporter (VGAT) transports β-alanine. *J Neurochem* **127**, 482–486 (2013).
38. Chaudhry, F. A. *et al.* The Vesicular GABA Transporter, VGAT, Localizes to Synaptic Vesicles in Sets of Glycinergic as Well as GABAergic Neurons. *The Journal of Neuroscience* **18**, 9733–9750 (1998).
39. Flores, C. E. *et al.* Activity-dependent inhibitory synapse remodeling through gephyrin phosphorylation. *Proceedings of the National Academy of Sciences* **112**, E65–E72 (2015).
40. Calamai, M. *et al.* Gephyrin Oligomerization Controls GlyR Mobility and Synaptic Clustering. *Journal of Neuroscience* **29**, 7639–7648 (2009).
41. Kim, S. *et al.* Impaired formation of high-order gephyrin oligomers underlies gephyrin dysfunction-associated pathologies. *iScience* **24**, 102037 (2021).
42. Yu, W. *et al.* Gephyrin clustering is required for the stability of GABAergic synapses. *Molecular and Cellular Neuroscience* **36**, 484–500 (2007).
43. Yu, W. & Blas, A. L. D. Gephyrin expression and clustering affects the size of glutamatergic synaptic contacts. *J Neurochem* **104**, 830–845 (2008).
44. Gross, G. G. *et al.* Recombinant Probes for Visualizing Endogenous Synaptic Proteins in Living Neurons. *Neuron* **78**, 971–985 (2013).
45. Feng, G. *et al.* Dual-requirement for gephyrin in glycine receptor clustering and molybdoenzyme activity. *Science (1979)* **282**, 1321–1324 (1998).
46. Bannai, H. *et al.* Activity-Dependent Tuning of Inhibitory Neurotransmission Based on GABAAR Diffusion Dynamics. *Neuron* **62**, 670–682 (2009).

47. Pfeiffer, F., Simler, R., Grenningloh, G. & Betz, H. Monoclonal antibodies and peptide mapping reveal structural similarities between the subunits of the glycine receptor of rat spinal cord. *Proc Natl Acad Sci U S A* **81**, 7224–7227 (1984).
48. Chamma, I. *et al.* Mapping the dynamics and nanoscale organization of synaptic adhesion proteins using monomeric streptavidin. *Nat Commun* **7**, (2016).
49. Khayenko, V. & Maric, H. M. Innovative affinitätsbasierte Markierungen für die High-End-Mikroskopie. *BIOspektrum* **27**, 709–712 (2021).
50. Ries, J., Kaplan, C., Platonova, E., Eghlidi, H. & Ewers, H. A simple, versatile method for GFP-based super-resolution microscopy via nanobodies. *Nat Methods* **9**, 582–584 (2012).
51. Fang, T. *et al.* Nanobody immunostaining for correlated light and electron microscopy with preservation of ultrastructure. *Nat Methods* **15**, 1029–1032 (2018).
52. Dong, J.-X. *et al.* A toolbox of nanobodies developed and validated for use as intrabodies and nanoscale immunolabels in mammalian brain neurons. *Elife* **8**, 1–25 (2019).
53. Maric, H. M. *et al.* Gephyrin-binding peptides visualize postsynaptic sites and modulate neurotransmission. *Nat Chem Biol* **13**, 153–160 (2017).
54. Kuhse, J. *et al.* Phosphorylation of gephyrin in hippocampal neurons by cyclin-dependent kinase CDK5 at Ser-270 is dependent on collybistin. *Journal of Biological Chemistry* **287**, 30952–30966 (2012).
55. Khater, I. M., Nabi, I. R. & Hamarneh, G. A Review of Super-Resolution Single-Molecule Localization Microscopy Cluster Analysis and Quantification Methods. *Patterns* **1**, 100038 (2020).
56. Culley, S., Tosheva, K. L., Matos Pereira, P. & Henriques, R. SRRF: Universal live-cell super-resolution microscopy. *Int J Biochem Cell Biol* **101**, 74–79 (2018).
57. Fritschy, J. M., Harvey, R. J. & Schwarz, G. Gephyrin: where do we stand, where do we go? *Trends Neurosci* **31**, 257–264 (2008).
58. dos Reis, R. *et al.* Complex regulation of Gephyrin splicing is a determinant of inhibitory postsynaptic diversity. *Nat Commun* **13**, 3507 (2022).
59. Tyagarajan, S. K. *et al.* Extracellular signal-regulated kinase and glycogen synthase kinase 3β regulate gephyrin postsynaptic aggregation and GABAergic synaptic function in a calpain-dependent mechanism. *Journal of Biological Chemistry* **288**, 9634–9647 (2013).
60. Tretter, V. *et al.* Molecular basis of the γ-aminobutyric acid a receptor α3 subunit interaction with the clustering protein gephyrin. *Journal of Biological Chemistry* **286**, 37702–37711 (2011).
61. Kasaragod, V. B. & Schindelin, H. Structure of Heteropentameric GABAA Receptors and Receptor-Anchoring Properties of Gephyrin. *Front Mol Neurosci* **12**, (2019).
62. Meyer, G., Kirsch, J., Betz, H. & Langosch, D. Identification of a gephyrin binding motif on the glycine receptor β subunit. *Neuron* **15**, 563–572 (1995).
63. Schrader, N. *et al.* Biochemical Characterization of the High Affinity Binding between the Glycine Receptor and Gephyrin. *Journal of Biological Chemistry* **279**, 18733–18741 (2004).
64. Kim, E. Y. *et al.* Deciphering the structural framework of glycine receptor anchoring by gephyrin. *EMBO J* **25**, 1385–1395 (2006).
65. Maric, H. M. *et al.* Design and Synthesis of High-Affinity Dimeric Inhibitors Targeting the Interactions between Gephyrin and Inhibitory Neurotransmitter Receptors. *Angewandte Chemie International Edition* **54**, n/a-n/a (2014).
66. Schulte, C. *et al.* High-throughput Determination of Protein Affinities using Unmodified Peptide Libraries in Nanomolar Scale. *iScience* 101898 (2020) doi:10.1016/j.isci.2020.101898.
67. Maric, H. M., Kasaragod, V. B. & Schindelin, H. Modulation of gephyrin-glycine receptor affinity by multivalency. *ACS Chem Biol* **9**, 2554–2562 (2014).
68. Frank, R. Spot-synthesis: an easy technique for the positionally addressable, parallel chemical synthesis on a membrane support. *Tetrahedron* **48**, 9217–9232 (1992).

69. Dikmans, A., Beutling, U., Schmeisser, E., Thiele, S. & Frank, R. SC2: A novel process for manufacturing multipurpose high-density chemical microarrays. *QSAR Comb Sci* **25**, 1069–1080 (2006).
70. Brautigam, C. A., Zhao, H., Vargas, C., Keller, S. & Schuck, P. Integration and global analysis of isothermal titration calorimetry data for studying macromolecular interactions. *Nat Protoc* **11**, 882–894 (2016).
71. Raveh, B., London, N. & Schueler-Furman, O. Sub-angstrom modeling of complexes between flexible peptides and globular proteins. *Proteins: Structure, Function and Bioinformatics* **78**, 2029–2040 (2010).
72. Hanus, C., Ehrensperger, M. V. & Triller, A. Activity-dependent movements of postsynaptic scaffolds at inhibitory synapses. *Journal of Neuroscience* **26**, 4586–4595 (2006).
73. Specht, C. G. *et al.* Regulation of glycine receptor diffusion properties and gephyrin interactions by protein kinase C. *EMBO Journal* **30**, 3842–3853 (2011).
74. Heilemann, M. *et al.* Subdiffraction-resolution fluorescence imaging with conventional fluorescent probes. *Angewandte Chemie International Edition* **47**, 6172–6176 (2008).
75. Lampe, A., Haucke, V., Sigrist, S. J., Heilemann, M. & Schmoranzer, J. Multi-colour direct STORM with red emitting carbocyanines. *Biol Cell* **104**, 229–237 (2012).
76. Ester, M., Kriegel, H.-P., Sander, J., Xu, X. & others. A density-based algorithm for discovering clusters in large spatial databases with noise. in *Kdd* vol. 96 226–231 (1996).
77. Schindelin, J. *et al.* Fiji: an open-source platform for biological-image analysis. *Nat Methods* **9**, 676–682 (2012).
78. Bolte, S. & Cordelières, F. P. A guided tour into subcellular colocalization analysis in light microscopy. *J Microsc* **224**, 213–232 (2006).
79. De Chaumont, F. *et al.* Icy: An open bioimage informatics platform for extended reproducible research. *Nat Methods* **9**, 690–696 (2012).
80. Hartley, J. M., Zhang, R., Gudheti, M., Yang, J. & Kopeček, J. Tracking and quantifying polymer therapeutic distribution on a cellular level using 3D dSTORM. *Journal of Controlled Release* **231**, 50–59 (2016).
81. Kaloyanova, S. *et al.* Water-Soluble NIR-Absorbing Rylene Chromophores for Selective Staining of Cellular Organelles. *J Am Chem Soc* **138**, 2881–2884 (2016).
82. Prior, P. *et al.* Primary structure and alternative splice variants of gephyrin, a putative glycine receptor-tubulin linker protein. *Neuron* **8**, 1161–1170 (1992).
83. Pennacchietti, F. *et al.* Nanoscale Molecular Reorganization of the Inhibitory Postsynaptic Density Is a Determinant of GABAergic Synaptic Potentiation. *The Journal of Neuroscience* **37**, 1747–1756 (2017).
84. Tang, A.-H. *et al.* A trans-synaptic nanocolumn aligns neurotransmitter release to receptors. *Nature* **536**, 210–214 (2016).
85. Schneider Gasser, E. M. *et al.* Immunofluorescence in brain sections: Simultaneous detection of presynaptic and postsynaptic proteins in identified neurons. *Nat Protoc* **1**, 1887–1897 (2006).
86. Cappaert, N. L. M., van Strien, N. M. & Witter, M. P. *The rat nervous system.* (Academic Press, 2015). doi:10.1016/B978-0-12-374245-2.00020-6.
87. Santuy, A., Rodríguez, J. R., DeFelipe, J. & Merchán-Pérez, A. Study of the size and shape of synapses in the juvenile rat somatosensory cortex with 3D electron microscopy. *eNeuro* **5**, (2018).
88. Silva, C. & McNaughton, N. Are periaqueductal gray and dorsal raphe the foundation of appetitive and aversive control? A comprehensive review. *Prog Neurobiol* **177**, 33–72 (2019).
89. Kakizaki, T., Sakagami, H., Sakimura, K. & Yanagawa, Y. A glycine transporter 2-Cre knock-in mouse line for glycinergic neuron-specific gene manipulation. *IBRO Rep* **3**, 9–16 (2017).
90. Villa, K. L. *et al.* Inhibitory Synapses Are Repeatedly Assembled and Removed at Persistent Sites In Vivo. *Neuron* **89**, 756–769 (2016).
91. Dobie, F. A. & Craig, A. M. Inhibitory Synapse Dynamics: Coordinated Presynaptic and Postsynaptic Mobility and the Major Contribution of Recycled Vesicles to New Synapse Formation. *Journal of Neuroscience* **31**, 10481–10493 (2011).

92. Wierenga, C. J. Live imaging of inhibitory axons: Synapse formation as a dynamic trial-and-error process. *Brain Res Bull* **129**, 43–49 (2017).
93. Schneider, A. F. L., Benz, L. S., Lehmann, M. & Hackenberger, C. P. R. Cell-Permeable Nanobodies Allow Dual-Color Super-Resolution Microscopy in Untransfected Living Cells. *Angewandte Chemie International Edition* **60**, 22075–22080 (2021).
94. Schneider, A. F. L., Kithil, M., Cardoso, M. C., Lehmann, M. & Hackenberger, C. P. R. Cellular uptake of large biomolecules enabled by cell-surface-reactive cell-penetrating peptide additives. *Nat Chem* **13**, 530–539 (2021).
95. Riddles, P. W., Blakeley, R. L. & Zerner, B. Reassessment of Ellman's reagent. in 49–60 (1983). doi:10.1016/S0076-6879(83)91010-8.
96. Adessi, C. & Soto, C. *Converting a Peptide into a Drug: Strategies to Improve Stability and Bioavailability*. *Current Medicinal Chemistry* vol. 9 (2002).
97. Roberts, M. & Harris, J. *Chemistry for peptide and protein PEGylation*. *Advanced Drug Delivery Reviews* vol. 54 www.elsevier.com/locate/drugdeliv (2002).
98. Pierzyńska-Mach, A., Janowski, P. A. & Dobrucki, J. W. Evaluation of acridine orange, LysoTracker Red, and quinacrine as fluorescent probes for long-term tracking of acidic vesicles. *Cytometry Part A* **85**, 729–737 (2014).
99. Won, S., Levy, J. M., Nicoll, R. A. & Roche, K. W. MAGUKs: multifaceted synaptic organizers. *Current Opinion in Neurobiology* vol. 43 94–101 Preprint at https://doi.org/10.1016/j.conb.2017.01.006 (2017).
100. Ye, F., Zeng, M. & Zhang, M. Mechanisms of MAGUK-mediated cellular junctional complex organization. *Current Opinion in Structural Biology* vol. 48 6–15 Preprint at https://doi.org/10.1016/j.sbi.2017.08.006 (2018).
101. Shiokawa, H., Kaftan, E. J., MacDermott, A. B. & Tong, C. K. NR2 subunits and NMDA receptors on lamina II inhibitory and excitatory interneurons of the mouse dorsal horn. *Mol Pain* **6**, (2010).
102. Hill, M. D. *et al.* Efficacy and safety of nerinetide for the treatment of acute ischaemic stroke (ESCAPE-NA1): a multicentre, double-blind, randomised controlled trial. *The Lancet* **395**, 878–887 (2020).
103. Bach, A. *et al.* Selectivity, efficacy and toxicity studies of UCCB01-144, a dimeric neuroprotective PSD-95 inhibitor. *Neuropharmacology* **150**, 100–111 (2019).
104. Aarts, M. *et al.* Treatment of Ischemic Brain Damage by Perturbing NMDA Receptor- PSD-95 Protein Interactions. *Science (1979)* **298**, 846–850 (2002).
105. Bach, A. *et al.* A high-affinity, dimeric inhibitor of PSD-95 bivalently interacts with PDZ1-2 and protects against ischemic brain damage. *Proceedings of the National Academy of Sciences* **109**, 3317–3322 (2012).
106. London, N., Raveh, B. & Schueler-Furman, O. Druggable protein-protein interactions - from hot spots to hot segments. *Current Opinion in Chemical Biology* vol. 17 952–959 Preprint at https://doi.org/10.1016/j.cbpa.2013.10.011 (2013).
107. Rosell, M. & Fernández-Recio, J. Hot-spot analysis for drug discovery targeting protein-protein interactions. *Expert Opinion on Drug Discovery* vol. 13 327–338 Preprint at https://doi.org/10.1080/17460441.2018.1430763 (2018).
108. Wang, X., Ni, D., Liu, Y. & Lu, S. Rational Design of Peptide-Based Inhibitors Disrupting Protein-Protein Interactions. *Frontiers in Chemistry* vol. 9 Preprint at https://doi.org/10.3389/fchem.2021.682675 (2021).
109. Schulte, C. & Maric, H. M. Expanding GABAAR pharmacology via receptor-associated proteins. *Current Opinion in Pharmacology* vol. 57 98–106 Preprint at https://doi.org/10.1016/j.coph.2021.01.004 (2021).
110. Khayenko, V. & Maric, H. M. Targeting GABAAR-Associated Proteins: New Modulators, Labels and Concepts. *Front Mol Neurosci* **12**, 1–10 (2019).
111. Pfeiffer, F., Graham, D. & Betz, H. Purification by affinity chromatography of the glycine receptor of rat spinal cord. *Journal of Biological Chemistry* **257**, 9389–9393 (1982).
112. Kneussel, M., Hermann, A., Kirsch, J. & Betz, H. Hydrophobic Interactions Mediate Binding of the Glycine Receptor β-Subunit to Gephyrin. *J Neurochem* **72**, 1323–1326 (1999).

113. Hughes, L. D., Rawle, R. J. & Boxer, S. G. Choose Your Label Wisely: Water-Soluble Fluorophores Often Interact with Lipid Bilayers. *PLoS One* **9**, e87649 (2014).
114. Virant, D. *et al.* A peptide tag-specific nanobody enables high-quality labeling for dSTORM imaging. *Nat Commun* **9**, 930 (2018).
115. Sauer, M. Localization microscopy coming of age: from concepts to biological impact. *J Cell Sci* **126**, 3505–3513 (2013).
116. Fang, M. *et al.* Downregulation of gephyrin in temporal lobe epilepsy neurons in humans and a rat model. *Synapse* **65**, 1006–1014 (2011).
117. Förstera, B. *et al.* Irregular RNA splicing curtails postsynaptic gephyrin in the cornu ammonis of patients with epilepsy. *Brain* **133**, 3778–3794 (2010).
118. Tretter, V. *et al.* Gephyrin, the enigmatic organizer at GABAergic synapses. *Front Cell Neurosci* **6**, (2012).
119. Mao, X., Sokpor, G., Staiger, J., Nguyen, H. P. & Tuoc, T. Mapping of domain-mediated protein-protein interaction by SPOT peptide assay. *STAR Protoc* **2**, 100503 (2021).
120. Touti, F., Gates, Z. P., Bandyopadhyay, A., Lautrette, G. & Pentelute, B. L. In-solution enrichment identifies peptide inhibitors of protein–protein interactions. *Nat Chem Biol* **15**, 410–418 (2019).
121. Lau, Y. H., de Andrade, P., Wu, Y. & Spring, D. R. Peptide stapling techniques based on different macrocyclisation chemistries. *Chem Soc Rev* **44**, 91–102 (2015).

Appendix

A. Gephyrin mono- and dimeric binders, microarray sequences

FSIG	FSIVG04K*	FSIVGS09K*	FSIVGSLP02G
FSIK*	FSIVG05K*	FSIVGS10K*	FSIVGSLP03G
FSI01K*	FSIVG06K*	FSIVGS11K*	FSIVGSLP04G
FSI02K*	FSIVG07K*	FSIVGSLG	FSIVGSLP05G
FSI03K*	FSIVG08K*	FSIVGSLK*	FSIVGSLP06G
FSI04K*	FSIVG09K*	FSIVGSL01K*	FSIVGSLP07G
FSI05K*	FSIVG10K*	FSIVGSL02K*	FSIVGSLP08G
FSI06K*	FSIVG11K*	FSIVGSL03K*	FSIVGSLP09G
FSI07K*	FSIVGG	FSIVGSL04K*	FSIVGSLP10G
FSI08K*	FSIVG01G	FSIVGSL05K*	FSIVGSLP11G
FSI09K*	FSIVG02G	FSIVGSL06K*	YSIVGRYPG
FSI10K*	FSIVG03G	FSIVGSL07K*	YSIVGRYPK*
FSI11K*	FSIVG04G	FSIVGSL08K*	YSIVGRYP01K*
FSIVG	FSIVG05G	FSIVGSL09K*	YSIVGRYP02K*
FSIVK*	FSIVG06G	FSIVGSL10K*	YSIVGRYP03K*
FSIV01K*	FSIVG07G	FSIVGSL11K*	YSIVGRYP04K*
FSIV02K*	FSIVG08G	FSIVGSLPK*	YSIVGRYP05K*
FSIV03K*	FSIVG09G	FSIVGSLP01K*	YSIVGRYP06K*
FSIV04K*	FSIVG10G	FSIVGSLP02K*	YSIVGRYP07K*
FSIV05K*	FSIVG11G	FSIVGSLP03K*	YSIVGRYP08K*
FSIV06K*	FSIVGSG	FSIVGSLP04K*	YSIVGRYP09K*
FSIV07K*	FSIVGSK*	FSIVGSLP05K*	YSIVGRYP10K*
FSIV08K*	FSIVGS01K*	FSIVGSLP06K*	YSIVGRYP11K*
FSIV09K*	FSIVGS02K*	FSIVGSLP07K*	
FSIV10K*	FSIVGS03K*	FSIVGSLP08K*	
FSIV11K*	FSIVGS04K*	FSIVGSLP09K*	
FSIVGK*	FSIVGS05K*	FSIVGSLP10K*	
FSIVG01K*	FSIVGS06K*	FSIVGSLP11K*	
FSIVG02K*	FSIVGS07K*	FSIVGSLPG	
FSIVG03K*	FSIVGS08K*	FSIVGSLP01G	

B. LC-MS profiling of peptide probes

VK7: Cyanine5-YSIVGSYPRRRRRRRRR

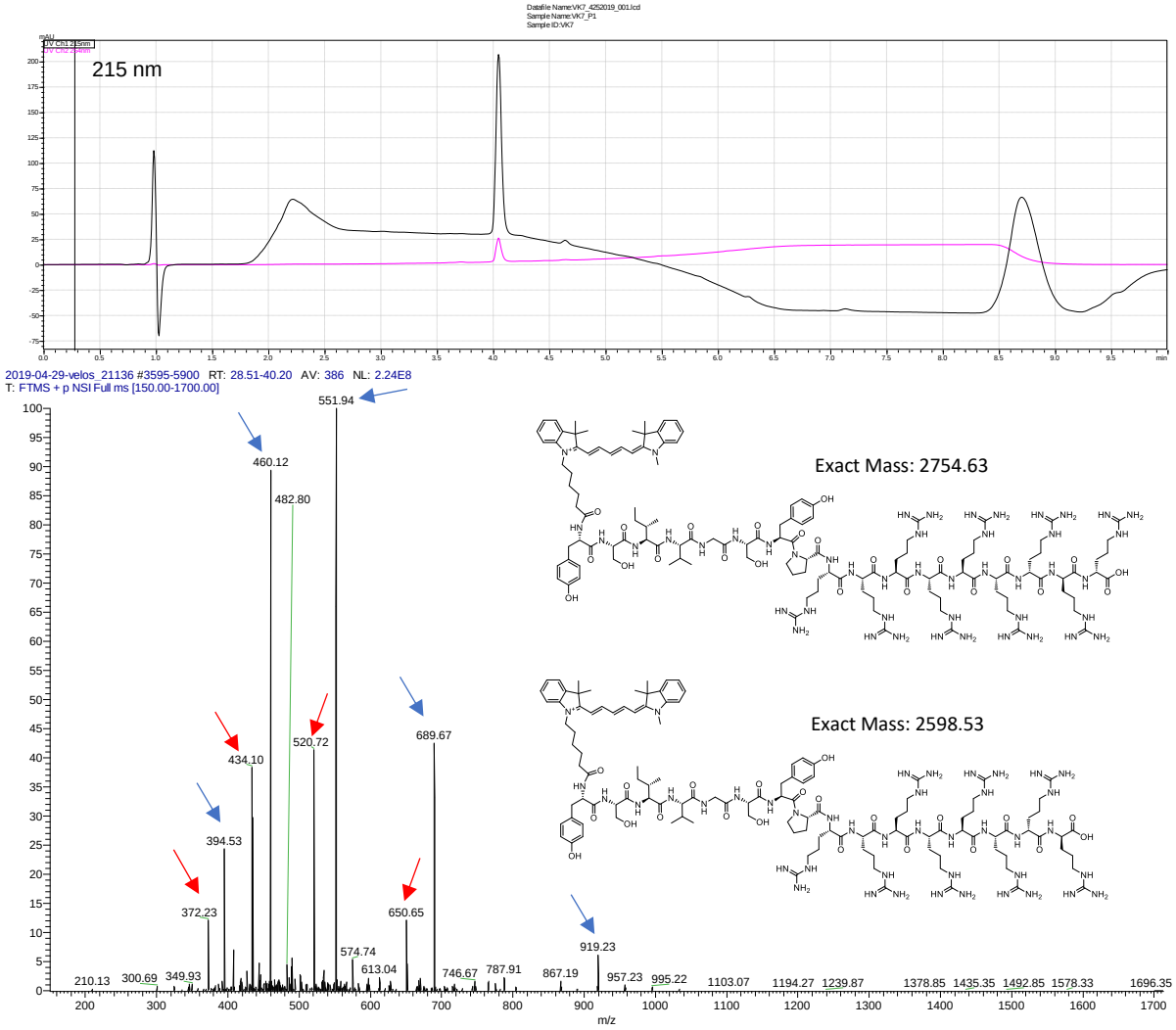

The peptide YSIVGSYPRRRRRRRRR (9 arginines) was purchased from ChinaPeptides with noted 95% purity and used directly for further conjugation with fluorophores. Post hoc MS analysis showed the presence of the expected product (blue arrows) with a less abundant YSIVGSYPRRRRRRRR fluorophore conjugated peptide (8 arginines, red arrows).

VK10: Cyanine5-YSIVGSYPR

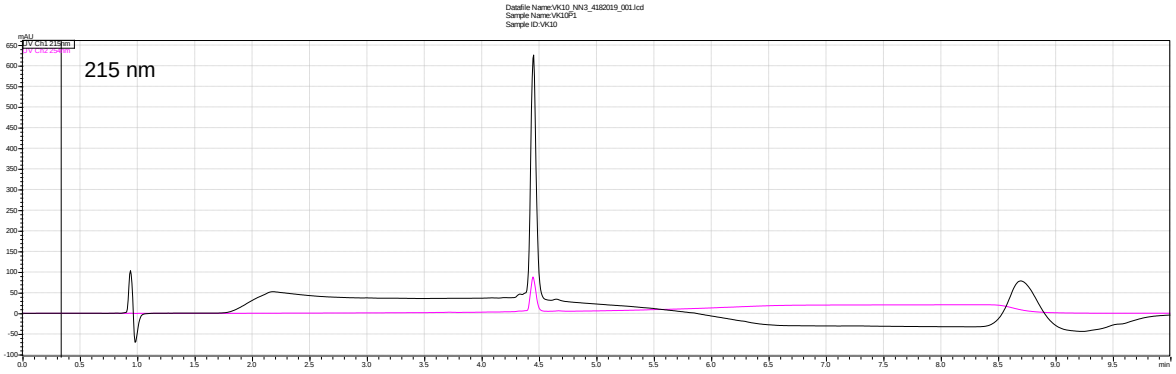

2019-04-24-velos_21105 #4767-5146 RT: 39.45-41.49 AV: 71 NL: 5.88E8
T: FTMS + p NSI Full ms [150.00-1700.00]

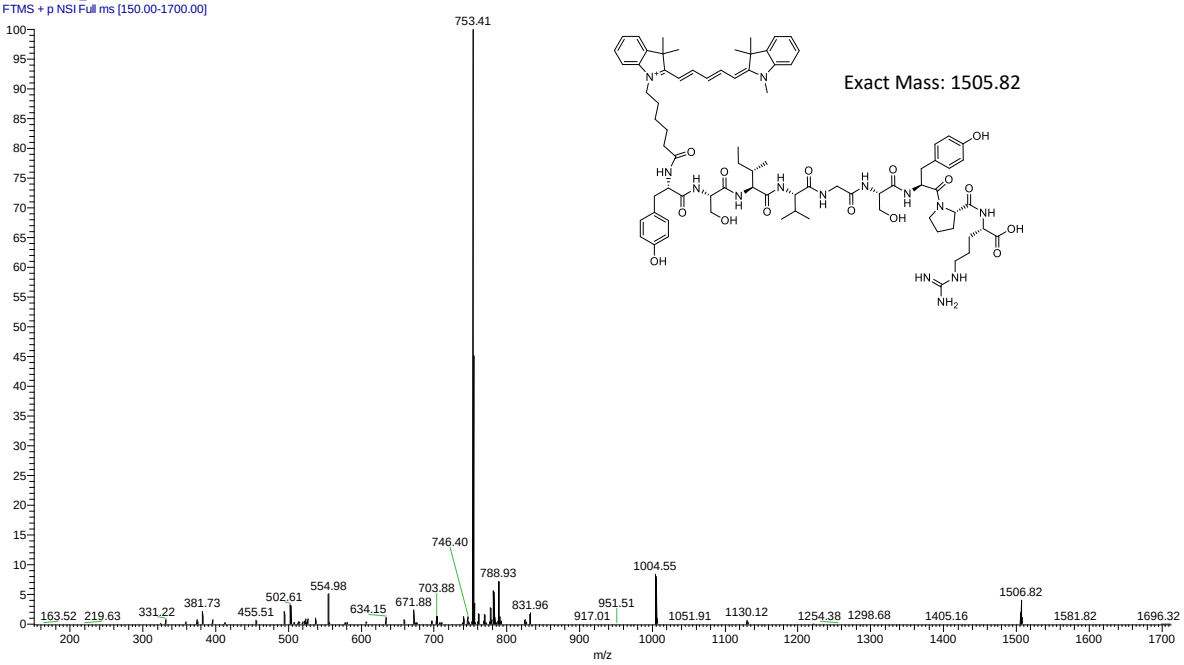

VK11: Perylene monoimide-YSIVGSYPRRRRRRRRR

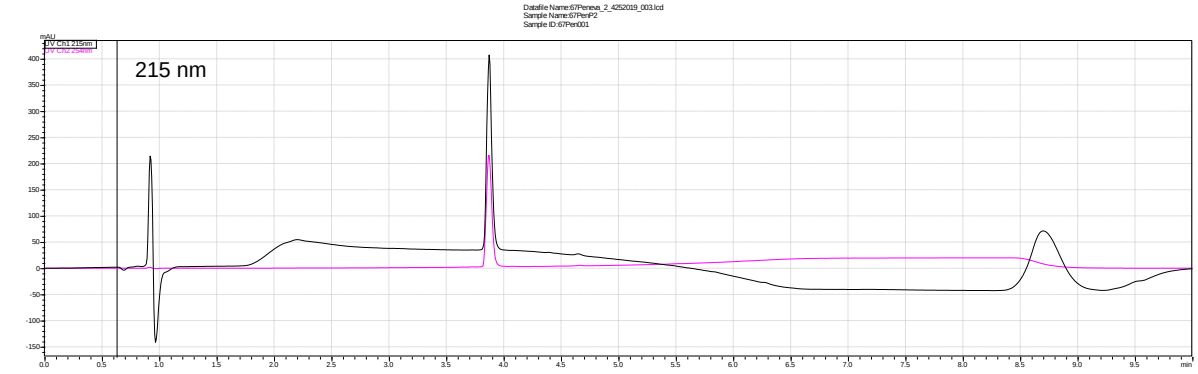

2019-04-29-velos_21133 #4258-5218 RT: 35.09-40.01 AV: 160 NL: 1.21E8
T: FTMS + p NSI Full ms [150.00-1700.00]

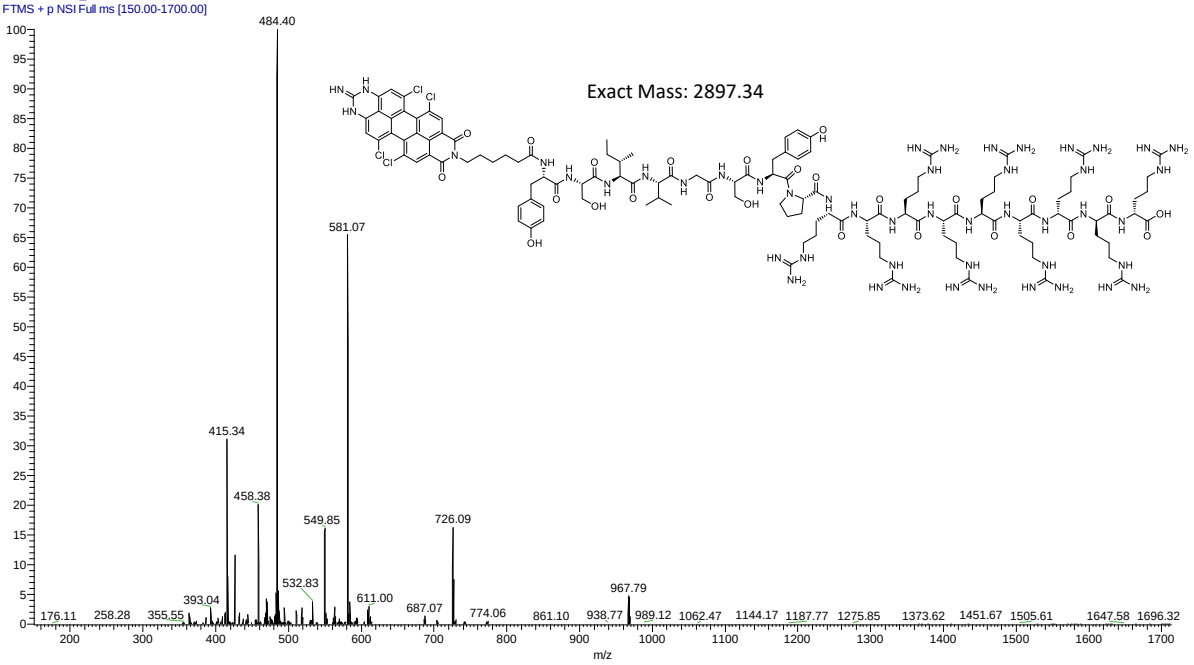

VK13: Cyanine5-FSIVGSYP6R

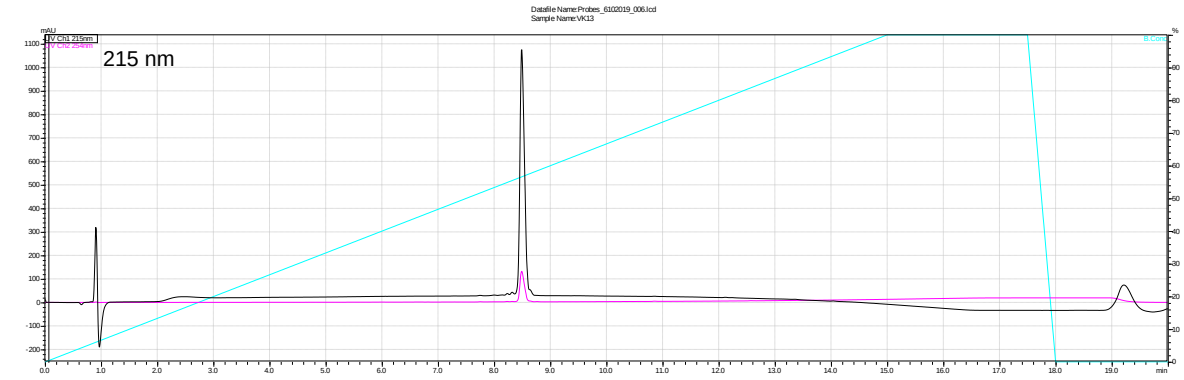

2019-06-11-velos_21409 #4201-5202 RT: 34.94-40.24 AV: 175 NL: 3.51E8
T: FTMS + p NSI Full ms [150.00-1700.00]

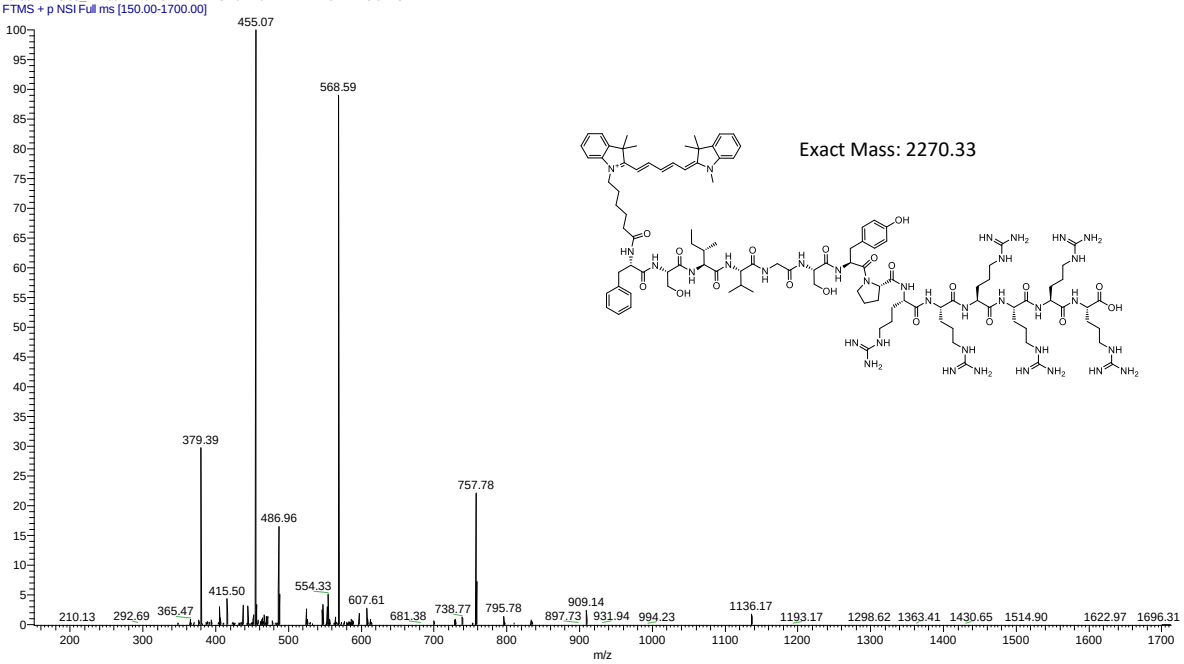

VK14: Sulfo-cyanine5-YSIVGSYP9R

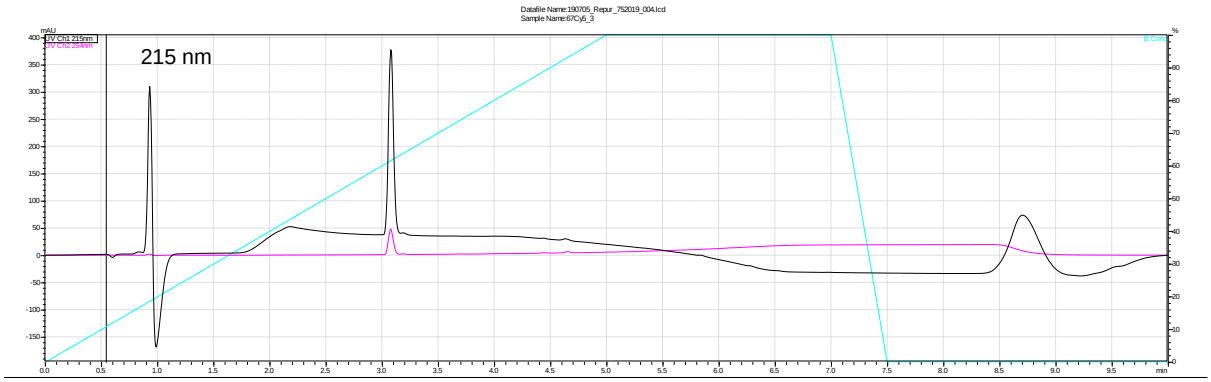

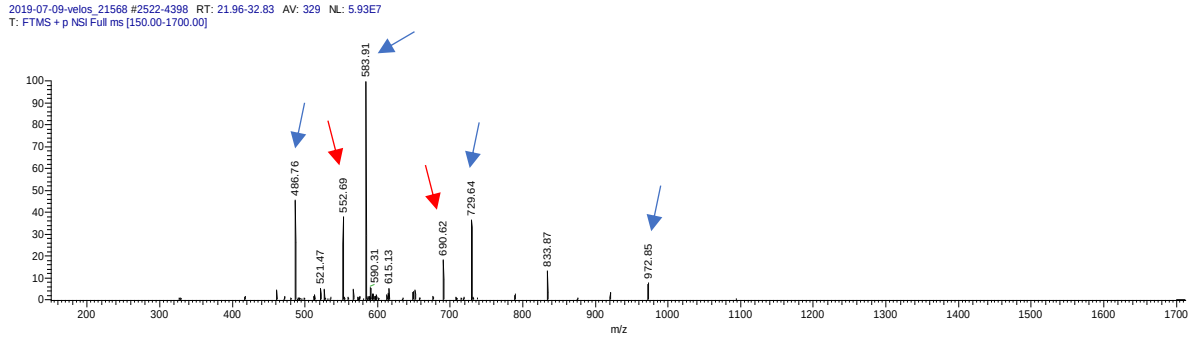

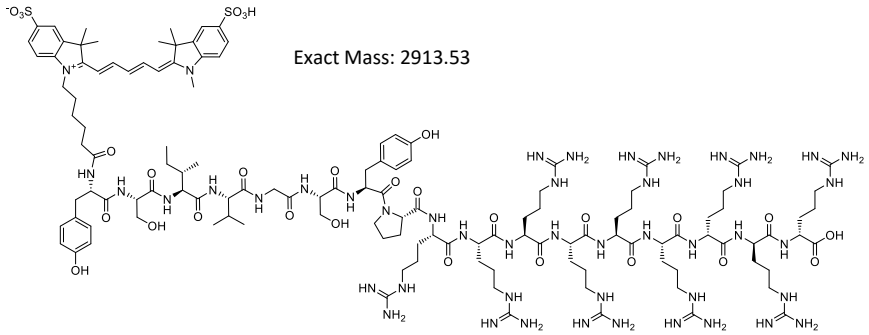

Exact Mass: 2913.53

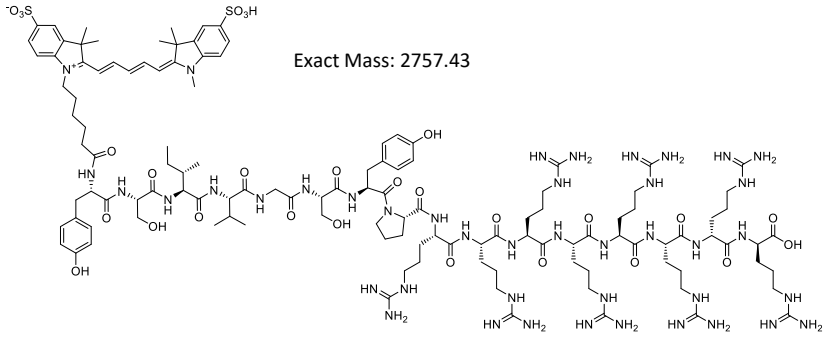

Exact Mass: 2757.43

The peptide YSIVGSYPRRRRRRRRR (9 arginines) was purchased from ChinaPeptides with noted 95% purity and used directly for further conjugation with fluorophores. Post hoc MS analysis showed the presence of the expected product (blue arrows) and minor presence of YSIVGSYPRRRRRRRR fluorophore conjugated peptide (8 arginines, red arrows).

SyliteM: Sulfo-cyanine5-FSIVGSYP6R

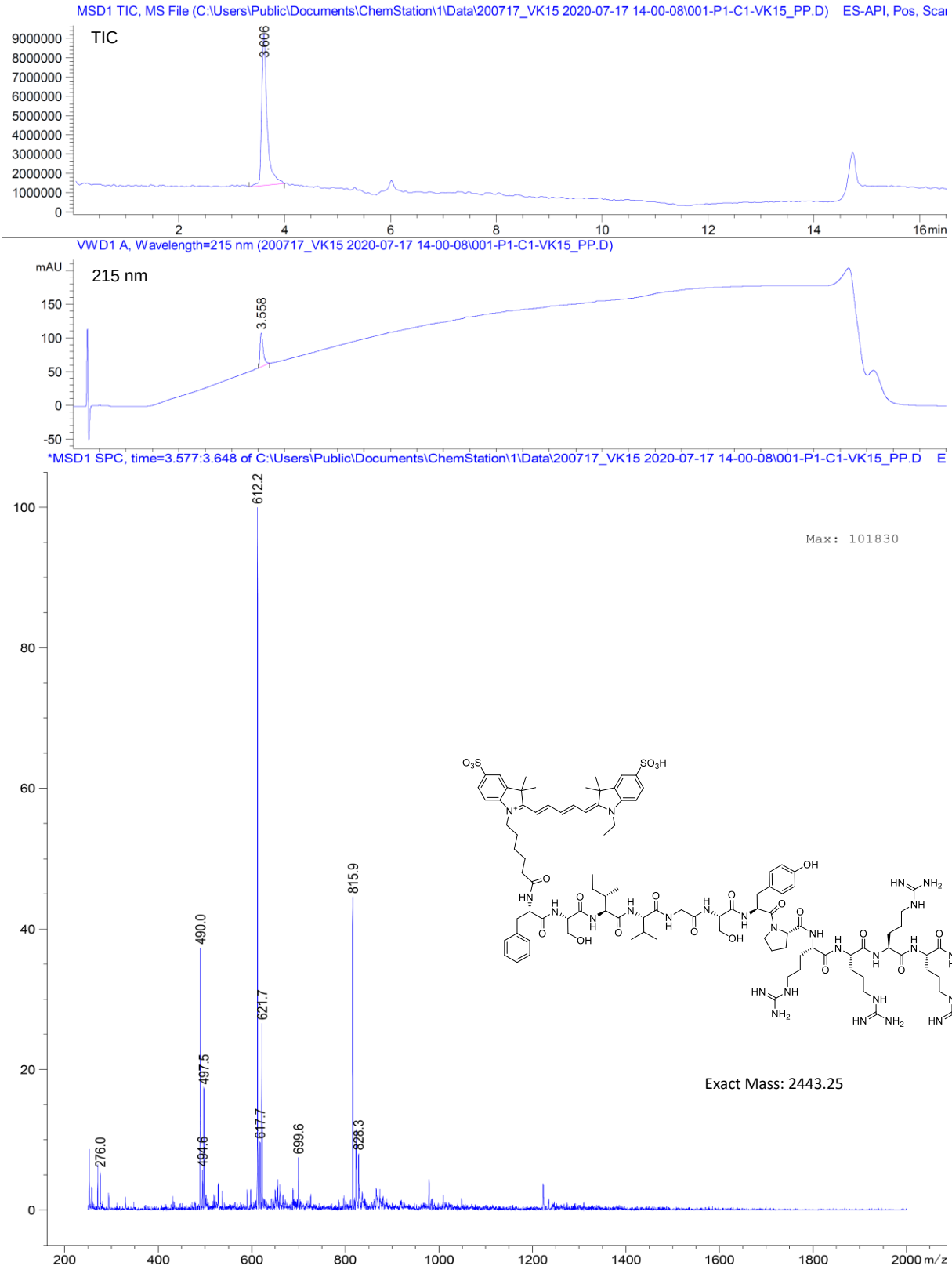

Exact Mass: 2443.25

Sylite (Cy5)

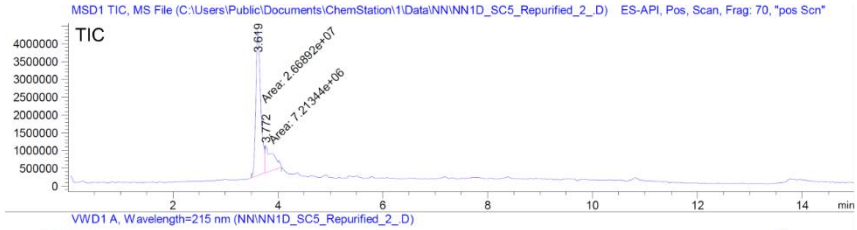

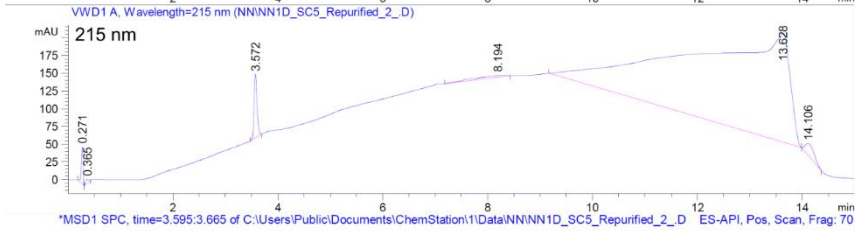

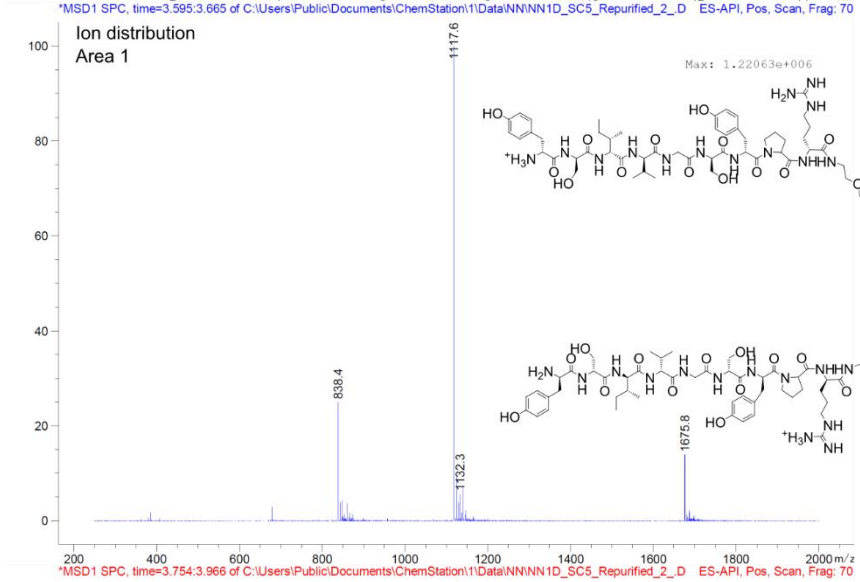

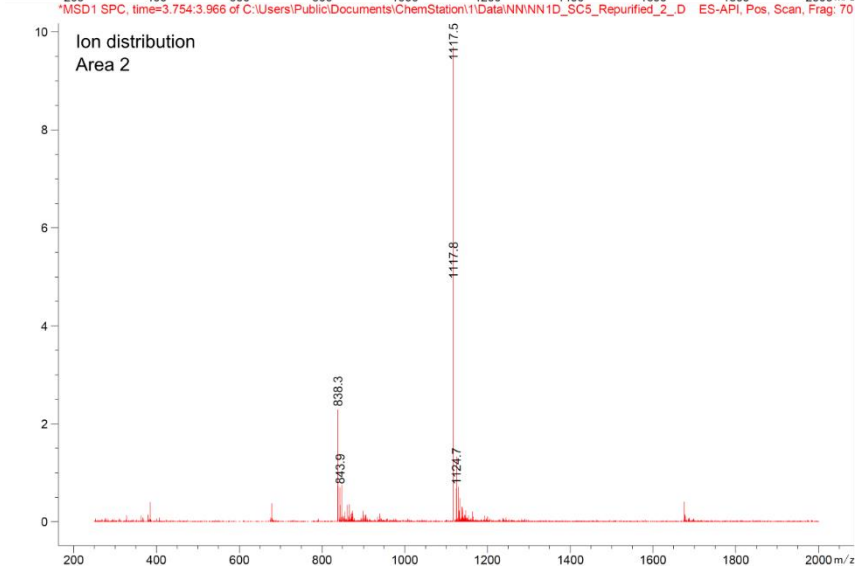

Molecular weight: 3352,89

SyliteCy3

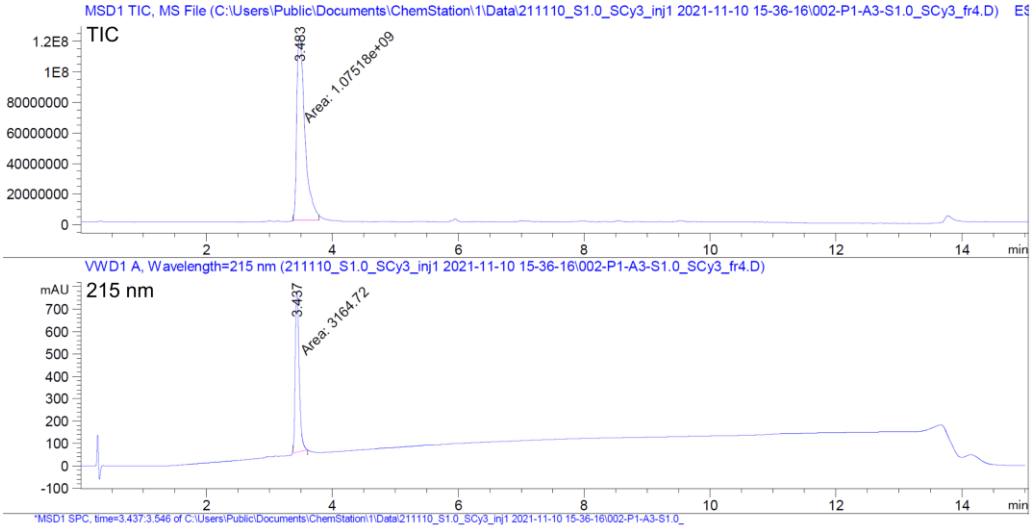

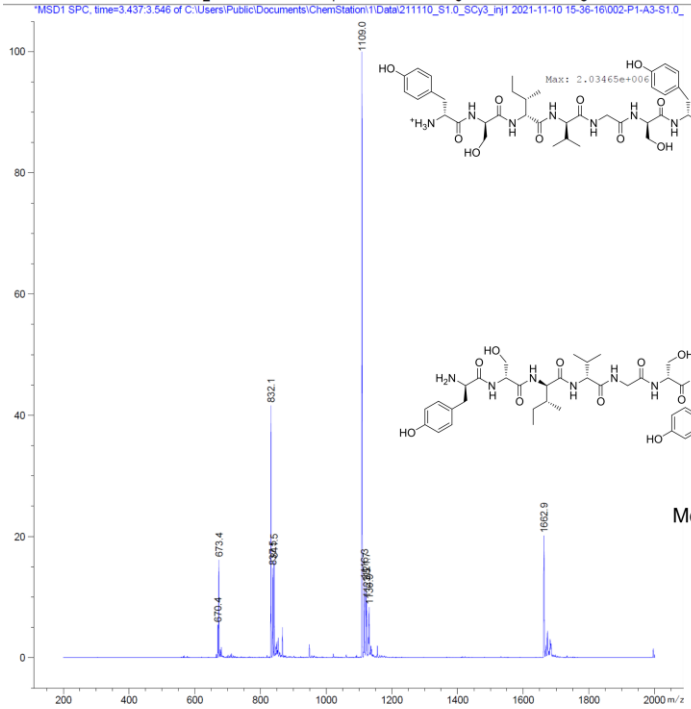

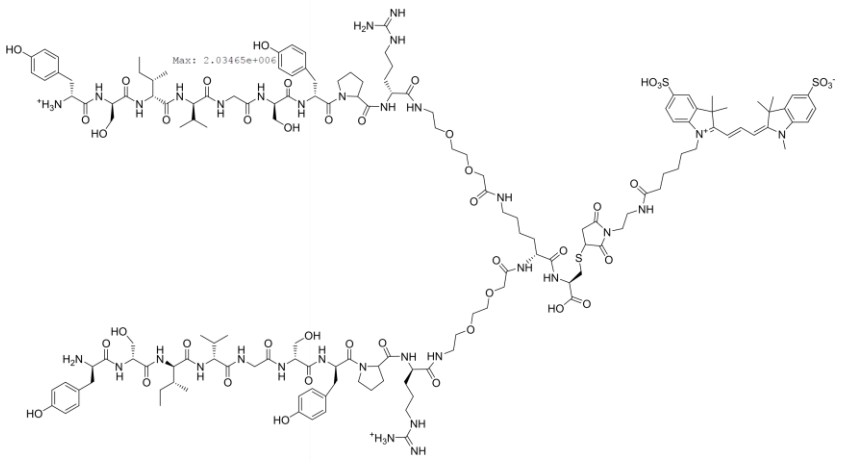

Molecular Weight: 3326.85

C5-2xIETAV – PSD-95 binding fluorescent probe

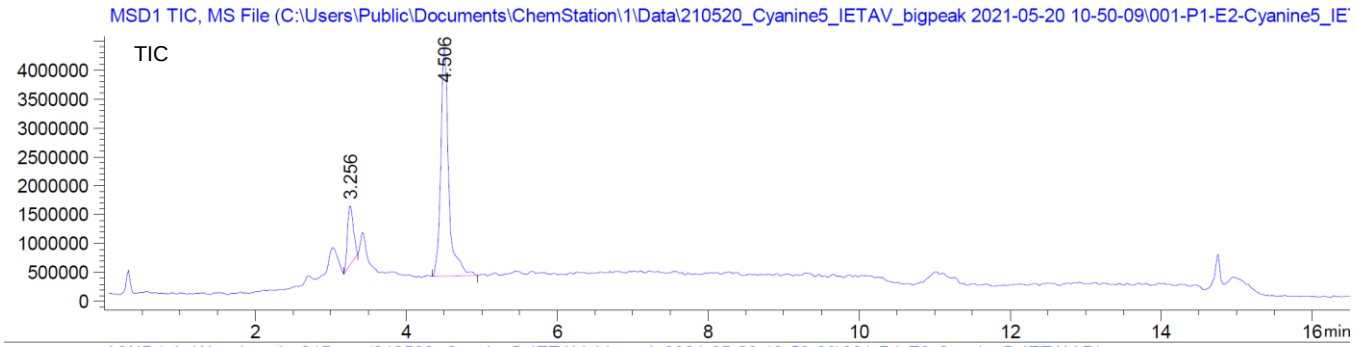

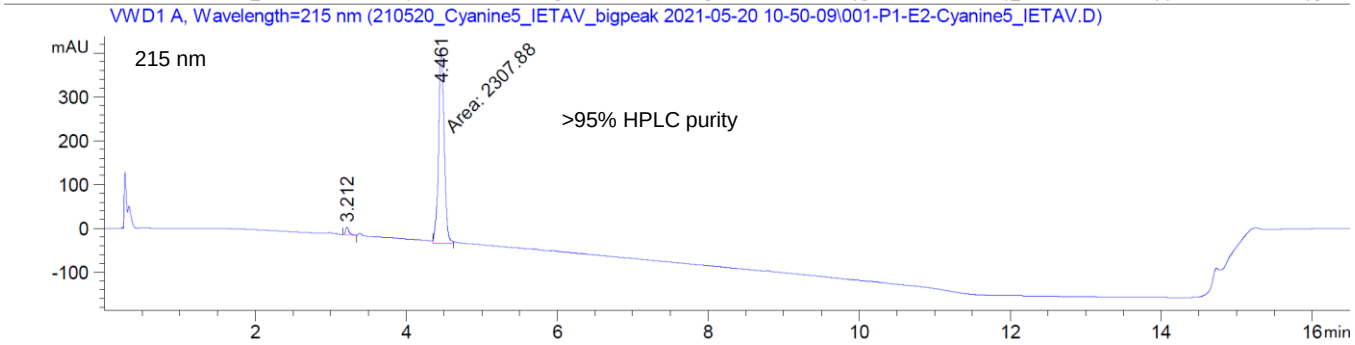

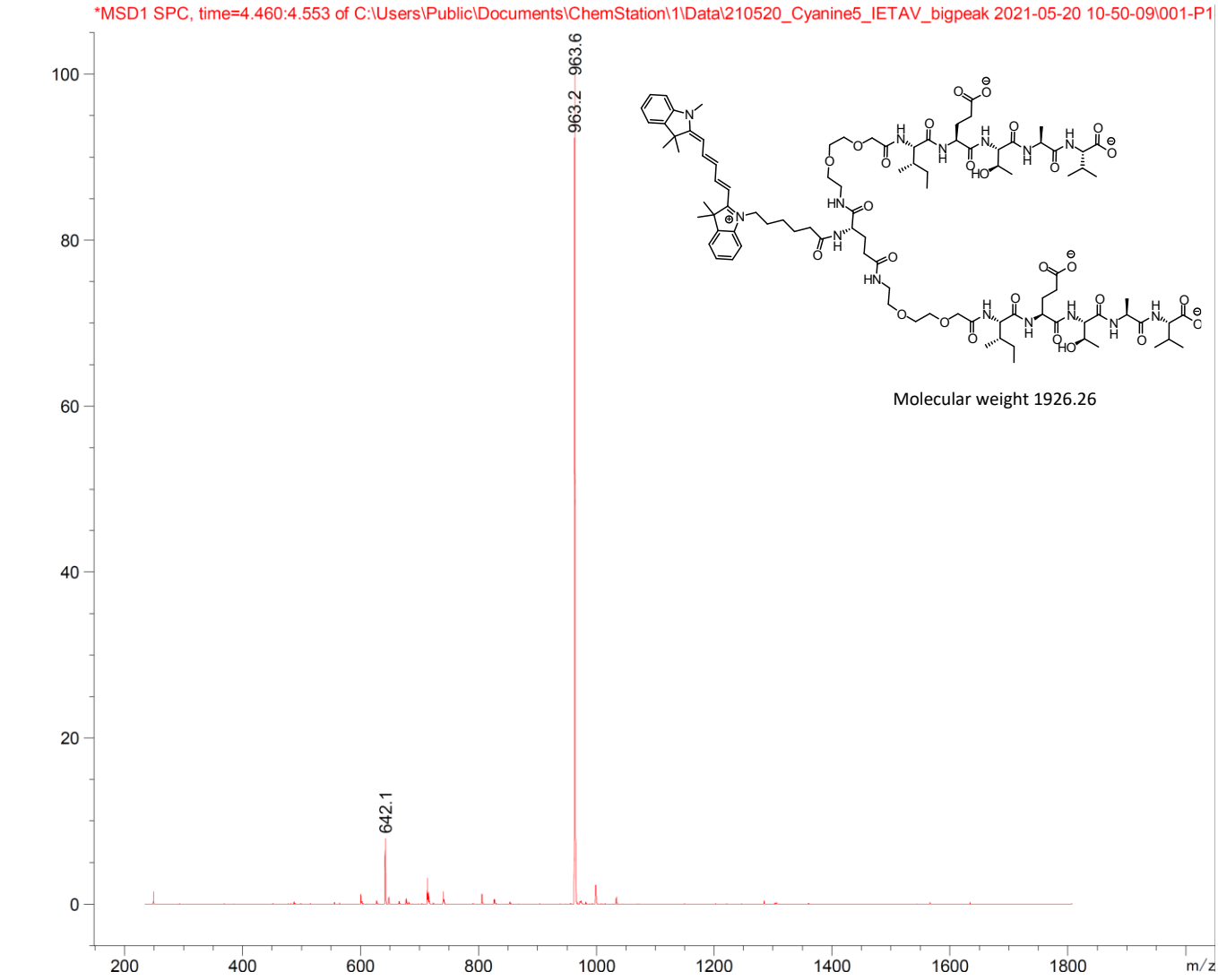

Molecular weight 1926.26

TNB-CPP – thiol reactive cell penetrating peptide (CPP)

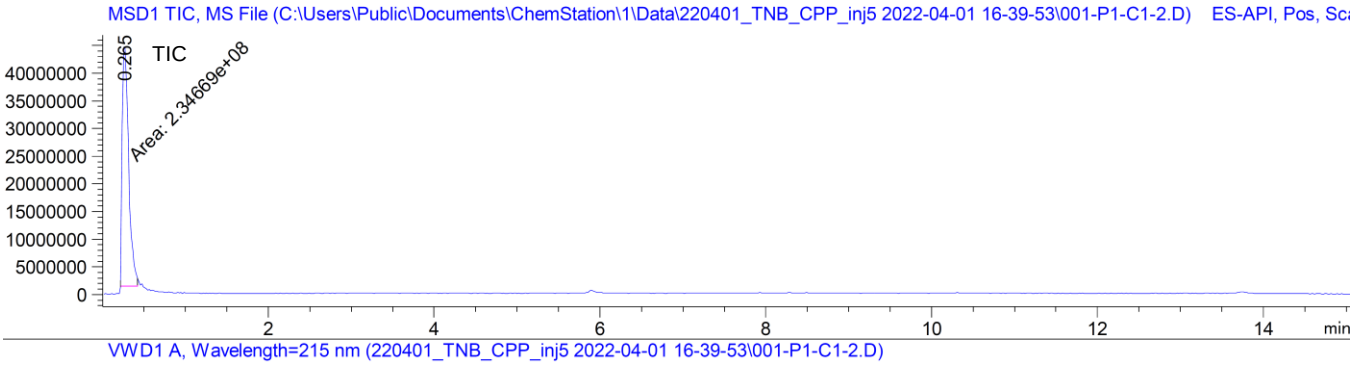

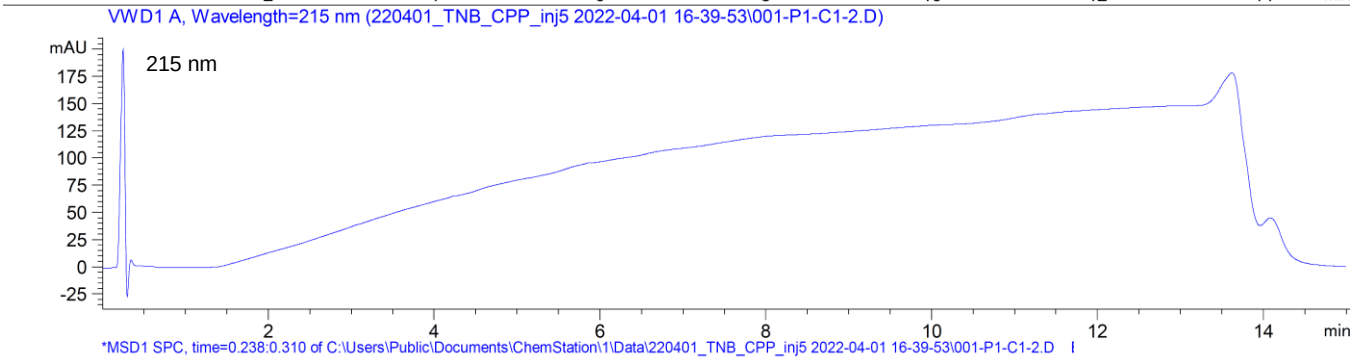

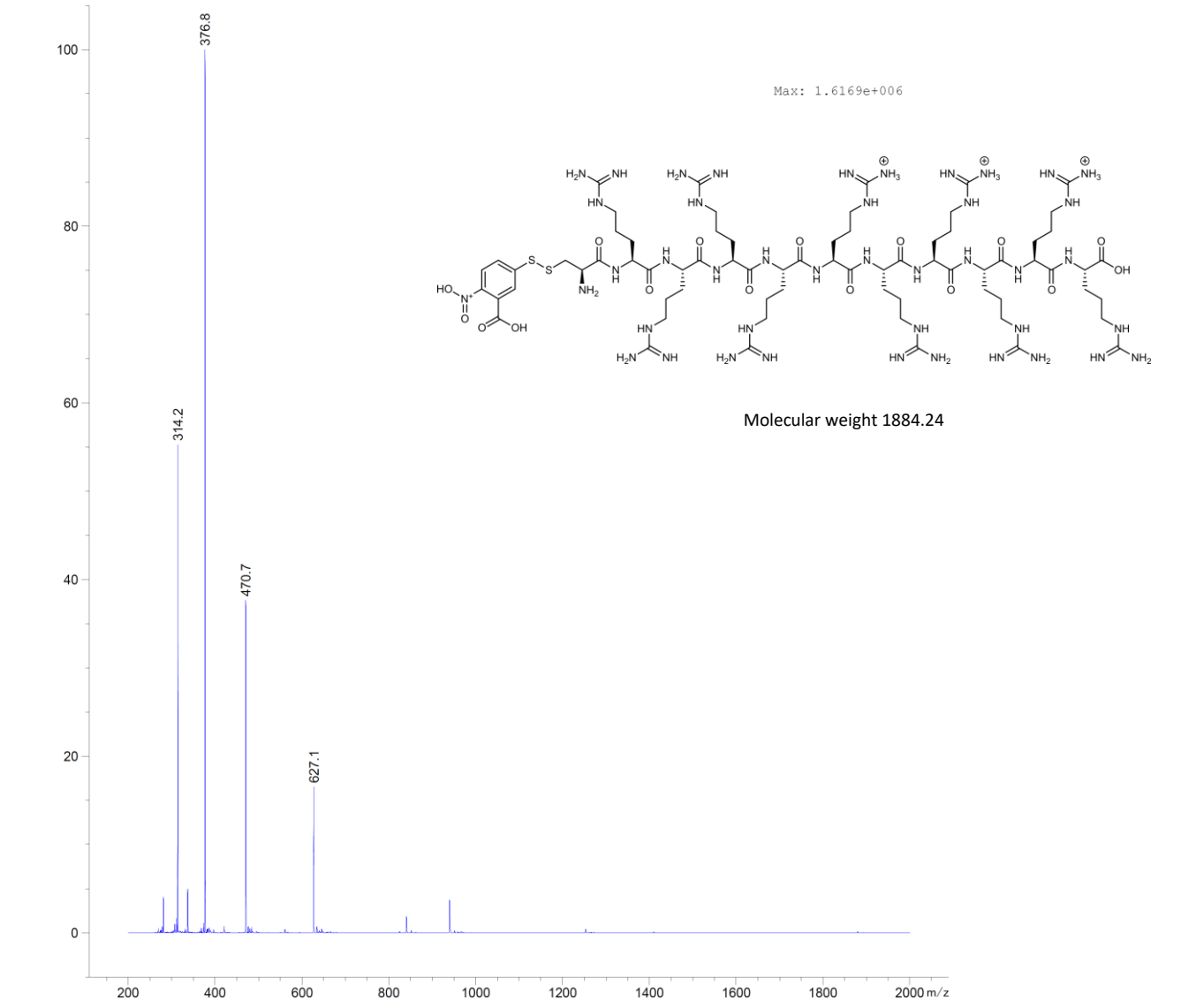

Molecular weight 1884.24

TNB-peg-CPP – thiol reactive cell penetrating peptide with a peg handle (CPP_2)

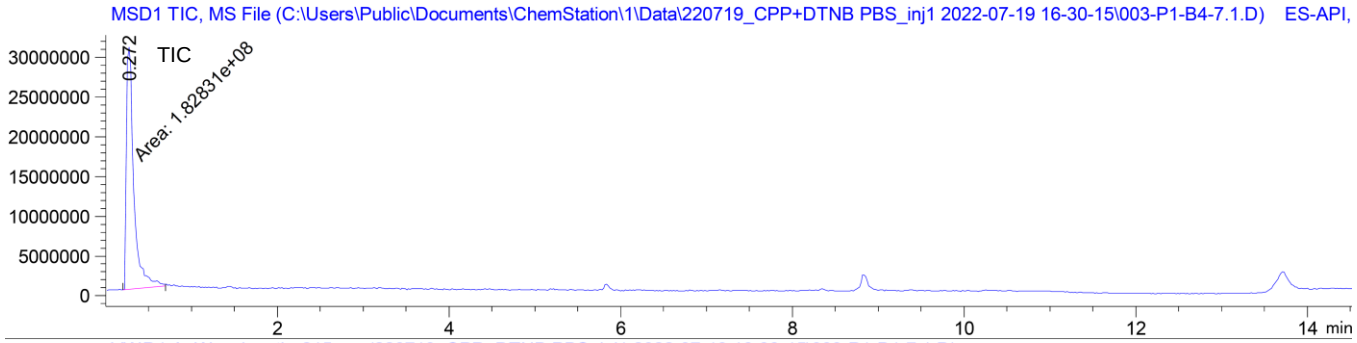

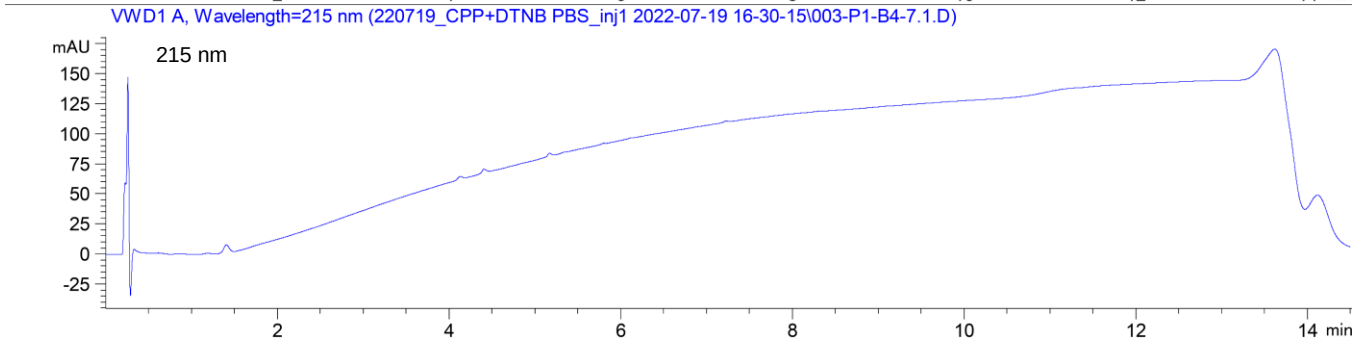

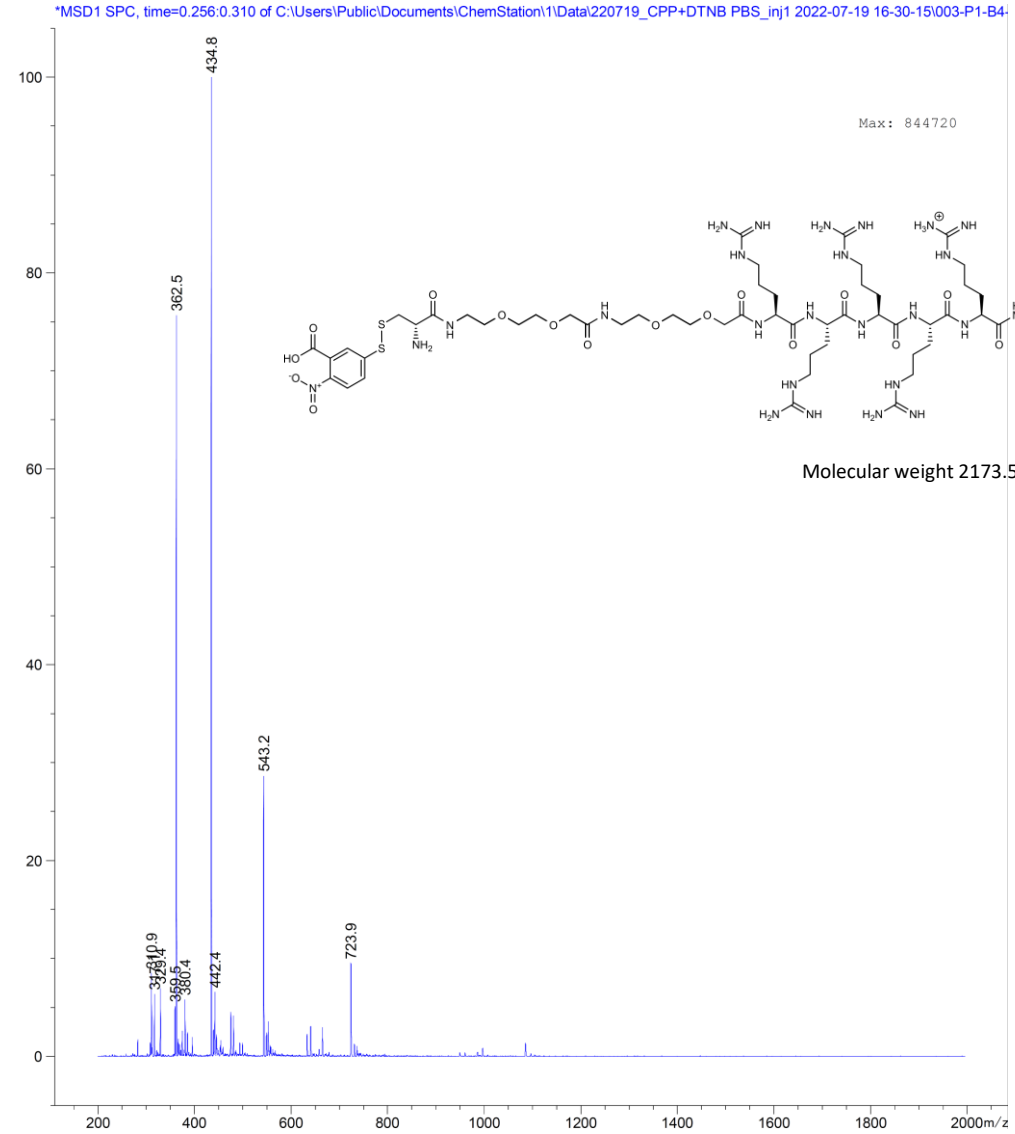

Molecular weight 2173.57

Sylite 1.2

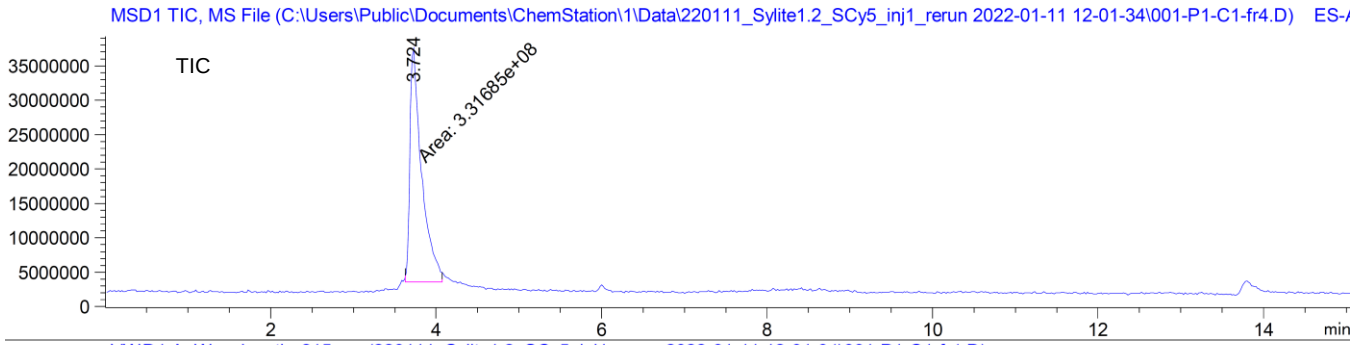

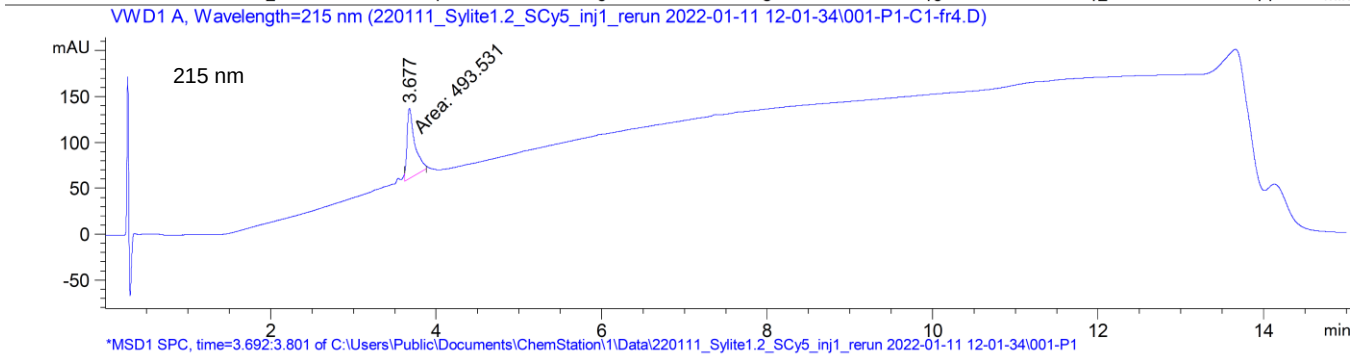

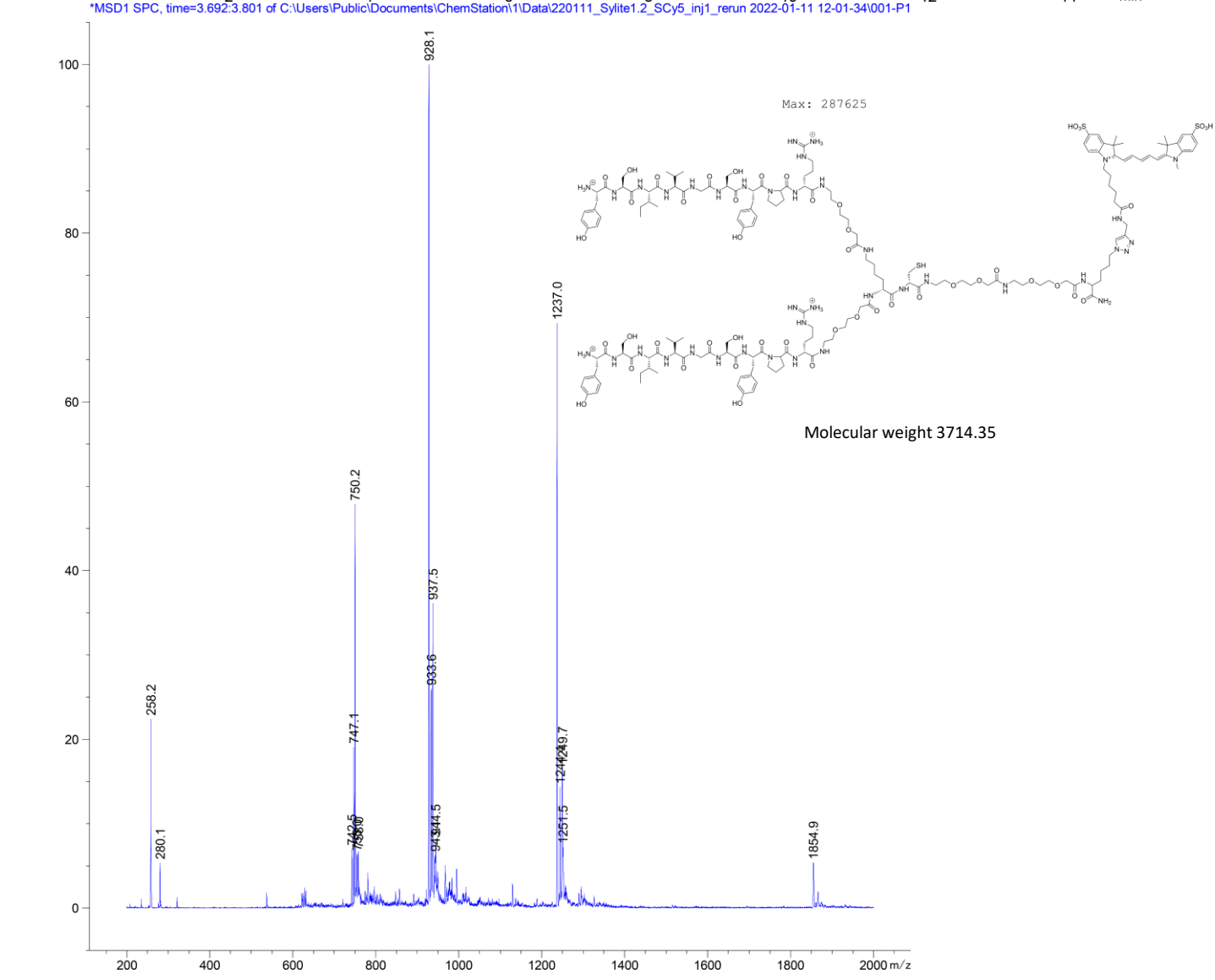

Molecular weight 3714.35

MH1

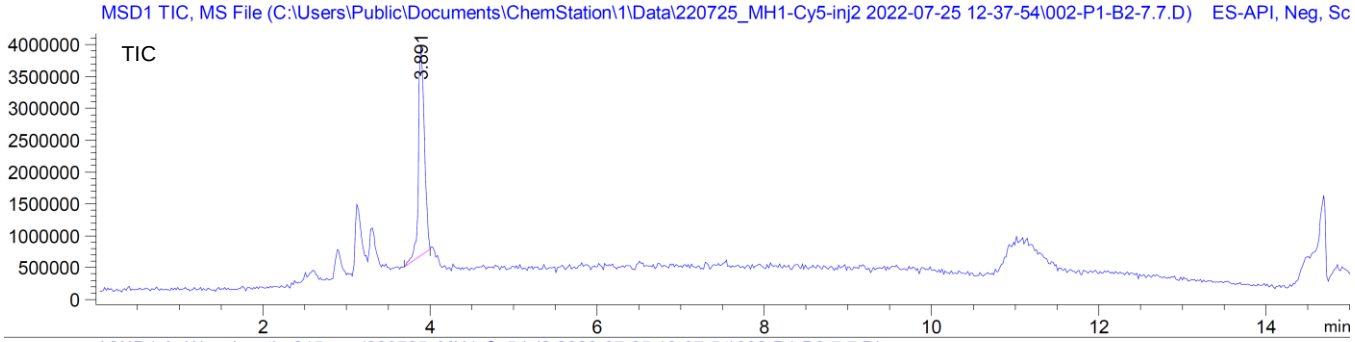

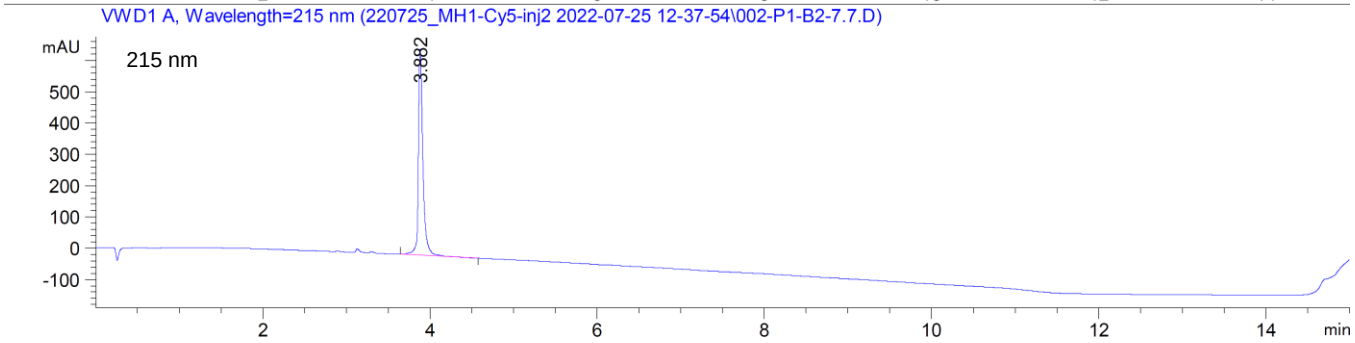

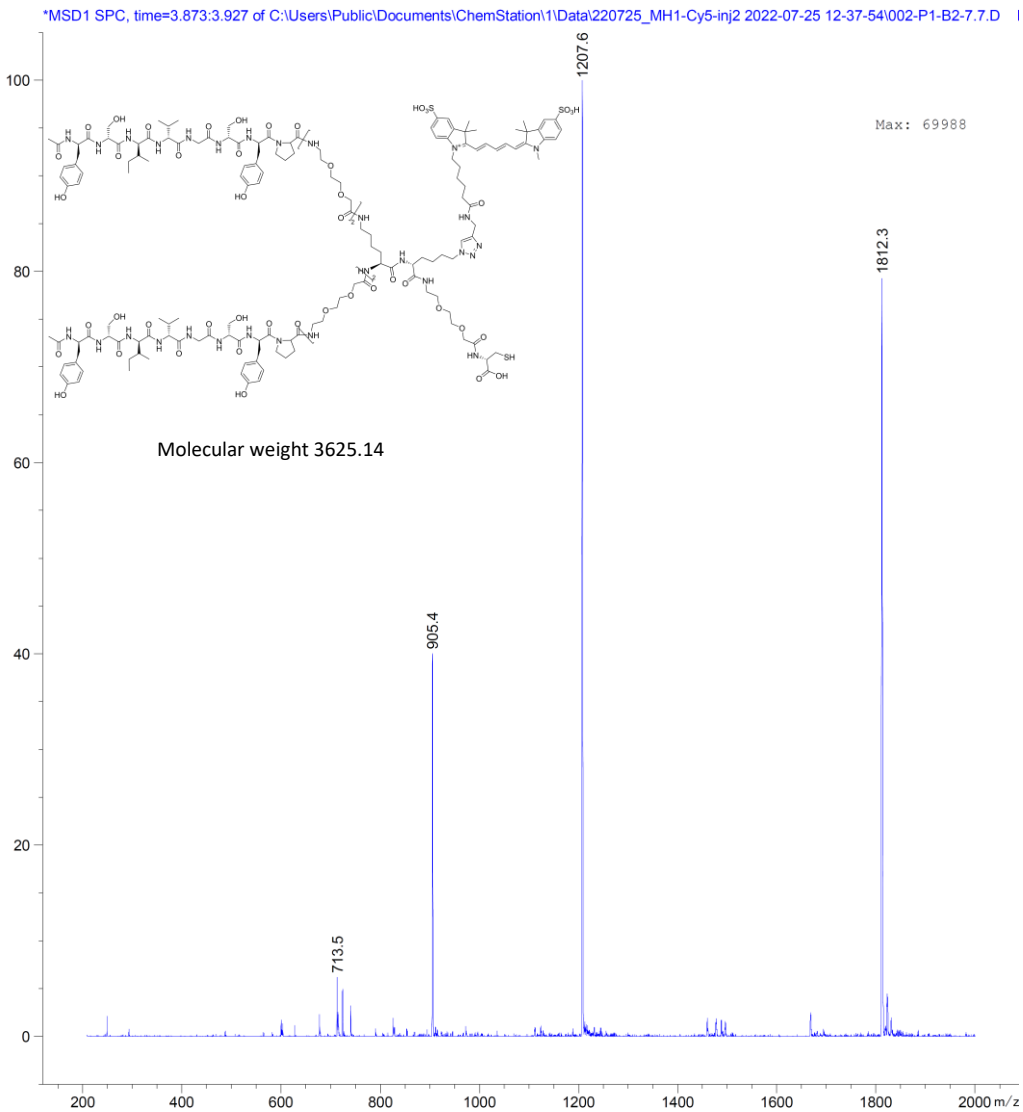

Molecular weight 3625.14

MH1peg

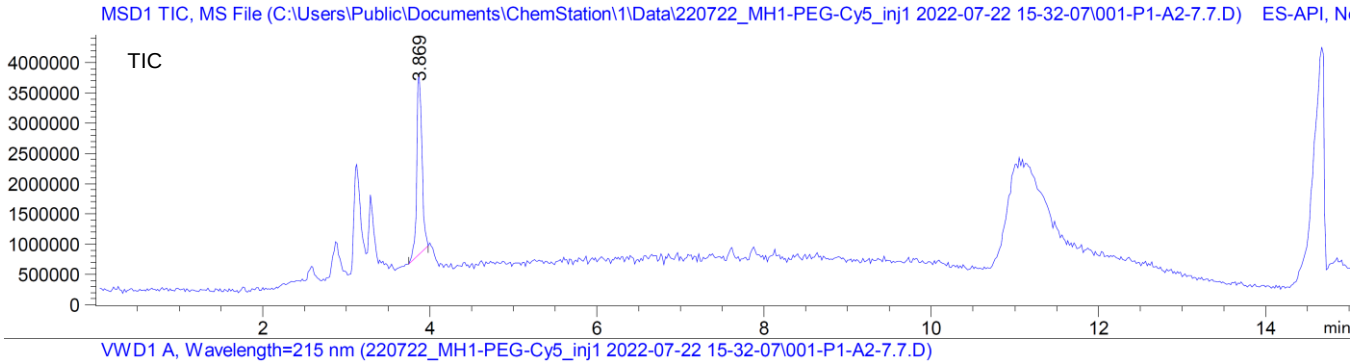

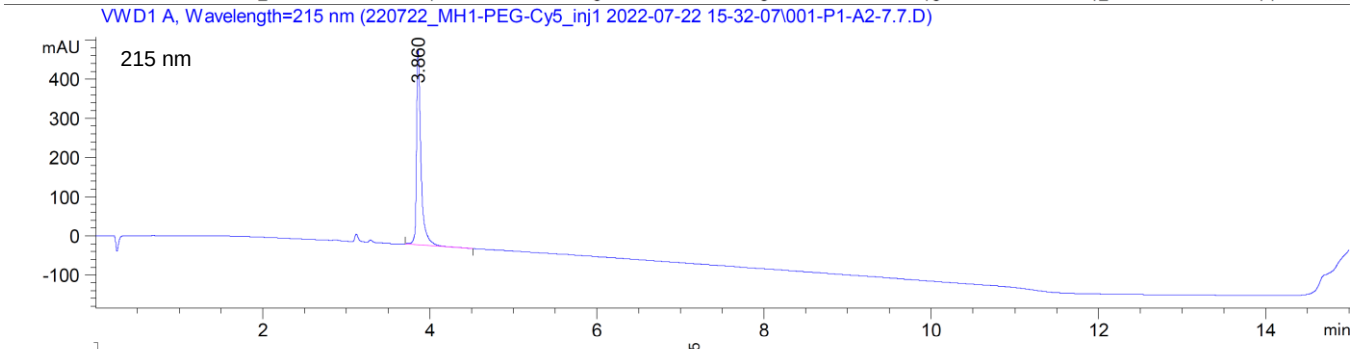

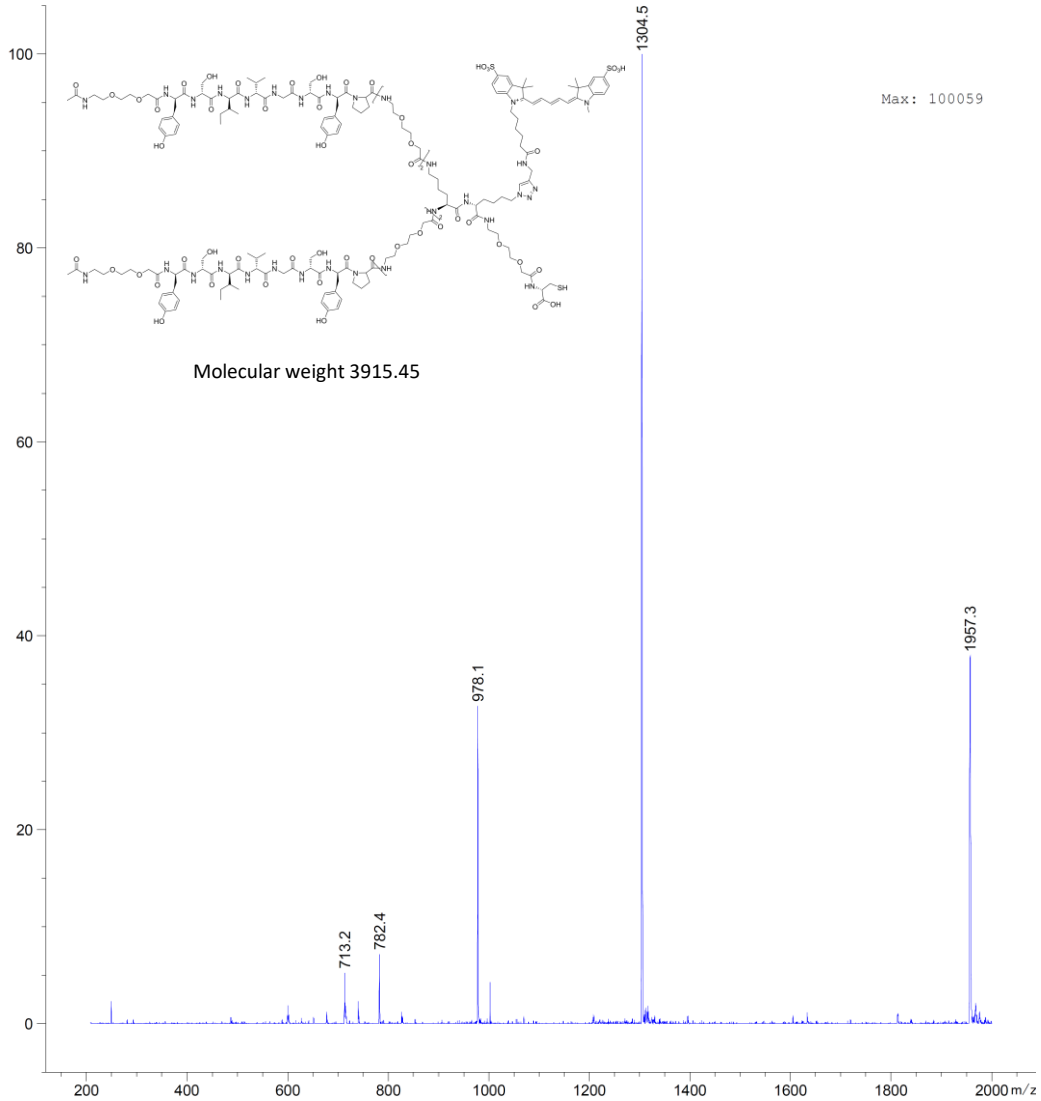

Molecular weight 3915.45

VK16

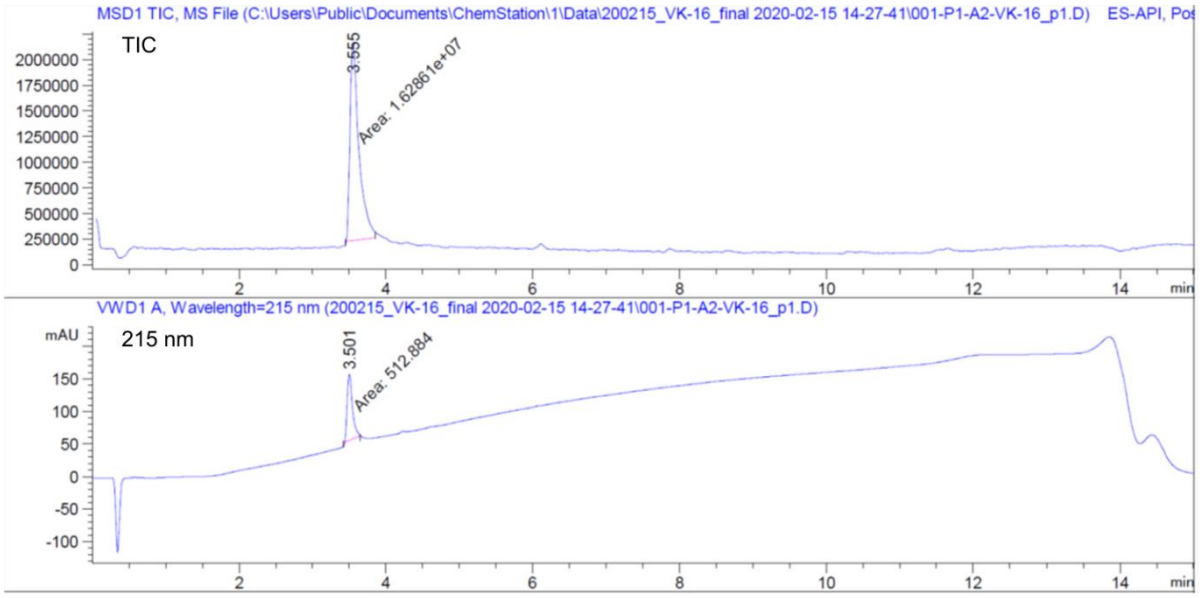
MSD1 TIC, MS File (C:\Users\Public\Documents\ChemStation\1\Data\200215_VK-16_final 2020-02-15 14-27-41\001-P1-A2-VK-16_p1.D) ES-API, Pos
TIC
3.555
Area: 1.62861e+07
2000000
1750000
1500000
1250000
1000000
750000
500000
250000
0
2
4
6
8
10
12
14
min
VWD1 A, Wavelength=215 nm (200215_VK-16_final 2020-02-15 14-27-41\001-P1-A2-VK-16_p1.D)
mAU
215 nm
3.501
Area: 512.884
150
100
50
0
-50
-100
2
4
6
8
10
12
14
min

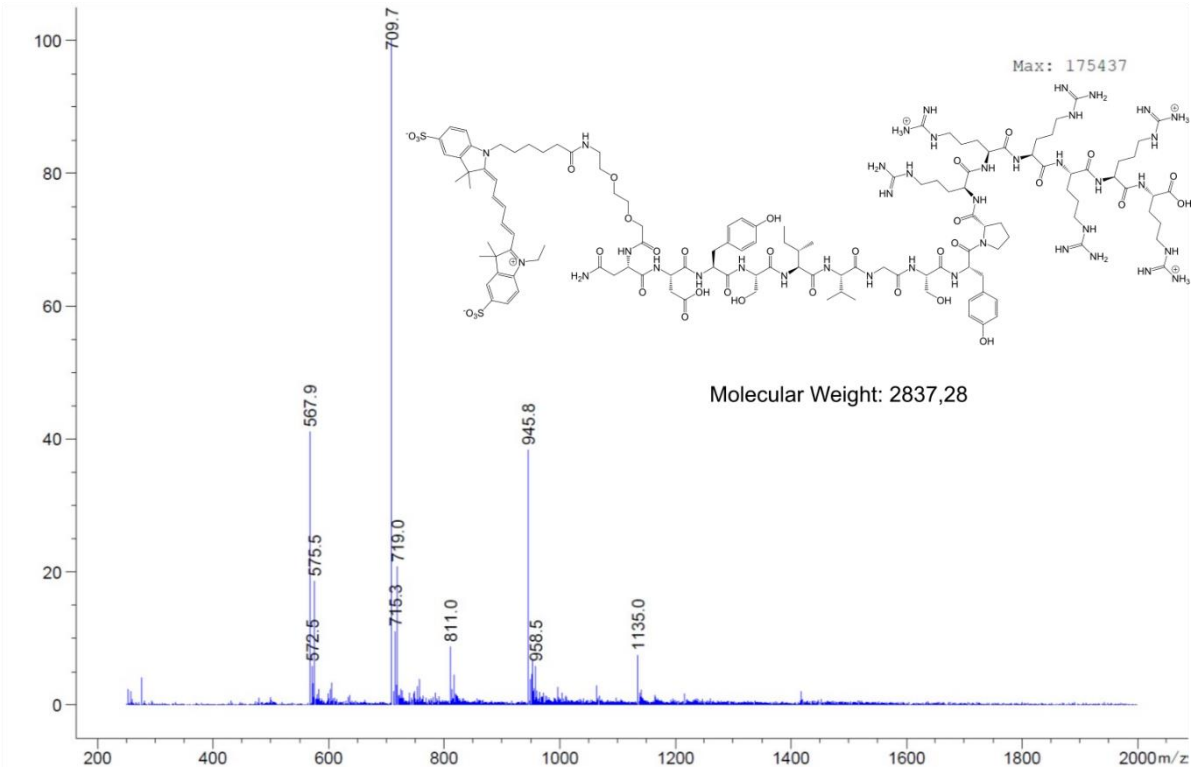
709.7
Max: 175437
Molecular Weight: 2837,28
567.9
945.8
575.5
719.0
572.6
715.3
811.0
958.5
1135.0
100
80
60
40
20
0
200
400
600
800
1000
1200
1400
1600
1800
2000
m/z

VK17

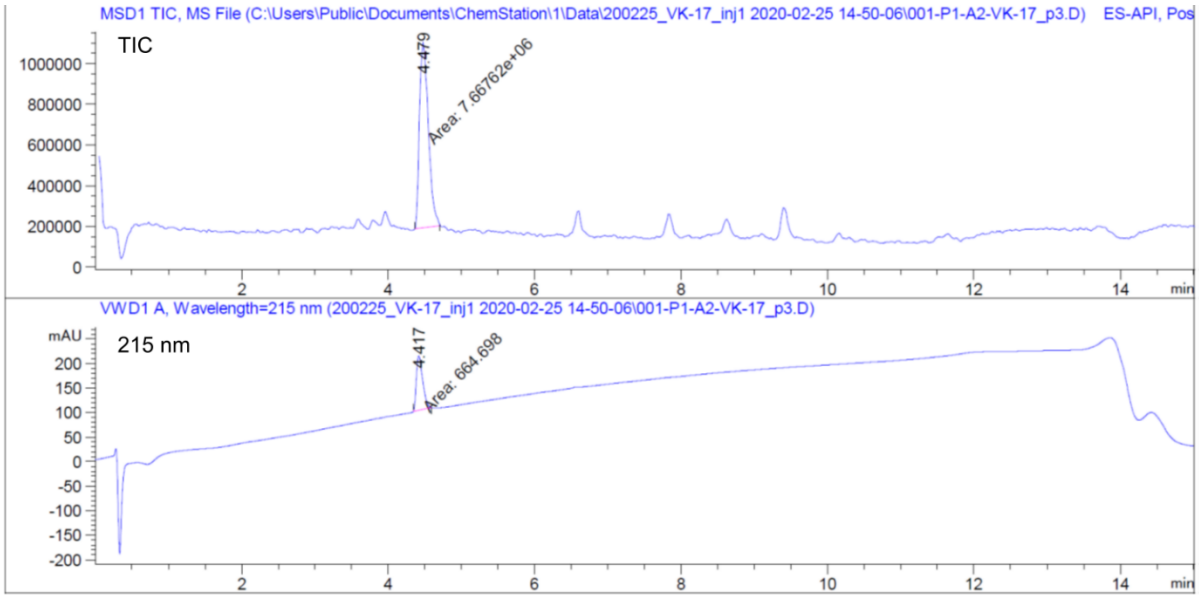
MSD1 TIC, MS File (C:\Users\Public\Documents\ChemStation\1\Data\200225_VK-17_inj1 2020-02-25 14-50-06\001-P1-A2-VK-17_p3.D) ES-API, Pos
TIC
4.479
Area: 7.66762e+06
VWD1 A, Wavelength=215 nm (200225_VK-17_inj1 2020-02-25 14-50-06\001-P1-A2-VK-17_p3.D)
215 nm
4.417
Area: 664.698
mAU
min

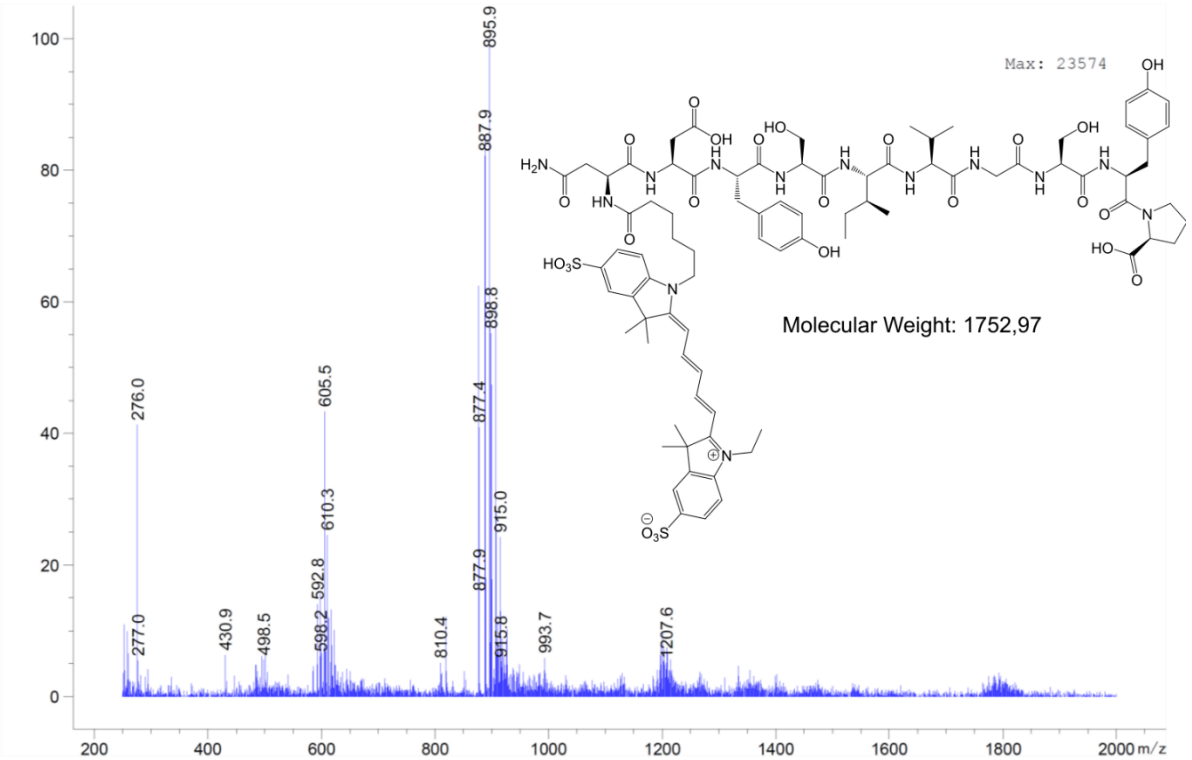
Max: 23574
Molecular Weight: 1752,97
m/z

VK18

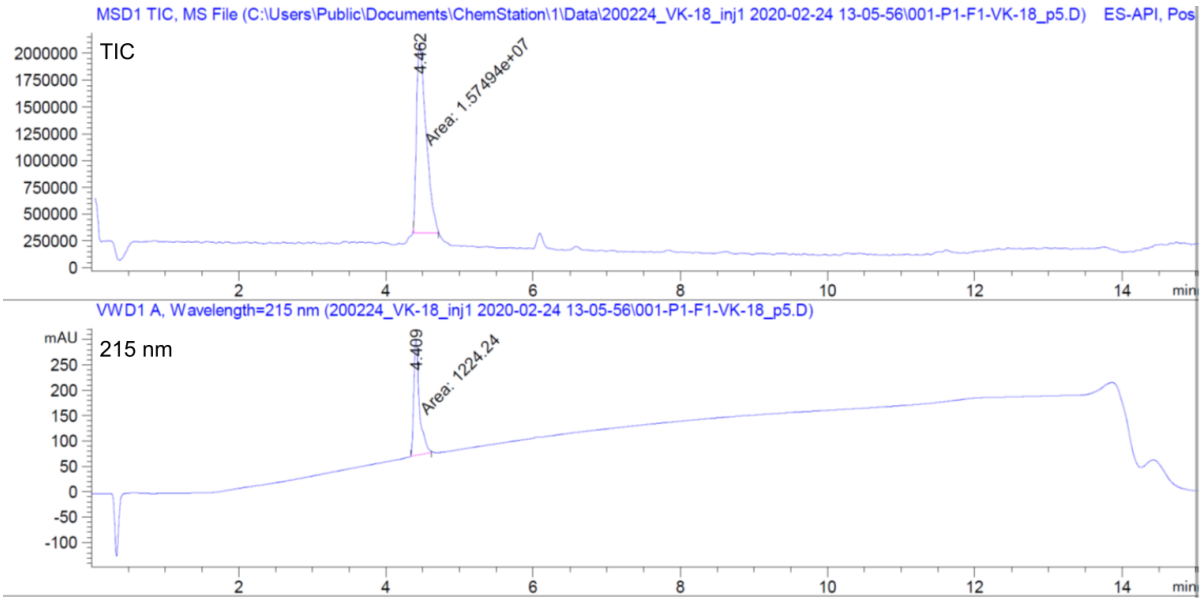
MSD1 TIC, MS File (C:\Users\Public\Documents\ChemStation\1\Data\200224_VK-18_inj1 2020-02-24 13-05-56\001-P1-F1-VK-18_p5.D) ES-API, Pos
TIC
4.462
Area: 1.57494e+07
VWD1 A, Wavelength=215 nm (200224_VK-18_inj1 2020-02-24 13-05-56\001-P1-F1-VK-18_p5.D)
215 nm
4.409
Area: 1224.24
mAU
min

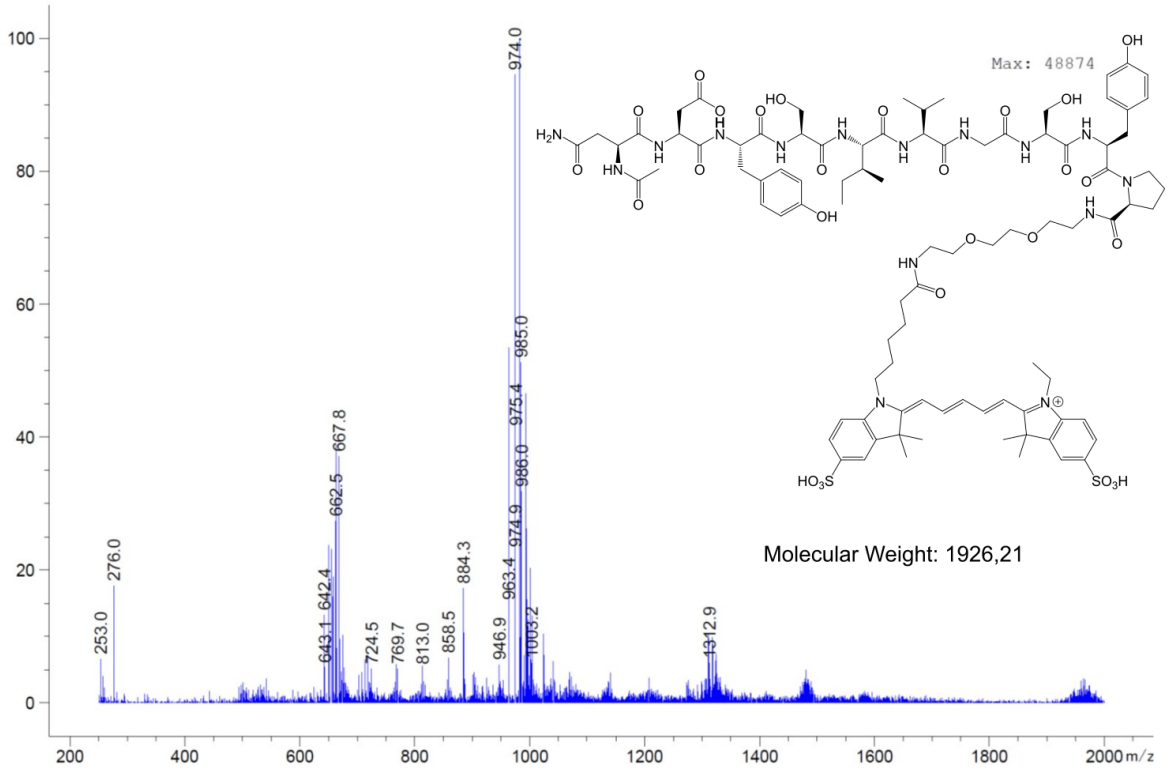
Max: 48874
974.0
985.0
975.4
667.8
662.5
986.0
974.9
884.3
963.4
276.0
642.4
643.1
724.5
769.7
813.0
858.5
946.9
1003.2
1312.9
253.0
Molecular Weight: 1926,21
m/z

VK20

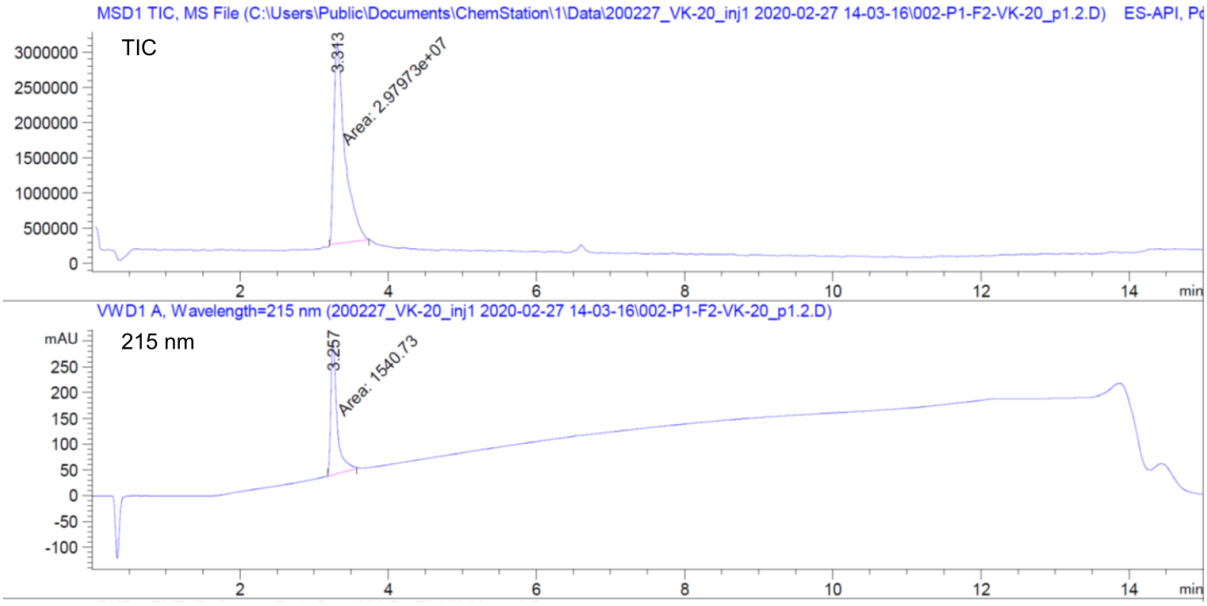
MSD1 TIC, MS File (C:\Users\Public\Documents\ChemStation\1\Data\200227_VK-20_inj1 2020-02-27 14-03-16\002-P1-F2-VK-20_p1.2.D) ES-API, Pd
TIC
3.313
Area: 2.97973e+07
VWD1 A, Wavelength=215 nm (200227_VK-20_inj1 2020-02-27 14-03-16\002-P1-F2-VK-20_p1.2.D)
215 nm
3.257
Area: 1540.73
mAU
min

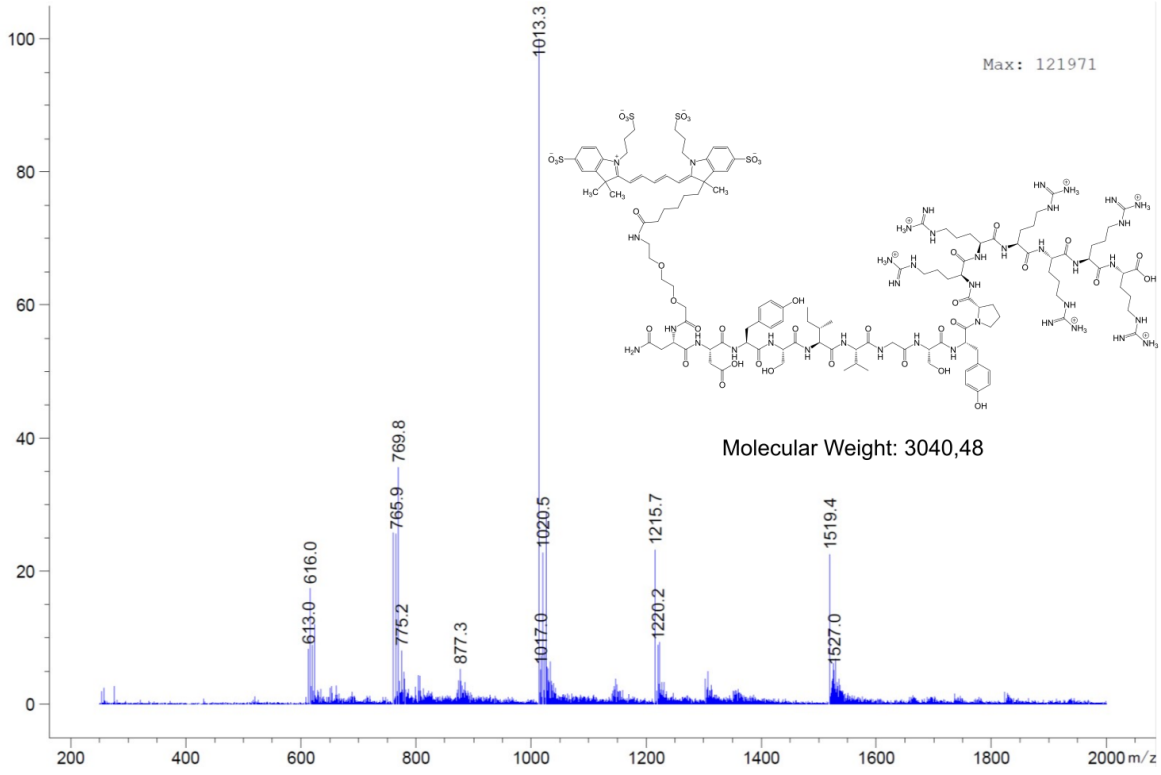
Max: 121971
1013.3
769.8
765.9
616.0
613.0
775.2
877.3
1020.5
1017.0
1215.7
1220.2
1519.4
1527.0
Molecular Weight: 3040,48
m/z

VK21

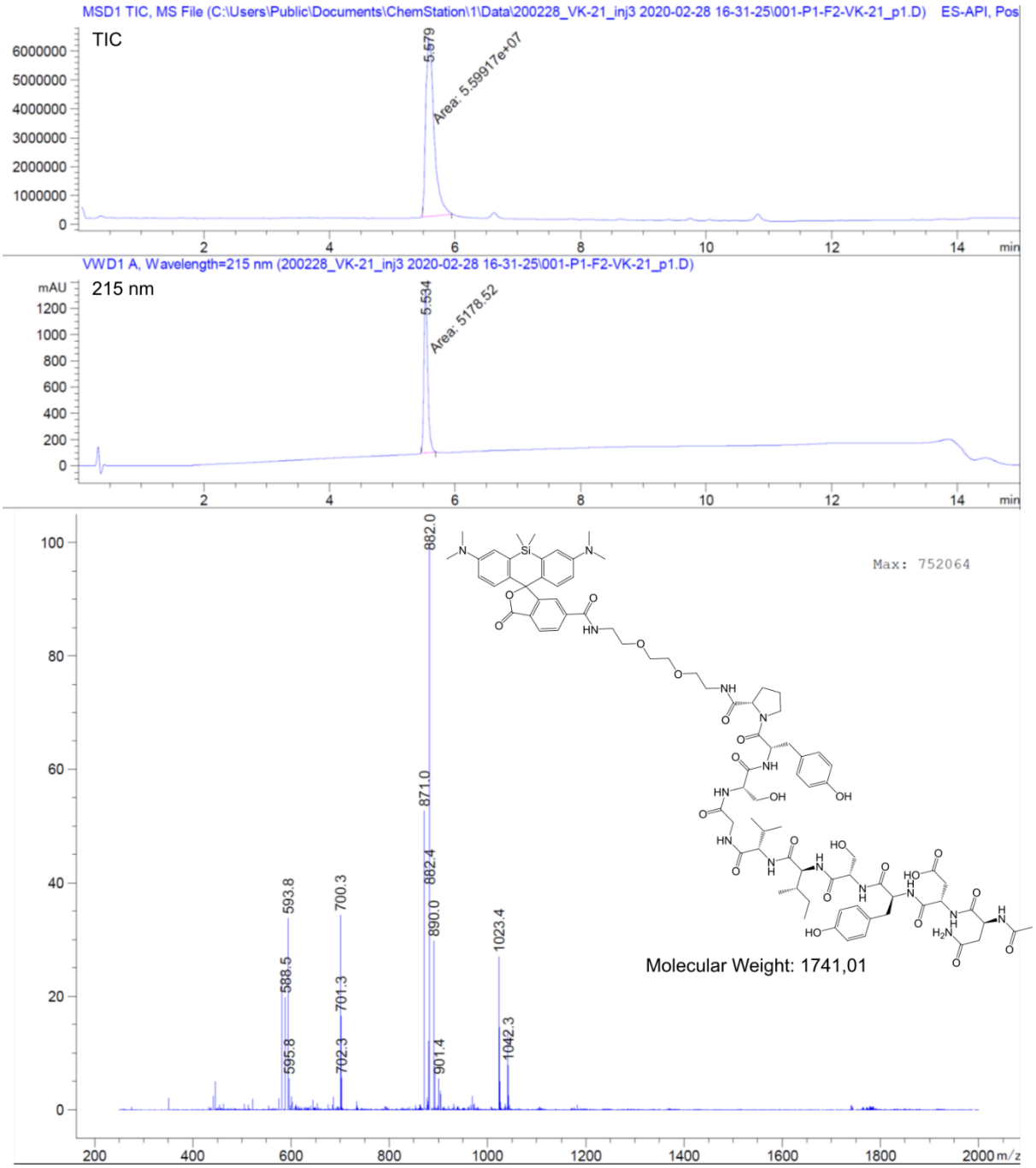
MSD1 TIC, MS File (C:\Users\Public\Documents\ChemStation\1\Data\200228_VK-21_inj3 2020-02-28 16-31-25\001-P1-F2-VK-21_p1.D) ES-API, Pos
TIC
5.579
Area: 5.59917e+07
VWD1 A, Wavelength=215 nm (200228_VK-21_inj3 2020-02-28 16-31-25\001-P1-F2-VK-21_p1.D)
215 nm
5.534
Area: 5178.52
Max: 752064
882.0
871.0
882.4
890.0
593.8
588.5
595.8
700.3
701.3
702.3
901.4
1023.4
1042.3
Molecular Weight: 1741,01

VK22

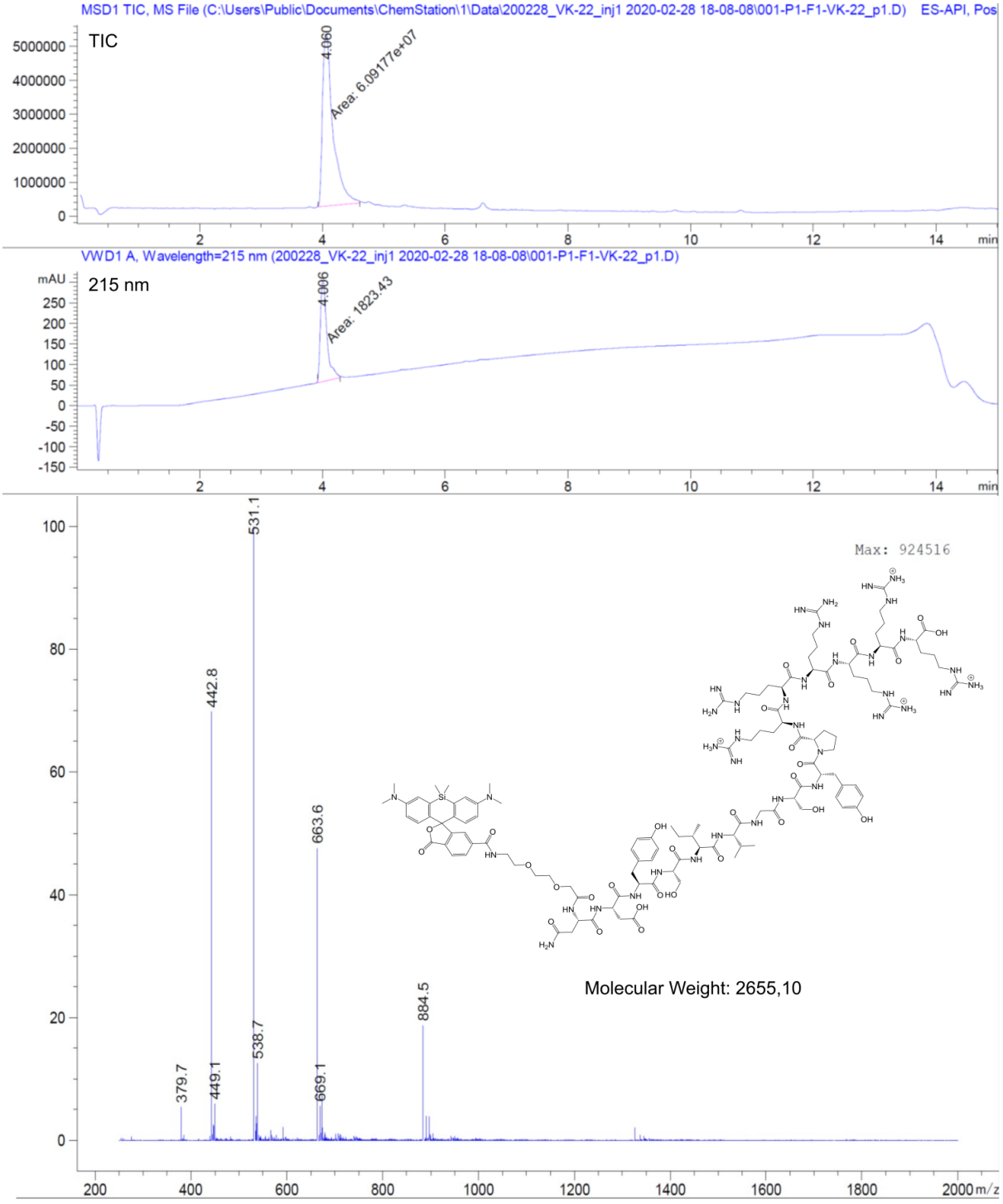
MSD1 TIC, MS File (C:\Users\Public\Documents\ChemStation\1\Data\200228_VK-22_inj1 2020-02-28 18-08-08\001-P1-F1-VK-22_p1.D) ES-API, Pos
TIC
4.060
Area: 6.09177e+07
VWD1 A, Wavelength=215 nm (200228_VK-22_inj1 2020-02-28 18-08-08\001-P1-F1-VK-22_p1.D)
215 nm
4.006
Area: 1823.43
Max: 924516
531.1
442.8
663.6
538.7
884.5
379.7
449.1
669.1
Molecular Weight: 2655,10
m/z

DVK1

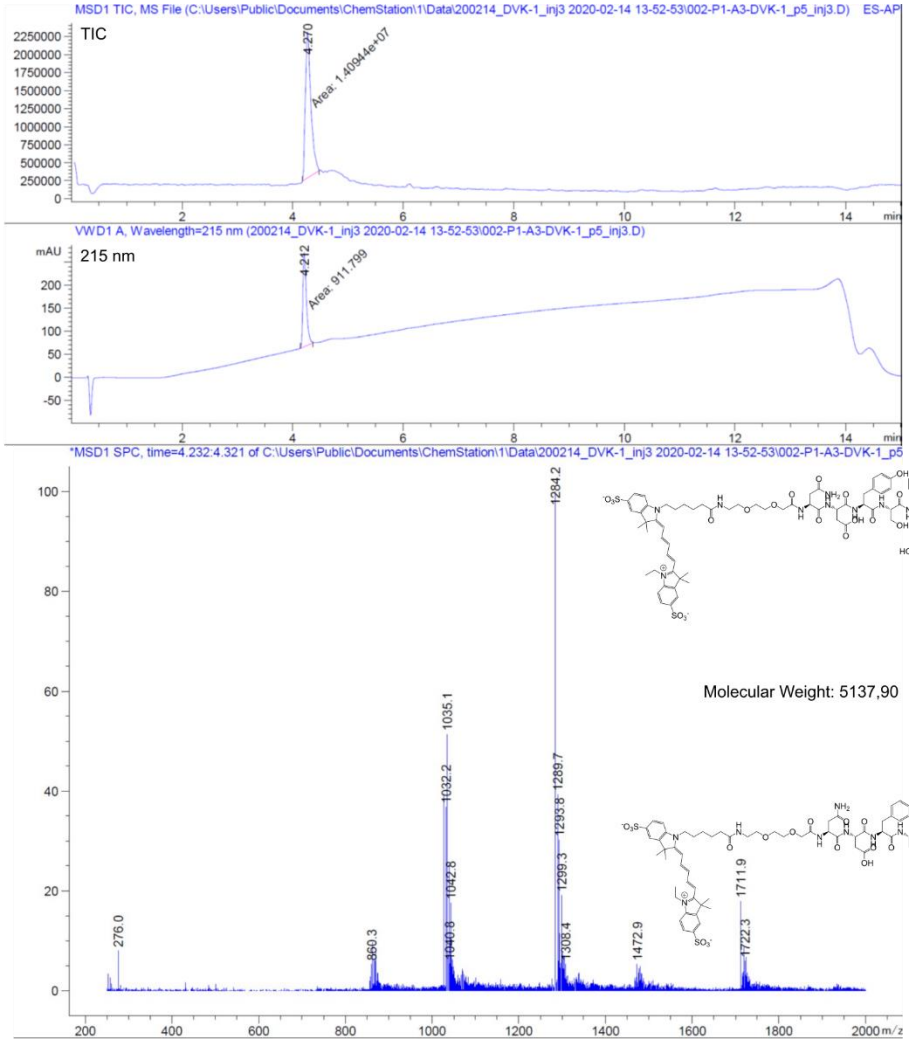
MSD1 TIC, MS File (C:\Users\Public\Documents\ChemStation\1\Data\200214_DVK-1_inj3 2020-02-14 13-52-53\002-P1-A3-DVK-1_p5_inj3.D) ES-API
TIC
4.270
Area: 1.40944e+07
VWD1 A, Wavelength=215 nm (200214_DVK-1_inj3 2020-02-14 13-52-53\002-P1-A3-DVK-1_p5_inj3.D)
mAU
215 nm
4.212
Area: 911.799
min
*MSD1 SPC, time=4.232:4.321 of C:\Users\Public\Documents\ChemStation\1\Data\200214_DVK-1_inj3 2020-02-14 13-52-53\002-P1-A3-DVK-1_p5
1284.2
1035.1
1032.2
1289.7
1293.8
1299.3
1042.8
1040.8
1308.4
1711.9
1722.3
1472.9
860.3
276.0
m/z
Molecular Weight: 5137,90

DVK2

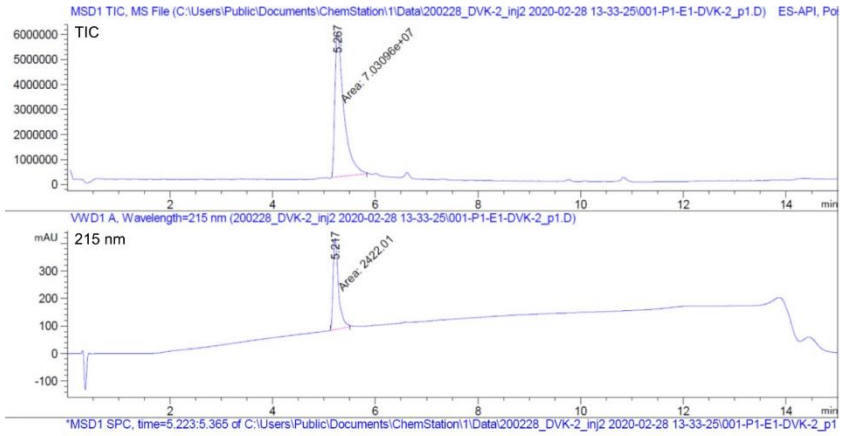
MSD1 TIC, MS File (C:\Users\Public\Documents\ChemStation\1\Data\200228_DVK-2_inj2 2020-02-28 13-33-25\001-P1-E1-DVK-2_p1.D) ES-API, Pol
TIC
5.267
Area: 7.03096e+07
VWD1 A, Wavelength=215 nm (200228_DVK-2_inj2 2020-02-28 13-33-25\001-P1-E1-DVK-2_p1.D)
mAU
215 nm
5.217
Area: 2422.01
min

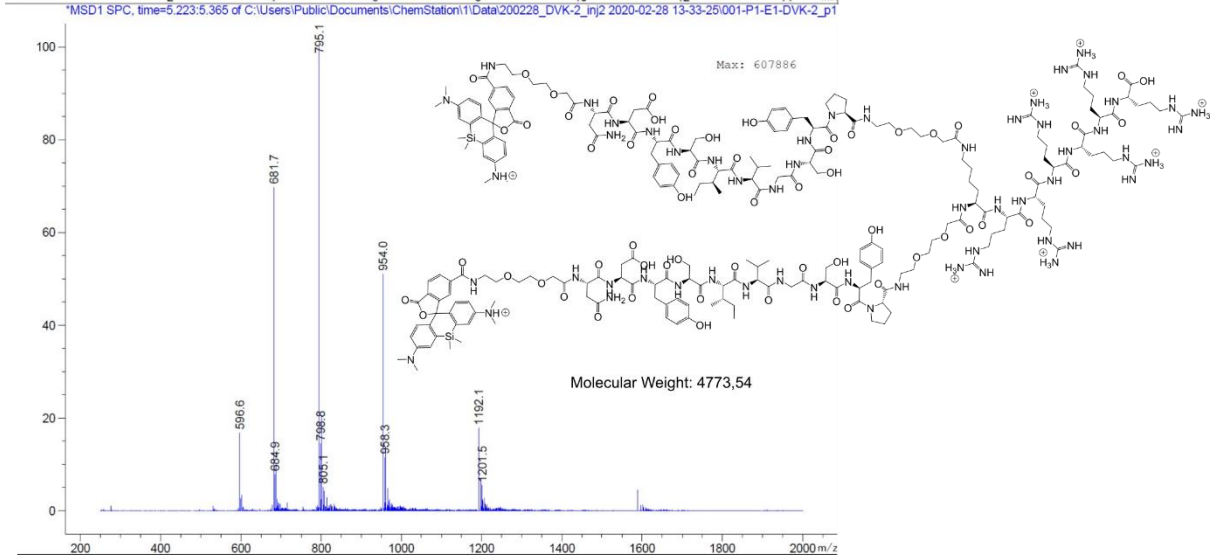
*MSD1 SPC, time=5.223:5.365 of C:\Users\Public\Documents\ChemStation\1\Data\200228_DVK-2_inj2 2020-02-28 13-33-25\001-P1-E1-DVK-2_p1
Max: 607886
Molecular Weight: 4773,54
795.1
681.7
954.0
596.6
684.9
798.8
805.1
958.3
1192.1
1201.5
m/z

C. Gephyrin overlapping fragments, microarray sequences

MATEGMILTNHDHQI	SKENILRASHSAVDI	IGHDIKRGECVLAKG	TTPXEXPRAQATSRL	TTPXEXPRAQATSRL
EGMILTNHDHQIRVG	NILRASHSAVDITKV	DIKRGECVLAKGTHM	XEXPRAQATSRLSTA	XEXPRAQATSRLSTA
ILTNHDHQIRVGVLT	RASHSAVDITKVARR	RGECVLAKGTHMGPS	-	-
NHDHQIRVGVLTVSD	HSAVDITKVARRHRM	CVLAKGTHMGPSEIG	-	-
HQIRVGVLTVSDSCF	VDITKVARRHRMSPF	AKGTHMGPSEIGLLA	-	-
RVGVLTVSDSCFRNL	TKVARRHRMSPFPLT	THMGPSEIGLLATVG	LPRDTASLSTTPSEX	LPRDTASLSTTPSEX
VLTVSDSCFRNLAED	ARRHRMSPFPLTSMD	GPSEIGLLATVGVTE	DTASLSTTPSEXPRA	DTASLSTTPSEXPRA
VSDSCFRNLAEDRSG	HRMSPFPLTSMDKAF	EIGLLATVGVTEVEV	SLSTTPSEXPRAQAT	SLSTTPSEXPRAQAT
SCFRNLAEDRSGINL	SPFPLTSMDKAFITV	LLATVGVTEVEVNKF	TTPSEXPRAQATSRL	TTPSEXPRAQATSRL
RNLAEDRSGINLKDL	PLTSMDKAFITVLEM	TVGVTEVEVNKFPVV	SEXPRAQATSRLSTA	SEXPRAQATSRLSTA
AEDRSGINLKDLVQD	SMDKAFITVLEMTPV	VTEVEVNKFPVVAVM	-	-
RSGINLKDLVQDPSL	KAFITVLEMTPVLGT	VEVNKFPVVAVMSTG	-	-
INLKDLVQDPSLLGG	ITVLEMTPVLGTEII	NKFPVVAVMSTGNEL	-	-
KDLVQDPSLLGGTIS	LEMTPVLGTEIINYR	PVVAVMSTGNELLNP	LPRDTASLSTTPXES	LPRDTASLSTTPXES
VQDPSLLGGTISAYK	TPVLGTEIINYRDGM	AVMSTGNELLNPEDD	DTASLSTTPXESPRA	DTASLSTTPXESPRA
PSLLGGTISAYKIVP	LGTEIINYRDGMGRV	STGNELLNPEDDLLP	SLSTTPXESPRAQAT	SLSTTPXESPRAQAT
LGGTISAYKIVPDEI	EIINYRDGMGRVLAQ	NELLNPEDDLLPGKI	TTPXESPRAQATSRL	TTPXESPRAQATSRL
TISAYKIVPDEIEEI	NYRDGMGRVLAQDVY	LNPEDDLLPGKIRDS	XESPRAQATSRLSTA	XESPRAQATSRLSTA
AYKIVPDEIEEIKET	DGMGRVLAQDVYAKD	EDDLLPGKIRDSNRS	-	-
IVPDEIEEIKETLID	GRVLAQDVYAKDNLP	LLPGKIRDSNRSTLL	-	-
DEIEEIKETLIDWCD	LAQDVYAKDNLPPFP	GKIRDSNRSTLLATI	-	-
EEIKETLIDWCDEKE	DVYAKDNLPPFPASV	RDSNRSTLLATIQEH	LPRDTASLSTTPXEX	LPRDTASLSTTPXEX
KETLIDWCDEKELNL	AKDNLPPFPASVKDG	NRSTLLATIQEHGYP	DTASLSTTPXEXPRA	DTASLSTTPXEXPRA
LIDWCDEKELNLILT	NLPPFPASVKDGYAV	TLLATIQEHGYPTIN	SLSTTPXEXPRAQAT	SLSTTPXEXPRAQAT
WCDEKELNLILTTGG	PFPASVKDGYAVRAA	ATIQEHGYPTINLGI	TTPXEXPRAQATSRL	TTPXEXPRAQATSRL
EKELNLILTTGGTGF	ASVKDGYAVRAADGP	QEHGYPTINLGIVGD	XEXPRAQATSRLSTA	XEXPRAQATSRLSTA
LNLILTTGGTGFAPR	KDGYAVRAADGPGDR	GYPTINLGIVGDNPD	-	-
ILTTGGTGFAPRDVT	YAVRAADGPGDRFII	TINLGIVGDNPDDLL	-	-
TGGTGFAPRDVTPEA	RAADGPGDRFIIGES	LGIVGDNPDDLLNAL	-	-
TGFAPRDVTPEATKE	DGPGDRFIIGESQAG	VGDNPDDLLNALNEG	LPRDTASLSTTPSEX	LPRDTASLSTTPSEX
APRDVTPEATKEVIE	GDRFIIGESQAGEQP	NPDDLLNALNEGISR	DTASLSTTPSEXPRA	DTASLSTTPSEXPRA
DVTPEATKEVIEREA	FIIGESQAGEQPTQT	DLLNALNEGISRANV	SLSTTPSEXPRAQAT	SLSTTPSEXPRAQAT
PEATKEVIEREAPGM	GESQAGEQPTQTVMP	NALNEGISRANVIIT	TTPSEXPRAQATSRL	TTPSEXPRAQATSRL
TKEVIEREAPGMALA	QAGEQPTQTVMPGQV	NEGISRANVIITSGG	SEXPRAQATSRLSTA	SEXPRAQATSRLSTA
VIEREAPGMALAMLM	EQPTQTVMPGQVMRV	ISRANVIITSGGVSM	-	-
REAPGMALAMLMGSL	TQTVMPGQVMRVTTG	ANVIITSGGVSMGEK	-	-
PGMALAMLMGSLNVT	VMPGQVMRVTTGAPI	IITSGGVSMGEKDYL	-	-
ALAMLMGSLNVTPLG	GQVMRVTTGAPIPCG	SGGVSMGEKDYLKQV	LPRDTASLSTTPXES	LPRDTASLSTTPXES
MLMGSLNVTPLGMLS	MRVTTGAPIPCGADA	VSMGEKDYLKQVLDI	DTASLSTTPXESPRA	DTASLSTTPXESPRA
GSLNVTPLGMLSRPV	TTGAPIPCGADAVVQ	GEKDYLKQVLDIDLH	SLSTTPXESPRAQAT	SLSTTPXESPRAQAT
NVTPLGMLSRPVCGI	APIPCGADAVVQVED	DYLKQVLDIDLHAQI	TTPXESPRAQATSRL	TTPXESPRAQATSRL
PLGMLSRPVCGIRGK	PCGADAVVQVEDTEL	KQVLDIDLHAQIHFG	XESPRAQATSRLSTA	XESPRAQATSRLSTA
MLSRPVCGIRGKTLI	ADAVVQVEDTELIRE	LDIDLHAQIHFGRVF	-	-
RPVCGIRGKTLIINL	VVQVEDTELIRESDD	DLHAQIHFGRVFMKP	-	-
CGIRGKTLIINLPGS	VEDTELIRESDDGTE	AQIHFGRVFMKPGLP	-	-
RGKTLIINLPGSKKG	TELIRESDDGTEELE	HFGRVFMKPGLPTTF	LPRDTASLSTTPXEX	LPRDTASLSTTPXEX
TLIINLPGSKKGSQE	IRESDDGTEELEVRI	RVFMKPGLPTTFATL	DTASLSTTPXEXPRA	DTASLSTTPXEXPRA
INLPGSKKGSQECFQ	SDDGTEELEVRILVQ	MKPGLPTTFATLDID	SLSTTPXEXPRAQAT	SLSTTPXEXPRAQAT
PGSKKGSQECFQFIL	GTEELEVRILVQARP	GLPTTFATLDIDGVR	TTPXEXPRAQATSRL	TTPXEXPRAQATSRL
KKGSQECFQFILPAL	ELEVRILVQARPGQD	TTFATLDIDGVRKII	XEXPRAQATSRLSTA	XEXPRAQATSRLSTA
SQECFQFILPALPHA	VRILVQARPGQDIRP	ATLDIDGVRKIIFAL		
CFQFILPALPHAIDL	LVQARPGQDIRPIGH	DIDGVRKIIFALPGN		
FILPALPHAIDLLRD	ARPGQDIRPIGHDIK	GVRKIIFALPGNPVS		
PALPHAIDLLRDAIV	GQDIRPIGHDIKRGE	KIIFALPGNPVSAVV		
PHAIDLLRDAIVKVK	IRPIGHDIKRGECVL	FALPGNPVSAVVTCN		
IDLLRDAIVKVKEVH	IGHDIKRGECVLAKG	PGNPVSAVVTCNLFV		
LRDAIVKVKEVHDEL	DIKRGECVLAKGTHM	PVSAVVTCNLFVVPA		
AIVKVKEVHDELEDL	RGECVLAKGTHMGPS	AVVTCNLFVVPALRK		
KVKEVHDELEDLPSP	CVLAKGTHMGPSEIG	TCNLFVVPALRKMQG		

EVHDELEDLPSPPPP	AKGTHMGPSEIGLLA	LFVVPALRKMQGILD
DELEDLPSPPPPLSP	THMGPSEIGLLATVG	VPALRKMQGILDPRP
EDLPSPPPPLSPPPT	GPSEIGLLATVGVTE	LRKMQGILDPRPTII
PSPPPPLSPPPTTSP	EIGLLATVGVTEVEV	MQGILDPRPTIIKAR
PPPLSPPPTTSPHKQ	LLATVGVTEVEVNKF	ILDPRPTIIKARLSC
LSPPPTTSPHKQTED	TVGVTEVEVNKFPVV	PRPTIIKARLSCDVK
PPTTSPHKQTEDKGV	VTEVEVNKFPVVAVM	TIIKARLSCDVKLDP
TSPHKQTEDKGVQCE	VEVNKFPVVAVMSTG	KARLSCDVKLDPRPE
HKQTEDKGVQCEEEE	NKFPVVAVMSTGNEL	LSCDVKLDPRPEYHR
TEDKGVQCEEEEEEK	PVVAVMSTGNELLNP	DVKLDPRPEYHRCIL
KGVQCEEEEEEKKDS	AVMSTGNELLNPEDD	LDPRPEYHRCILTWH
QCEEEEEEKKDSGVA	STGNELLNPEDDLLP	RPEYHRCILTWHHQE
EEEEEKKDSGVASTE	NELLNPEDDLLPGKI	YHRCILTWHHQEPLP
EEKKDSGVASTEDSS	LNPEDDLLPGKIRDS	CILTWHHQEPLPWAQ
KDSGVASTEDSSSSH	EDDLLPGKIRDSNRS	TWHHQEPLPWAQSTG
GVASTEDSSSSHITA	LLPGKIRDSNRSTLL	HQEPLPWAQSTGNQM
STEDSSSSHITAAAL	GKIRDSNRSTLLATI	PLPWAQSTGNQMSSR
DSSSSHITAAALAAK	RDSNRSTLLATIQEH	WAQSTGNQMSSRLMS
SSHITAAALAAKIPD	NRSTLLATIQEHGYP	STGNQMSSRLMSMRS
ITAAALAAKIPDSII	TLLATIQEHGYPTIN	NQMSSRLMSMRSANG
AALAAKIPDSIISRG	ATIQEHGYPTINLGI	SSRLMSMRSANGLLM
AAKIPDSIISRGVQV	QEHGYPTINLGIVGD	LMSMRSANGLLMLPP
IPDSIISRGVQVLPR	GYPTINLGIVGDNPD	MRSANGLLMLPPKTE
SIISRGVQVLPRDTA	TINLGIVGDNPDDLL	ANGLLMLPPKTEQYV
SRGVQVLPRDTASLS	LGIVGDNPDDLLNAL	LLMLPPKTEQYVELH
VQVLPRDTASLSTTP	VGDNPDDLLNALNEG	LPPKTEQYVELHKGE
LPRDTASLSTTPSES	NPDDLLNALNEGISR	KTEQYVELHKGEVVD
DTASLSTTPSESPRA	DLLNALNEGISRANV	QYVELHKGEVVDVMV
SLSTTPSESPRAQAT	NALNEGISRANVIIT	ELHKGEVVDVMVIGRL
TTPSESPRAQATSRL	NEGISRANVIITSGG	-
SESPRAQATSRLSTA	ISRANVIITSGGVSM	-
PRAQATSRLSTASCP	ANVIITSGGVSMGEK	-
QATSRLSTASCPTPK	IITSGGVSMGEKDYL	LPRDTASLSTTPSEX
SRLSTASCPTPKVQS	SGGVSMGEKDYLKQV	DTASLSTTPSEXPRA
STASCPTPKVQSRCS	VSMGEKDYLKQVLDI	SLSTTPSEXPRAQAT
SCPTPKVQSRCSSKE	GEKDYLKQVLDIDLH	TTPSEXPRAQATSRL
TPKVQSRCSSKENIL	DYLKQVLDIDLHAQI	SEXPRAQATSRLSTA
VQSRCSSKENILRAS	KQVLDIDLHAQIHFG	-
RCSSKENILRASHSA	LDIDLHAQIHFGRVF	-
	DLHAQIHFGRVFMKP	-
	AQIHFGRVFMKPGLP	LPRDTASLSTTPXES
	HFGRVFMKPGLPTTF	DTASLSTTPXESPRA
	RVFMKPGLPTTFATL	SLSTTPXESPRAQAT
	MKPGLPTTFATLDID	TTPXESPRAQATSRL
	GLPTTFATLDIDGVR	XESPRAQATSRLSTA
	TTFATLDIDGVRKII	-
	ATLDIDGVRKIIFAL	-
	DIDGVRKIIFALPGN	-
	GVRKIIFALPGNPVS	LPRDTASLSTTPXEX
	KIIFALPGNPVSAVV	DTASLSTTPXEXPRA
	FALPGNPVSAVVTCN	SLSTTPXEXPRAQAT

D. Sylite IP-MS analysis

Sylite			
Protein names	**Unique Peptides**	**Log10 LFQ intensity**	**Log2 enrichment over control**
Tubulin alpha-4A chain	5	9.743956372	0.584659494
Serine/threonine-protein phosphatase 6 cat	5	8.743862388	1.165271614
Protein arginine N-methyltransferase 5	5	9.05422991	3.045182858
Histone deacetylase 6	7	9.017158598	1.011423821
Ras-related protein Rab-18	4	8.709643023	1.686198086
AP-3 complex subunit beta-2	10	8.881652798	1.667806449
Gephyrin;Molybdopterin adenylyltransferas	20	9.935602981	1.915168585
Ubiquitin-like modifier-activating enzyme 6	7	9.002900069	2.379527982
Tumor protein D52	6	9.466689716	0.829065762
CD166 antigen	5	8.747419577	1.502311769
Desmoplakin	11	8.933548024	1.880167352
26S proteasome non-ATPase regulatory sub	9	9.225696872	0.773465349
Dynamin-2	3	9.307175012	3.334602811
Cell adhesion molecule 3	6	9.283595183	2.995593321
Hypoxanthine-guanine phosphoribosyltrans	11	10.00449334	0.679598224
Sodium- and chloride-dependent GABA tran	4	8.679872866	1.578396554
Enoyl-CoA delta isomerase 1, mitochondrial	6	9.219741661	3.047408762
Protein S100-B	5	10.96715937	0.62275033
Peroxisomal multifunctional enzyme type 2;	4	8.868879446	2.108930696
Guanine nucleotide-binding protein G(I)/G(S	3	9.686975708	0.812033782
E3 ubiquitin-protein ligase RBX1;E3 ubiquitin	3	8.877670756	2.270320786
Eukaryotic translation initiation factor 4E	3	9.027920136	2.272716186
Ras-related protein Ral-A	3	8.782164352	1.543762875
ATP synthase subunit e, mitochondrial	3	8.903008549	2.354138905
26S proteasome non-ATPase regulatory sub	5	8.682560212	1.811575104
Haloacid dehalogenase-like hydrolase doma	9	9.679709461	0.619611003
Synaptic vesicle glycoprotein 2B	4	8.804091705	1.315536085
UPF0600 protein C5orf51 homolog	3	9.006508828	2.073758606
Endonuclease domain-containing 1 protein	5	9.038461196	2.33728129
Hydroxymethylglutaryl-CoA synthase, cytop	5	8.908988723	2.125199697
LYR motif-containing protein 4	4	8.795261141	2.438112278
tr|Q8R5L1|Q8R5L1_MOUSE Complement co	4	9.557435014	0.676720944
UPF0696 protein C11orf68 homolog	4	8.792405699	1.445165084
Mitochondrial intermembrane space import	3	8.993502362	2.465625161
Protein S100;Protein S100-A1	3	9.652681385	0.700450053
GTP-binding protein Di-Ras1	3	8.766650752	1.71735903
Propionyl-CoA carboxylase alpha chain, mito	5	8.737931746	1.794738904
Trifunctional enzyme subunit beta, mitocho	4	8.739548612	1.361098945
Ubiquitin-like-conjugating enzyme ATG3	7	9.649325121	0.627128638
Cytochrome b-c1 complex subunit 7	4	8.984648809	2.063895649
Gamma-soluble NSF attachment protein	6	8.993039232	2.610455389
Arginine--tRNA ligase, cytoplasmic	3	8.649957615	1.476441609
ADP-ribosylation factor-like protein 2	3	8.729091861	1.08527878
Mitochondrial-processing peptidase subunit	4	8.777600795	1.571389005
Hyaluronan and proteoglycan link protein 1	5	9.022469613	2.755531644
Galactokinase	5	9.057399817	2.428822808
Small acidic protein	4	9.070148736	2.812445209
EH domain-containing protein 1	5	8.749767225	1.886600732
Dynactin subunit 3	7	8.689734951	1.895263895

SyliteM			
Protein names	**Unique Peptides**	**Log10 LFQ intensity**	**Log2 enrichment over control**
Abl interactor 2	4	8.840237869	1.627386384
Nuclear ubiquitous casein and cyclin-depen	7	9.443122112	3.046228545
Receptor-type tyrosine-protein phosphatase	4	9.249687428	3.176006515
NFU1 iron-sulfur cluster scaffold homolog, n	5	9.283888938	3.08854551
Cysteine protease ATG4B	5	8.972128752	2.517726771
Endophilin-A3	7	9.147583582	1.952476758
Amyloid beta A4 protein;N-APP;Soluble APP	6	9.425322238	3.329284422
Ran-binding protein 3	9	8.992252986	2.022561274
Gephyrin;Molybdopterin adenylyltransferas	20	9.869988142	2.456814084
UPF0587 protein C1orf123 homolog	5	9.18110008	2.427189177
Protein DDI1 homolog 2	5	9.091666958	3.060621454
Protein Shroom2	7	8.85836874	2.138436695
Cytoplasmic dynein 1 intermediate chain 2	5	9.092299477	2.681451784
tr|A2RTH5|A2RTH5_MOUSE Leucine carbox	12	9.379831068	3.267400004
Protein-glutamate O-methyltransferase	3	9.119222887	2.076670806
Protein archease	6	9.204255678	2.945472274
Glycogen synthase kinase-3 alpha	7	8.904060635	1.646585718
Proline-rich transmembrane protein 2	4	9.196507792	2.605882308
Ephexin-1	9	9.067070856	2.762141717
Serine/threonine-protein kinase B-raf	7	9.026042721	2.478157015
Polyadenylate-binding protein-interacting pr	8	8.936201984	2.129552827
Hsc70-interacting protein	13	10.23225896	1.253853898
Ribose-phosphate pyrophosphokinase 1;Rib	4	9.097187873	3.201202868
E3 ubiquitin-protein ligase ARIH1	6	9.046104787	2.546357422
Cell adhesion molecule 3	2	9.174554035	2.999962336
Ubiquitin-protein ligase E3A	9	8.912136997	2.470247476
Transcriptional activator protein Pur-beta	6	8.971164477	2.177525217
Importin subunit alpha-4	10	9.385445394	1.711882851
Acidic leucine-rich nuclear phosphoprotein 3	12	10.33459447	1.21896867
Guanidinoacetate N-methyltransferase	3	8.944255595	1.573382505
Guanylate cyclase soluble subunit beta-1	7	8.70808081	1.609104882
Phospholipid hydroperoxide glutathione per	5	8.897868909	1.604865811
Target of Myb protein 1	7	9.14160653	2.715353062
Neurofilament light polypeptide	3	8.752547791	1.776759407
Neuroendocrine protein 7B2;N-terminal pep	4	9.148602655	2.886125195
Secretogranin-1;CCB peptide;PE-11	10	9.185060283	2.865366559
Methylmalonyl-CoA mutase, mitochondrial	5	9.010130277	2.531885435
Ubiquitin-like protein 4A	5	8.814786798	1.827951872
Vitamin D-binding protein	7	9.013258665	2.508293265
AP-1 complex subunit gamma-1	2	8.580331833	1.782811289
GDP-L-fucose synthase	3	8.906399696	1.806946983
Talin-1	10	8.825302758	2.588304338
Metallothionein-3	5	9.51771041	3.126959315
Ras-related protein Rab-5C	4	8.971864716	2.172112131
Ran GTPase-activating protein 1	5	8.917941161	1.790169097
Secretogranin-3	5	8.905239843	2.11038256
Stathmin	11	10.20696073	2.193589206
UV excision repair protein RAD23 homolog A	4	8.908849459	1.721768167
Tyrosine-protein phosphatase non-receptor	6	9.007705114	2.631910804

Endoplasmic reticulum resident protein 29	4	8.940262408	1.728015066
Neurogranin;NEUG(55-78)	2	10.11126251	2.745650847
Eukaryotic translation initiation factor 4E	6	9.055493007	2.168945363
Na(+)/H(+) exchange regulatory cofactor NH	9	9.272352241	2.034139864
Neuroplastin	3	9.306746608	3.944703967
Hematological and neurological expressed 1	3	9.121165748	3.503906028
Cytochrome b-c1 complex subunit 6, mitoch	3	9.104998949	2.516299516
Heterogeneous nuclear ribonucleoprotein U	4	8.747761278	2.136095077
Nucleobindin-1	15	9.442495447	1.984893254
Sorting nexin-12	6	8.799478399	2.430535836
S-adenosylmethionine synthase isoform typ	12	9.789841493	1.861210732
Tubulin--tyrosine ligase-like protein 12	9	8.756095756	2.197543506
Ubiquitin-conjugating enzyme E2 Z	8	9.336419705	3.563773643
Eukaryotic translation initiation factor 3 sub	3	8.788430001	1.791708573
Protein prune homolog 2	4	9.021396057	2.352930017
Synergin gamma	6	8.767541734	1.906236676
Src substrate cortactin	10	9.211254068	1.926669615
GTPase HRas;GTPase HRas, N-terminally pro	4	9.093736785	2.472404486
Nucleophosmin	4	8.739287468	1.92875029
Transcription intermediary factor 1-beta	8	9.076713245	2.186517729
Endophilin-A2	4	8.998812755	2.482440144
Sorting nexin-6;Sorting nexin-6, N-terminally	8	8.970249219	2.119110525
tr|Q91V89|Q91V89_MOUSE Serine/threonir	5	8.948183042	1.651657358
Glutaredoxin-related protein 5, mitochondri	3	9.122215878	2.681899123
Heterogeneous nuclear ribonucleoprotein A	3	8.844042042	2.354830652
N-terminal EF-hand calcium-binding protein	7	9.422606253	1.617052957
Eukaryotic translation initiation factor 4B	8	8.687947893	1.537475183
Protein FAM49A	6	9.30992811	1.956827769
PITH domain-containing protein 1	6	8.951536646	2.525865936
DCN1-like protein 2;DCN1-like protein	6	8.726466391	1.576064566
WD repeat-containing protein 37	9	9.342521373	2.146190144
tr|Q8CFX3|Q8CFX3_MOUSE Protocadherin 1	4	9.027634966	2.135578403
Poly(ADP-ribose) glycohydrolase ARH3	5	9.054766218	2.263852602
5-oxoprolinase	4	9.087461966	2.80591609
Protein farnesyltransferase subunit beta	4	8.815537903	2.163154128
Sulfite oxidase, mitochondrial	6	9.001214325	2.203861284
COP9 signalosome complex subunit 8	3	9.012837225	2.125057521
Peroxisomal biogenesis factor 19	4	9.011824096	2.474097818
UPF0696 protein C11orf68 homolog	7	8.859660578	2.264658074
Cell cycle and apoptosis regulator protein 2	7	8.829400272	1.612870534
Phosphate carrier protein, mitochondrial	3	9.237342629	3.140988826
Immunity-related GTPase family Q protein	9	9.060848873	1.647359195
Inorganic pyrophosphatase 2, mitochondria	12	9.684674841	2.053000945
ATP-dependent RNA helicase DDX1	11	9.288092655	3.740157619
Protein BRICK1	4	9.119486836	2.452183731
Glycine cleavage system H protein, mitochor	3	9.596035999	1.77335315
Adenylate kinase isoenzyme 5	2	8.418152081	1.59905039
Homer protein homolog 3	5	9.403292145	3.557556818
Adrenodoxin-like protein, mitochondrial	3	8.850254029	2.015084
RWD domain-containing protein 1	6	8.957410924	2.157244497
Heat shock factor-binding protein 1	4	9.139028547	2.351928408

26S proteasome non-ATPase regulatory sub	5	8.716854395	1.967814782
Vacuolar protein sorting-associated protein	6	8.813854421	1.936384367
Gamma-soluble NSF attachment protein	7	9.301203679	3.419673434
COP9 signalosome complex subunit 7a	3	9.238196699	3.023611179
Parathymosin	7	10.45055701	3.159189989
Nucleolar protein 3	4	9.269582986	2.86813258
Synapse-associated protein 1	4	9.239524703	3.080585246
Charged multivesicular body protein 4b	9	9.161487791	3.328427049
Sorting nexin-5	11	9.384675923	3.372258826
N-acetyl-D-glucosamine kinase	6	9.258014363	3.05459226
Ethylmalonyl-CoA decarboxylase	5	8.797059695	1.879258466
ATP synthase subunit d, mitochondrial	7	9.513430698	4.508290006
Calsyntenin-1;Soluble Alc-alpha;CTF1-alpha	6	8.940700722	2.848112276
Protein SET	7	9.881994865	1.245237688
Nucleosome assembly protein 1-like 5	4	8.974760316	2.027583761
Cell cycle exit and neuronal differentiation p	7	9.290457564	2.606475804
Protein NDRG3	4	8.86119975	1.753399906
Prostaglandin E synthase 3	9	10.67739705	1.548659392
RAC-gamma serine/threonine-protein kinas	8	9.093071306	2.935456966
STIP1 homology and U box-containing prote	4	8.981088887	2.109410011
Adenylate kinase 4, mitochondrial	3	8.712338177	2.285924931
Protein kinase C and casein kinase substrate	8	9.124960451	3.220362229
EH domain-containing protein 1	5	8.810528222	2.20788491
SUMO-activating enzyme subunit 2	12	9.698387659	1.180774345
ADP-ribosylation factor GTPase-activating pr	6	9.017742664	2.219402408

E. Gephyrin isoform sequences

GPHN_1 736 AA long 79,76 kDa

MATEGMILTNHDHQIRVGVLTVSDSCFRNLAEDRSGINLKDLVQDPSLLGGTISAYKIVPDEIEEIKETLIDWCDE
KELNLILTTGGTGFAPRDVTPEATKEVIEREAPGMALAMLMGSLNVTPLGMLSRPVCGIRGKTLIINLPGSKKGSQ
ECFQFILPALPHAIDLLRDAIVKVKEVHDELEDLPSPPPPLSPPPTTSPHKQTEDKGVQCEEEEEEKKDSGVASTE
DSSSSHITAAALAAKIPDSIISRGVQVLPRDTASLSTTPSESPRAQATSRLSTASCPTPKVQSRCSSKENILRASH
SAVDITKVARRHRMSPFPLTSMDKAFITVLEMTPVLGTEIINYRDGMGRVLAQDVYAKDNLPPFPASVKDGYAVRA
ADGPGDRFIIGESQAGEQPTQTVMPGQVMRVTTGAPIPCGADAVVQVEDTELIRESDDGTEELEVRILVQARPGQD
IRPIGHDIKRGECVLAKGTHMGPSEIGLLATVGVTEVEVNKFPVVAVMSTGNELLNPEDDLLPGKIRDSNRSTLLA
TIQEHGYPTINLGIVGDNPDDLLNALNEGISRADVIITSGGVSMGEKDYLKQVLDIDLHAQIHFGRVFMKPGLPTT
FATLDIDGVRKIIFALPGNPVSAVVTCNLFVVPALRKMQGILDPRPTIIKARLSCDVKLDPRPEYHRCILTWHHQE
PLPWAQSTGNQMSSRLMSMRSANGLLMLPPKTEQYVELHKGEVVDVMVIGRL

GPHN_5 455 AA long 49,62 kDa

MATEGMILTNHDHQIRVGVLTGHSAVDITKVARRHRMSPFPLTSMDKAFITVLEMTPVLGTEIINYRDGMGRVLAQ
DVYAKDNLPPFPASVKDGYAVRAADGPGDRFIIGESQAGEQPTQTVMPGQVMRVTTGAPIPCGADAVVQVEDTELI
RESDDGTEELEVRILVQARPGQDIRPIGHDIKRGECVLAKGTHMGPSEIGLLATVGVTEVEVNKFPVVAVMSTGNE
LLNPEDDLLPGKIRDSNRSTLLATIQEHGYPTINLGIVGDNPDDLLNALNEGISRADVIITSGGVSMGEKDYLKQV
LDIDLHAQIHFGRVFMKPGLPTTFATLDIDGVRKIIFALPGNPVSAVVTCNLFVVPALRKMQGILDPRPTIIKARL
SCDVKLDPRPEYHRCILTWHHQEPLPWAQSTGNQMSSRLMSMRSANGLLMLPPKTEQYVELHKGEVVDVMVIGRL

GPHN_6 769 AA long 83,48 kDa

MATEGMILTNHDHQIRVGVLTVSDSCFRNLAEDRSGINLKDLVQDPSLLGGTISAYKIVPDEIEEIKETLIDWCDE
KELNLILTTGGTGFAPRDVTPEATKEVIEREAPGMALAMLMGSLNVTPLGMLSRPVCGIRGKTLIINLPGSKKGSQ
ECFQFILPALPHAIDLLRDAIVKVKEVHDELEDLPSPPPPLSPPPTTSPHKQTEDKGVQCEEEEEEKKDSGVASTE
DSSSSHITAAALAAKIPDSIISRGVQVLPRDTASLSTTPSESPRAQATSRLSTASCPTPKQIRRPDESKGVASRVG
SLKYLLSLGDFVHKTFKVQSRCSSKENILRASHSAVDITKVARRHRMSPFPLTSMDKAFITVLEMTPVLGTEIINY
RDGMGRVLAQDVYAKDNLPPFPASVKDGYAVRAADGPGDRFIIGESQAGEQPTQTVMPGQVMRVTTGAPIPCGADA
VVQVEDTELIRESDDGTEELEVRILVQARPGQDIRPIGHDIKRGECVLAKGTHMGPSEIGLLATVGVTEVEVNKFP
VVAVMSTGNELLNPEDDLLPGKIRDSNRSTLLATIQEHGYPTINLGIVGDNPDDLLNALNEGISRADVIITSGGVS
MGEKDYLKQVLDIDLHAQIHFGRVFMKPGLPTTFATLDIDGVRKIIFALPGNPVSAVVTCNLFVVPALRKMQGILD
PRPTIIKARLSCDVKLDPRPEYHRCILTWHHQEPLPWAQSTGNQMSSRLMSMRSANGLLMLPPKTEQYVELHKGEV
VDVMVIGRL

GPHN_7 409 AA long 44,43 kDa

MATEGMILTNHDHQIRVGVLTDGMGRVLAQDVYAKDNLPPFPASVKDGYAVRAADGPGDRFIIGESQAGEQPTQTV
MPGQVMRVTTGAPIPCGADAVVQVEDTELIRESDDGTEELEVRILVQARPGQDIRPIGHDIKRGECVLAKGTHMGP
SEIGLLATVGVTEVEVNKFPVVAVMSTGNELLNPEDDLLPGKIRDSNRSTLLATIQEHGYPTINLGIVGDNPDDLL
NALNEGISRADVIITSGGVSMGEKDYLKQVLDIDLHAQIHFGRVFMKPGLPTTFATLDIDGVRKIIFALPGNPVSA
VVTCNLFVVPALRKMQGILDPRPTIIKARLSCDVKLDPRPEYHRCILTWHHQEPLPWAQSTGNQMSSRLMSMRSAN
GLLMLPPKTEQYVELHKGEVVDVMVIGRL

GPHN_8 757 AA long 82,37 kDa

MATEGMILTNHDHQIRVGVLTVSDSCFRNLAEDRSGINLKDLVQDPSLLGGTISAYKIVPDEIEEIKETLIDWCDE
KELNLILTTGGTGFAPRDVTPEATKEVIEREAPGMALAMLMGSLNVTPLGMLSRPVCGIRGKTLIINLPGSKKGSQ
ECFQFILPALPHAIDLLRDAIVKVKEVHDELEDLPSPPPPLSPPPTTSPHKQTEDKGVQCEEEEEEKKDSGVASTE
DSSSSHITAAALAAKIPDSIISRGVQVLPRDTASLSTTPSESPRAQATSRLSTASCPTPKLHSRLEGLKDELWRNR
GYDLRVQSRCSSKENILRASHSAVDITKVARRHRMSPFPLTSMDKAFITVLEMTPVLGTEIINYRDGMGRVLAQDV
YAKDNLPPFPASVKDGYAVRAADGPGDRFIIGESQAGEQPTQTVMPGQVMRVTTGAPIPCGADAVVQVEDTELIRE
SDDGTEELEVRILVQARPGQDIRPIGHDIKRGECVLAKGTHMGPSEIGLLATVGVTEVEVNKFPVVAVMSTGNELL
NPEDDLLPGKIRDSNRSTLLATIQEHGYPTINLGIVGDNPDDLLNALNEGISRADVIITSGGVSMGEKDYLKQVLD

IDLHAQIHFGRVFMKPGLPTTFATLDIDGVRKIIFALPGNPVSAVVTCNLFVVPALRKMQGILDPRPTIIKARLSC
DVKLDPRPEYHRCILTWHHQEPLPWAQSTGNQMSSRLMSMRSANGLLMLPPKTEQYVELHKGEVVDVMVIGRL

GPHN_10 515 AA long 55,99 kDa

MATEGMILTNHDHQIRVGVLTVSDSCFRNLAEDRSGINLKDLVQDPSLLGGTISAYKIVPDEIEEIKETLIDWCDE
KELNLILTTGGTGFAPRDVTPEATKEVIEREAPGMALAMLMGSLNVTPLGMLSRPVCGIRGKTLIINLPGSKKGSQ
ECFQFILPALPHAIDLLRDAIVKVKEVHDELEDLPSPPPPLSPPPTTSPHKQTEDKGVQCEEEEEEKKDSGVASTE
DSSSSHITAAALAAKIPDSIISRGVQVLPRDTASLSTTPSESPRAQATSRLSTASCPTPKLLNPEDDLLPGKIRDS
NRSTLLATIQEHGYPTINLGIVGDNPDDLLNALNEGISRADVIITSGGVSMGEKDYLKQVLDIDLHAQIHFGRVFM
KPGLPTTFATLDIDGVRKIIFALPGNPVSAVVTCNLFVVPALRKMQGILDPRPTIIKARLSCDVKLDPRPEYHRCI
LTWHHQEPLPWAQSTGNQMSSRLMSMRSANGLLMLPPKTEQYVELHKGEVVDVMVIGRL

GPHN_14 705 AA long 76,34 kDa

MATEGMILTNHDHQIRVGVLTVSDSCFRNLAEDRSGINLKDLVQDPSLLGGTISAYKIVPDEIEEIKATKEVIERE
APGMALAMLMGSLNVTPLGMLSRPVCGIRGKTLIINLPGSKKGSQECFQFILPALPHAIDLLRDAIVKVKEVHDEL
EDLPSPPPPLSPPPTTSPHKQTEDKGVQCEEEEEEKKDSGVASTEDSSSSHITAAALAAKIPDSIISRGVQVLPRD
TASLSTTPSESPRAQATSRLSTASCPTPKVQSRCSSKENILRASHSAVDITKVARRHRMSPFPLTSMDKAFITVLE
MTPVLGTEIINYRDGMGRVLAQDVYAKDNLPPFPASVKDGYAVRAADGPGDRFIIGESQAGEQPTQTVMPGQVMRV
TTGAPIPCGADAVVQVEDTELIRESDDGTEELEVRILVQARPGQDIRPIGHDIKRGECVLAKGTHMGPSEIGLLAT
VGVTEVEVNKFPVVAVMSTGNELLNPEDDLLPGKIRDSNRSTLLATIQEHGYPTINLGIVGDNPDDLLNALNEGIS
RADVIITSGGVSMGEKDYLKQVLDIDLHAQIHFGRVFMKPGLPTTFATLDIDGVRKIIFALPGNPVSAVVTCNLFV
VPALRKMQGILDPRPTIIKARLSCDVKLDPRPEYHRCILTWHHQEPLPWAQSTGNQMSSRLMSMRSANGLLMLPPK
TEQYVELHKGEVVDVMVIGRL

GPHN_28 445 AA long 48,58 kDa

MATEGMILTNHDHQIRVGVLTVSDSCFRNLAEDRSGINLKDLVQDPSLLGGTISAYKIVPDEIEEIKETLIDWCDE
KELNLILTTGGTGFAPRDVTPEATKEVIEREAPGMALAMLMGSLNVTPLGMLSRPVCGIRGKTLIINLPGSKKGSQ
ECFQFILPALPHAIDLLRDAIVKVKEVHDELEDLPSPPPPLSPPPTTSPHKQTEDKGVQCEEEEEEKKDSGVASTE
DSSSSHITAAALAAKIPDSIISRGVQVLPRDTASLSTTPSESPRAQATSRLSTASCPTPKDYLKQVLDIDLHAQIH
FGRVFMKPGLPTTFATLDIDGVRKIIFALPGNPVSAVVTCNLFVVPALRKMQGILDPRPTIIKARLSCDVKLDPRP
EYHRCILTWHHQEPLPWAQSTGNQMSSRLMSMRSANGLLMLPPKTEQYVELHKGEVVDVMVIGRL

GPHN_32 628 AA long 67,57 kDa

MATEGMILTNHDHQIRVGVLTVSDSCFRNLAEDRSGINLKDLVQDPSLLGGTISAYKIVPDEIEEIKETLIDWCDE
KELNLILTTGGTGFAPRDVTPEATKEVIEREAPGMALAMLMGSLNVTPLGMLSRPVCGIRGKTLIINLPGSKKGSQ
ECFQFILPALPHAIDLLRDAIVKVKEVHDELEDLPSPPPPLSPPPTTSPHKQTEDKGVQCEEEEEEKKDSGVASTE
DSSSSHITAAALAAKIPDSIISRGVQVLPRDTASLSTTPSESPRAQATSRLSTASCPTPKVQSRCSSKENILRASH
SAVDITKVARRHRMSPFPLTSMDKAFITVLEMTPVLGTEIINYRDGMGRVLAQDVYAKDNLPPFPASVKDGYAVRA
ADGPGDRFIIGESQAGEQPTQTVMPGQVMRVTTGAPIPCGADAVVQVEDTELIRESDDGTEELEVRILVQARPGQD
IRPIGHDIKRGECVLAKGTHMGPSEIGLLATVGVTEVEVNKFPVVAVMSTGNELLNPEDDLLPGKIRDSNRSTLLA
TIQEHGYPTINLGIVGDNPDDLLNALNEGISRADVIITSGGVSMGEKDYLKQVLDIDLHAQIHFGRVFMKPGLPTT
FATLDIDGVRKIIFALPVIV

GPHN_42 669 AA long 72,16 kDa

MATEGMILTNHDHQIRVGVLTVSDSCFRNLAEDRSGINLKDLVQDPSLLGGTISAYKIVPDEIEEIKETLIDWCDE
KELNLILTTGGTGFAPRDVTPEATKEVIEREAPGMALAMLMGSLNVTPLGMLSRPVCGIRGKTLIINLPGSKKGSQ
ECFQFILPALPHAIDLLRDAIVKVKEVHDELEDLPSPPPPLSPPPTTSPHKQTEDKGVQCEEEEEEKKDSGVASTE
DSSSSHITAAALAAKIPDSIISRGVQVLPRDTASLSTTPSESPRAQATSRLSTASCPTPKVQSRCSSKENILRASH
SAVDITKVARRHRMSPFPLTSMDKAFITVLEMTPVLGTEIINYRDGMGRVLAQDVYAKDNLPPFPASVKDGYAVRA
ADGPGDRFIIGESQAGEQPTQTVMPGQVMRVTTGAPIPCGADAVVQVEDTELIRESDDGTEELEVRILVQARPGQD
IRPIGHDIKRGECVLAKGTHMGPSEIGLLATVGVTEVEVNKFPVVAVMSTGNELLNPEDDLLPGKIRDSNRSTLLA
TIQEHGYPTINLGIVGDNPDDLLNALNEGISRADVIITSGGVSMGEKDYLKQVLDIDLHAQIHFGRVFMKPGLPTT
FATLDIDGVRKIIFALPGNQMSSRLMSMRSANGLLMLPPKTEQYVELHKGEVVDVMVIGRL

GPHN_49 528 AA long 57,45 kDa

MATEGMILTNHDHQIRVGVLTVSDSCFRNLAEDRSGINLKDLVQDPSLLGGTISAYKIVPDEIEEIKETLIDWCDE
KELNLILTTGGTGFAPRDVTPEKFPTFPFCGLQKGATKEVIEREAPGMALAMLMGSLNVTPLGMLSRPVCGIRGKT
LIINLPGSKKGSQECFQFILPALPHAIDLLRDAIVKVKEVHDELEDLPSPPPPLSPPPTTSPHKQTEDKGVQCEEE
EEEKKDSGVASTEDSSSSHITAAALAAKIPDSIISRGVQVLPRDTASLSTTPSESPRAQATSRLSTASCPTPKLLN
PEDDLLPGKIRDSNRSTLLATIQEHGYPTINLGIVGDNPDDLLNALNEGISRADVIITSGGVSMGEKDYLKQVLDI
DLHAQIHFGRVFMKPGLPTTFATLDIDGVRKIIFALPGNPVSAVVTCNLFVVPALRKMQGILDPRPTIIKARLSCD
VKLDPRPEYHRCILTWHHQEPLPWAQSTGNQMSSRLMSMRSANGLLMLPPKTEQYVELHKGEVVDVMVIGRL

F. Vector maps

Gephyrin isoform vector map. All isoforms have the same scaffold, the only change is the gephyrin coding sequence.

Gephyrin isoform constructs

pLVX-hSyn-Flag-V5-mScarlett-IHRES-ZsGreen1 (version Eral)
pLVX-hSyn-Flag-V5-mScarlett-GPHN-1-IHRES-ZsGreen1 (version Eral)
pLVX-hSyn-Flag-V5-mScarlett-GPHN-5-IRES-ZsGreen1 (version Eral)
pLVX-hSyn-Flag-V5-mScarlett-GPHN-6-IRES-ZsGreen1 (version Eral)
pLVX-hSyn-Flag-V5-mScarlett-GPHN-7-IRES-ZsGreen1 (version Eral)
pLVX-hSyn-Flag-V5-mScarlett-GPHN-8-IRES-ZsGreen1 (version Eral)
pLVX-hSyn-Flag-V5-mScarlett-GPHN-10-IRES-ZsGreen1 (version Eral)
pLVX-hSyn-Flag-V5-mScarlett-GPHN-14-IRES-ZsGreen1 (version Eral)
pLVX-hSyn-Flag-V5-mScarlett-GPHN-28-IRES-ZsGreen1 (version Eral)
pLVX-hSyn-Flag-V5-mScarlett-GPHN-32-IRES-ZsGreen1 (version Eral)
pLVX-hSyn-Flag-V5-mScarlett-GPHN-42-IRES-ZsGreen1 (version Eral)
pLVX-hSyn-Flag-V5-mScarlett-GPHN-49-IRES-ZsGreen1 (version Eral)

Plasmid map

pLVX-hSyn-Flag-V5-mScarlett-GPHN-1-IRES-ZsGreen1 (version Eral)

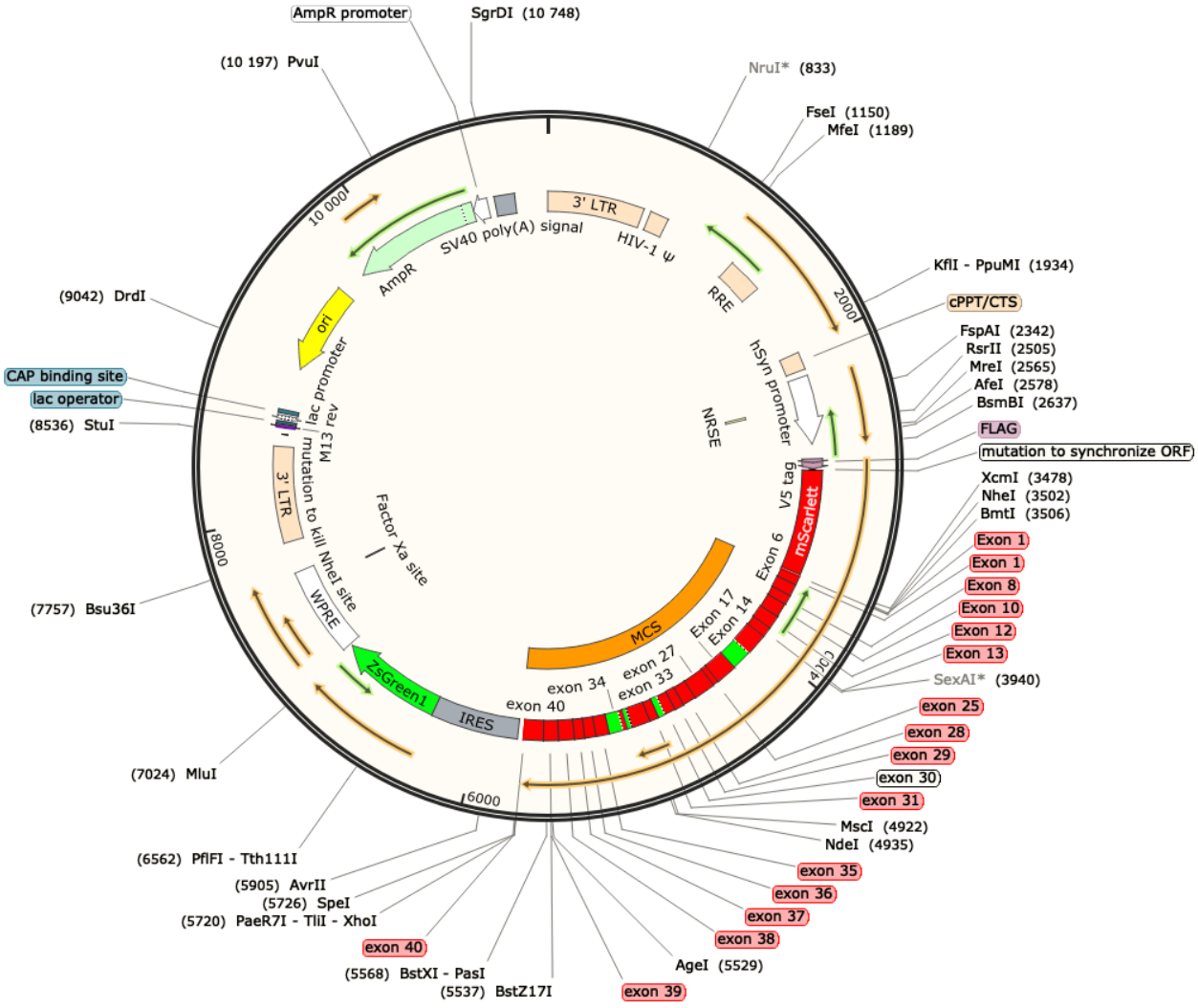

Floxed synaptophysin vector map

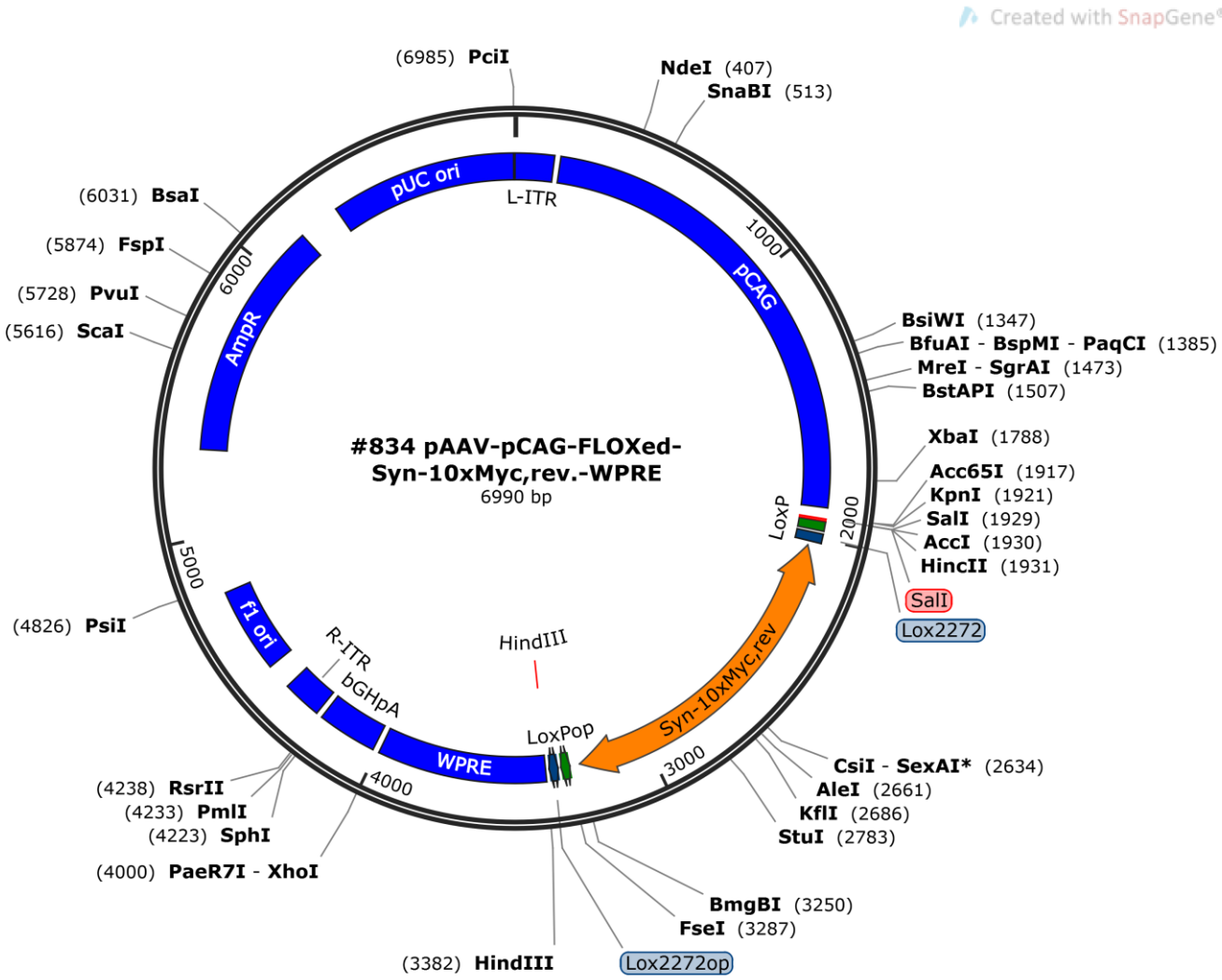

Coff/Fon eYFP vector map

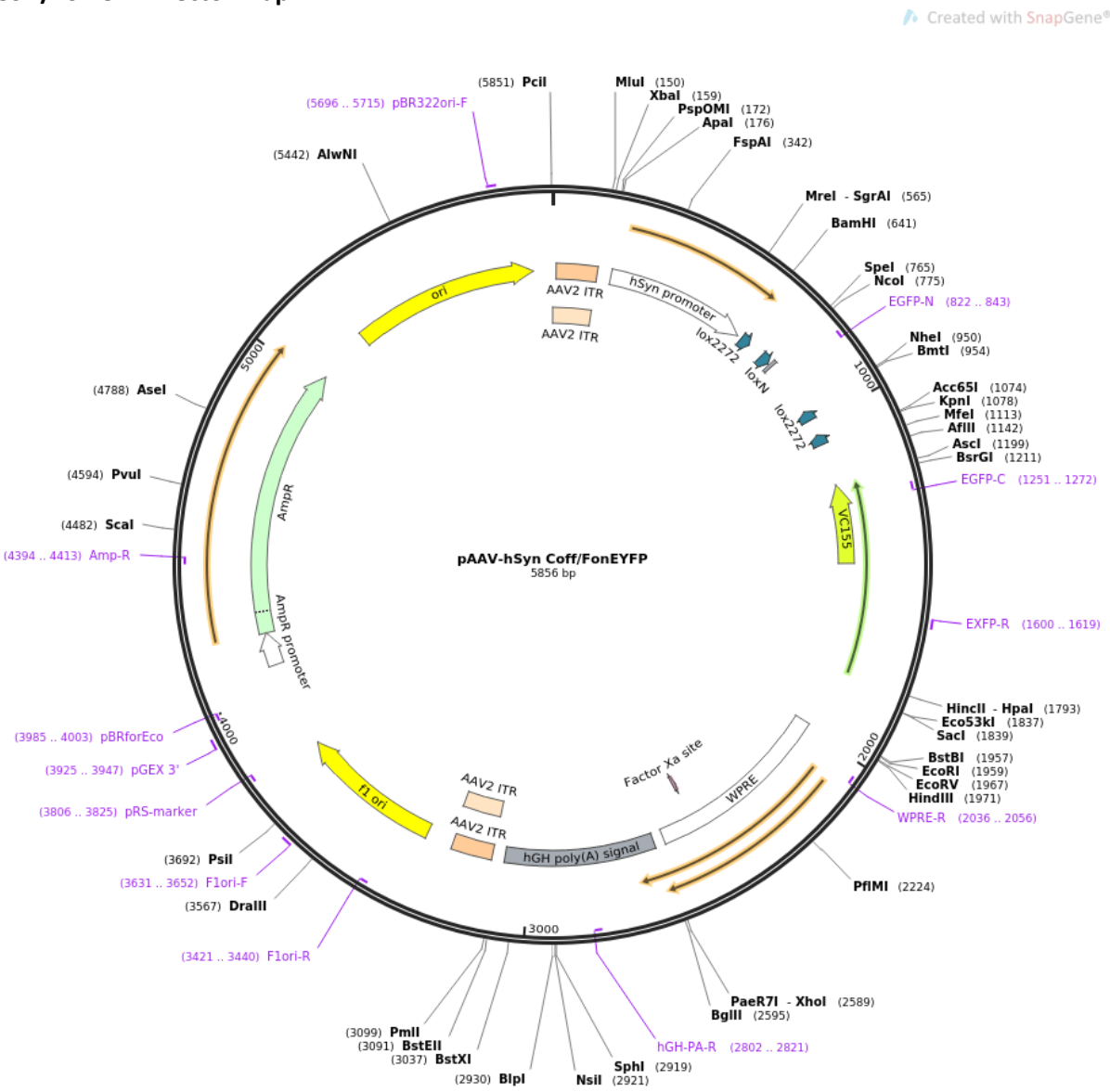

PSD-95-eGFP vector map

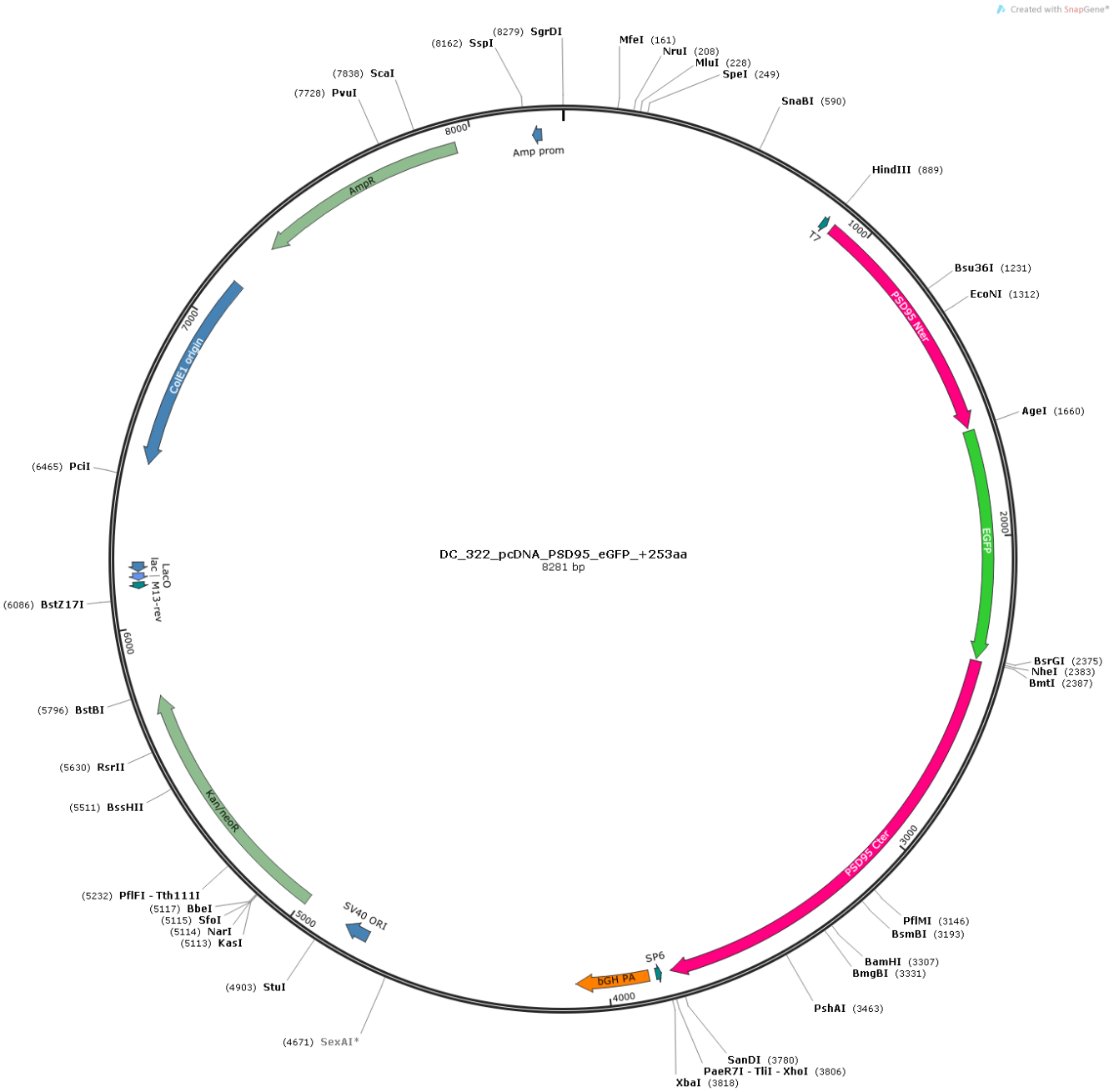

G. Macro and script for Image analysis

Macro	Mode of operation	Utilization
I	• renaming the data format	• conversion of the proprietary image format to .tiff • data import
II	• averages the image set to one image (noise reduction) • sets greyscale representation of intensities • sets the min and max values for the intensity display	• averaging of image series
III	• creates a binary mask and inverses the image • measures the image background and subtracts the background	• subtraction of the image background
IV	• opens corresponding channel images iteratively • automatically analyses the images in JACoP plugin and measures the colocalization	• colocalization analysis
V	• creates a binary mask corresponding to fluorescent protein location in the cell/object of interest • tracks the binary mask in the target channel and measures the average intensity in ROI	• measurement of intensity in fluorescent protein rich regions in all color channels

Macro I:

```
path = File.openDialog("Select a File");
oldname = File.getName(path);
run("Bio-Formats Macro Extensions");
Ext.setId(path);
Ext.getCurrentFile(file);
Ext.getSeriesCount(seriesCount);
for (s=1; s<=seriesCount; s++) {
        run("Bio-Formats Importer", "open=&path autoscale color_mode=Default view=Hyperstack stack_order=XYCZT series_"+s);
        oldtitle = getTitle();
        newtitle = replace(oldtitle, oldname + " - ", "");
        out_path = getDirectory("image") + newtitle;
        saveAs("tiff", out_path);
        run("Close All");
  }
```

Macro II:

```
dir1 = getDirectory("Select directory to average");
list = getFileList(dir1);
SaveDir = getDirectory("Select output directory");
for (g=0; g<list.length; g++) {
        open(dir1 + list[g]);
        originalImageName = getTitle();
        selectWindow(originalImageName);
        run("Z Project...", "projection=[Average Intensity]");
        selectWindow("AVG_" + originalImageName);
        run("Grays");
        //run("Brightness/Contrast...");
        setMinAndMax(150, 2500);
        save(SaveDir + originalImageName);
```

```
	close();
	close();
}
```

Macro III:

```
dir1 = getDirectory("Select image directory");
list = getFileList(dir1);
SaveDir = getDirectory("Select results directory");
	run("Set Measurements...", "area mean standard min integrated median redirect=Nondecimal=3");
	for (g=0; g<list.length; g++) {
	ch1name = list[g];
	//Identifier = "-Probe";
	print(ch1name);
	open(dir1 + ch1name);
	//rename (g + Identifier);
	//creating a binary mask
	selectWindow(ch1name);
	run("Duplicate...", "title=Dup.tif");
	selectWindow("Dup.tif");
	run("Median...", "radius=5");
	run("Maximum...", "radius=5");
	run("Minimum...", "radius=5");
	setAutoThreshold("Default dark");
	setThreshold(250, 65535);

	setOption("BlackBackground", true);
	run("Convert to Mask");
	run("Make Inverse");
	roiManager("Add");
	RunningNumber = g + 1;
	roiManager("Save", SaveDir + ch1name + ".roi");
	selectWindow("Dup.tif");
	close();
//Mask done
selectWindow(ch1name);
roiManager("Select", 0);
	run("Measure");
	BG = getResult("Mean");
	print(BG);
	selectWindow(ch1name);
	run("Select None");
	run("Subtract...", "value=BG");
	setMinAndMax(0, 10000);
	save(SaveDir + ch1name);
	close();
	roiManager("reset");
}
selectWindow("Results");
saveAs("Measurements", SaveDir + "Results.tsv");
selectWindow("ROI Manager");
	run("Close");
}
```

Macro IV:

```
//Coloc measurement 2 folders, JACoP
function parseJACoP() { //Log to table function
	//Get the log window
	logdump = split(getInfo("log"), "\n");
```

```
	thrVals = false;
	imgA = -1;
	imgB= -1;
	Pc = -1;
	Oc = -1;
	OcThr = -1;
	k1Thr = -1;
	k1 = -1;
	k2Thr = -1;
	k2 = -1;
	thrA = -1;
	thrB = -1;
	M1 = -1;
	M2 = -1;
	M1Thr = -1;
	M2Thr = -1;
	a = -1;
	b = -1;
	R = -1;
	icq = -1;
	for (i=0; i<logdump.length; i++) {
		if (startsWith(logdump[i], "Image A"))
			imgA = substring(logdump[i], 9, lengthOf(logdump[i]));
		if (startsWith(logdump[i], "Image B"))
			imgB = substring(logdump[i], 9, lengthOf(logdump[i]));
		if (startsWith(logdump[i], "Pearson's Coefficient"))
			Pc = parseFloat(substring(logdump[i+1], 2, lengthOf(logdump[i+1])));

		if (startsWith(logdump[i], "Overlap Coefficient"))
			if (thrVals) {
				OcThr = parseFloat(substring(logdump[i+1], 2, lengthOf(logdump[i+1])));
			} else {
				Oc = parseFloat(substring(logdump[i+1], 2, lengthOf(logdump[i+1])));
			}
		if (startsWith(logdump[i], "k1=")) {
			if (thrVals) {
				k1Thr = parseFloat(substring(logdump[i], 3, lengthOf(logdump[i])));
			} else {
				k1 = parseFloat(substring(logdump[i], 3, lengthOf(logdump[i])));
			}
		}
		if (startsWith(logdump[i], "k2=")) {
			if (thrVals) {
				k2Thr = parseFloat(substring(logdump[i], 3, lengthOf(logdump[i])));
			} else {
				k2 = parseFloat(substring(logdump[i], 3, lengthOf(logdump[i])));
			}
		}
		if (startsWith(logdump[i], "Using thresholds")) {
			thrA = parseFloat(substring(logdump[i], indexOf(logdump[i], "=")+1, indexOf(logdump[i], "and")-
1));
			thrB = parseFloat(substring(logdump[i], lastIndexOf(logdump[i], "=")+1, lastIndexOf(logdump[i],
")")));
			thrVals = true;
		}
		if (startsWith(logdump[i], "Manders' Coefficients (original):")) {
			M1 = parseFloat(substring(logdump[i+1], 3, 8));
```

```
                        M2 = parseFloat(substring(logdump[i+2], 3, 8));
                }
                if (startsWith(logdump[i], "Manders' Coefficients (using threshold")) {
                        M1Thr = parseFloat(substring(logdump[i+1], 3, 8));
                        M2Thr = parseFloat(substring(logdump[i+2], 3, 8));
                }
                if (startsWith(logdump[i], "Cytofluorogram's parameters:")) {
                        a = parseFloat(substring(logdump[i+1], 3, 8));
                        b = parseFloat(substring(logdump[i+2], 3, 8));
                        R = parseFloat(substring(logdump[i+3], 25, 30));
                }
                if (startsWith(logdump[i], "ICQ"))
                        icq = parseFloat(substring(logdump[i], 5, lengthOf(logdump[i])));
        }
        n=nResults;
        setResult("Pearson's", n, Pc);
        setResult("Overlap Coefficient (no threshold)", n, Oc);
        setResult("k1 (no threshold)", n, k1);
        setResult("k2 (no threshold)", n, k2);
        setResult("M1 (no threshold)", n, M1);
        setResult("M2 (no threshold)", n, M2);
        setResult("ThrA", n, thrA);
        setResult("ThrB", n, thrB);
        setResult("Correlation Coefficient", n, R);
        setResult("Overlap Coefficient", n, OcThr);
        setResult("k1", n, k1Thr);
        setResult("k2", n, k2Thr);
        setResult("M1", n, M1Thr);
        setResult("M2", n, M2Thr);
        setResult("Li's ICQ", n, icq);
        setResult("Cytofluorogram Slope", n, a);
        setResult("Cytofluorogram Intercept", n, b);
}
//Function end
dir1 = getDirectory("Select Green image directory");
list = getFileList(dir1);
dir2 = getDirectory("Select Far-Red image directory");
SaveDir = getDirectory("Select results directory");
for (g=0; g<list.length; g++) {
        ch1name = list[g];
        RefCh = "R";
        TargetCh = "FR";
        ch2name = replace(ch1name, RefCh, TargetCh)
        open(dir1 + ch1name);
        open(dir2 + ch2name);
        run("JACoP ", "imga=["+ch1name+"] imgb=["+ch2name+"] thra=400 thrb=160 pearson mm");
        parseJACoP();
        // Clear log window
        print("\\Clear");
        close(ch1name);
        close(ch2name);
}
saveAs("Measurements", SaveDir + "ColocData.tsv");
```

Macro V:

```
dir1 = getDirectory("Select reference image directory");
list = getFileList(dir1);
```

```
dir2 = getDirectory("Select target image directory");
SaveDir = getDirectory("Select output directory");
for (g=0; g<list.length; g++) {
	RunningNumber = g + 1;
	ch1name = list[g];
	RefCh = "R";
	TargetCh = "FR";
	ch2name = replace(ch1name, RefCh, TargetCh);
	print(ch1name);
	open(dir1 + ch1name);
//creating a Mask from a reference channel ROI [R]
	selectWindow(ch1name);
	run("Duplicate...", "title=Dup.tif");
	selectWindow("Dup.tif");
	run("Median...", "radius=5");
	run("Maximum...", "radius=5");
	run("Minimum...", "radius=5");
	setAutoThreshold("Default dark");
	setThreshold(600, 65535);
	setOption("BlackBackground", true);
	run("Convert to Mask");
	run("Create Selection");
	roiManager("Add");
	roiManager("Save", SaveDir + RunningNumber + ".roi");
	selectWindow("Dup.tif");
	close();
//Mask done
//creating 2nd Mask
	selectWindow(ch1name);
	run("Duplicate...", "title=Dup.tif");
	selectWindow("Dup.tif");
	setAutoThreshold("Default dark");
	setThreshold(4000, 65535);
	setOption("BlackBackground", true);
	run("Convert to Mask");
	run("Create Selection");
	roiManager("Add");
	roiManager("Select", 1);
	roiManager("Save", SaveDir + RunningNumber + "-punctae" + ".roi");
	selectWindow("Dup.tif");
	close();
//Mask done
//3rd mask for mScarlet-gephyrin controls
	selectWindow(ch1name);
	run("Duplicate...", "title=Dup.tif");
	selectWindow("Dup.tif");
	run("Median...", "radius=5");
	run("Maximum...", "radius=5");
	run("Minimum...", "radius=5");
	setAutoThreshold("Default dark");
	setThreshold(1000, 65535);
	setOption("BlackBackground", true);
	run("Convert to Mask");
	run("Create Selection");
	roiManager("Add");
	roiManager("Select", 2);
	roiManager("Save", SaveDir + RunningNumber + "-foreGFP" + ".roi");
```

```
		selectWindow("Dup.tif");
		close();
		//Mask done
		selectWindow(ch1name);
		roiManager("Select", 0);
		run("Measure");
		roiManager("Select", 1);
		run("Measure");
		roiManager("Select", newArray(0,1));
		roiManager("XOR");
		run("Measure");
		roiManager("Select", 2);
		run("Measure");
		close();
		open(dir2 + ch2name);
		roiManager("Select", 0);
		run("Measure");
		roiManager("Select", 1);
		run("Measure");
		roiManager("Select", newArray(0,1));
		roiManager("XOR");
		run("Measure");
		roiManager("Select", 2);
		run("Measure");
		close();
		roiManager("reset");
}
selectWindow("Results");
saveAs("Measurements", SaveDir + "Results.tsv");
run("Close");
selectWindow("ROI Manager");
run("Close");
```

H. Icy 2.0.3.0 protocol for single synapse segmentation and intensity recording

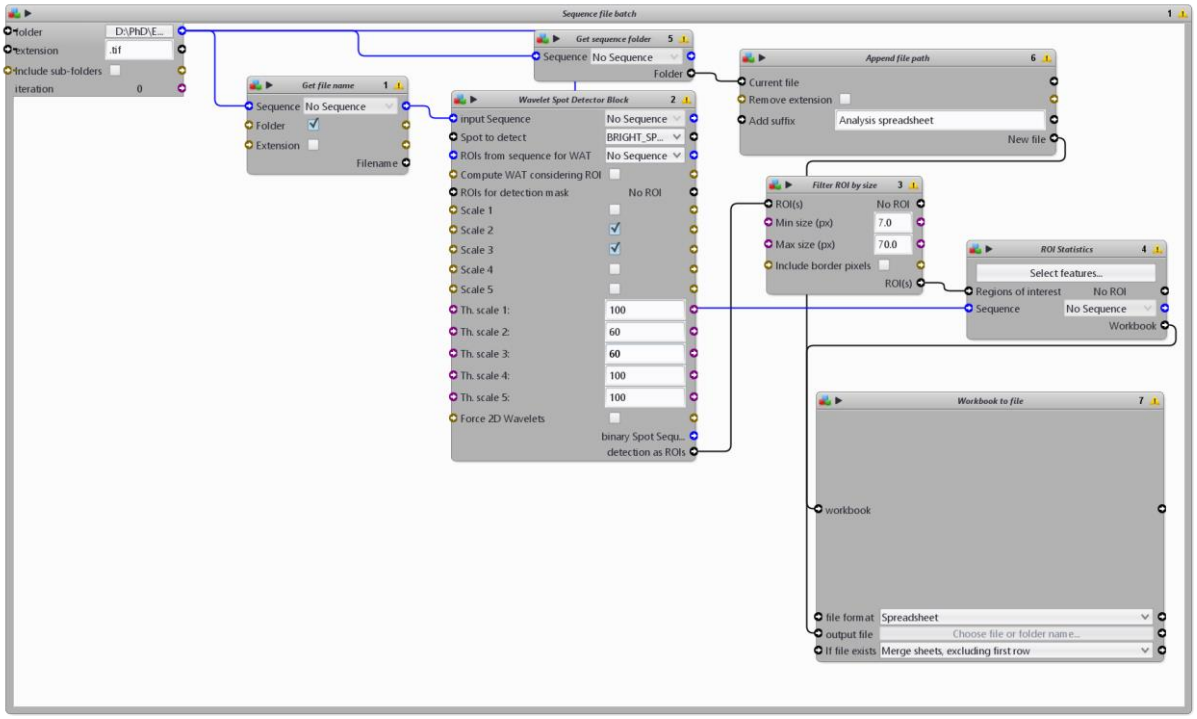

Affidavit

I hereby confirm that my thesis entitled "Functional peptide-based probes for the visualization of inhibitory synapses" is the result of my own work. I did not receive any help or support from commercial consultants. All sources and / or materials applied are listed and specified in the thesis.

Furthermore, I confirm that this thesis has not yet been submitted as part of another examination process neither in identical nor in similar form.

Würzburg,

Place, Date Signature

Eidesstattliche Erklärung

Hiermit erkläre ich an Eides statt, die Dissertation "Funktionelle peptidbasierte Sonden zur Visualisierung von hemmenden Synapsen" eigenständig, d.h. insbesondere selbständig und ohne Hilfe eines kommerziellen Promotionsberaters, angefertigt und keine anderen als die von mir angegebenen Quellen und Hilfsmittel verwendet zu haben.

Ich erkläre außerdem, dass die Dissertation weder in gleicher noch in ähnlicher Form bereits in einem anderen Prüfungsverfahren vorgelegen hat.

Würzburg,

Ort, Datum Unterschrift